Coordination Chemistry Reviews 255 (2011) 1834–1920

Contents lists available at ScienceDirect

Coordination Chemistry Reviews

journal homepage: www.elsevier.com/locate/ccr

Review

Lanthanides and actinides: Annual survey of their organometallic chemistry covering the year 2008

Frank T. Edelmann*

Chemisches Institut der Otto-von-Guericke-Universität Magdeburg, D-39106 Magdeburg, Germany

Contents

* Fax: +49 391 6712933.
E-mail address: frank.edelmann@ovgu.de

0010-8545/$ – see front matter
doi:10.1016/j.ccr.2011.03.007

ARTICLE INFO

Article history:
Received 24 February 2011
Accepted 8 March 2011
Available online 16 March 2011

Keywords:
Lanthanides
Actinides
Cyclopentadienyl complexes
Cyclooctatetraenyl complexes
Organometallic chemistry

ABSTRACT

This review summarizes the progress in organo-*f*-element chemistry during the year 2008. A continuing trend in organolanthanide research is a strong emphasis on applications of organolanthanide complexes in homogeneous catalysis and, to a lesser extent, materials science. Roughly 20% of all relevant papers published in 2008 were in the area of organoactinide chemistry which continues to produce exciting results.

1. Introduction

This review summarizes the progress in organo-*f*-element chemistry during the year 2008. This year witnessed again a significant increase of publications in the field over 2007. A continuing trend in organolanthanide research is a strong emphasis on applications of organolanthanide complexes in homogeneous catalysis and, to a lesser extent, materials science. Roughly 20% of all relevant papers published in 2008 were in the area of organoactinide chemistry, although the latter continues to produce exciting results (*cf.* Sections 3.1–3.4). In this review mainly regular scientific papers are covered, while patents and conference abstracts, etc. have mostly been excluded.

2. Lanthanides

2.1. Lanthanide carbonyls

Isolable binary lanthanide carbonyls still remain elusive, but transient species continue to be subjects of experimental and theoretical investigations. The interaction of metal atoms with small molecules (*i.e.*, CO, O_2, CO_2, H_2, and CH_4) is of considerable interest because of its importance in a great number of catalytic processes. Among these small molecules, carbon monoxide is one of the most important in transition-metal chemistry from an academic or an industrial viewpoint. In this context reactions of laser-ablated lanthanide atoms with CO have been investigated. The adsorption properties of a single CO molecule on Sc_n (n = 2–13) clusters have been studied by means of a density functional theory with the generalized gradient approximation. Two adsorption patterns were identified. Pattern a (n = 3, 4, 6, 8, 11, and 12), CO binds to hollow site while Pattern b (n = 5, 7, 9, 10, and 13), CO binds to bridge site accompanied by significantly lengthening of the Sc–Sc bond. The adsorption energy exhibits clear size-dependent variation and odd–even oscillation for n < 10 and reaches the peak at n = 5, 7, and 9, implying their high chemical reactivity. Similar variations were noted in C–O bond length, vibrational frequency, and charge transferred between CO and the clusters. This can be understood in light of the adsorption pattern, the atomic motif, and the relative stability of the bare Sc clusters. Compared with the free Sc clusters, the magnetic nature remains upon adsorption except n = 2, 4, 12, and 13. Particularly, the moments of n = 13 reduce significantly from 19 to $5\mu_B$, implying the adsorption plays an attenuation influence on the magnetism of the cluster [1]. The interaction of carbon monoxide with 3*d* metal dimers (scandium through zinc) has been examined using six different exchange-correlation density functionals. Results were compared to the relevant experimental values and to other theoretical investigations when available, and the overall agreement has been obtained. The ground state of Sc_2CO was predicted to be $^1A'$, which has an asymmetrically bridging and side-on-bonded CO ligand. The C–O stretching vibrational frequency of the ground state of Sc_2CO was calculated to be 1237.6 cm^{-1}, which is consistent with the experimental value (1193.4 cm^{-1}) and previous calculations. The C–O bond length (1.321 Å) is much longer than the value of the free CO molecule (1.140 Å) calculated at the same level of theory, implying that the C–O bond is highly activated in this side-on bonded Sc_2CO species. The Sc–Sc bond length in Sc_2CO is elongated by 0.111 Å relative to the naked Sc_2 [2]. Reactions of laser-ablated lanthanide atoms (except for radioactive Pm) with carbon dioxide molecules in solid argon have been investigated using matrix-isolation infrared spectroscopy. On the basis of isotopic shifts, mixed isotopic splitting patterns, and CCl_4-doping experiments, the resulting lanthanide oxocarbonyl complexes have been identified. Density functional theory calculations have been performed on these products, which support the experimental assignments of the infrared spectra. Infrared spectroscopic studies of these lanthanide complexes combined with theoretical calculations revealed that the early lanthanide (La–Sm) oxocarbonyl complexes adopt *trans*-configurations, the europium and ytterbium ones adopt side-on-bonded modes (Eu-(η^2-OC)O and Yb-(η^2-OC)O), and the late lanthanoid (Gd–Lu) ones adopt *cis*-configurations. Natural bond orbital analysis indicated that the formation of the lanthanoid oxocarbonyl complexes involves the promotion of 6*s* and 4*f* electrons into the metal valence shell [3].

2.2. Lanthanide hydrocarbyls

2.2.1. Homoleptic compounds

The gas-phase reactivity of doubly charged lanthanide cations, Ln^{2+} (Ln = La, Ce, Pr, Nd, Sm, Eu, Gd, Tb, Dy, Ho, Er, Tm, Yb, Lu), with alkanes (methane, ethane, propane, *n*-butane) and alkenes (ethene, propene, 1-butene) was studied by Fourier transform ion cyclotron resonance mass spectrometry. The reaction products consisted of different combinations of doubly charged organometallic ions (adducts or species formed *via* metal ion induced hydrogen, dihydrogen, alkyl, or alkane eliminations from the hydrocarbons) and singly charged ions that resulted from electron, hydride, or methide transfers from the hydrocarbons to the metal ions. The only lanthanide cations capable of activating the hydrocarbons to form doubly charged organometallic ions were La^{2+}, Ce^{2+}, Gd^{2+}, and Tb^{2+}, which have ground-state or low-lying d^1 electronic configurations. Lu^{2+}, with an accessible d^1 electronic configuration but a rather high electron affinity, reacted only through transfer channels. The remaining Ln^{2+} reacted *via* transfer channels or adduct formation. The different accessibilities of d^1 electronic configurations and the range of electron affinities of the Ln^{2+} cations allowed for a detailed analysis of the trends for metal(2+) reactivity and the conditions for the occurrence of bond activation, adduct formation, and electron, hydride, and methide transfers [4].

2.2.2. Heteroleptic compounds

The bulky hydro-tris(3-^{t}Bu-5-Me-pyrazolyl)borate ligand, ($Tp^{tBu,Me}$, =Tp′), a second generation Trofimenko "scorpionate", has previously been used to prepare heteroleptic "(Tp′)LnER" (Ln = Yb(II) and Sm(II)) type complexes, including hydrocarbyl species. Thus it appeared tempting to test this ligand with the strongly reducing "non-classical" divalent lanthanide ions Tm(II), Dy(II), or Nd(II). One of the most remarkable achievements in 2008 organolanthanide chemistry was certainly the successful synthesis of the first heteroleptic Tm(II) complexes, including the Tm(II)-hydrocarbyl, (Tp′)Tm[CH(SiMe$_3$)$_2$]. Addition of KTp′ to a THF solution of TmI_2 at room temperature in a glovebox (He/N_2 atmosphere), followed by simple work-up afforded dark green (Tp′)TmI(THF) in moderate yield. Although isolable, complex (Tp′)TmI(THF) undergoes slow decomposition both in solution and in the solid state, when kept at −30 °C. Pure (Tp′)TmI(THF) can be recovered from small amounts of decomposed material (appearance of white solid) by recrystallization from diethyl ether. Despite its delicate nature, the iodo complex was found to be a useful starting material for the synthesis of a selected number of heteroleptic Tm(II) complexes. Thus simple salt metathesis gave the dark brown Tm(II)-hydrocarbyl (Tp′)Tm[CH(SiMe$_3$)$_2$], dark brown (Tp′)Tm[N(SiMe$_3$)$_2$], and the dark green triethylborohydride complex (Tp′)Tm(μ-HBEt$_3$)(THF). The complexes were fully characterized and the solid-state structures were established by single-crystal X-ray studies. The most remarkable compound in this series is (Tp′)Tm[CH(SiMe$_3$)$_2$], with a Tm(II)-hydrocarbyl bond, the first time such σ-alkyl species could be isolated. The Tm(II) center is bonded to a classical κ^3-scorpionate and an almost planar CH(SiMe$_3$)$_2$ hydrocarbyl ligand, with the sum of the angles involving non-hydrogen atoms bonded to C1 being 351°. One hydrocarbyl $SiMe_3$ group is wedged between two pyrazolyl ligands while the other $SiMe_3$ points toward the ^{t}Bu group on the third pyrazole ring. Steric repulsion between the latter two groups certainly contributes to the observed distorted tetrahedral coordination geometry of Tm, but electronic factors must also play a role. There are indications of agostic Tm(II)—CH interactions

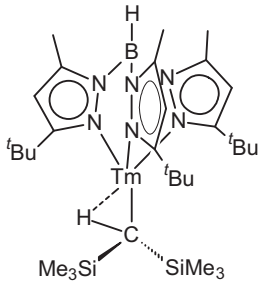

Scheme 1.

(Scheme 1), a common feature with electron deficient lanthanide centers, as is the case with complex (Tp′)Tm[CH(SiMe$_3$)$_2$] [5].

Unusual Lewis acid-stabilized methylidene and oxoscandium complexes have been prepared and structurally characterized. When (PNP)$ScCl_2$ (PNP$^-$ = N[2-P(CHMe$_2$)$_2$-4-methylphenyl]) was treated with 2 equiv. of $LiCH_3$·LiBr complex, the dimethyl derivative (PNP)Sc(CH$_3$)$_2$ was isolated in 58% yield after workup of the reaction mixture (Scheme 2). Treating of the dimethyl complex with 2 equiv. or an excess of Al(CH$_3$)$_3$ in benzene at 25 °C resulted in the clean, gradual formation of a new product along with methane extrusion, as inferred by ^{1}H NMR spectroscopy. The new resonance in the ^{31}P NMR spectrum of this complex was uninformative due to the broad line widths. The ^{1}H NMR spectrum was also rather uninformative at room temperature, revealing a very broad peak centered at −0.20 ppm. However, the notable presence of a singlet at 0.69 ppm integrating to two protons suggested the formation of a methylidene unit. The latter CH_2 resonance was unambiguously correlated to the ^{13}C NMR resonance at 28.8 ppm by HMQC NMR experiments. Cooling the NMR solution of this newly isolated product to −50 °C shifted the CH_2 resonance to 0.75 ppm in the ^{1}H NMR spectrum and also resolved the resonance at −0.20 ppm to suggest the formation of an organometallic complex having three inequivalent –CH_3 environments with the same ratio of hydrogens.

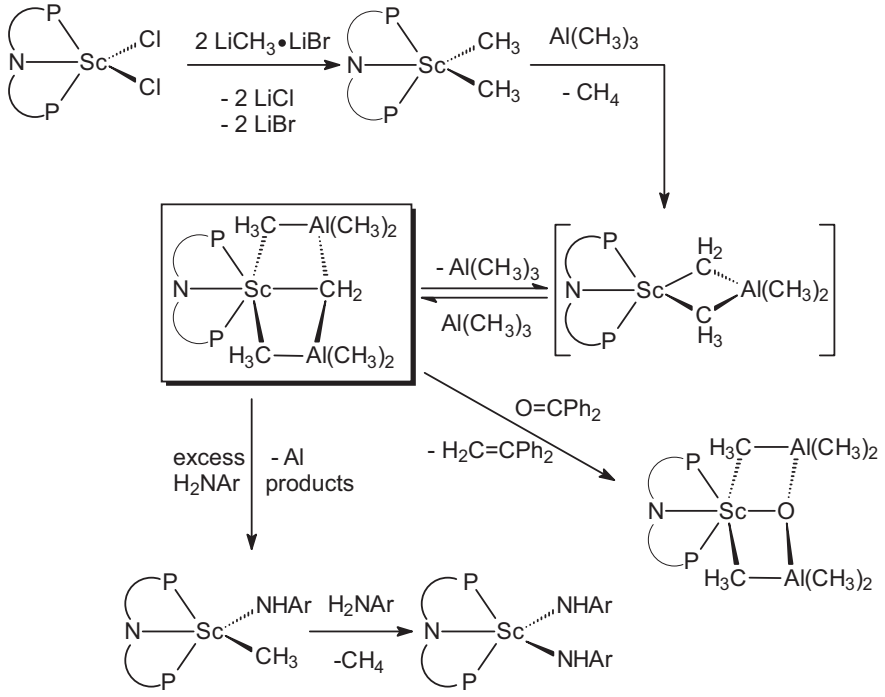

Scheme 2. For simplicity, the PNP cartoon represents N[2-P(CHMe$_2$)$_2$-4-methylphenyl]$_2^-$.

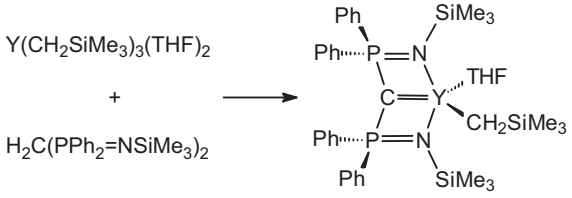

Scheme 3.

Due to these interesting spectroscopic signatures, the structural connectivity of this new scandium complex was elucidated by single crystal X-ray diffraction studies. These confirmed the molecular structure of the first mononuclear scandium methylidene, (PNP)Sc(μ_3-CH_2)(μ_2-CH_3)$_2$[Al(CH_3)$_2$]$_2$, stabilized by two Al(CH_3)$_3$ ligands in a *pseudo*-transoid fashion [6].

The new methylene complex could be protonated with an excess of H_2NAr (Ar = 2,6-*i*Pr$_2$C$_6$H$_3$) to quickly form the anilide-methyl (PNP)Sc(NHAr)(CH_3) intermediate and after 12 h ultimately produce the bis(anilide) (PNP)Sc(NHAr)$_2$ quantitatively (Scheme 2). The connectivity of the latter complex was inferred by single crystal X-ray diffraction analysis and NMR spectral data and the fact that it could be prepared independently by the reaction of (PNP)ScCl_2 with 2 equiv. of LiNHAr. When a solution of the methylene complex was added to O=CPh_2 in benzene, an immediate reaction occurred. Examination of the mixture by ^{31}P and ^{1}H NMR evinced clean formation of a new *C*2 symmetric Sc complex. Notably, the methylidene resonance originally present in (PNP)Sc(μ_3-CH_2)(μ_2-CH_3)$_2$[Al(CH_3)$_2$]$_2$ was absent, suggesting that this ligand had been transformed or replaced. However, the resonances corresponding to the bridging and terminal methyl moieties in the two Al(CH_3)$_3$ groups were fluxional even to −50 °C, unlike those observed for complex (PNP)Sc(μ_3-CH_2)(μ_2-CH_3)$_2$[Al(CH_3)$_2$]$_2$. Based on this evidence and the formation of the terminal olefin, H_2C=CPh_2, the new product was proposed to be the Lewis acid stabilized scandium oxo complex (PNP)Sc(μ_3-O)(μ_2-CH_3)$_2$[Al(CH_3)$_2$]$_2$, depicted in Scheme 2. Its solid state structure further supported the proposed connectivity, revealing a three-coordinate oxo-ligand bridged by one Sc and two Al atoms. The metrical parameters closely resembled those for the methylene precursor, with the only significant exception being the shorter Sc–O bond length 2.008(2) Å, thus leading to a tucked-in appearance of the ScOC_2Al_2 skeleton. The latter distance is longer than scandium alkoxide distances (∼1.9 Å) but shorter than dative Sc←:OR_2 resulting from a coordinating ether (∼2.2 Å) [6].

Synthesis and structural characterization of an yttrium–alkyl–alkylidene complex have also been achieved in 2008. Addition of toluene to a cold (−78 °C) 1:1 molar mixture of Y(CH_2SiMe_3)$_3$(THF)$_2$ and H_2C(PPh_2=N$SiMe_3$)$_2$ afforded a clear, pale yellow solution on warming to room temperature with stirring overnight. Work-up and recrystallization from a hexane–toluene mixture afforded colorless crystals of the yttrium–alkyl–alkylidene complex (Scheme 3) in moderate yield (43%), but inspection of the crude mother liquor by NMR spectroscopy indicated that the reaction is essentially quantitative and the isolated yield is a result of the high solubility of the product [7].

An X-ray diffraction study showed the presence of the first structurally authenticated, monomeric yttrium–alkyl–alkylidene complex. DFT calculations showed, however, that the formal Y=C double bond in fact possesses a calculated bond order significantly lower than one, and this is only moderately larger than the *bona fide* Y–C single bond in the same molecule. The two lone pairs on the alkylidene center remain essentially localized, and thus a dipolar description, Y^+–C^-, appears most appropriate [7].

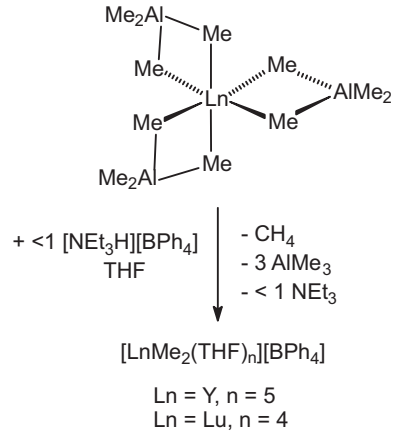

Scheme 4.

The synthesis, structure, and reactivity of two families of rare-earth metal complexes containing discrete methyl cations [LnMe$_{(2-x)}$(THF)$_n$]$^{(1+x)+}$ (x = 0, 1) have been investigated. When the tris(tetramethylaluminates) Ln(AlMe_4)$_3$ (Ln = Y, Lu) were treated with less than 1 equiv. of [NR_3H][BPh_4], the dimethyl cations [LnMe$_2$(THF)$_n$][BPh_4] were obtained (Scheme 4) [8].

Dicationic methyl complexes of the rare-earth metals of the formula [LnMe(THF)$_n$][BAr_4]$_2$ (Ln = Sc, Y, La–Nd, Sm, Gd–Lu; Ar = Ph, C_6H_4F-4) were synthesized, by protonolysis of either the "ate" complexes [Li_3LnMe$_6$(THF)$_n$] (Ln = Sc, Y, Gd–Lu) or the tris(tetramethylaluminate) Ln(AlMe_4)$_3$ (Ln = La–Nd, Sm, Dy, Gd) with ammonium borates [NR_3H][BAr_4] in THF. The number of coordinated THF ligands varied from n = 5 (Ln = Sc, Tm) to n = 6 (Ln = La, Y, Sm, Dy, Ho). The configuration of representative examples was determined by X-ray diffraction studies and confirmed by density-functional theory calculations. The highly polarized bonding between the methyl group and the rare-earth metal center results in a reactivity pattern dominated by the carbanionic character and the pronounced Lewis acidity: the dicationic methyl complex [YMe(THF)$_6$]$^{2+}$ inserted benzophenone as an electrophile to give the alkoxy complex [Y(OCMePh_2)(THF)$_5$]$^{2+}$. Nucleophilic addition of a soft anion X^- (X^- = I^-, BH_4^-) led to the monocationic methyl complexes [YMe(X)(THF)$_5$]$^+$ (Scheme 5) [8].

A series of three-coordinate chromium complexes sharing the common molecular fragment "(nacnac)Cr" (nacnac$^-$ = [ArNC(^{t}Bu)]$_2$CH, Ar = 2,6-^{i}Pr$_2$C$_6$H$_3$) have been investigated. Depending on the nature of the third ligand, L^-, these complexes can adopt either distorted T-shaped or Y-shaped coordination geometries. Density functional theory calculations and molecular orbital analyses in combination with a

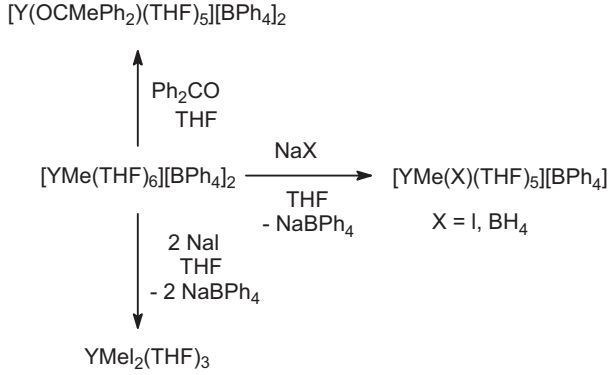

Scheme 5.

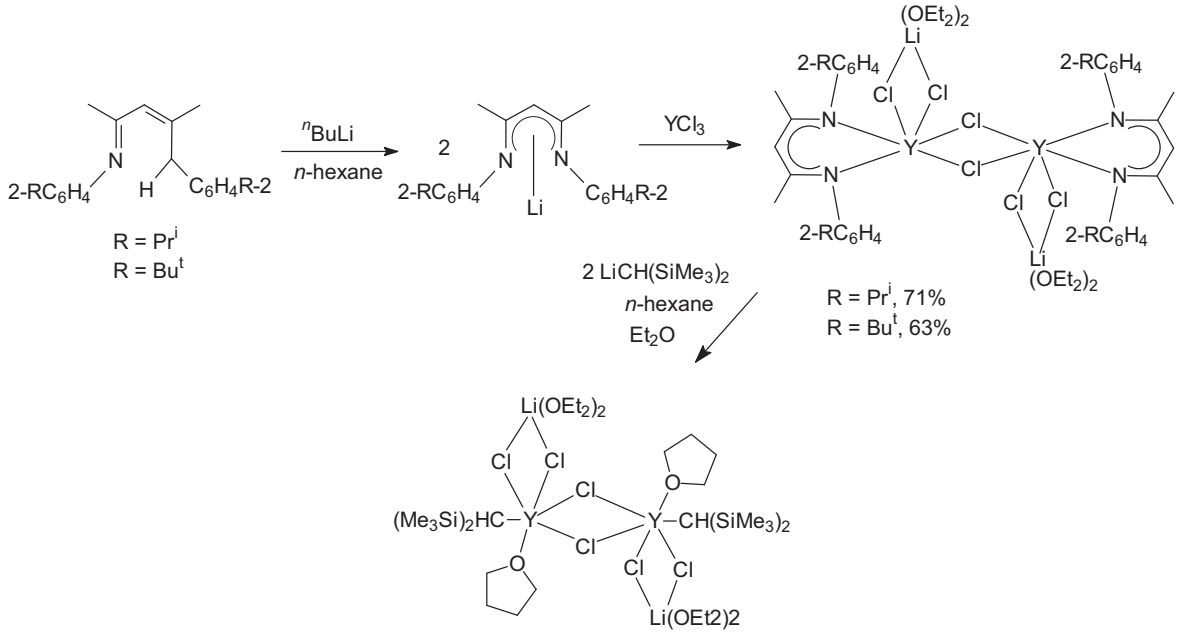

Scheme 6.

detailed molecular fragment energy decomposition were used to establish an intuitive concept of the key electronic structure patterns that determine the coordination geometry of preference. The relationship between electronics at the metal center and coordination geometry was extended to include the putative neutral three-coordinate high-spin complex of Sc(II), which was predicted to adopt the Y-shaped geometry [9]. In a related preparative investigation the synthesis and selected reactions of a series of crystalline mono(β-diiminato) yttrium chlorides have been studied (Scheme 6). A surprising result was the formation of a dimeric "ate"-complex upon treatment of a chloro precursor with $LiCH(SiMe_3)_2$ followed by recrystallization form a THF/Et_2O/*n*-hexane mixture. In the course of this unusual reaction the β-diiminato ligands are replaced by the carbanion rather than Cl^-. The product is a centrosymmetrical dimer with distorted octahedral coordination geometry around yttrium [10].

A mono(alkyl) yttrium complex stabilized by a bulky chelating ethylenediamido ligand was synthesized according to Scheme 7 and isolated in the form of orange crystals. Apparently only the 2,6-diisopropylphenyl substituent introduces sufficient steric shielding to stabilize the yttrium alkyl compound well enough to allow isolation and spectroscopic characterization. Analogous chelates containing a Lu(III) center or the less bulky mesityl or phenyl substituents decomposed rapidly, as observed frequently for alkyl complexes of rare-earth metal cations [11].

Reaction of anhydrous YCl_3 with 1 equiv. of the arylamido lithium reagent 2,6-^{i}Pr$_2$C$_6$H$_3$NSi^{i}Pr$_3$Li gave an anionic mono-arylamido-ligated yttrium dichloride complex {[2,6-^{i}Pr$_2$C$_6$H$_3$NSi^{i}Pr$_3$]YCl$_2$(THF)}$_2$[LiCl(THF)$_2$], which with 4 equiv. of $LiCH_2SiMe_3$ afforded an anionic arylamido-ligated yttrium tris(alkyl) complex [2,6-^{i}Pr$_2$C$_6$H$_3$NSi^{i}Pr$_3$]Y(CH$_2$SiMe$_3$)$_3$Li(THF)$_2$ (Scheme 8). Both complexes were characterized by NMR, elementary analysis, and X-ray structural determination [12].

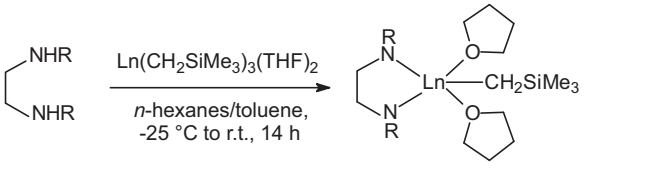

Scheme 7.

The synthesis, DFT studies, and reactions of scandium and yttrium dialkyl cations containing neutral *fac*-N_3 and *fac*-S_3 donor ligands have been reported. Reaction of Sc(CH$_2$SiMe$_3$)$_3$(THF)$_2$ with 1,4,7-trithiacyclononane gave Sc([9]aneS$_3$)(CH$_2$SiMe$_3$)$_3$, the first organometallic group 3 complex of [9]aneS$_3$ ([9]aneS$_3$ = 1,4,7-trithiacyclononane). The corresponding reaction for yttrium gave equilibrium mixtures of Y([9]aneS$_3$)(CH$_2$SiMe$_3$)$_3$ and starting materials (Scheme 9) [13].

Density functional theory (DFT) was used to compare the energies of formation and metal–ligand interaction energies for M([9]aneS$_3$)R$_3$ with those for the previously reported *fac*-N_3 donor complexes M(*fac*-N$_3$)R$_3$ (R = Me or CH$_2$SiMe$_3$; *fac*-N$_3$ = 1,4,7-trimethyltriazacyclononane (Me$_3$[9]aneN$_3$) or HC(Me$_2$pz)$_3$). Reaction of M(CH$_2$SiMe$_3$)$_3$(THF)$_2$ with [NHMe$_2$Ph][BAr$^F_4$] (Ar^F = C$_6$F$_5$) in the presence of a face-capping ligand L (L = HC(Me$_2$pz)$_3$, Me$_3$[9]aneN$_3$, or [9]aneS$_3$) gave the cationic complexes [M(L)(CH$_2$SiMe$_3$)$_2$(THF)]$^+$ (Scheme 10), which have been structurally characterized for M = Sc and L = [9]aneS$_3$ [13].

The corresponding base-free cations [M(L)(CH$_2$SiMe$_3$)$_2$]$^+$ were studied by ^{29}Si NMR spectroscopy and/or DFT and found to possess *β*-Si–C agostic alkyl groups in most instances. The isolated cations [Sc(*fac*-N$_3$)(CH$_2$SiMe$_3$)$_2$(THF)]$^+$ underwent THF substitution reactions with $OPPh_3$ or pyridine, Sc-alkyl migratory insertion with carbodiimides, and C–H bond metathesis with PhC≡CH [13]. Rare-earth metal alkyl and hydride complexes stabilized by a cyclen-derived [NNNN] macrocyclic ancillary ligand, 1,4,7-trimethyl-1,4,7,10-tetraazacyclododecane (=Me$_3$TACDH), have been reported. Reactions of the tris(alkyl) complexes Ln(CH$_2$SiMe$_3$)$_3$(THF)$_2$ with an equimolar amount of Me$_3$TACDH in pentane afforded the corresponding dialkyl complexes (Me$_3$TACD)Ln(CH$_2$SiMe$_3$)$_2$ (Ln = Y, Ho, Lu) in moderate to good isolated yields with concomitant formation of tetramethylsilane (Scheme 11) [14].

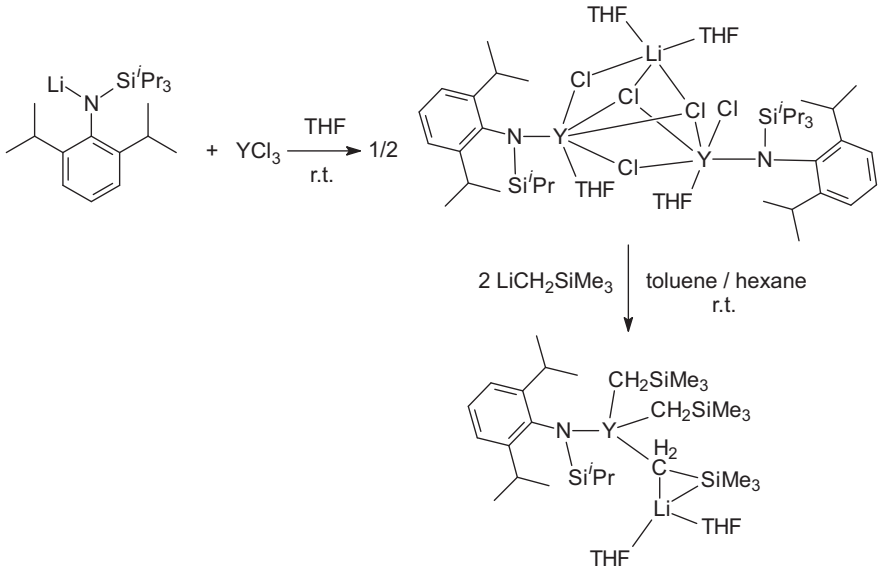

Scheme 8.

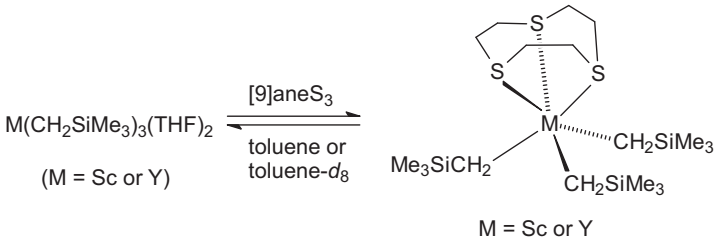

Scheme 9.

The alkyl complexes (Me$_3$TACD)Ln(CH$_2$SiMe$_3$)$_2$ (Ln = Y, Ho, Lu) were found to react with dihydrogen or PhSiH$_3$ at room temperature to give the dihydride complexes [Ln(Me$_3$TACD)H$_2$]$_3$ (Ln = Y, Ho, Lu) which were isolated in 65–75% yields (Scheme 11). In the ^{1}H NMR spectrum of the yttrium and lutetium complexes, the hydride resonance was recorded at δ 6.37 (m) and 9.81 (s) ppm, respectively. The X-ray diffraction study of [Y(Me$_3$TACD)H$_2$]$_3$ revealed a trinuclear structure with an interatomic Y–Y distance of 3.5164(9) Å. The compound represents a rare example for trinuclear lanthanide hydrides, and its structure was well reproduced using DFT methods. A slightly longer Y–Y distance of 3.55 Å and six almost equivalent Y–H bonds (2.19 and 2.23 Å) were calculated. An NBO analysis of the density indicated that the cohesion of the structure is due to the Y–H bonds. At the second order perturbation theory, Y–Y interactions were found (50 kcal mol^{-1}), accounting for the increase in stability of [Y(Me$_3$TACD)H$_2$]$_3$. The calculated ^{1}H NMR chemical shift of δ 6.15 ppm is also in good agreement with the experiment. Each eight-coordinate yttrium center bonded to four nitrogen atoms of the Me$_3$TACD ligand and four bridging hydrides adopts a square antiprism coordination geometry. The three vectors joining the amide nitrogen with the opposite amine in each mononuclear unit are arranged in a head-to-tail fashion to form a regular triangle, most likely due to reduction of the steric hindrance between the adjacent NMe groups on the TACD macrocycles. The hydride [Y(Me$_3$TACD)H$_2$]$_3$ was obtained as a single isomer. This is consistent with the ^{1}H and ^{13}C NMR spectra, indicating a set of eight and four signals, respectively, attributable to only one kind of the TACD ring [14]. Within the course of a related investigation a new neutral tridentate 1,4,6-trimethyl-6-pyrrolidin-1-yl-1,4-diazepane (=L) was prepared. Reaction of L with the trialkyls M(CH$_2$SiMe$_3$)$_3$(THF)$_2$ (M = Sc, Y) and tribenzyls M(CH$_2$Ph)$_3$(THF)$_3$ (M = Sc, La) yielded trialkyl complexes (L)M(CH$_2$SiMe$_3$)$_3$ (M = Sc, Y) and tribenzyl complexes (L)M(CH$_2$Ph)$_3$ (M = Sc, La) (Scheme 12) [15].

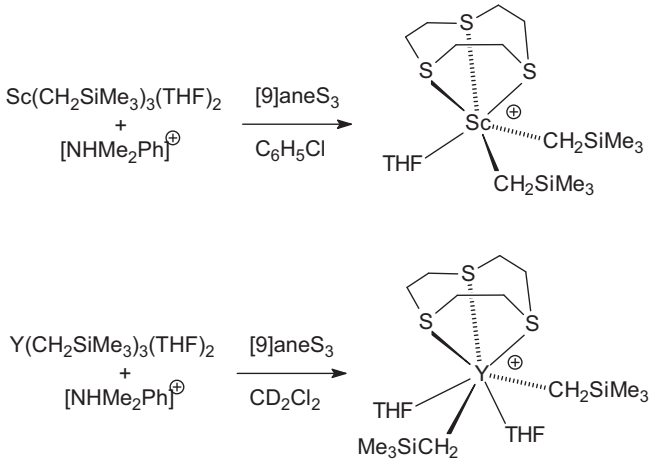

Scheme 10.

New benzyl complexes have also been prepared with scandium and lutetium. Reaction of ScCl$_3$(THF)$_3$ with benzyl potassium afforded Sc(CH$_2$Ph)$_3$(THF)$_3$. In the solid state the coordination polyhedron is a distorted octahedron, in which the benzyl groups are located in a facial arrangement on one side of the molecule. One of the coordinated THF molecules could be removed by trituration with toluene and recrystallization of Sc(CH$_2$Ph)$_3$(THF)$_3$ from toluene to give Sc(CH$_2$Ph)$_3$(THF) (Scheme 13) [16].

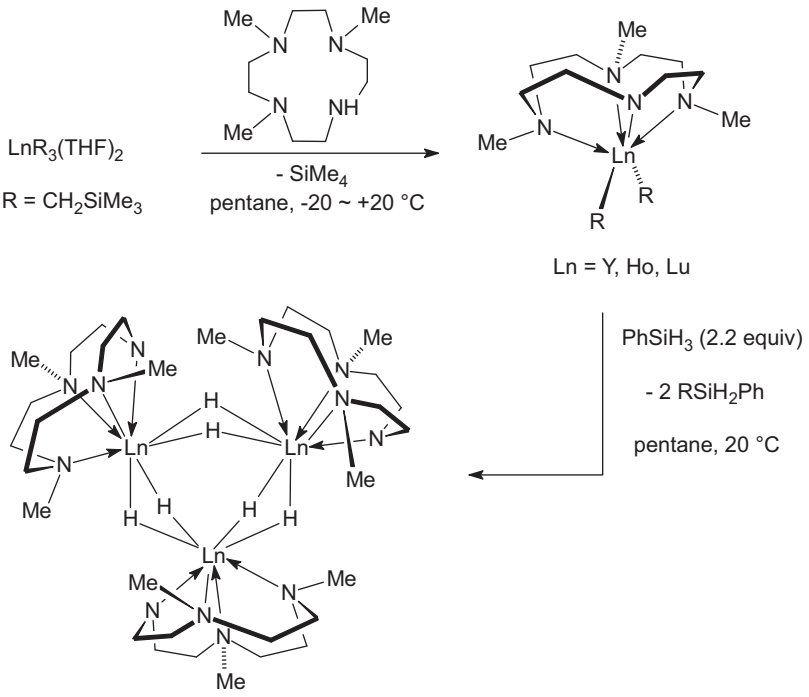

Scheme 11.

A significantly different compound was obtained by starting the transmetalation reaction at −196 °C. Under these conditions the reaction of $ScCl_3$ with KCH_2Ph led to a two-dimensional coordination polymer of the composition $[Sc(CH_2Ph)_5K_2(THF)_3]_n$, in which the scandium atom is surrounded by five benzyl groups in a trigonal bipyramidal fashion (Scheme 14). Under the same reaction conditions, but using $LuCl_3$ as the starting material, the analogue of the scandium tribenzyl complex, $Lu(CH_2Ph)_3(THF)_3$ (Scheme 13), was obtained, which can also be induced to lose a coordinated THF ligand to give $Lu(CH_2Ph)_3(THF)_2$ [16].

In a similar manner, the isolation of $Sc(CH_2Xy\text{-}3,5)_3(THF)_2$ (Scheme 15) was achieved, and the desired compound could be purified by recrystallization from toluene/hexanes. The yield of the pure product was consistently 60% [17].

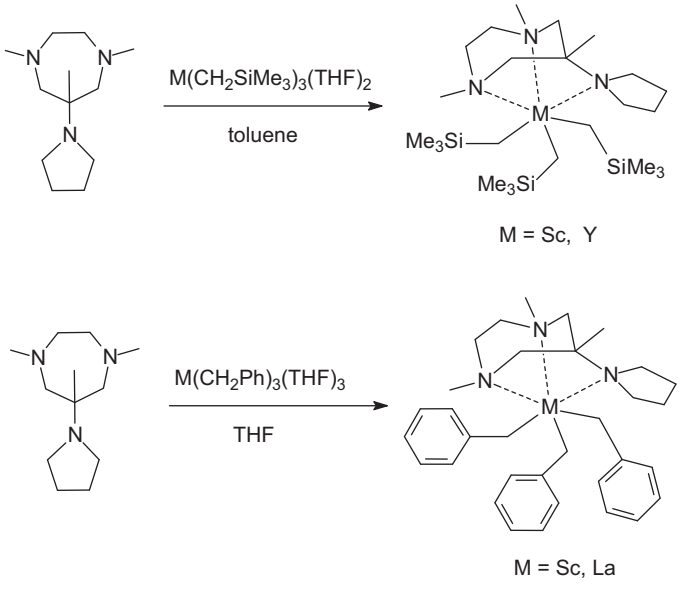

Scheme 12.

In a comparative study, strategies for the synthesis of lanthanum dialkyl complexes with monoanionic ancillary ligands have been evaluated. The synthesis of such lanthanum dialkyl complexes with monoanionic ancillary ligands $[L]^-$ was pursued by three different strategies: (a) *in situ* peralkylation of $LaBr_3(THF)_4$ with 3 equiv. of $LiCH_2SiMe_3$ followed by reaction with LH (Scheme 16); (b) reaction of isolated $La(CH_2Ph)_3(THF)_3$ with LH (Scheme 17); (c) stepwise salt metathesis on $LaBr_3(THF)_4$. Methods (a) and (b) generally work well for triazacyclononane-amide and amidinate ligands, but are unsuitable for the sterically demanding β-diketiminate $[HC(MeCNAr)_2]^-$ (Ar = 2,6-^{i}Pr$_2$C$_6$H$_3$) due to its high affinity for the Li cation and the sluggish reactivity of the diketimine [18].

Nevertheless, the β-diketiminate lanthanum dibenzyl complex $[HC(MeCNAr)_2]La(CH_2Ph)_2(THF)$ could be obtained by first reacting $LaBr_3(THF)_4$ with $K[HC(MeCNAr)_2]$ to form $[HC(MeCNAr)_2]LaBr_2(THF)_2$ and subsequent reaction of this dibromide complex with 2 equiv. of $PhCH_2K$ (Scheme 18). When this reaction mixture is warmed, the product decomposes by H-abstraction from one of the diketiminate methyl groups and ligand redistribution, forming the coordination polymer $[\{\mu\text{-}\eta^2\text{:}\eta^1\text{-ArNC(Me)CHC(CH}_2\text{)NAr}\}_2La\{K(THF)_4\}]_\infty$ [18].

The complexes $(L)M(CH_2SiMe_3)_3$ (M = Sc, Y) could be converted to their corresponding ionic compounds $[(L)M(CH_2SiMe_3)_2(THF)][B(C_6H_5)_4]$ (M = Sc, Y) by reaction with $[PhNMe_2H][B(C_6H_5)_4]$ in THF, while the complexes $(L)M(CH_2Ph)_3$ (M = Sc, La) could be converted to cationic species $[(L)M(CH_2Ph)_2]^+$ by reaction with $[PhNMe_2H][B(C_6F_5)_4]$ in C_6D_5Br in the absence of THF (Scheme 19) [15].

In a related study, a mono(amidinato) yttrium dialkyl complex was synthesized and characterized. Treatment of the tris(aminobenzyl)yttrium complex $Y(o\text{-}CH_2C_6H_4NMe_2)_3$ with 1 equiv. of the amidine ligand *N,N′*-bis(2,6-diisopropylphenyl)benzamidine (=NCNdippH) in THF or toluene afforded the corresponding mono(amidinate) bis(aminobenzyl) complex in 85% yield (Scheme 20). The complex was fully characterized by NMR spectroscopy, elemental analysis, and X-ray crystallography. The NCNdipp unit is bonded to the Y center through its two N atoms, as observed in other amidinate com-

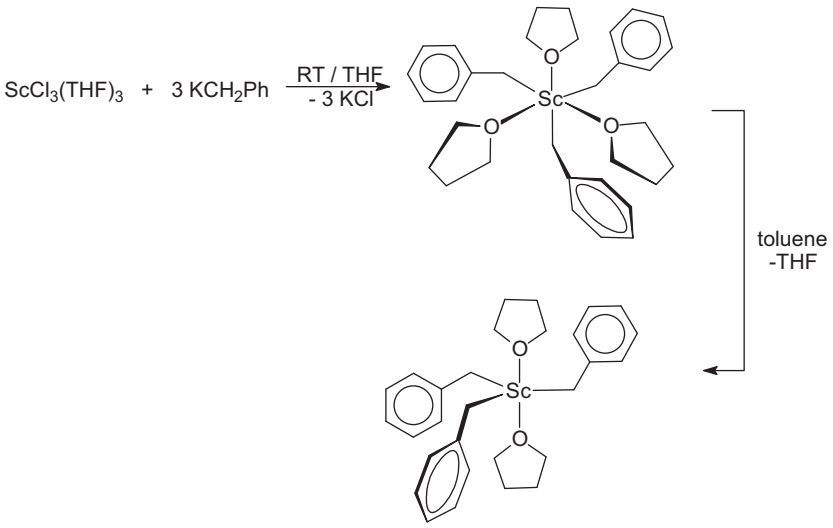

Scheme 13.

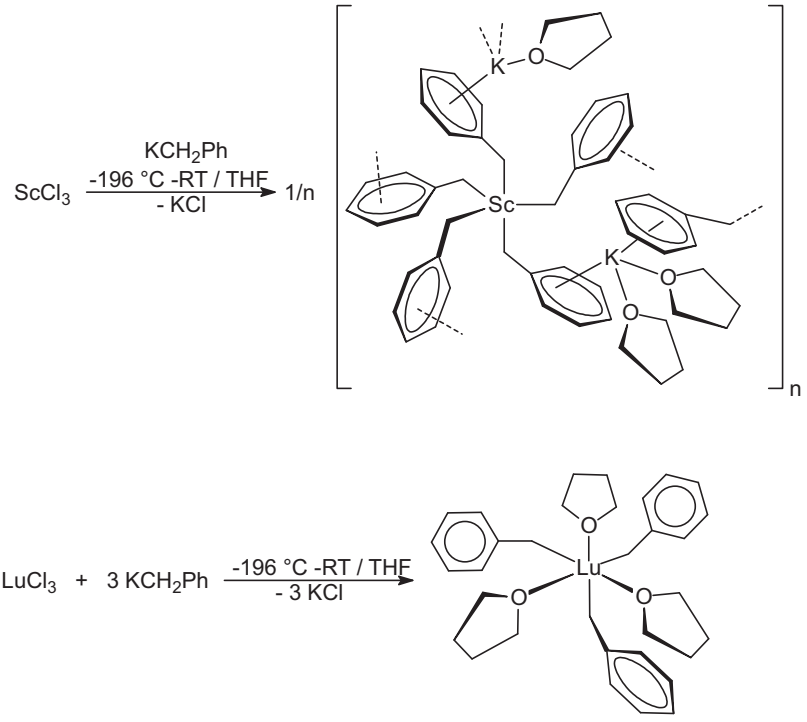

Scheme 14.

plexes. The two aminobenzyl groups are bonded to the Y atom in a chelating fashion through both the N atom and the benzyl carbon atom. Intramolecular coordination of the amino group means that the complex does not possess a THF co-ligand, in contrast with the THF-containing CH_2SiMe_3 analogue (NCNdipp)Y(CH_2SiMe_3)$_2$(THF) [19].

4,4′-Di-*tert*-butyl-2,2′-bipyridyl (^{t}Bu$_2$bpy) was found to stabilize the thermally sensitive Lu(CH_2SiMe_3)$_3$ unit, giving the isolable lutetium(III) (trimethylsilyl)methyl complex (^{t}Bu$_2$bpy)Lu(CH_2SiMe_3)$_3$ as an orange solid in 83% yield (Scheme 21) [20].

This tris(alkyl) complex does not undergo alkane elimination, and it readily reacts with Ph_3COH, H_2N-2,6-^{i}Pr$_2$C$_6$H$_3$, H_2N-2,4,6-^{t}Bu$_3$C$_6$H$_2$, and *N*,*N*′-dicyclohexylcarbodiimide (DCHCDI) to afford a variety of Lu(III) tris(alkoxide), tris(amide), mono(amide) bis(alkyl), and amidinate bis(alkyl) compounds. These reactions are summarized in Scheme 22 [20].

Reaction of the amide bis(alkyl) complex (^{t}Bu$_2$bpy)Lu(NH-2,4,6-^{t}Bu$_3$C$_6$H$_2$)(CH_2SiMe_3)$_2$ with triphenylphosphine oxide according to Scheme 23 afforded ($Ph_3P{=}O$)$_2$Lu(NH-2,4,6-^{t}Bu$_3$C$_6$H$_2$)(CH_2SiMe_3)$_2$, showing that the bidentate ^{t}Bu$_2$bpy ligand can be displaced [20].

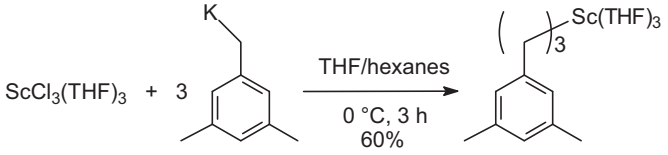

Scheme 15.

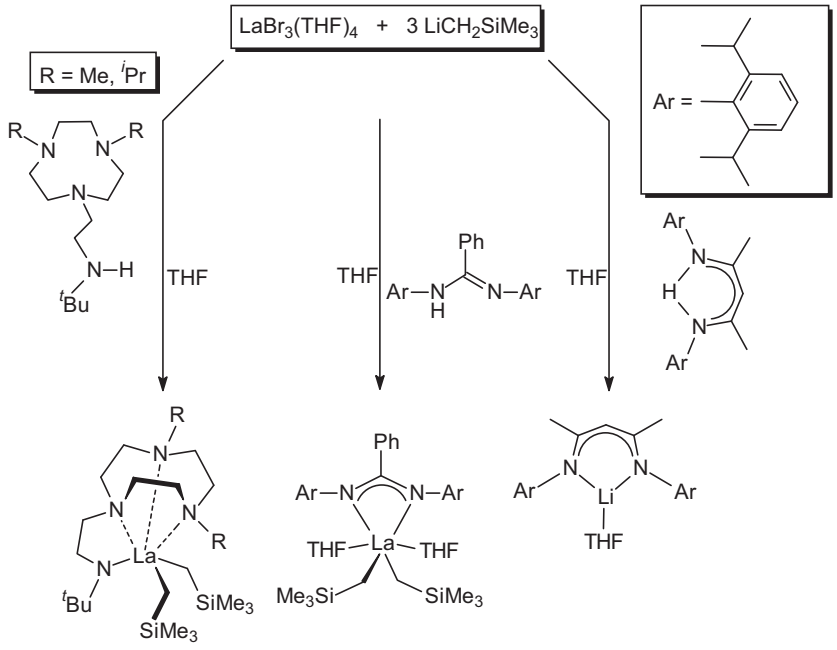

Scheme 16.

Lutetium alkyl complexes supported by a monoanionic, tridentate ligand system formed by the dearomatization and functionalization of a 2,2′:6′,2″-terpyridine have been treated with 2,4,6-triphenylaniline or the fluorinated anilines 4-$FC_6H_4NH_2$ and $C_6F_5NH_2$ to give both terminal mono(amide) and bis(amide) lutetium(III) complexes (Scheme 24), which have been fully characterized. The product [^{t}Bu$_3$(2′-Me$_3$SiCH$_2$)tpy]Lu[NH(2,4,6-Ph$_3$C$_6$H$_2$)]$_2$ has been structurally characterized. Heating either product (benzene-d_6, 60 °C, 20 days or toluene-d_8, 75 °C, 1 day) did not result in the formation of a lutetium-imido species as monitored by ^{1}H NMR spectroscopy; higher temperatures afforded intractable materials [21].

Three new tridentate NNN ligand precursors, CH_3C(2,6-^{i}Pr$_2$C$_6$H$_3$NH)CHC(CH$_3$)(NCH$_2$CH$_2$-D) (D = NMe$_2$, NEt$_2$, N((CH$_2$CH$_2$)$_2$CH$_2$)), were synthesized. Subsequent metalations with *in situ* generated Ln(CH$_2$SiMe$_3$)$_3$(THF)$_n$ (Ln = Nd, Sm, Y, Lu) provided six solvent-free dialkyllanthanide complexes (Scheme 25). Five of the new complexes were characterized by single-crystal X-ray diffraction, which showed that the pendant arm D bonds to the lanthanide ion in the solid state. The NMR

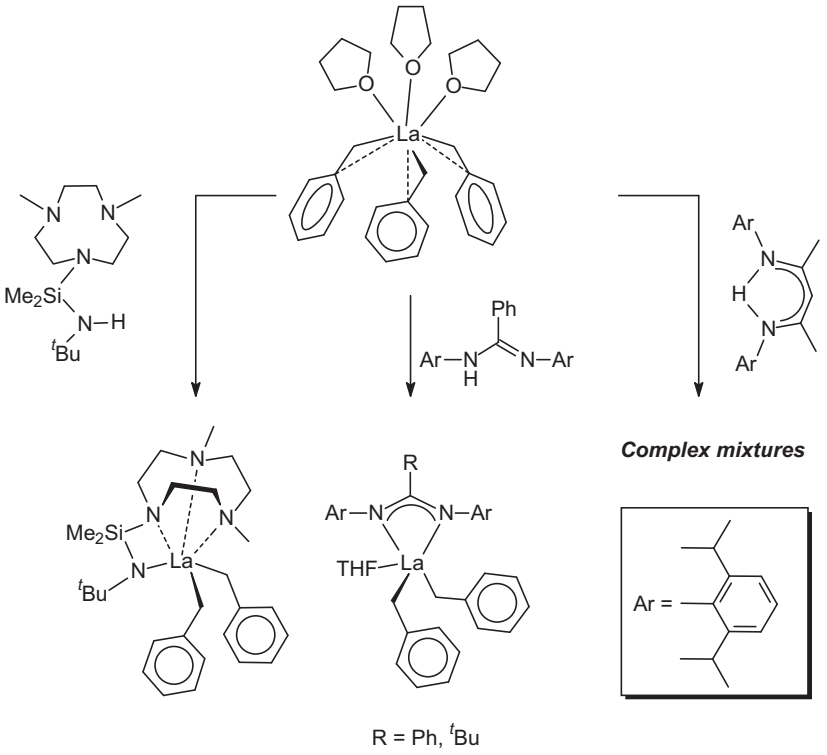

Scheme 17.

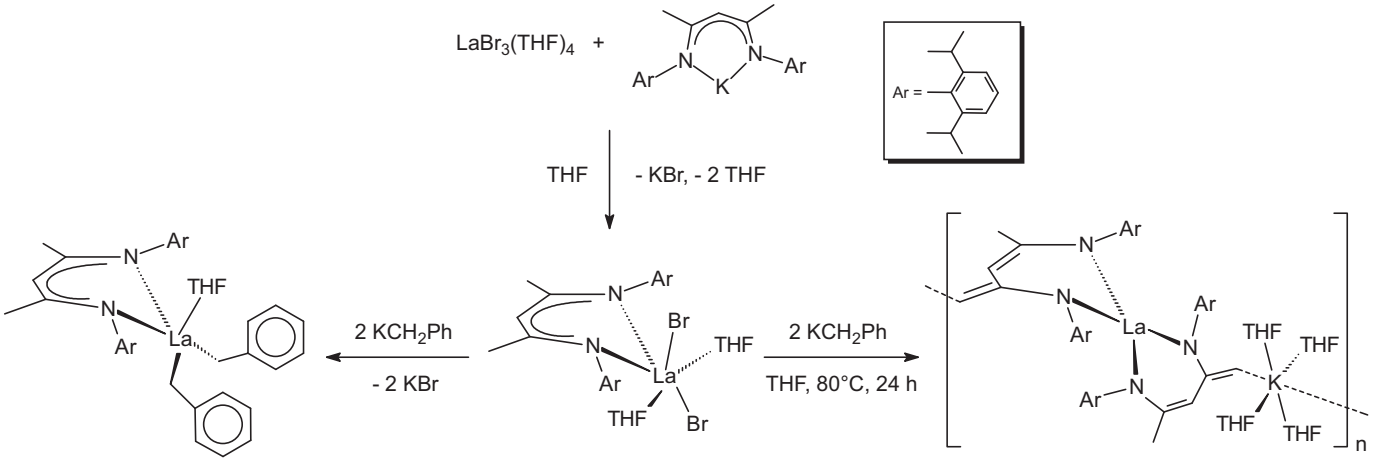

Scheme 18.

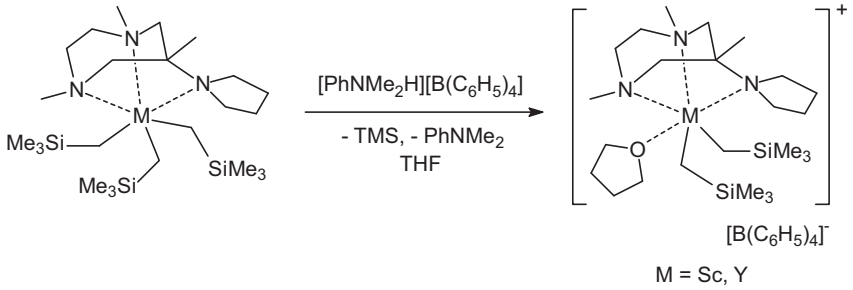

Scheme 19.

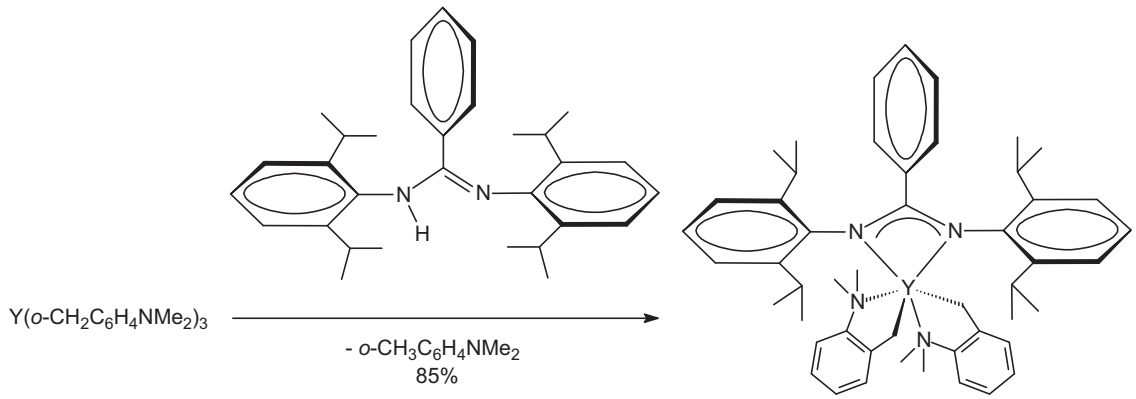

Scheme 20.

spectra of these complexes in C_6D_6 showed that such coordination is retained in solution [22].

A series of new thiophene–NPN ligand supported rare-earth metal bis(alkyl) complexes have been prepared by the reaction of rare-earth metal tris(alkyl)s with the corresponding HL^{1-4} ligands *via* alkane elimination. The synthetic routes are outlined in Schemes 26 and 27. With one exception all these complexes are monomeric with a coordinating THF molecule. Each metal ion is coordinated by a NPN ligand, two *trans*-located alkyl groups, and a THF molecule, forming a distorted trigonal-bipyramidal geometry. Only the scandium derivative of HL^3 is THF-free, adopting a distorted tetrahedron geometry [23].

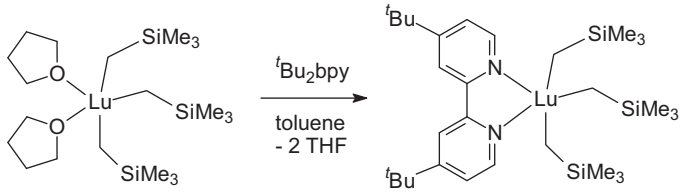

Scheme 21.

In a related study the synthesis and thermal behavior of dimethyl scandium complexes featuring anilido-phosphinimine ancillary ligands have been investigated. In the course of this work a family of *N*,*N*-donor ligands [1-(NHAr)-2-(PR_2 = NAr')C_6H_4] (Ar = 2,6-^{i}Pr$_2$C$_6$H$_3$, R = Me, Ph; Ar′ = 2,4,6-Me$_3$C$_6$H$_2$, 2-^{i}PrC$_6$H$_4$, 2,6-^{i}Pr$_2$C$_6$H$_3$) has been prepared and fully characterized by multinuclear NMR spectroscopy and X-ray crystallography. Lithiation of the N–H unit and subsequent salt metathesis protocols with $ScCl_3THF_3$ provided an avenue to organometallic scandium complexes. The resultant base-free monomeric dichlorides, $LScCl_2$,

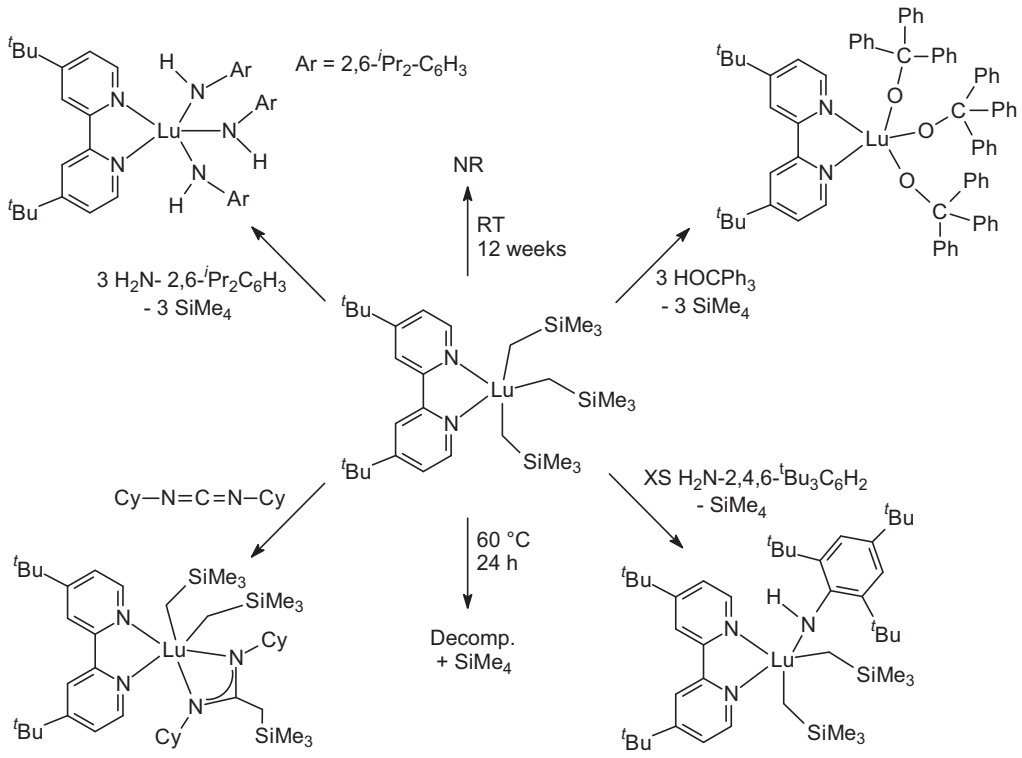

Scheme 22.

have been fully characterized by NMR spectroscopy as well as X-ray crystallography. Alkylation of the dichlorides using MeLi resulted in clean formation of dialkyl complexes $LScMe_2$ (Scheme 28) [24].

Thermolysis of these materials under argon and hydrogen led to monomeric or dimeric decomposition products as a result of C–H activation of the ligand. Analysis of these results provides a qualitative assessment of the metalative resistance of each ligand framework. In one case, an interesting dimeric product resulting from C–H activation has been obtained upon reaction with H_2. Typical thermolysis and hydrogenation reactions are summarized in Scheme 29 [24].

New rare-earth metal bis(alkyl)s bearing an iminophosphonamido ligand have been prepared according to Scheme 30 *via* protonolysis reaction between rare earth metal tris(alkyl)s and the corresponding iminophosphonamines. The products are analogous monomers of THF solvates. Each metal ion coordinates to an η^2-chelated NPN ligand and two *cis*-located alkyl groups, adopting tetrahedral geometry [25].

A PNP pincer ligand set has been successfully employed to synthesize a unique dimeric lanthanide phosphinidene complex. A key intermediate in this synthesis is a dialkyl derivative. As illustrated in Scheme 31, reaction of the PNP ligands (R = ^{i}Pr, Ph) with $Lu(CH_2SiMe_3)_3(THF)_2$ at room temperature in pentane and toluene, respectively, gave the corresponding lutetium bis(alkyl) complexes as yellow solids in good isolated yield. The crystal structure determination of the compound with R = ^{i}Pr revealed a distorted square pyramidal geometry about the Lu(III) metal center with one alkyl group in the apical position and the PNP^{i}Pr ligand and the other alkyl group forming the pyramid base. As shown in Scheme 31, reaction of a toluene solution of the PNP^{i}Pr compound with 1 equiv. of $MesPH_2$ (Mes = 2,4,6-$Me_3C_6H_2$) at 80 °C for 12 h afforded the novel Lu(III) phosphinidene complex as a cherry red solid in 52% isolated yield [26].

The tridentate ligand *N*-[2-{(2,6-diisopropylphenylimino) methyl}phenyl]quinolin-8-amine (HL) was prepared and employed in organolanthanide chemistry. Treatment of HL with 1 equiv. of $Ln(CH_2SiMe_3)_3(THF)_2$ afforded the corresponding rare-earth metal bis(alkyl) complexes $LLn(CH_2SiMe_3)_2(THF)_n$ (Ln = Sc, n = 0; Y, n = 1; Lu, n = 0) in high yields (Scheme 32). Variable-temperature ^{1}H NMR spectral analysis showed that these complexes are fluxional at room temperature. The Sc and Lu complexes were found to be THF-free, where the metal center adopts a square-pyramidal geometry, while in the Y derivative the metal center generated a distorted octahedral geometry owing to the coordination of a THF molecule [27].

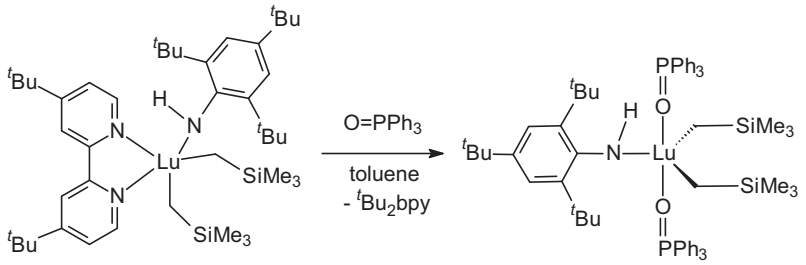

Scheme 23.

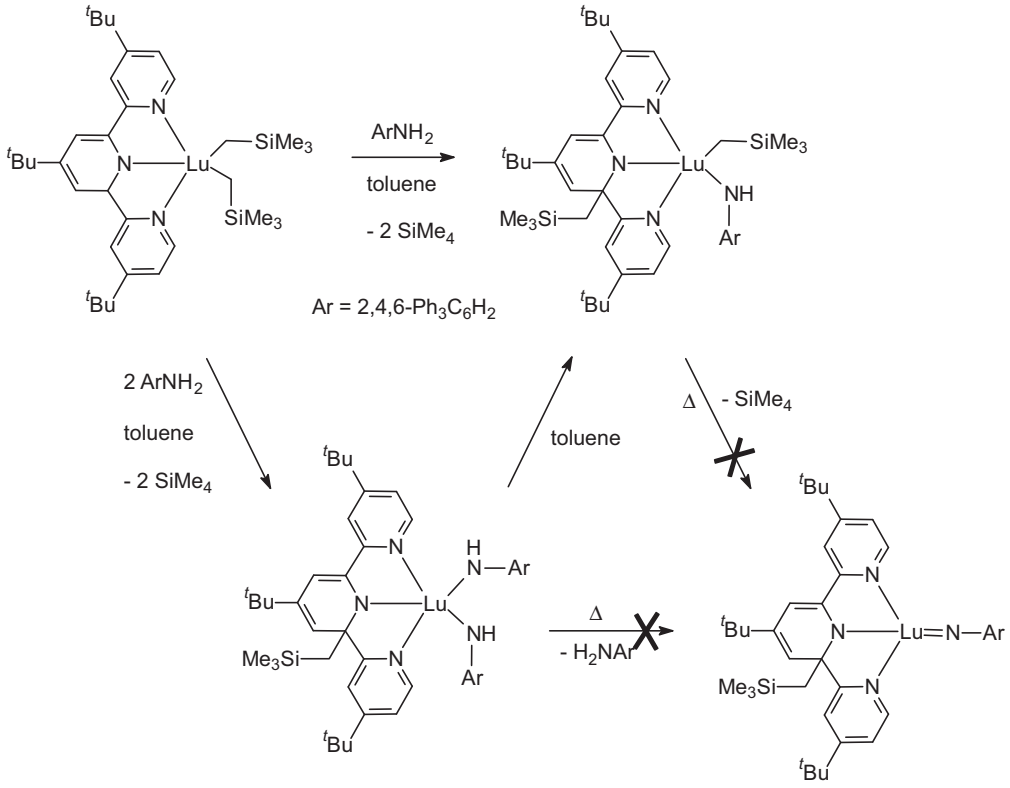

Scheme 24.

O_2 activation and hydrolysis of Salan rare-earth metal alkyl complexes have been reported. A Salan-ligated yttrium alkyl complex, $L_1Y(CH_2SiMe_3)(THF)$ (Salan = L^1: [2-O-3,5-$^tBu_2C_6H_2CH_2N(CH_3)CH_2]_2$), was exposed to an oxygen/nitrogen atmosphere to give a bimetallic alkoxide complex, $[L^1Y(\mu\text{-}OCH_2SiMe_3)]_2$ (Scheme 33) [28].

In contrast, the lutetium counterparts $L^1Lu(CH_2SiMe_3)(THF)$ and $L^2Lu(CH_2SiMe_3)(THF)$ (L^2: [2-O-3-$^tBuC_6H_2CH_2N(CH_3)CH_2]_2$) were hydrolyzed with moist nitrogen to afford the mixed hydroxy/silyloxy complexes $[L^{1,2}Lu(\mu\text{-}OSiMe_3)(\mu\text{-}OH)LuL^{1,2}]$ (Scheme 34) [28].

In a related study, the thioether-functionalized bis(phenolato) ligands shown in Scheme 35 have been employed to stabilize rare-earth metal alkyl and hydrido complexes [29].

Rare-earth metal alkyl complexes with the tridentate [OSO]-type and tetradentate [OSSO]-type bis(phenolato) ligands, $(L)Ln(CH_2SiMe_3)(THF)_n$ (LH_2 = 2,2′-thio-bis(6-*tert*-butyl-4-methylphenol) ($tbmpH_2$), 1,3-dithiapropanediyl-bis (6-*tert*-butyl-4-methylphenol) ($mtbmpH_2$), 1,4-dithiabutanediyl-bis(6-*tert*-butyl-4-methylphenol) ($etbmpH_2$); Ln = Y, Sc, Lu, Ho), were synthesized from the reactions of the tris(alkyl) complexes $Ln(CH_2SiMe_3)_3(THF)_2$ with the corresponding bis(phenol) *via* alkane elimination as illustrated in Scheme 36. The alkyl complexes were characterized by NMR spectroscopy (Y, Sc, Lu) and elemental analysis as well as by X-ray crystal structure analyses [29].

The reaction of the holmium alkyl complexes with $PhSiH_3$ resulted in the formation of the corresponding hydrido complexes $[Ho(L)(\mu\text{-}H)(THF)_n]_2$ (L = tbmp, n = 3; L = etbmp, n = 2). The formation of the yttrium analogues could be observed by NMR spectroscopy. Some of the products shown in Scheme 36 were found to be efficient catalysts for olefin hydrosilylation [29].

The first xylene-bridged bis(*N*-heterocyclic carbene) (bis(NHC))-ligated CCC-pincer rare-earth metal dibromides $(PBNHC)LnBr_2(THF)$ (PBNHC = 2,6-(2,4,6-$Me_3C_6H_2NCHCHNCCH_2)_2C_6H_3$; Ln = Sc, Lu, Sm) have been prepared by *in situ* treatment of a THF suspension of 2,6-bis(1-mesitylimidazolium methyl)-1-bromobenzene dibromides ((PBNHC-Br)·2HBr) and lanthanide trichlorides ($LnCl_3$) with dropwise addition of ^{n}BuLi at room temperature (Scheme 37). The overall molecular structure of these complexes was determined to be an isostructural monomer of a THF solvate. The monoanionic xylene-bridged bis(NHC)s bond to the central metal as a tridentate CCC-pincer moiety in a κ*C*:κ*C*:κ*C*′ mode, which, in combination with the two *trans*-located bromo units, generates a twisted tetragonal–bipyramidal geometry [30].

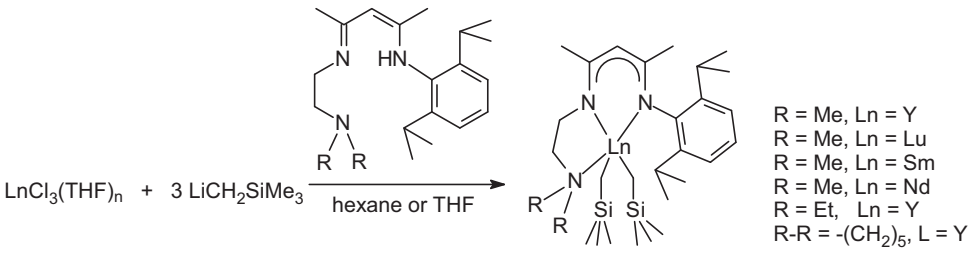

Scheme 25.

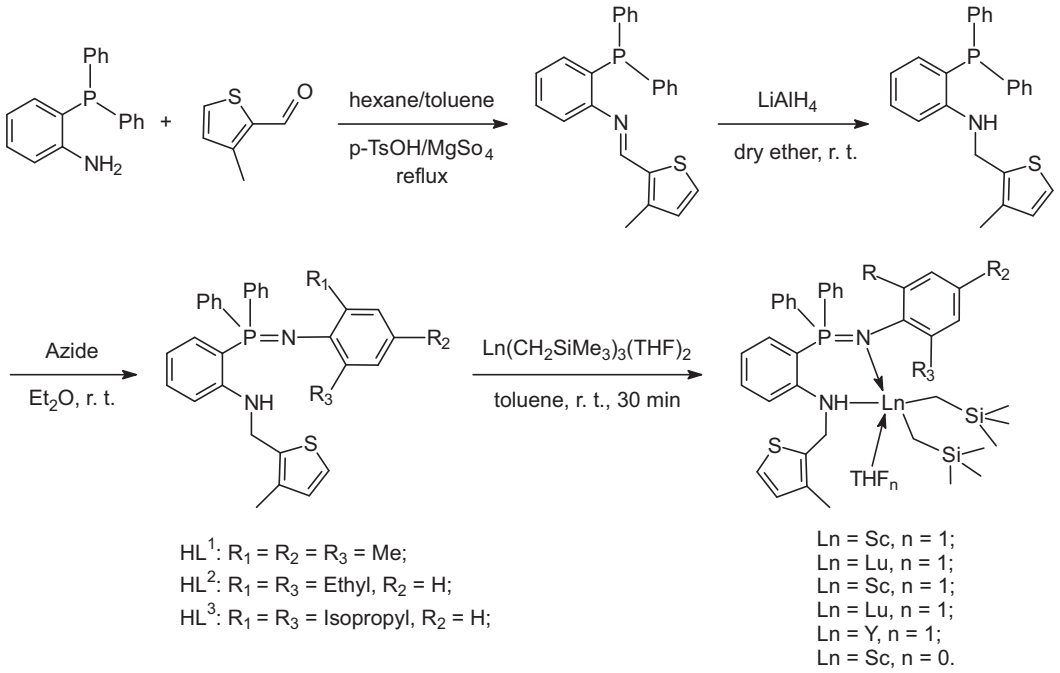

Scheme 26.

Three salicylaldiminato-functionalized *N*-heterocyclic carbene lanthanide bromides L_2LnBr (Ln = Nd, Sm, Er; L = [3,5-^{t}Bu$_2$-2-(O)C$_6$H$_2$CH = NCH$_2$CH$_2$(C{NCHCHN^{i}Pr})]) with early to late lanthanide metals were conveniently synthesized in moderate yields by a protonolysis strategy *via* the direct reaction of LiLn(N^{i}Pr$_2$)$_4$ with [H$_2$L]Br. A plausible intermediate in this reaction is the bis(amide) species shown in Scheme 38. All complexes were characterized by X-ray crystal determinations [31].

Structure–reactivity relationships of amido-pyridine-supported rare-earth metal alkyl complexes have been investigated in greater detail. Treatment of rare-earth metal dialkyl complexes with group 13 cocatalysts is a prominent approach to generate homogeneous catalysts active in olefin polymerization. Reaction of Ln(CH$_2$SiMe$_3$)$_3$(THF)$_2$ with the monovalent imino-amido-pyridine 2-{(2,6-^{i}Pr$_2$C$_6$H$_3$)N = CMe}-6-{(2,6-^{i}Pr$_2$C$_6$H$_3$)NHCMe$_2$}C$_5$H$_3$N (H**L2**) gives donor solvent-free discrete dialkyl compounds [**L2**]Ln(CH$_2$SiMe$_3$)$_2$ (Ln = Sc, Y, Lu) (Scheme 39). In the solid state the scandium derivative is isostructural to the previously reported lutetium complex [32].

Activation by borate cocatalysts [Ph$_3$C][B(C$_6$F$_5$)$_4$] and [PhNMe$_2$H][B(C$_6$F$_5$)$_4$] produces ion pairs (Scheme 40) that polymerize ethylene in moderate yields (activity: Sc > Lu). Cationization with *N*-[tris(pentafluorophenyl)borane]-3*H*-indole gives inactive species. ^{1}H/^{13}C/^{11}B/^{19}F NMR spectroscopy was applied to examine the interaction of the rare-earth metal dialkyl complexes with the boron cocatalysts. In contrast to the monoalkyl diamido-pyridine compounds [**L1**]Ln(CH$_2$SiMe$_3$)(THF)$_x$ (H**L1** = 2,6-{(2,6-^{i}Pr$_2$C$_6$H$_3$)NHCH$_2$}C$_5$H$_3$N), the dialkyl imino-amido-pyridine complexes do not polymerize methyl methacrylate [32].

Amidopyridinate ligands have also been employed for the selective assembly of trinuclear rare-earth alkyl hydrido clusters. For this purpose, bulky (2,6-diisopropylphenyl)[6-(2,4,6-triisopropylphenyl)pyridin-2-yl]amine (Ap*-H) was used as the

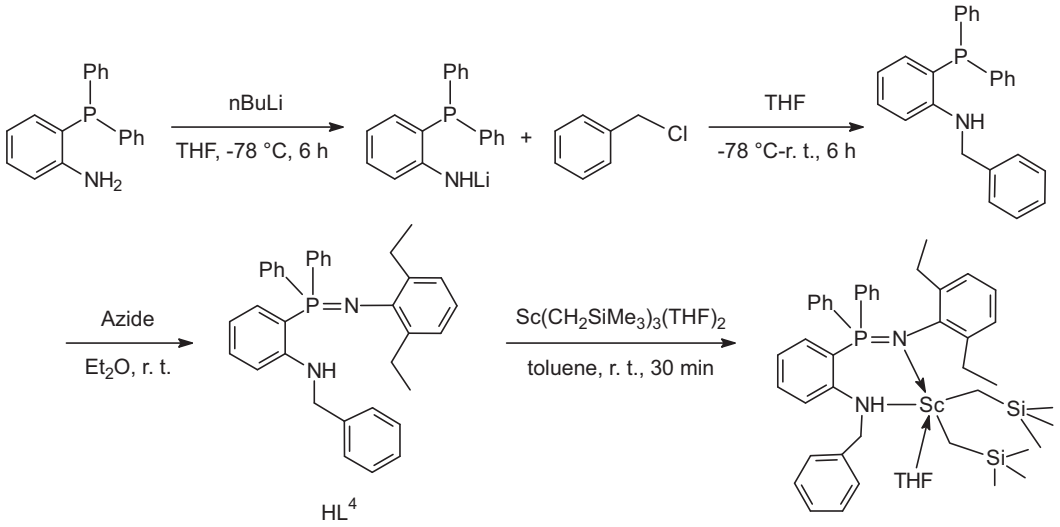

Scheme 27.

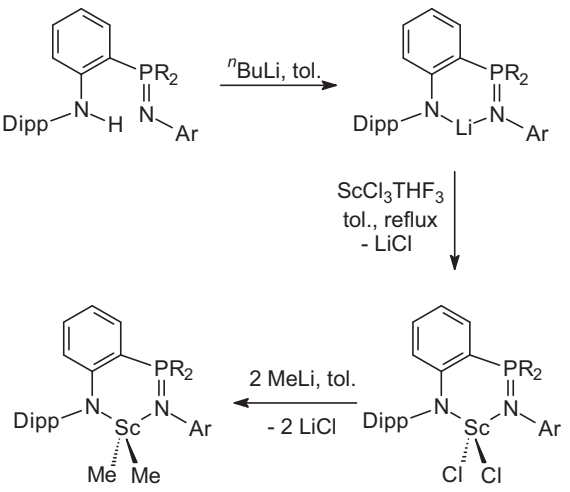

Scheme 28.

ligand precursor for the preparation of the aminopyridinato dichloride, dialkyl, and alkyl hydrido complexes of yttrium and lutetium. Reactions of anhydrous $LnCl_3$ (Ln = Y, Lu) with an equimolar amount of Ap*Li(Et_2O) in THF at 20 °C afforded the "ate" complexes Ap*LnCl(THF)(μ-Cl)$_2$Li(THF)$_2$ (Ln = Y, Lu) (Scheme 41), which were isolated after recrystallization from THF–hexane mixtures as pale yellow crystals in 78 and 85% yields, respectively. The yttrium derivative has been characterized by an X-ray diffraction study, which revealed its monomeric structure [33].

Alkylation of the "ate" complexes with 2 equiv. of $LiCH_2SiMe_3$ in hexane at 0 °C allowed the synthesis of the salt-free dialkyl complexes Ap*Ln(CH_2SiMe_3)$_2$(THF) (Ln = Y, Lu), which were obtained after recrystallization from pentane (Y) or hexane (Lu) at −20 °C in 68 and 75% yields, respectively (Scheme 42). The dialkyl complexes were also synthesized through alkane elimination from trialkyl complexes and parent aminopyridine in hexane at 0 °C [33].

Reactions of the dialkyls with both $PhSiH_3$ (1:2 molar ratio, 0 °C) and H_2 (5 atm, 15 °C, 24 h) smoothly occurred in hexane under the aforementioned conditions and resulted in the formation of the unusual trinuclear alkyl hydrido clusters (Ap*Ln)$_3$(μ_2-H)$_3$(μ_3-H)$_2$(CH_2SiMe_3)(THF)$_2$ (Ln = Y, Lu), which were isolated after recrystallization from hexane at −20 °C in 58 and 64% yields, respectively (Scheme 43). Surprisingly, all attempts to remove the remaining alkyl group and to obtain polyhydrido clusters consisting of Ap*LnH_2 units failed: the use of a 10-fold molar excess of $PhSiH_3$ or an increase in the reaction time with H_2 afforded only the same trinuclear alkyl hydrido clusters [33].

New chiral binaphthylamido alkyl "ate" and neutral yttrium and ytterbium complexes have been synthesized and characterized. X-ray structures have been obtained for the "ate" alkyl complexes [(*R*)-$C_{20}H_{12}(NC_5H_9)_2$]Y[(μ-Me)$_2$Li(THF)$_2$(μ-Me)Li(THF)] and [(*R*)-$C_{20}H_{12}(NC_5H_9)_2$]Ln[(μ-Me)$_2$Li(TMEDA)(μ-Me)Li(OEt_2)] (Ln = Y, Yb) as well as for the neutral complex [(*R*)-$C_{20}H_{12}(NC_5H_9)_2$]Y(CH_2SiMe_3)(DME). Both types of complexes could be easily prepared in a one-pot procedure according to Scheme 44 starting from yttrium and ytterbium chlorides [34].

Two complementary protocols for the synthesis of a wide range of scorpionate-supported rare-earth metal dialkyl complexes have been reported. Protonolysis of Ln(CH_2SiMe_3)$_3$(THF)$_2$ with $HTp^{tBu,Me}$ is the method of choice to obtain lanthanide(III) dialkyl complexes with the bulky $Tp^{tBu,Me}$ scorpionate (Ln = Y, Yb, Lu), whereas alkyl abstraction with thallium pyrazolylborates allows the synthesis of the full range of (Tp^{Me2})Ln(CH_2SiMe_3)$_2$(THF)

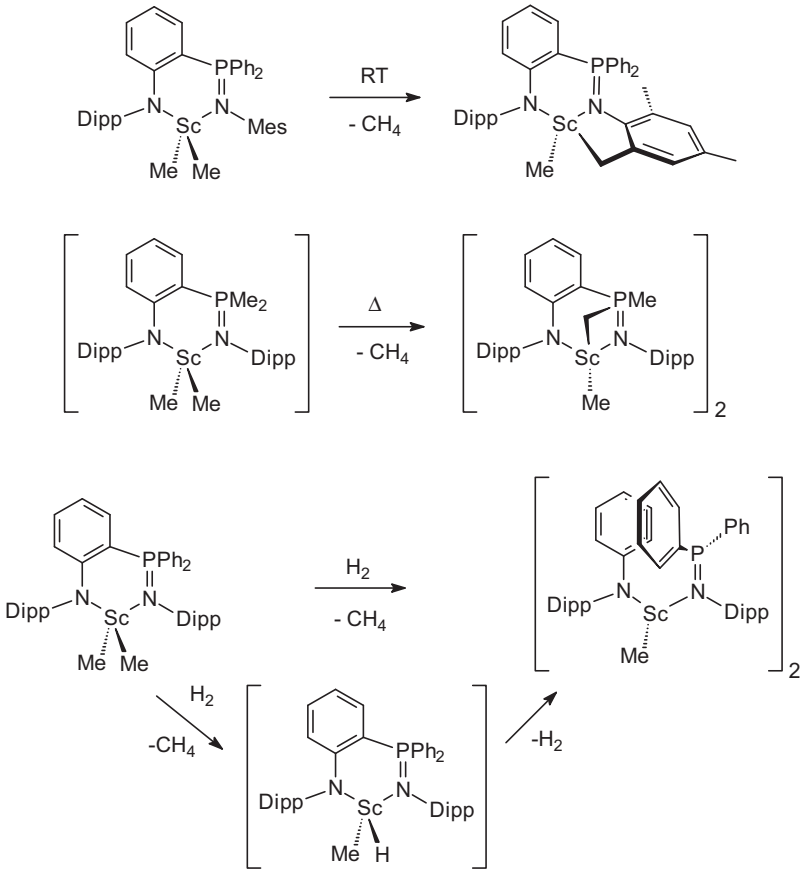

Scheme 29.

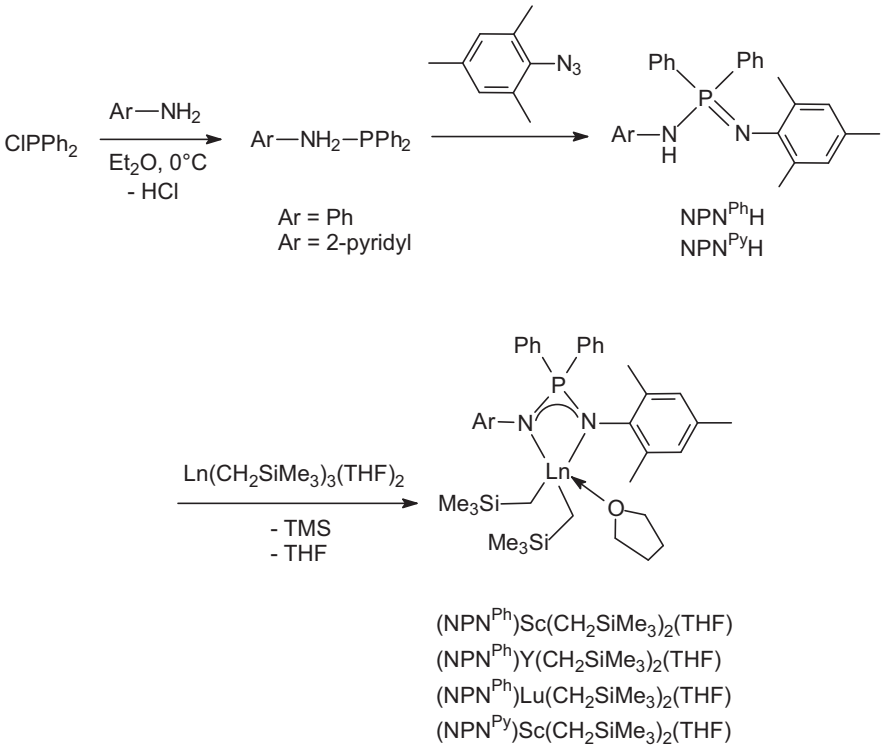

Scheme 30.

(Ln = Y, Nd, Sm, Yb, Lu) and even (Tp)Ln(CH_2SiMe_3)$_2$(THF) (Ln = Y, Yb, Lu) complexes. These synthetic pathways are summarized in Scheme 45 [35].

Hydrogenolysis of ($Tp^{R,R'}$)Ln(CH_2SiMe_3)$_2$(THF) (R = R′ = Me, H) successfully led to the isolation of the first non-cyclopentadienyl lanthanide dihydrides [($Tp^{R,R'}$)LnH_2]$_n$ (Scheme 46, n = 4). The structure of the dihydrides can be described as a polynuclear cluster framework which is maintained in solution and the nuclearity of which depends on the ligand and even the solvent used in their synthesis [35].

2.3. Lanthanide alkenyl and alkynyl compounds

Laser-ablated lanthanum atoms have been codeposited at 4 K with acetylene in excess argon. The products La(C_2H_2), $LaCCH_2$, HLaCCH, and $La_2(C_2H_2)$, have been formed in these experiments and characterized using IR spectroscopy on the basis of the results of the isotopic shifts, mixed isotopic splitting patterns, stepwise annealing, the change of reagent concentration and laser energy, and the comparison with theoretical predictions. Density functional theory calculations have also been performed on these

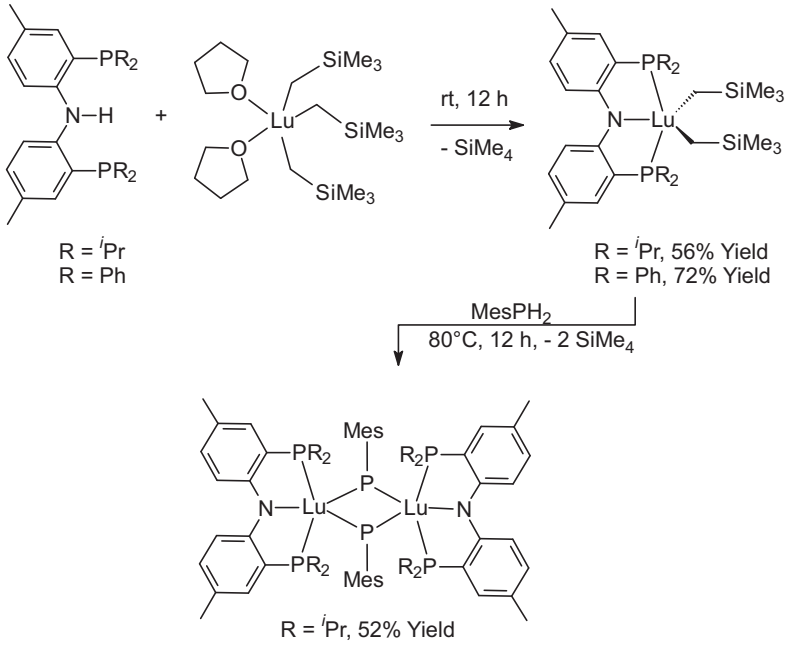

Scheme 31.

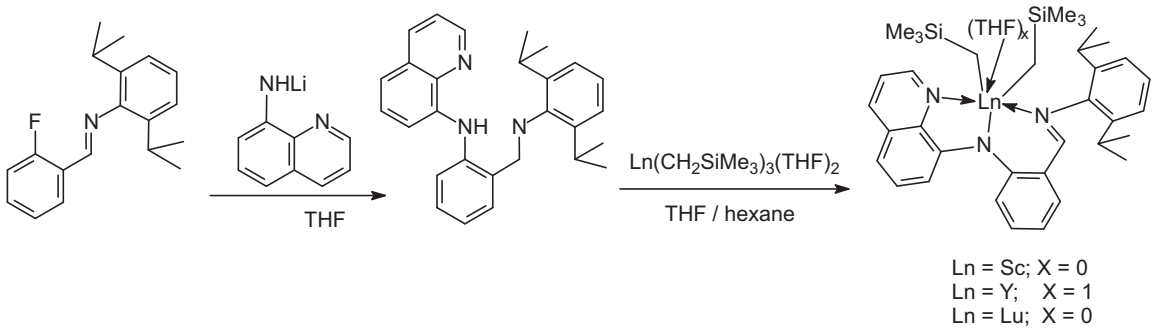

Scheme 32.

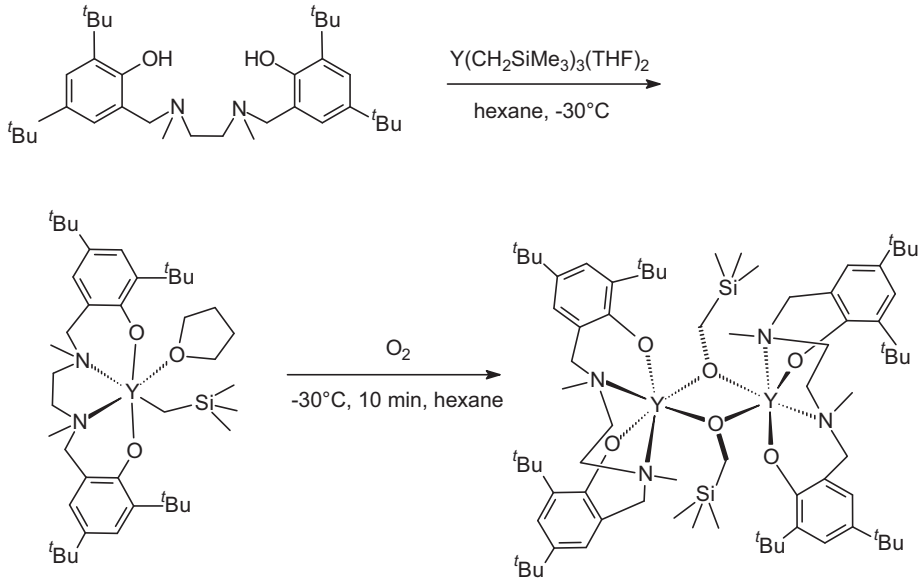

Scheme 33.

molecules. The agreement between the experimental and calculated vibrational frequencies, relative absorption intensities, and isotopic shifts supported the identification of these molecules from the matrix infrared spectra. Plausible reaction mechanisms have been proposed to account for the formation of these molecules [36].

2.4. Lanthanide cyclopentadienyl complexes

2.4.1. Cp_2Ln compounds

The redox-transmetalation ligand-exchange reaction of ytterbium metal with 2 equiv. of pentaphenylcyclopentadiene (C_5Ph_5H) and 1 equiv. of $HgPh_2$ in THF (Scheme 47) afforded the pale orange solvent-separated ion pair (SSIP) $[Yb(THF)_6][C_5Ph_5]_2$, which was characterized by single-crystal X-ray analysis [37].

Addition of toluene to the isolated SSIP led to the precipitation of the homoleptic sandwich complex $Yb(C_5Ph_5)_2$. Small amounts of dark green $Yb(C_5Ph_5)_2$ were also obtained by heating the divalent ytterbium acetylide precursor $Yb(CC^tBu)_2$ with pentaphenylcyclopentadiene in toluene at 60 °C (Scheme 48). Single-crystal X-ray analysis confirmed the highly symmetric structure of this complex with two parallel cyclopentadienyl ligands (Fig. 1). Oxidation and metal-ligand exchange reactions were also investigated for the

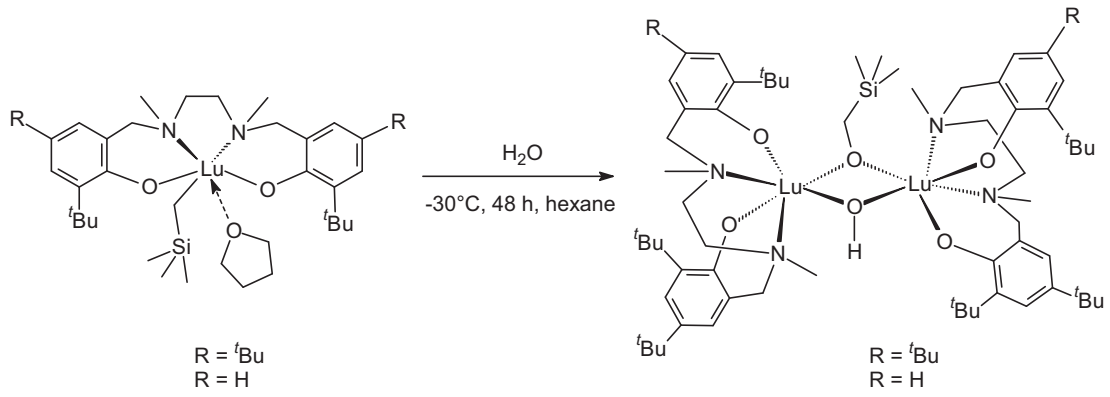

Scheme 34.

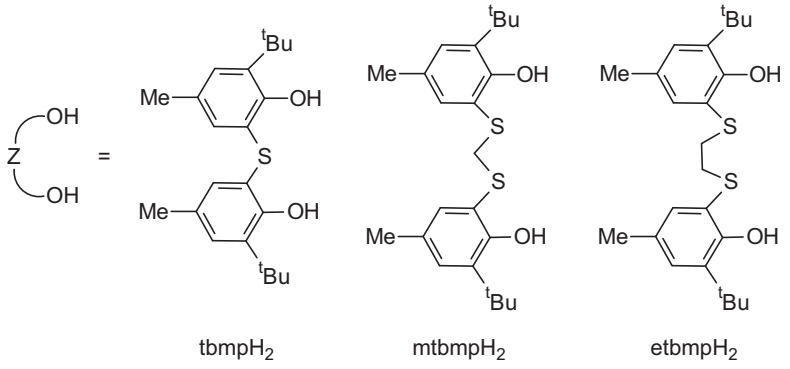

Scheme 35.

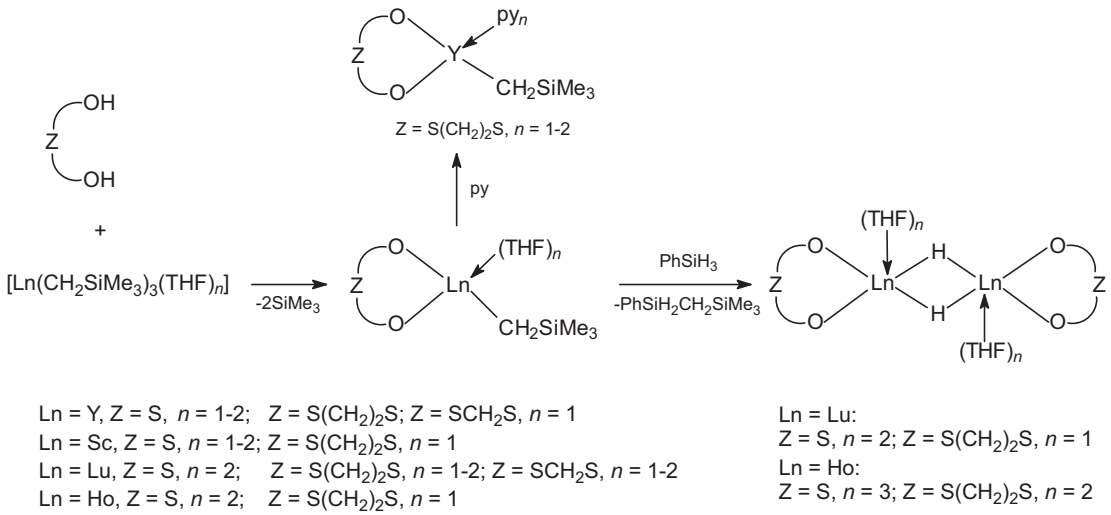

Scheme 36.

divalent ytterbium complex. Oxidation of the divalent Yb sandwich $Yb(C_5Ph_5)_2$ with different oxidizing agents were carried out in an attempt to obtain $(C_5Ph_5)_2YbX$ complexes (X = halide). Two different results were found depending on the strength of the oxidizing reagent. Oxidants as powerful as oxygen, *e.g.,* $PhICl_2$ or I_2, led to the formation of C_5Ph_5 radicals and YbX_3. Weaker oxidants, such as C_2Cl_6, did not react with $Yb(C_5Ph_5)_2$, even in boiling toluene. By contrast, all oxidants reacted readily with the SSIP $[Yb(THF)_6][C_5Ph_5]_2$ to give the C_5Ph_5 radical and YbX_3. Attempts to use an excess of $[Yb(THF)_6][C_5Ph_5]_2$ or $Yb(C_5Ph_5)_2$ led predominantly to unreacted starting material, and no $(C_5Ph_5)_2YbX$ or $(C_5Ph_5)YbX_2$ species could be identified [37].

The remarkable lanthanide chemistry of a new "superbulky" cyclopentadienyl ligand is summarized in Scheme 49. Given the fact that complexes containing the Ph_5C_5 ligand are very insoluble on account of their rigidity and high symmetry, the modified perarylated cyclopentadiene $(4\text{-}^{n}BuC_6H_4)_5C_5H$ (=$Cp^{BIG}H$) has been introduced. This ligand can be obtained in a simple high yield, one-pot procedure. Reaction of equimolar amounts of $Cp^{BIG}H$ with $(2\text{-}Me_2N\text{-benzyl})_3Y$ in benzene gave the half-sandwich complex $(Cp^{BIG})(2\text{-}Me_2N\text{-benzyl})_2Y$ as colorless, needle-like crystals (31% yield). However, the analogous reaction with $(2\text{-}Me_2N\text{-benzyl})_3Yb$ resulted in spontaneous reduction to the Yb^{II} metallocene $(Cp^{BIG})_2Yb$, which crystallized as dark green blocks. Most remark-

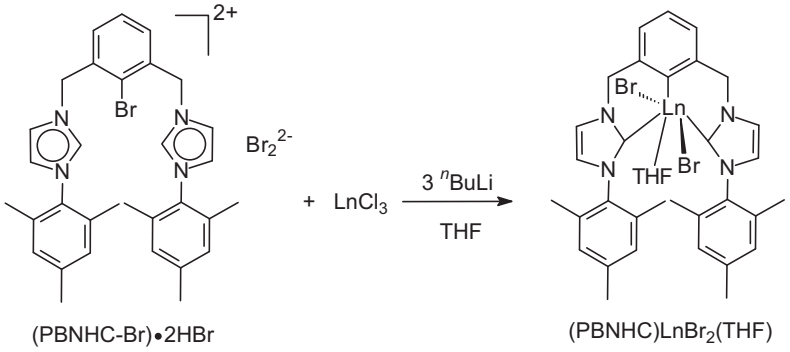

Scheme 37.

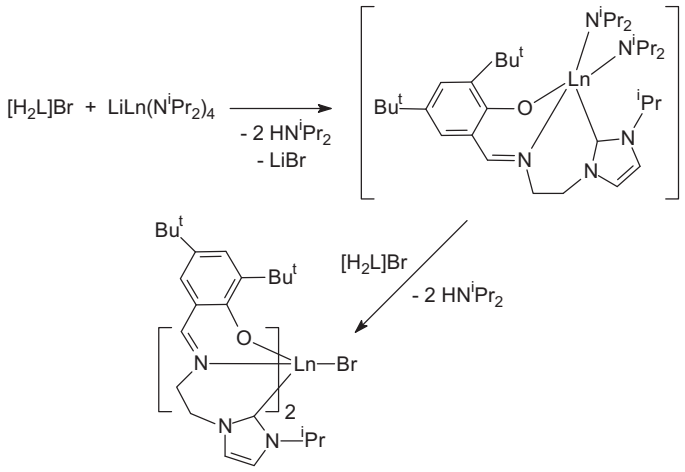

Scheme 38.

ably, however, this spontaneous reduction also occurred with samarium. The samarocene $(Cp^{BIG})_2Sm$, with the metal in its highly reactive 2+ oxidation state, was isolated in the form of red-brown crystals (36% yield). The instability of Sm^{II} against oxidation is well established (Sm^{3+}/Sm^{2+}, $E_{1/2} = -1.55$ V). SmI_2 is used as a versatile reducing agent in organic chemistry, and Cp^*_2Sm is even able to reduce molecular nitrogen. In this light, the spontaneous reduction of a Sm^{III} precursor to the samarocene $(Cp^{BIG})_2Sm^{II}$ is quite unusual [38].

2.4.2. $CpLnX_2$ compounds

A four-coordinate hydrogen atom has been unambiguously located, by single-crystal neutron diffraction for the first time, in the center of the tetrahedral metal complex $[(C_5Me_4SiMe_3)YH_2]_4(THF)$. As shown in Fig. 2, the core of the molecule consists of a tetranuclear cluster with one interstitial, one face-bridging, and six edge-bridging hydride ligands. The compound was prepared *via* the reaction of $(C_5Me_4SiMe_3)Y(CH_2SiMe_3)_2(THF)$ with gaseous H_2. Neutron data were collected on a 4 mm^3 crystal at the Quasi-Laue diffractometer VIVALDI at ILL (Grenoble) and on an 8 mm^3 crystal at the SXD diffractometer at ISIS (Didcot). The final agreement factor was $R = 8.9\%$ for 4171 reflections [39].

A tridentate [N,N,O]-Schiff-base, 3,5-^{t}Bu$_2$-2-(OH)-C_6H_2CH = N-8-C_9H_6N, (=LH) was prepared, and the corresponding sodium and ytterbium complexes were synthesized (Scheme 50) and characterized. Reaction of LH with NaH in THF at room temperature afforded the sodium salt of the Schiff-base as a dimer $[LNa(THF)]_2$. This dimer was treated with anhydrous $YbCl_3$ in THF to give, after workup, the monomeric ytterbium Schiff-base dichloride complex, $LYbCl_2(DME)$. This complex is a good precursor for the synthesis of corresponding ytterbium derivatives with aryloxide and cyclopentadienyl ligands. For example, a reaction with 2 equiv. of ArONa (ArO = –$OC_6H_3{}^tBu_2$-2,6) in THF afforded the desired solvent-free ytterbium aryloxide $LYb(OAr)_2$. In a similar manner, reaction of $LYbCl_2(DME)$ with 1 equiv. of $NaCH_3C_5H_4$ in THF gave the expected mono(methylcyclopentadienyl) product $LYb(CH_3C_5H_4)Cl(THF)$ in a good isolated yield. All these complexes were fully characterized including X-ray structure determination [40].

The synthesis, characterization and reactivity of heteroleptic rare-earth metal complexes supported by the carbon-bridged

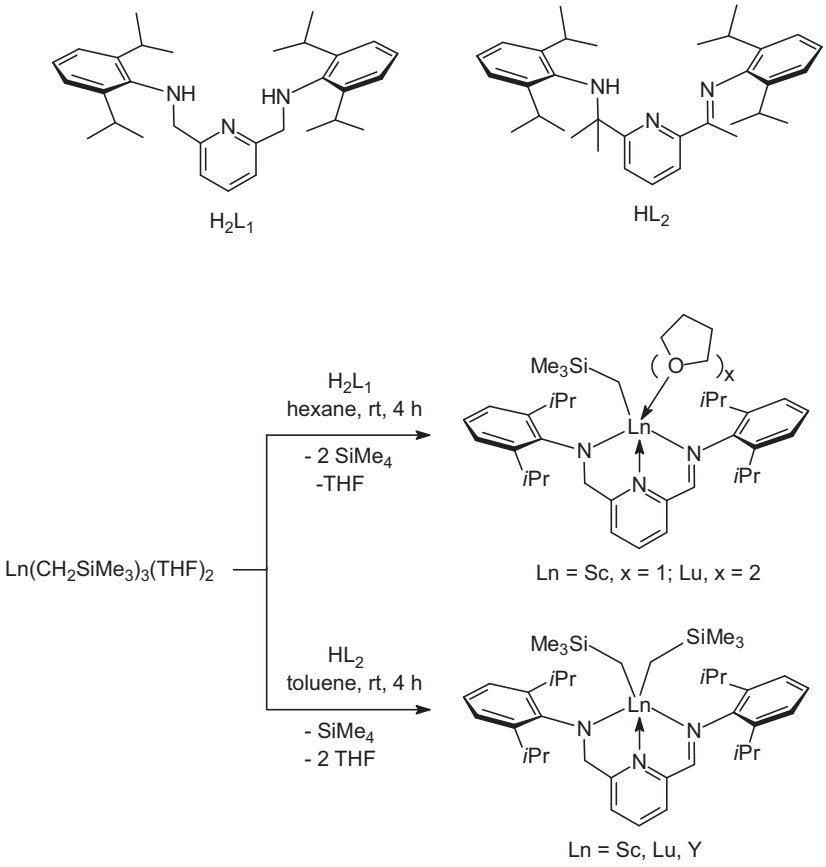

Scheme 39.

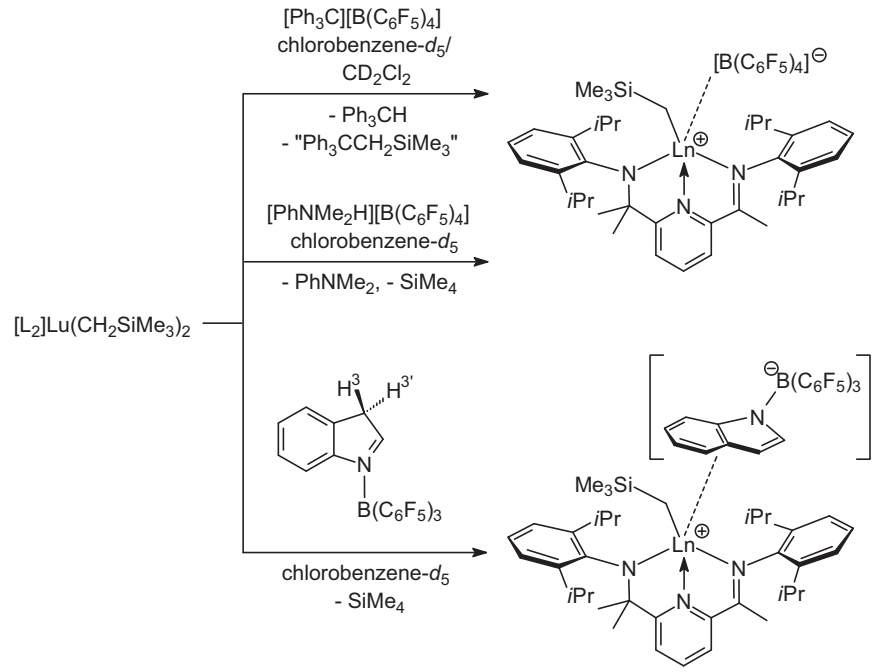

Scheme 40.

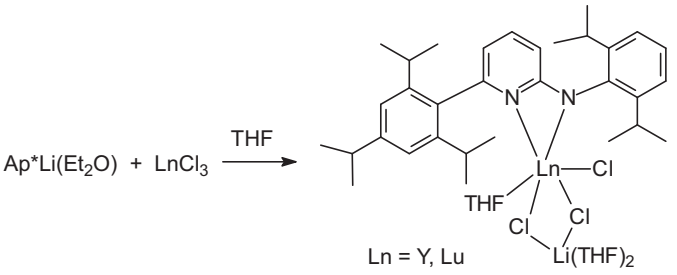

Scheme 41.

bis(phenolate) ligand 2,2′-methylene-bis(6-*tert*-butyl-4-methylphenoxo) ($MBMP^{2-}$) have been described. Reaction of $Cp_3Ln(THF)$ with $MBMPH_2$ in a 1:1.5 molar ratio in THF at 50 °C produced the heteroleptic rare-earth metal bis(phenolate) complexes $CpLn(MBMP)(THF)_n$ (Ln = La, n = 3; Ln = Yb, Y, n = 2) in nearly quantitative yields (Scheme 51) [41].

The residual C_5H_5 groups in the mono(cyclopentadienyl) complexes shown in Scheme 51 can be substituted by the bridged bis(phenolate) ligands at elevated temperature to give the neutral rare-earth metal bis(phenolate) complexes. It was found that the ionic radii have a profound effect on the structures of the final products. The La complex reacted with $MBMPH_2$ in a 1:0.5 molar ratio in toluene at 80 °C to produce a dinuclear complex (MBMP)La(THF)(μ-

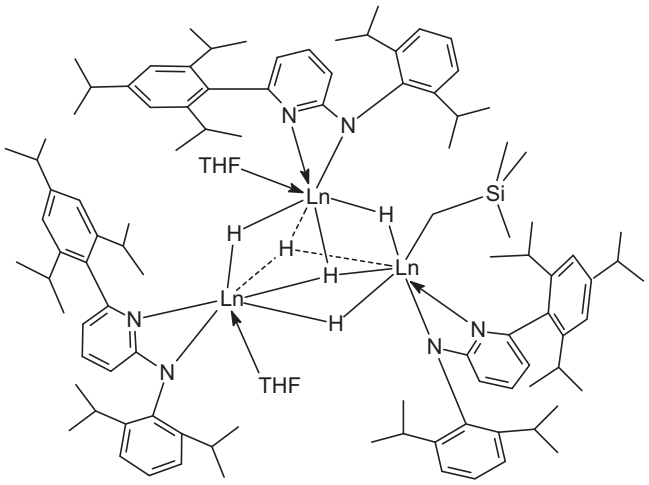

Scheme 43.

$MBMP)_2La(THF)_2$ in good isolated yield, whereas the Y and Yb complexes reacted with $MBMPH_2$ under the same conditions to give (MBMP)Ln(MBMPH)$(THF)_2$ (Ln = Yb, Y) as the final products, in which one hydroxyl group of the phenol is coordinated to the rare-earth metal in a neutral fashion (Scheme 52) [41].

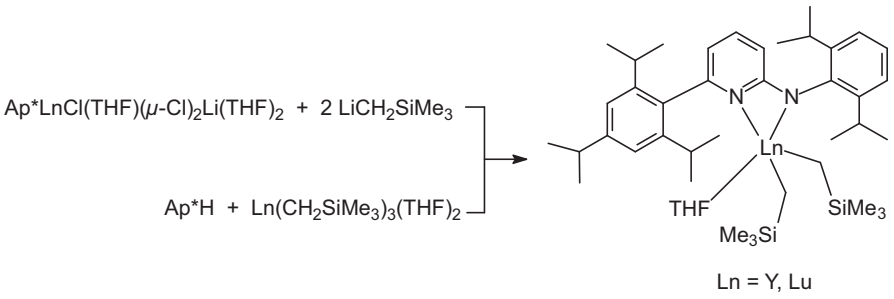

Scheme 42.

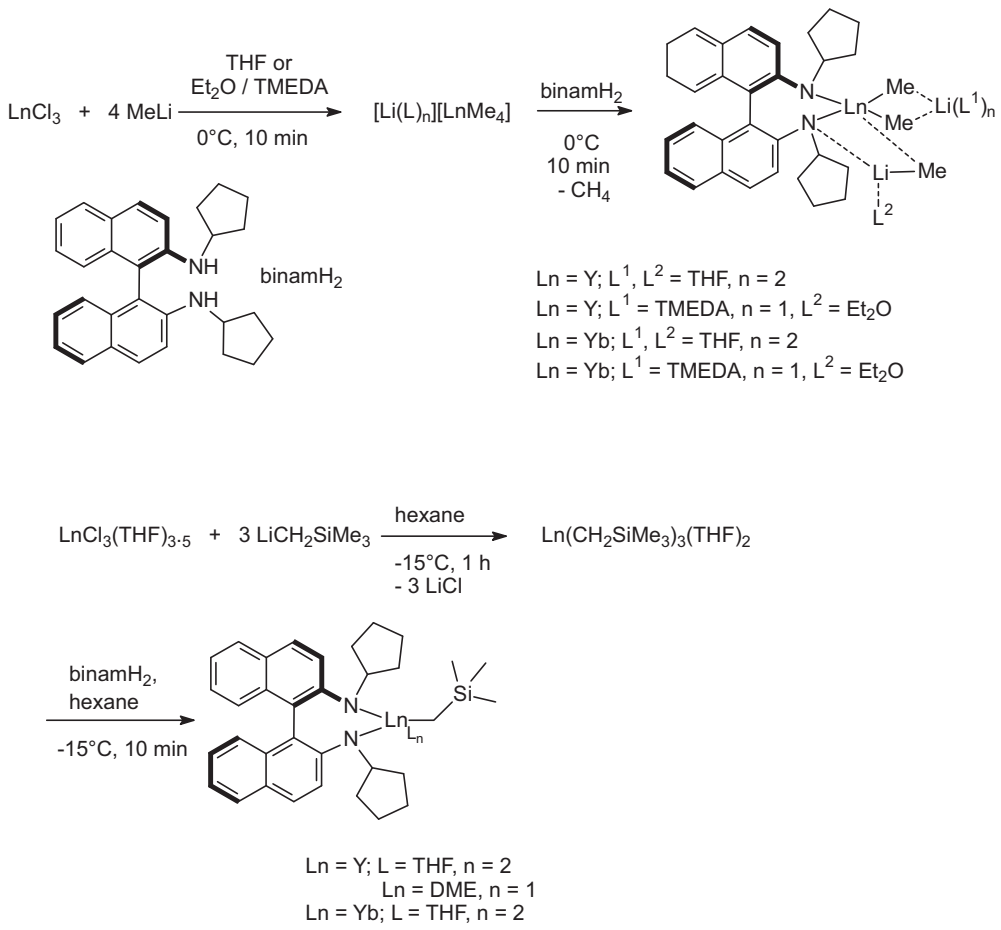

Scheme 44.

Rare-earth metal mixed hydride/aryloxide complexes bearing mono(cyclopentadienyl) ligands have been investigated. Hydrogenolysis of mono(cyclopentadienyl)-ligated rare-earth metal bis(alkyl) complexes $Cp'Ln(CH_2SiMe_3)_2(THF)$ (Ln = Y, Dy, Lu; $Cp' = C_5Me_4SiMe_3$) with $PhSiH_3$ afforded the mixed hydride/alkyl complexes $[Cp'Ln(\mu\text{-}H)(CH_2SiMe_3)(THF)]_2$ (Ln = Y, Dy, Lu). The overall structure of the resulting complexes is a C_2-symmetric dimer containing a planar symmetric Ln_2H_2 core at the center of the molecule. Deprotonation of the bulky phenol ArOH ($Ar = C_6H_2\text{-}^tBu_2\text{-}2,6\text{-}Me\text{-}4$) by the metal alkyl group of the dimeric alkyl hydrides led to the formation of the mixed hydride/aryloxide derivatives $[Cp'Ln(\mu\text{-}H)(OAr)]_2$ (Ln = Y, Dy, Lu), which again adopt the dimeric structure through hydride bridges with *trans*-accommodated terminal aryloxide groups (Scheme 53) [42].

The dimeric hydride/aryloxide complexes were found to react swiftly with CO_2 to generate the mixed formate/carbonate complexes $[Cp'Ln(\mu\text{-}\eta^1\text{:}\eta^1\text{-}O_2CH)(\mu\text{-}\eta^1\text{:}\eta^1\text{-}O_2COAr)]_2$ (Ln = Y, Dy, Lu)

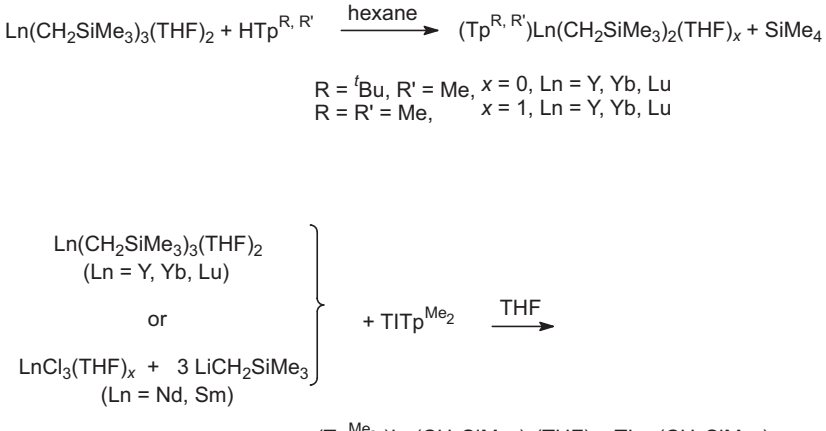

Scheme 45.

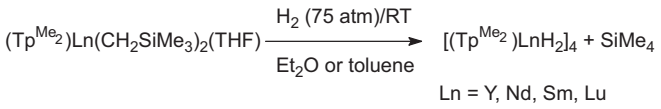

Scheme 46.

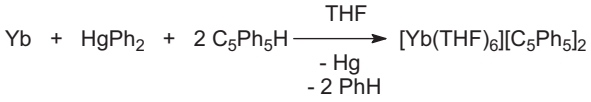

Scheme 47.

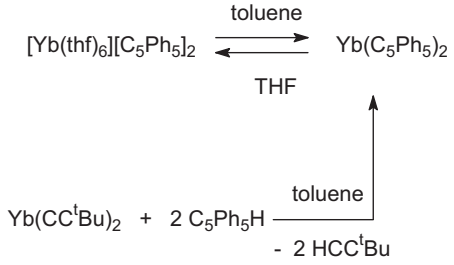

Scheme 48.

(Scheme 54). The two Cp′Ln fragments in these complexes are bridged by the formate and carbonate species, respectively, to form two square-pyramidal geometries around the metal centers [42].

Synthesis and catalytic properties of phenylene-bridged binuclear organolanthanide complexes have been reported. The syntheses required the use of unsolvated $Ln[N(SiHMe_2)_2]_3$ as starting materials. These precursors were prepared by a transamination route outlined in Scheme 55 [43].

Using the base-free $Ln[N(SiHMe_2)_2]_3$ complexes as highly effective protodeamination reagents, the binuclear lanthanide complexes *p*-bis{η^5-(2,3,4,5-tetramethylcyclopentadienyl)Ln[$N(SiHMe_2)_2]_2$}phenylene (=*p*-Ln_2, Ln = Y, La, Lu) and *m*-bis{η^5-(2,3,4,5-tetramethylcyclopentadienyl)La[$N(SiHMe_2)_2]_2$}phenylene (=*m*-La_2) were synthesized from the corresponding phenylene-linked tetramethylcyclopentadienes as shown in Scheme 56. The resulting products served as new types of multicenter homogeneous 4*f* catalysts (*cf.* Section 2.9.2) [43].

The acid–base reactions between the rare-earth metal tris-(*ortho*-*N*,*N*-dimethylaminobenzyl) complexes $Ln(CH_2C_6H_4NMe_2\text{-}o)_3$ with 1 equiv. of the silylene-linked cyclopentadiene-amine ligand $(C_5Me_4H)SiMe_2NH(C_6H_2Me_3$-2,4,6) afforded the corresponding half-sandwich aminobenzyl complexes $[Me_2Si(C_5Me_4)$-$(NC_6H_2Me_3$-2,4,6)]$Ln(CH_2C_6H_4NMe_2$-*o*)(THF) (Ln = Y, La, Pr, Nd, Sm, Gd, Lu) in 60–87% isolated yields (Scheme 57). The one-pot reaction between $ScCl_3$ and $[Me_2Si(C_5Me_4)(NC_6H_2Me_3$-2,4,6)]$Li_2$ followed by reaction with $LiCH_2C_6H_4NMe_2$-*o* in THF gave the scandium analogue $[Me_2Si(C_5Me_4)(NC_6H_2Me_3$-2,4,6)]$Sc(CH_2C_6H_4NMe_2$-*o*) in 67% isolated yield. The scandium derivative could not be prepared by the acid–base reaction between $Sc(CH_2C_6H_4NMe_2\text{-}o)_3$ and $(C_5Me_4H)SiMe_2NH(C_6H_2Me_3$-2,4,6) [44].

The subsequent reaction of the La derivative with 1 equiv. of Ph_2PH yielded the corresponding phosphide complex $[Me_2Si(C_5Me_4)(NC_6H_2Me_3$-2,4,6)]$La(PPh_2)(THF)_2$ (92% yield), which, on recrystallization from benzene, gave the dimeric

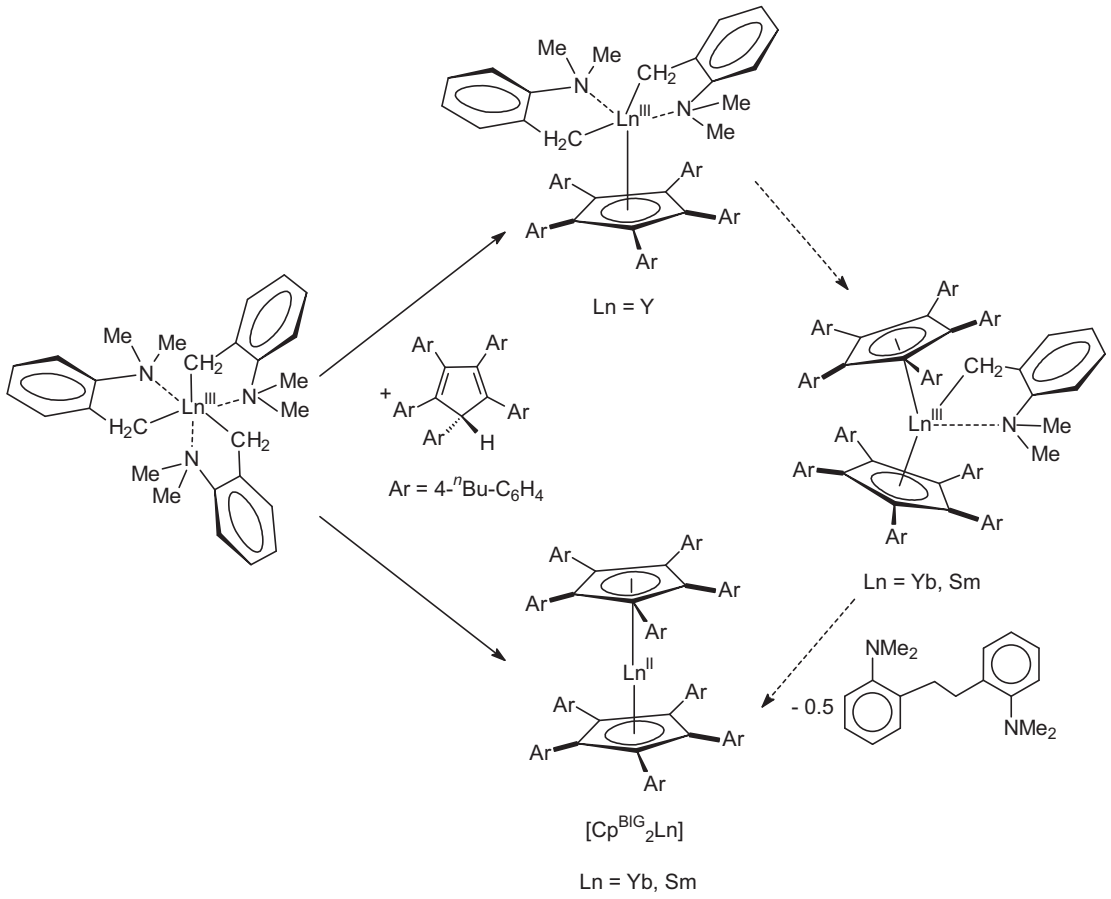

Scheme 49.

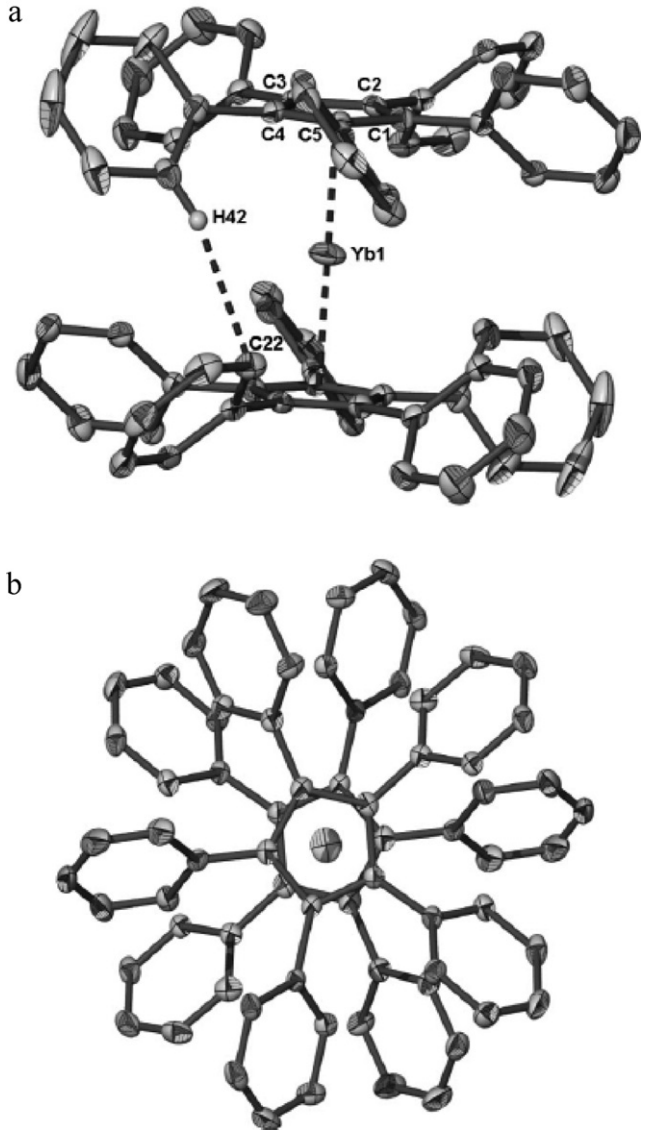

Fig. 1. Side view (a) and top view (b) of the molecular structure of $Yb(C_5Ph_5)_2$ with 50% probability ellipsoids [37].

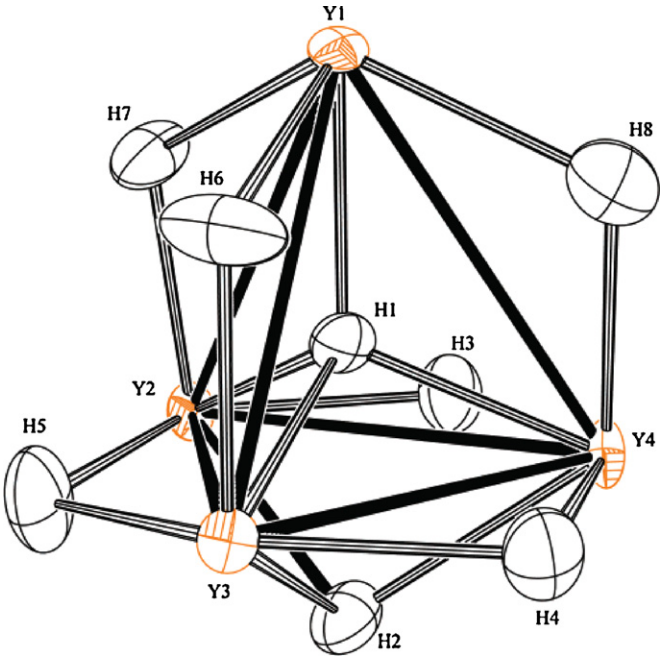

Fig. 2. ORTEP plot of the core of $[(C_5Me_4SiMe_3)YH_2]_4(THF)$ [39].

analogue $[\{Me_2Si(C_5Me_4)(NC_6H_2Me_3\text{-}2,4,6)\}La(PPh_2)]_2$ in 90% yield (Scheme 58). Addition of either of these complexes to $^iPrN{=}C{=}N^iPr$ in THF yielded the phosphaguanidinate complex $[Me_2Si(C_5Me_4)(NC_6H_2Me_3\text{-}2,4,6)]La[^iPrNC(PPh_2)N^iPr](THF)$, which, on recrystallization from ether, afforded the ether-coordinated structurally characterizable analogue $[Me_2Si(C_5Me_4)(NC_6H_2Me_3\text{-}2,4,6)]La[^iPrNC(PPh_2)N^iPr](OEt_2)$. The reaction of the phosphaguanidinate complexes with Ph_2PH in THF yielded the starting phosphide complex and the phosphaguanidine $^iPrN{=}C(PPh_2)NH^iPr$ [44].

Synthesis, structures, and reactivity of yttrium complexes of a phenanthrene-fused cyclopentadienyl have been investigated. The tris-alkyl complex $Y(CH_2SiMe_3)_3(THF)_2$ reacts with 1,2,3-trimethyl-1*H*-cyclopenta[*l*]phenanthrene (PCp*H) according to Scheme 59 to give $(PCp^*)Y(CH_2SiMe_3)_2(THF)$, characterized structurally by X-ray crystallography. VT-NMR spectra of the product revealed a dynamic equilibrium between the THF-free and mono(THF) solvate in solution [45].

The dialkyl complex $(PCp^*)Y(CH_2SiMe_3)_2(THF)$ undergoes substitution of THF by 2,2′-bipyridine (bipy) to give $(PCp^*)Y(CH_2SiMe_3)_2(bipy)$; the latter complex does not undergo ligand exchange in solution. Insertion reactions of $(PCp^*)Y(CH_2SiMe_3)_2(THF)$ with CO_2, Me_3SiNCO, and $^iPrN{=}C{=}NC^iPr$ afforded $(PCp^*)Y[\kappa^2\text{-}(O,O)\text{-}O_2C(CH_2SiMe_3)]_2$, $(PCp^*)Y[\kappa^2\text{-}(N,O)\text{-}(Me_3Si)NC(CH_2SiMe_3)O]_2$, and $(PCp^*)Y[\kappa^2\text{-}(N,N)\text{-}^iPrNC\text{-}(CH_2SiMe_3)N^iPr]_2$ (Scheme 60) [45].

Reaction of $(PCp^*)Y(CH_2SiMe_3)_2(THF)$ with 2 equiv. of $Me_3SiC{\equiv}CH$ afforded a terminal bis(acetylide) $(PCp^*)Y(C{\equiv}CSiMe_3)_2(THF)$ in solution; however, X-ray analysis of crystals obtained from a solution of $(PCp^*)Y(C{\equiv}CSiMe_3)_2(THF)$ showed that it dimerizes to $(\mu\text{-}C{\equiv}CSiMe_3)_2[(PCp^*)Y(C{\equiv}CSiMe_3)(THF)]_2$ (Scheme 61) [45].

The chemistry of Sc and Y compounds comprising NNCp hybrid scorpionate/cyclopentadienyl ligands has been further developed. Reaction of hybrid scorpionate/cyclopentadienyl ligands in the form of the lithium derivatives Li(bpzcp)(THF) [bpzcp = 2,2-bis(3,5-dimethylpyrazol-1-yl)-1,1-diphenylethylcyclo-pentadienyl], Li(bpztcp)(THF) [bpztcp = 2,2-bis(3,5-dimethylpyrazol-1-yl)-1-*tert*-butylethylcyclopentadienyl], and the *in situ*-generated "Li(bpzpcp)" [bpzpcp = 2,2-bis(3,5-dimethylpyrazol-1-yl)-1-phenylethylcyclopentadienyl] with $MCl_3(THF)_3$ afforded the group 3 halide compounds $(bpzcp)MCl_2(THF)$, $MCl_2(bpztcp)(THF)$, and $MCl_2(bpzpcp)(THF)$ (Scheme 62, M = Sc, Y) [46].

The H_2O adduct of $MCl_2(bpztcp)(THF)$, $YCl_2(bpztcp)(H_2O)$ (Scheme 63), was formed when a solution of the THF adduct was allowed to stand at room temperature in the presence of moisture. All complexes shown in Schemes 62 and 63 adopt a *pseudo*-octahedral structure with the heteroscorpionate ligands κ^2-NN-η^5-Cp-coordinated to the metal through the cyclopentadienyl group and two imino nitrogens of pyrazole rings [46].

The earlier reported alkyl heteroscorpionate scandium and yttrium complexes $(bpzcp)M(CH_2SiMe_3)_2$, were found to react with 2,6-dimethylphenol and 3,5-dimethylphenol as shown in Scheme 64 to give the bis(aryloxide) derivatives $[M(OAr)_2(bpzcp)]$ (M = Sc, Y; OAr = 2,6-dimethylphenoxide; M = Y, OAr = 3,5-dimethylphenoxide). The yttrium 2,6-dimethylphenoxide derivative underwent an interesting hydrolysis process to give the tetranuclear complex $[\{Y(bpzcp)\}(\mu\text{-}OH)_2(\mu_3\text{-}OH)\{Y(OAr)_2\}]_2$ [46].

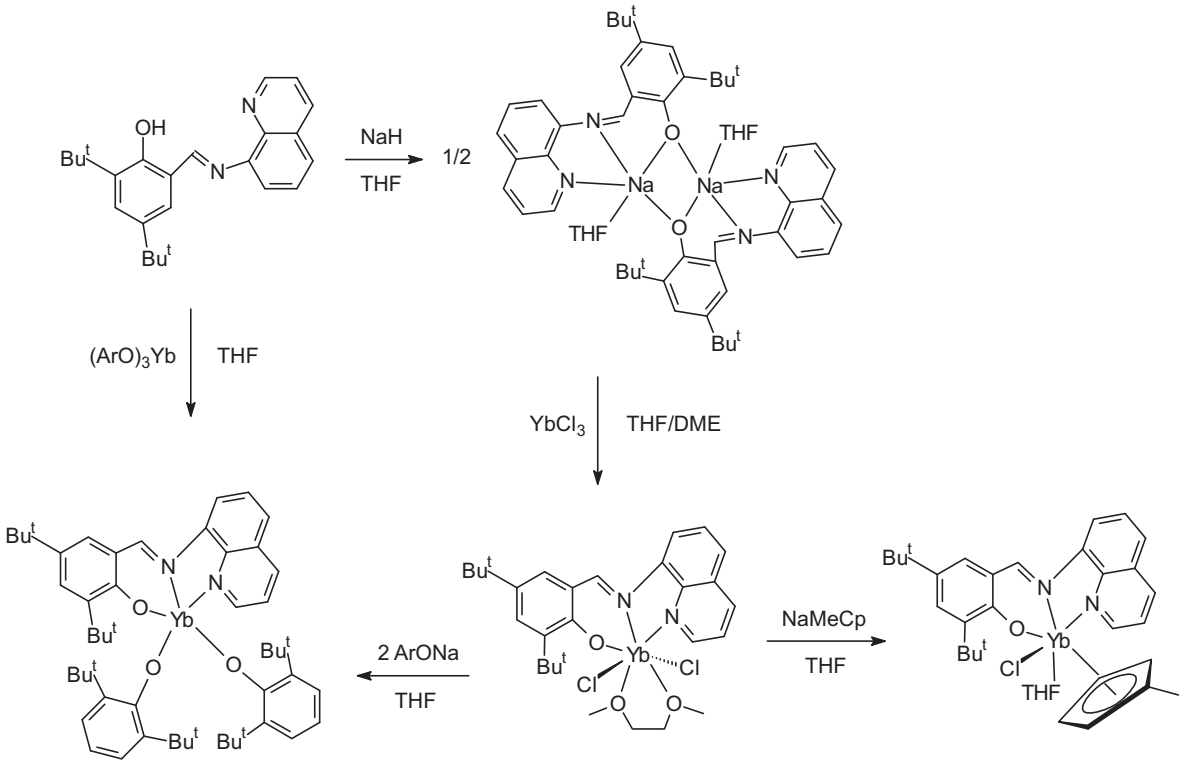

Scheme 50.

2.4.3. Cp_2LnX compounds

The compounds $[Cp_2Y(ONBn_2)]_2$ and $[Cp_2Sm(ONBn_2)]_2$ were prepared according to Scheme 65 by the reactions of Cp_3Ln (Ln = Y, Sm) with *N*,*N*-dibenzylhydroxylamine, Bn_2NOH (Bn = CH_2Ph) [47].

The trinuclear compound $Cp_5Y_3[ON(Me)CH_2CH_2(Me)NO]_2$ was obtained in a similar manner by the reaction of Cp_3Y and the bis(hydroxylamine) $HON(Me)CH_2CH_2(Me)NOH$ as shown in Scheme 66. All new rare-earth metal hydroxylamide complexes were characterized by NMR spectroscopy, single-crystal X-ray diffraction and elemental analysis. In all these complexes side-on-coordination of the hydroxylamide units was observed. The compounds are of dynamic nature in solution [47].

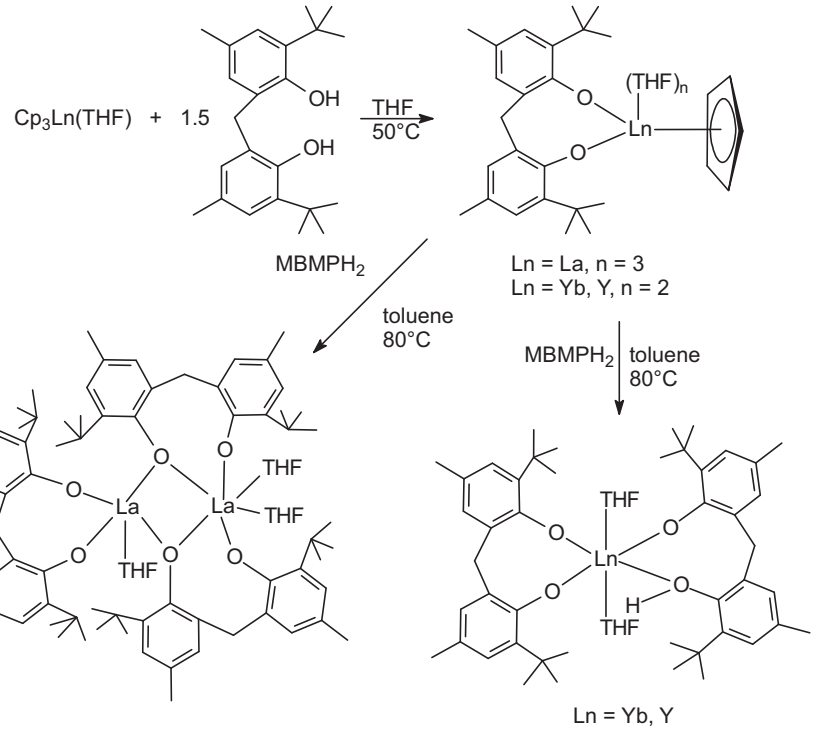

Scheme 51.

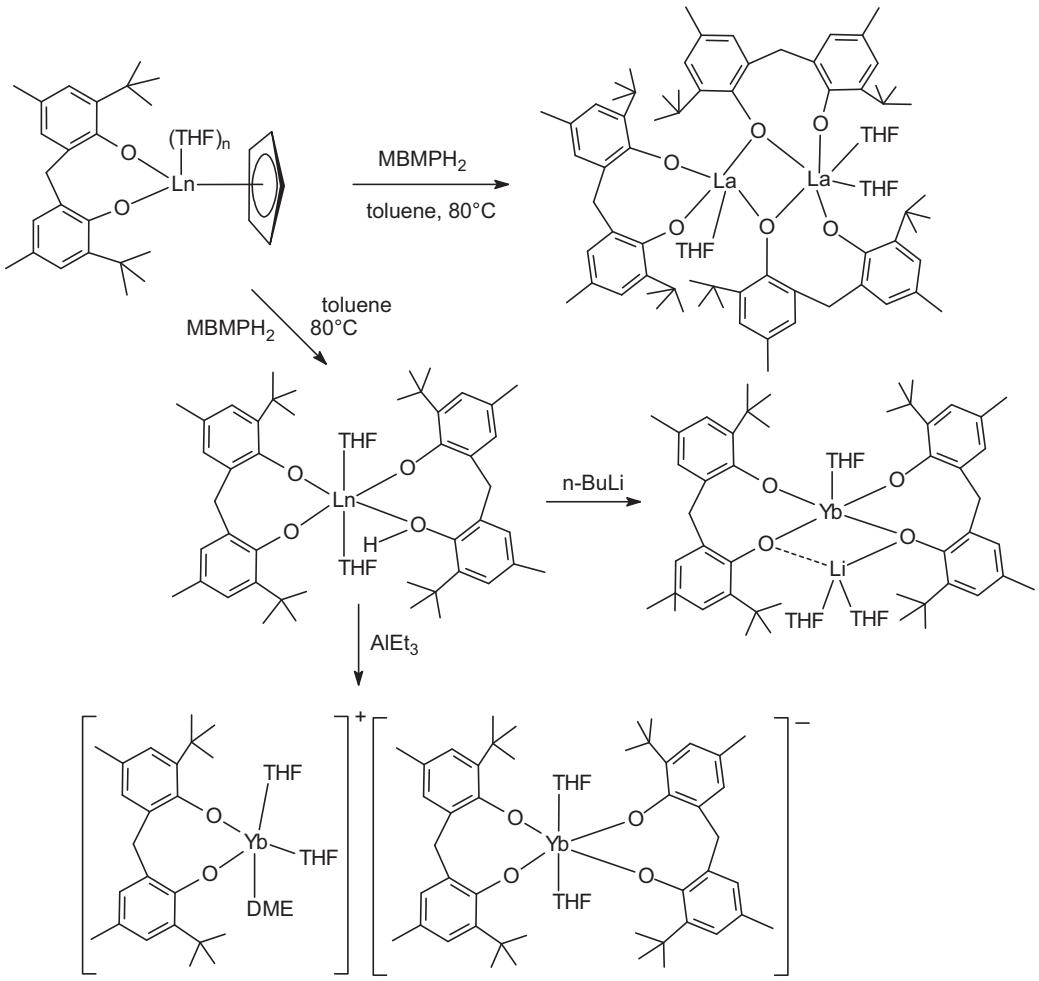

Scheme 52.

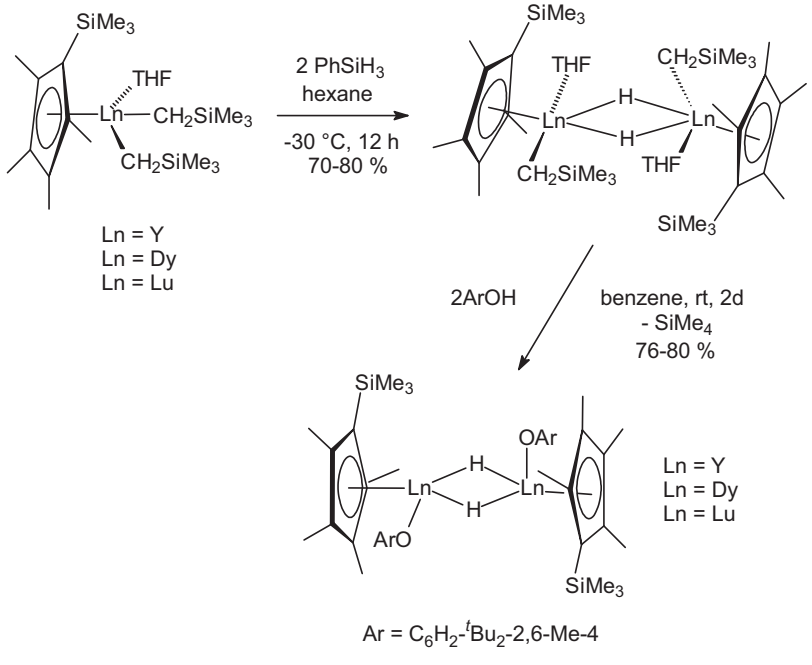

Scheme 53.

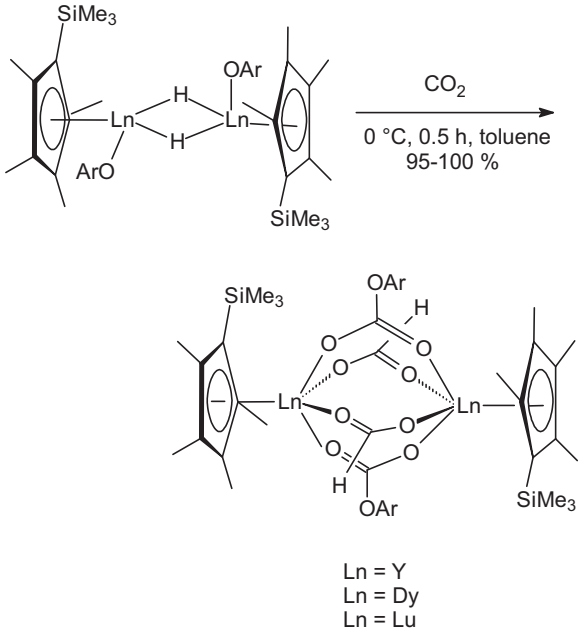

Scheme 54.

The compounds $Cp_2Ln[\kappa^3\text{-}4\text{-}NH(C_8N_2H_4)(2\text{-}NH_2C_6H_4)]$ (Ln = Er, Y) were synthesized by the reaction of $Cp_2LnN^iPr_2(THF)$ with anthranilonitrile, indicating a novel organolanthanide-mediated intermolecular nucleophilic addition/cyclization of anthranilonitrile. The products were isolated in moderate or high yields. Structural analysis revealed that an intermolecular nucleophilic addition/cyclization of anthranilonitrile took place accompanied by the elimination of HN^iPr_2 to form a novel $[4\text{-}NH(C_8N_2H_4)(2\text{-}NH_2C_6H_4)]^-$ ligand. It should be noted that the compounds could also be obtained from the reaction of $Cp_2LnN^iPr_2(THF)$ with 1 equiv. of anthranilonitrile under the same conditions in lower yields. A proposed mechanism for the formation of $Cp_2Ln[\kappa^3\text{-}4\text{-}NH(C_8N_2H_4)(2\text{-}NH_2C_6H_4)]$ (Ln = Er, Y) is illustrated in Scheme 67. The first step is protonolysis of the diisopropylamide ligand by an anthranilonitrile molecule to generate the intermediate **I**. A further nitrile group from another anthranilonitrile molecule inserts into the Ln–N bond of **I**, to give **A**, and then transforms into **B** through 1,3-hydrogen shift. The final products are formed by nitrile insertion and a 1,3 hydrogen shift again [48].

Insertion of ketenes into lanthanocene *n*-butylamide and imidazolate complexes has been investigated in detail (Scheme 68). Reaction of Cp_2LnNH^nBu with 1 equiv. of $Ph_2C{=}C{=}O$ in toluene affords dimeric complexes $[Cp_2Ln(OC(CHPh_2)N^nBu)]_2$ (Ln = Yb, Dy), derived from a formal insertion of the C=C bond of the ketene into the N–H bond. Treatment of $CpErCl_2$ with 2 equiv. of $LiNH^nBu$ followed by reaction with $Ph_2C{=}C{=}O$ affords a rearrangement product $[Cp_2Er(OC(CHPh_2)N^nBu)]_2$. Treatment of $[Cp_2Ln(\mu\text{-}Im)]_3$ (Im = imidazolate) with PhRC=C=O gives $[Cp_2Ln(\mu\text{-}OC(Im){=}CPhR)]_2$ (R = Et, Ln = Yb; R = Ph, Ln = Yb, Er). In contrast to the previous observations that $[Cp_2ErN^iPr_2]_2$ and $[Cp_2ErNHEt]_2$ react with ketenes to give di-insertion products, in the present cases the presence of excess of ketenes has no influence on the final product even with prolonged heating, and only mono-insertion products are isolated. All these complexes were characterized by elemental analysis, IR and mass spectrometry. The structures of the new complexes were also determined through X-ray single crystal diffraction analysis [49].

The reaction between monomeric bis(1,2,4-tri-*tert*-butylcyclopentadienyl)cerium hydride, Cp'_2CeH, and several hydrofluorobenzene derivatives has been investigated in great detail (Scheme 69). The aryl derivatives that are the primary products, $Cp'_2Ce(C_6H_{5-x}F_x)$ where $x = 1, 2, 3, 4$, were found to be thermally stable enough to be isolated in only two cases, since all of them decompose at different rates to Cp'_2CeF and a

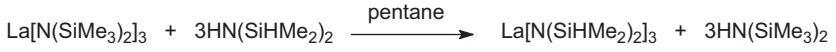

Scheme 55.

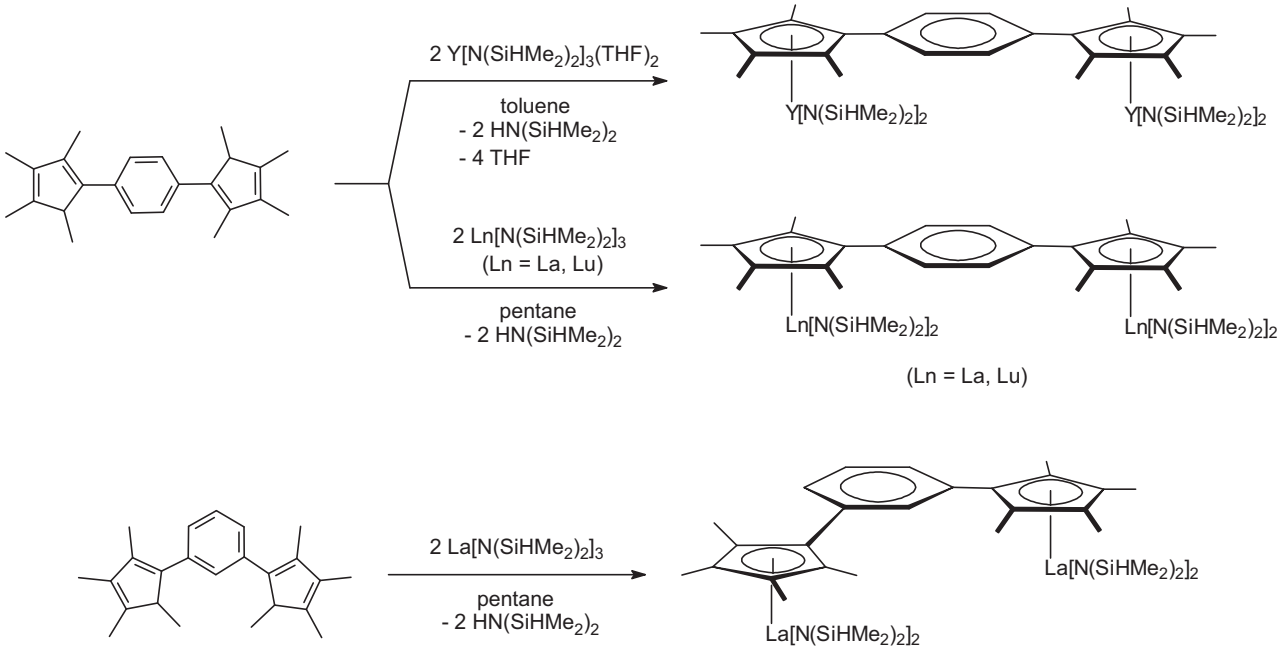

Scheme 56.

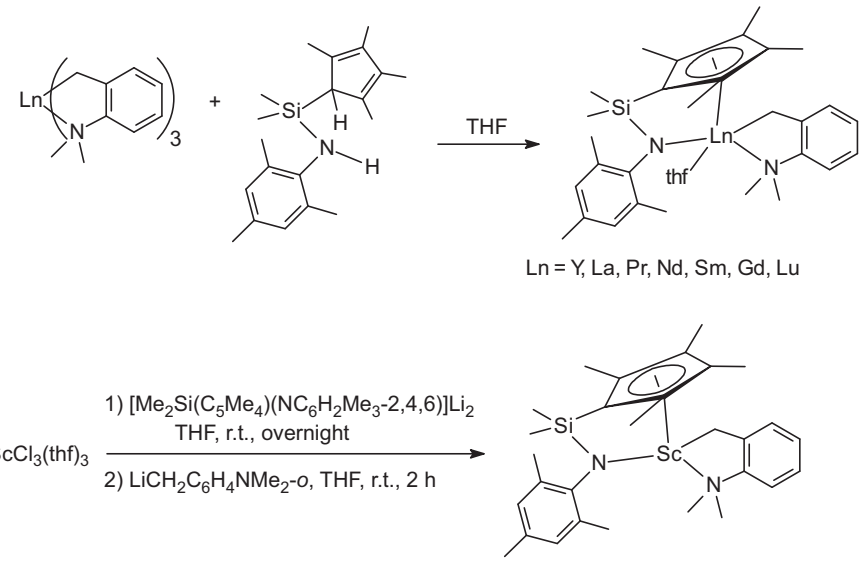

Scheme 57.

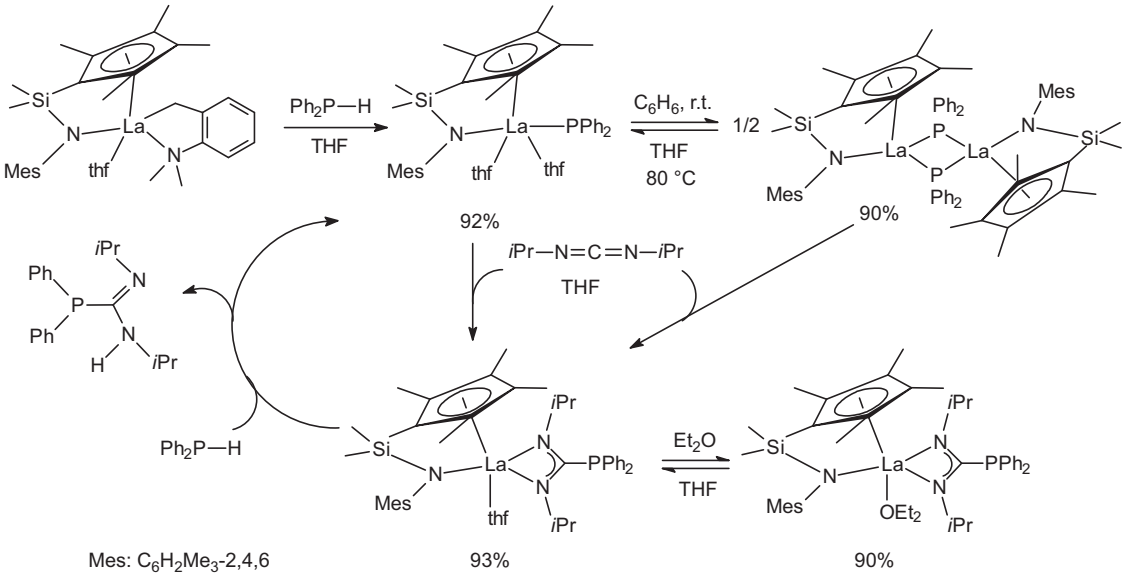

Scheme 58.

fluorobenzyne; the latter was trapped by either solvent when C_6D_6 was used or by a Cp′H ring when C_6D_{12} was the solvent. The trapped products were identified by GC/MS analysis after hydrolysis. The aryl derivatives were also generated cleanly by the reaction of the metallacycle Cp′[$(Me_3C)_2C_5H_2C(Me_2)CH_2$]Ce with a hydrofluorobenzene, and the resulting arylcerium products, in each case, were identified by their ^{1}H and ^{19}F NMR spectra at 20 °C [50].

2.4.4. Cp_3Ln and Cp_3LnL compounds

Notable among the highlights of organolanthanide chemistry is the isolation of stable mononuclear La^{II} compounds, in which the lanthanum oxidation state was confirmed by structural, spectroscopic, magnetic, and computational studies. Reaction of the colorless diamagnetic La^{III} compound Cp″$_3$La with a potassium mirror and [18]crown-6 in Et_2O or [2.2.2]cryptand in THF produced the crystalline complexes [K([18]c-6)(OEt_2)][Cp″$_3$La] and [K([2.2.2]crypt)][Cp″$_3$La], respectively (Scheme 70). Reduction with K and [18]crown-6 did not proceed cleanly, and the product was contaminated with a small amount of K([18]c-6)(Cp″). In contrast, the cryptand derivative was readily purified. Both La^{II} compounds were both isolated as very dark, blue-violet, paramagnetic crystals easily soluble in THF and sparingly so in Et_2O; addition of aromatic solvents to crystalline [K([18]c-6)(OEt_2)][Cp″$_3$La] led to immediate decomposition with the formation of a green precipitate. The recrystallized divalent lanthanum complexes showed remarkable stability both in the solid state and in the Et_2O solution (THF solutions decolorized slowly). The crown ether derivative was recovered from its Et_2O solution after storing at 10 °C for one year. X-ray crystallography revealed that both complexes contain well-

Scheme 59.

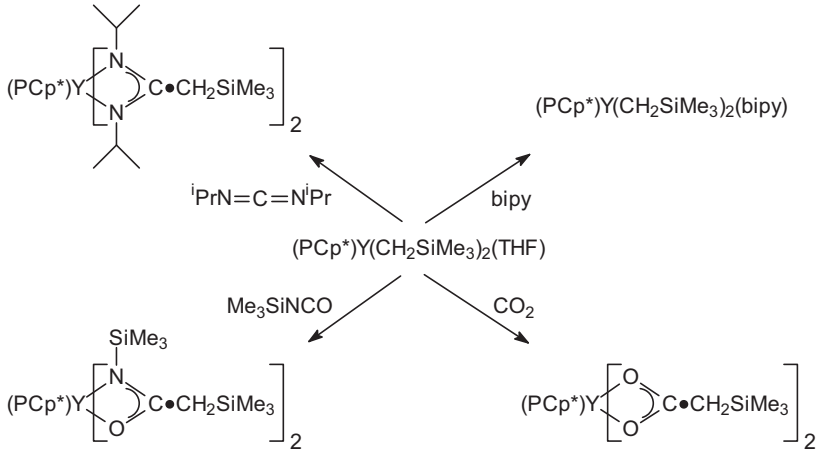

Scheme 60.

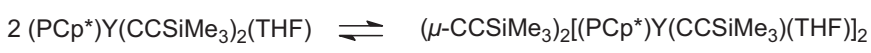

Scheme 61.

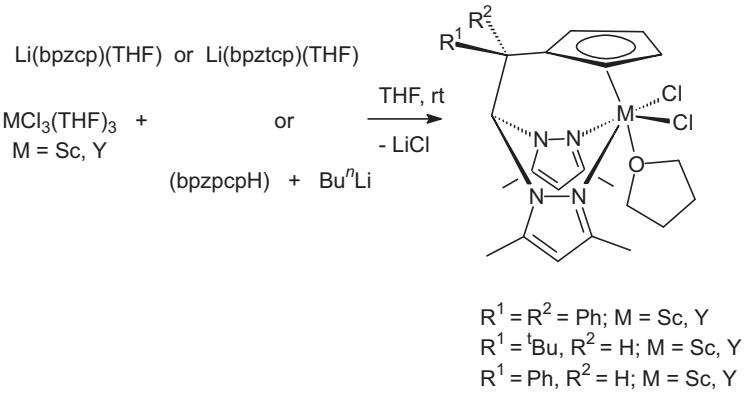

Scheme 62.

separated encapsulated potassium cations and $[Cp''_3La]^-$ anions [51].

Optical polarization measurements of oriented single crystals of $Pr(C_5Me_4H)_3$ were performed at room temperature. In order to separate "cold" and "hot" *f*–*f*-transitions and νC–H combination vibrations, the absorption spectra of KBr pellets of compound $Pr(C_5Me_4H)_3$ and $La(C_5Me_4H)_3$ were additionally recorded at *ca.* 77 K. To gather additional information about the wave-functions of the crystal field (CF) states of $Pr(C_5Me_4H)_3$, a magnetic circular dichroism spectrum was recorded as well. From the spectra obtained, a partial CF splitting pattern of $Pr(C_5Me_4H)_3$ was derived,

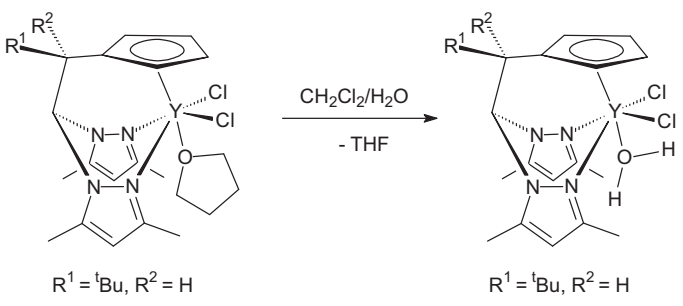

Scheme 63.

and simulated by fitting the free parameters of a phenomenological Hamiltonian, leading to a reduced r.m.s. deviation of 24.8 cm^{-1} for 24 assignments. On the basis of these phenomenological CF parameters, the global CF strength experienced by the Pr^{3+} central ion was estimated, and seems to be the largest ever encountered in Pr^{III} chemistry. The obtained Slater parameter F^2 and the spin–orbit coupling parameter ζ_{4f} allow the insertion of $Pr(C_5Me_4H)_3$ into empirical nephelauxetic and relativistic nephelauxetic series, respectively, of Pr^{III} compounds. With its low F^2 value, $Pr(C_5Me_4H)_3$ is the most covalent Pr^{III} compound (considering only *f* electrons) found to date. The experimentally based non-relativistic molecular orbital scheme (in the *f* range) of complex $Pr(C_5Me_4H)_3$ was determined and compared with the results of a previous Xα-SW calculation on the ψ trigonal planar model compound $Pr(\eta^5\text{-}C_5H_5)_3$. In the framework of the search for "polarized" luminescence transitions, polarized Raman spectra of $Pr(C_5Me_4H)_3$ were recorded too, and compared to the corresponding FIR and IR spectra run by means of pellets [52]. In a closely related study, the absorption spectra (in the IR/NIR/Vis/UV range) of $Ce(C_5Me_4H)_3$ and $La(C_5Me_4H)_3$ were recorded at room and low temperatures. From the spectra obtained, two alternative closely related crystal field (CF) splitting patterns of $Ce(C_5Me_4H)_3$ could be derived, and simulated by fitting the free parameters of a phenomenological Hamiltonian. The fact that the difference of the experimental energies of the barycenters

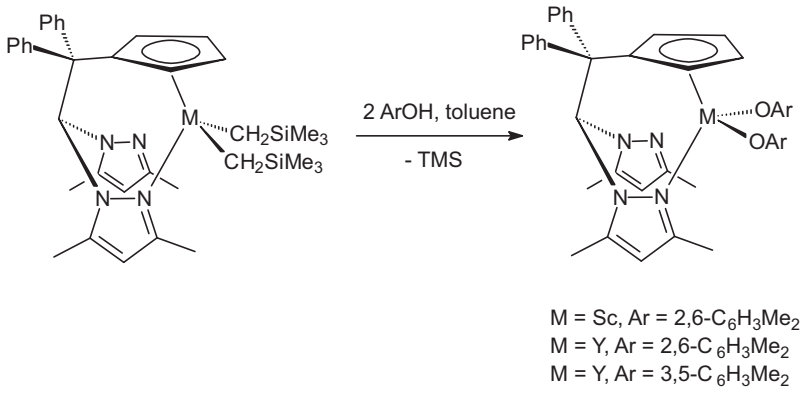

Scheme 64.

of CF levels of the multiplets $^2F_{7/2}$ and $^2F_{5/2}$ is larger than in the gaseous free Ce^{3+} ion ("anti"-relativistic nephelauxetic effect) could be explained by coupling effects of these multiplets *via* the CF, resulting in lower spin–orbit coupling parameters than in the case of the gaseous free Ce^{3+} ion. The experimentally derived CF splitting pattern of $Ce(C_5Me_4H)_3$ was compared with the predictions of previous non-relativistic SW-Xα and relativistic DV-Xα calculations [53].

2.4.5. Pentamethylcyclopentadienyl compounds

2.4.5.1. Mono(pentamethylcyclopentadienyl)lanthanide(III) compounds. The methoxide-bridged, hexanuclear, mixed-valence oxo-centered cluster $[K(THF)_6][Cp^*_6Sm_6(OMe)_8O]$ (Scheme 71) was obtained as a side-product from a reaction of the pental-

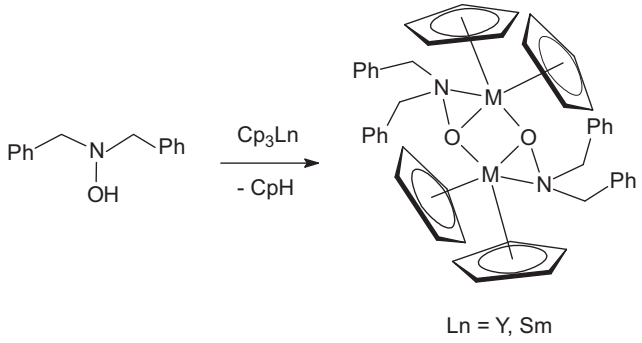

Scheme 65.

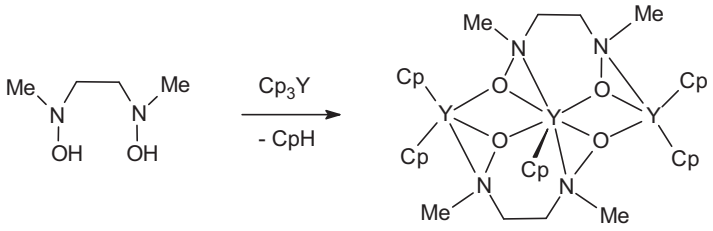

Scheme 66.

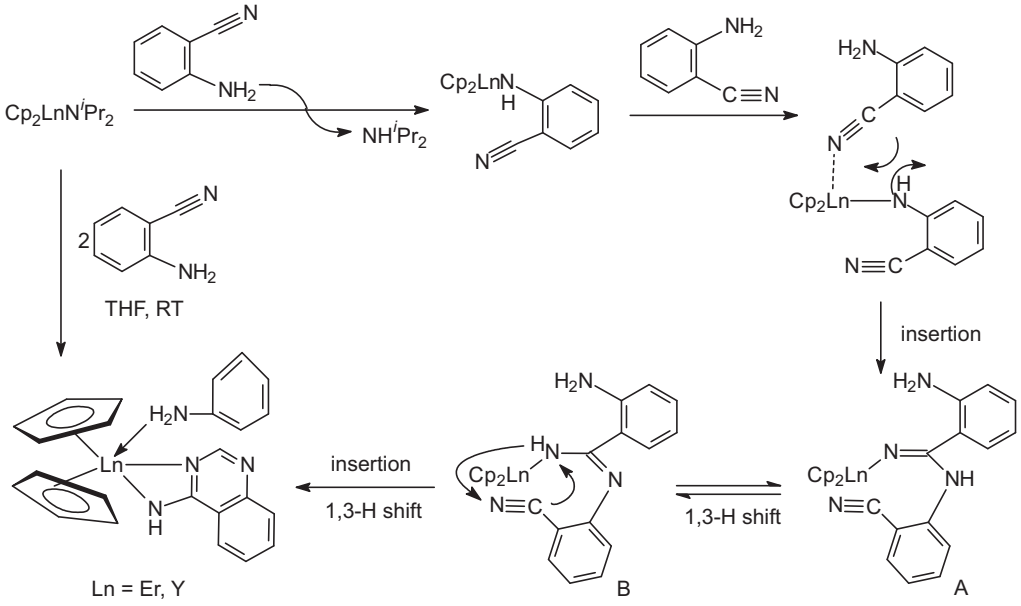

Scheme 67.

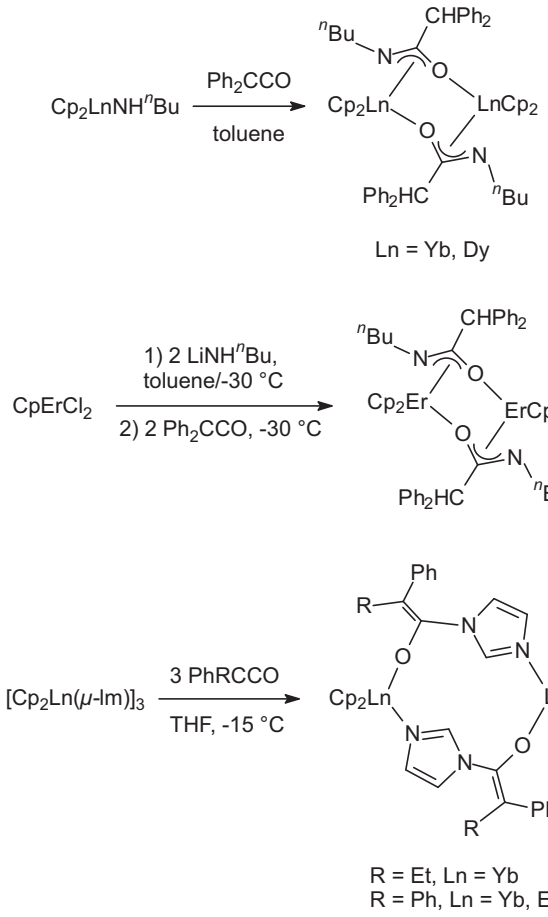

Scheme 68.

ene salt $K_2[C_8H_4\{Si^iPr_3\text{-}1,4\}_2]$ with $[Cp^*Sm(\mu\text{-}I)(THF)_2]_2$. X-ray crystallography showed the Sm(II)/Sm(III) mixed-valence cluster compound to contain a centrosymmetric hexanuclear array of Cp*Sm units, bridged by face-centered μ_3-methoxy groups, with

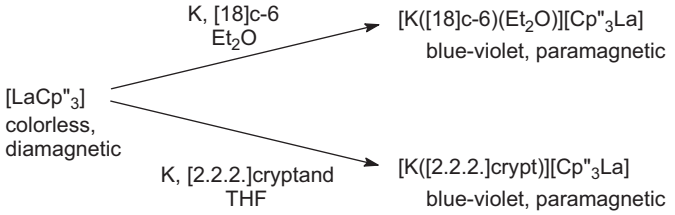

Scheme 70.

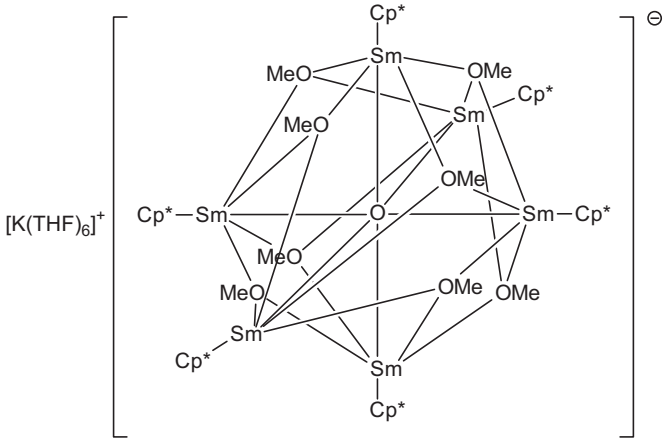

Scheme 71.

a central oxo unit. Presumably the oxo and methoxy groups in the cluster were derived from ring opening of THF [54].

Mono-Cp* lutetium complexes supported by a monoanionic, tridentate ligand system formed by dearomatization and functionalization of a 2,2′:6′,2″-terpyridine have been treated with the fluorinated anilines $4\text{-}FC_6H_4NH_2$ and $C_6F_5NH_2$ to give the corresponding terminal mono(amide)lutetium(III) complexes (Scheme 72), which have been fully characterized. The pentafluoroanilide derivative $[^tBu_3(2'\text{-}Me_3SiCH_2)tpy]Cp^*Lu\text{-}(NHC_6F_5)$ has been structurally characterized. The fluorinated anilide complexes $[^tBu_3(2'\text{-}Me_3SiCH_2)tpy]Cp^*Lu(NHAr_F)$ ($Ar_F = 4\text{-}FC_6H_4$, C_6F_5) pro-

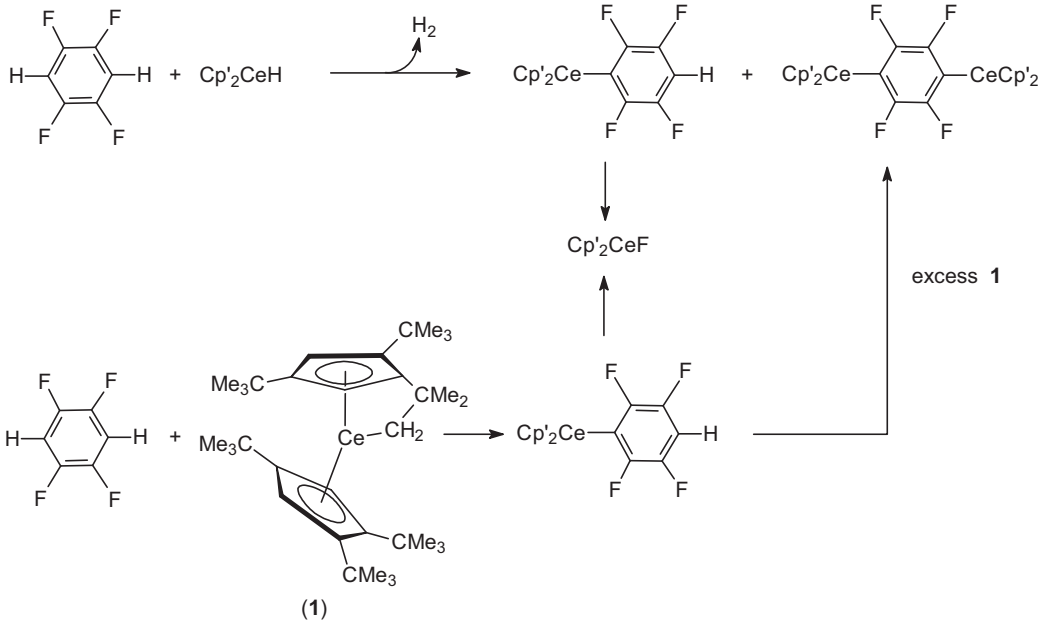

Scheme 69.

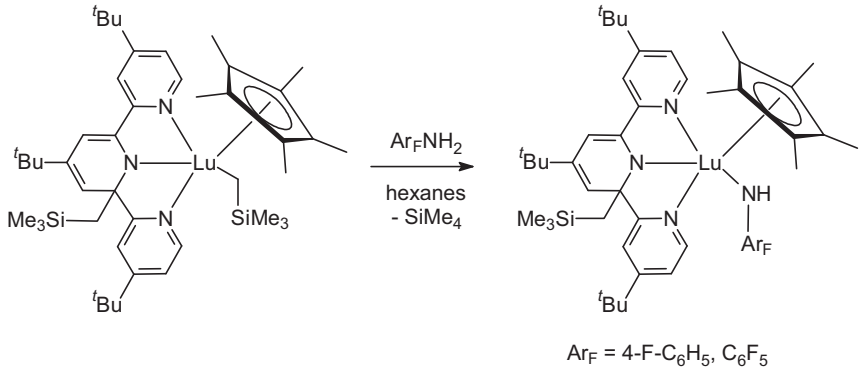

Scheme 72.

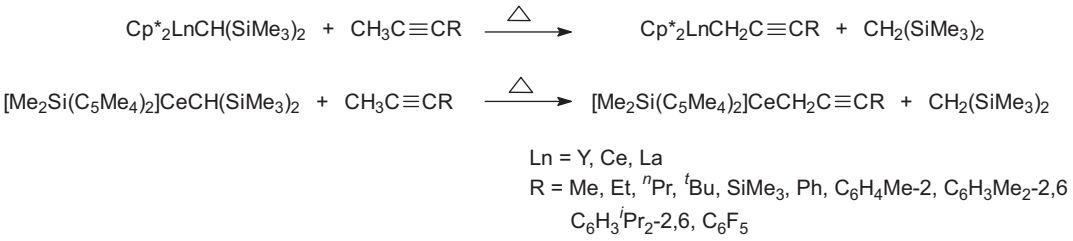

Scheme 73.

vide rare examples of lutetium organofluorine complexes, with the latter featuring an intramolecular F. . .H–C interaction that is present in both solid state and solution [21].

2.4.5.2. Bis(pentamethylcyclopentadienyl)lanthanide(III) compounds. The synthesis, structure, and reactivity of rare-earth metallocene η^3-propargyl/allenyl complexes have been studied in detail. Reactions of the alkyl complexes $Cp^*_2LnCH(SiMe_3)_2$ (Ln = Y, Ce, La) and $[Me_2Si(\eta^5\text{-}C_5Me_4)_2]CeCH(SiMe_3)_2$ with 1-methylalk-2-ynes $CH_3C{\equiv}CR$ (R = Me, Et, ^{n}Pr ^{t}Bu, $SiMe_3$, Ph, C_6H_4Me-2, $C_6H_3Me_2$-2,6, $C_6H_3{}^i Pr_2$-2,6, C_6F_5) according to Scheme 73 afforded the corresponding η^3-propargyl/allenyl complexes $Cp^*_2LnCH_2CCR$ and $[Me_2Si(\eta^5\text{-}C_5Me_4)_2]CeCH_2CCR$ *via* propargylic metalation. The hydride complexes $[Cp^*_2Ln(\mu\text{-}H)]_2$ (Ln = Y, Ce, La) react rapidly with $CH_3C{\equiv}CR$ to produce mixtures of insertion and propargylic metalation products, and the relative rate of these processes depends on the metal and alkyne substituent. Selected η^3-propargyl/allenyl complexes $Cp^*_2YCH_2CCR$ (R = Me, Ph), $Cp^*_2CeCH_2CCR$ (R = Me, Ph), $Cp^*_2CeCH(Me)CCEt$, $Cp^*_2LaCH_2CCR$ (R = Ph, $C_6H_3Me_2$-2,6) were obtained on a preparative scale and characterized by NMR spectroscopy, IR spectroscopy, and cryoscopy, and were also characterized by single-crystal X-ray diffraction. The reactions of the η^3-propargyl/allenyl complexes with Brønsted acids, such as alcohols and acetylenes, afforded the corresponding substituted allenes ($RCH{=}C{=}CH_2$) and 1-methylalk-2-ynes ($CH_3C{\equiv}CR$) as organic products, while reactions with Lewis bases, such as pyridine and THF, yielded the corresponding base adducts [55].

In a related study, diazomethane insertion into lanthanide- and yttrium-C(allyl) bonds has been investigated. It was found that (trimethylsilyl)diazomethane, Me_3SiCHN_2, is not metalated by the metallocene allyl complexes $Cp^*_2Ln(\eta^3\text{-}CH_2CHCH_2)$ but instead inserts to form the lanthanide hydrazonato complexes $Cp^*_2Ln[\eta^2(N,N')\text{-}RNN{=}CHSiMe_3]$ (R = $CH_2{=}CHCH_2$; Ln = Sm, La, Y).

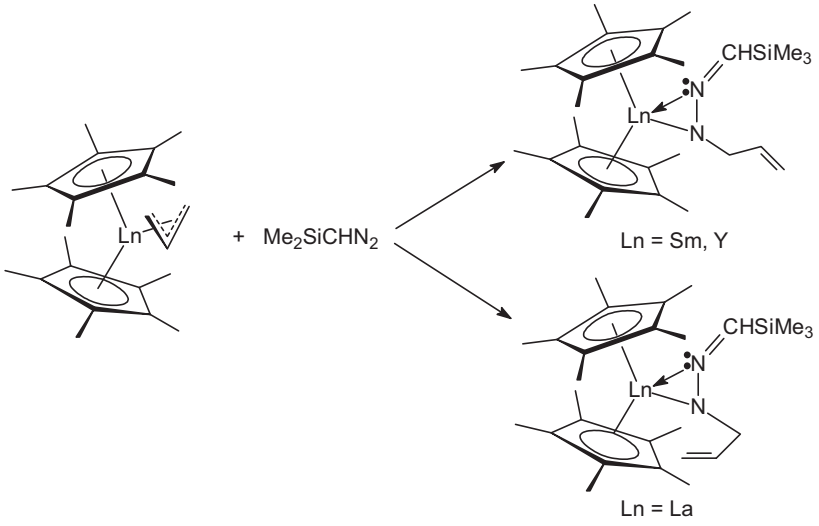

Scheme 74.

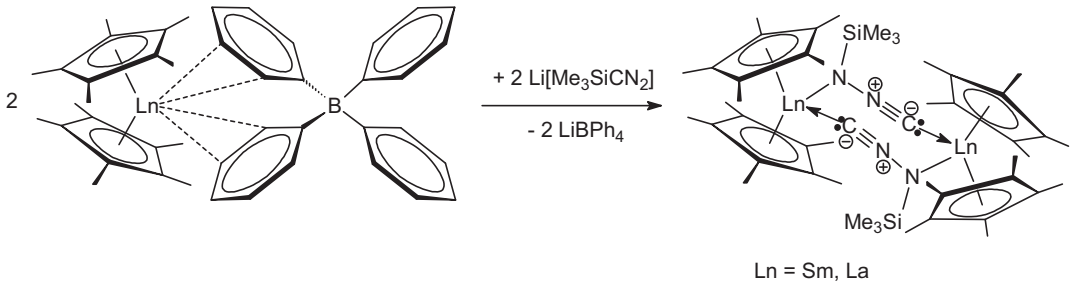

Scheme 75.

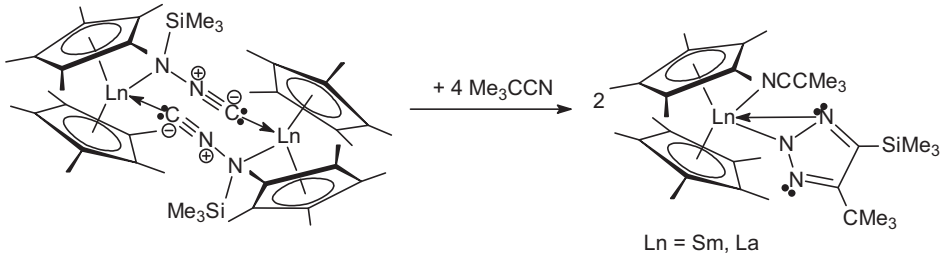

Scheme 76.

The reaction provides a facile route to crystallographically characterized hydrazonato complexes of yttrium and lanthanide metals. These hydrazonato ligands contain a tethered olefin derived from the allyl group and can be obtained from diazoalkanes that have a hydrogen substituent. Although the La, Y, and Sm complexes are isomorphous, the double bond in the allyl substituent is oriented toward La and away from Y and Sm (Scheme 74) [56].

The complexes $[Cp^*_2Ln][(\mu\text{-}Ph)_2BPh_2]$ (Ln = Sm, La) react with the salt obtained from ^{i}BuLi and Me_3SiCHN_2 in hexane (Scheme 75) to form products formulated as isomorphous bimetallic isocyanotrimethylsilyl amide complexes, $[Cp^*_2Ln\{\mu\text{-}N(SiMe_3)NC\}]_2$ (Ln = Sm, La) on the basis of structural and reactivity data. This requires a 1,3-silyl migration from carbon to nitrogen if the lithium salt has a carbon-bound silyl group [57].

The products shown in Scheme 75 react with nitriles to make products containing triazole rings. Reactivity was observed with acetonitrile, but crystal quality precluded definitive identification of the products. However, Me_3CCN reacts with both compounds to form the isomorphous 1,2,3-triazolato complexes $Cp^*_2Ln(NCCMe_3)[NNC(SiMe_3)C(CMe_3)N]$ (Scheme 76; Ln = Sm, La) that could be fully characterized by X-ray crystallography. The data clearly showed the heterocycle as a 1,2,3-triazole, a result that once again requires silyl migration if the starting materials have silyl groups bound to N and not C [57].

To probe this system further, the reaction of Me_3SiN_3 with the lanthanum precursor was examined. A trimeric azide product was obtained, $[Cp^*_2La\{CNN(SiMe_3)_2\}(\mu\text{-}N_3)]_3$ (Scheme 77) as an adduct of an isocyanide $(Me_3Si)_2NNC$ generated in the course of the reaction. The isolation of $(Me_3Si)_2NNC$ rather than $(Me_3Si)_2CN_2$ again supported the assignment of *N*-bound Me_3Si in the isocyanotrimethylsilyl amide complexes shown in Scheme 75 [57].

Reaction of the lanthanide metallocene allyl complexes, $Cp^*_2Ln(\eta^3\text{-}CH_2CHCH_2)(THF)$ (Ln = Ce, Sm, Y) with the bicyclic guanidine 1,3,4,6,7,8-hexahydro-2*H*-pyrimido[1,2-*a*]pyrimidine, Hhpp, forms a series of metallocene complexes, $Cp^*_2Ln(hpp)$ (Ln = Ce, Sm, Y) in which the $(hpp)^-$ anion coordinates as a terminal bidentate ligand (Scheme 78). Isomorphous structures were observed by X-ray crystallography regardless of the size of the metal [58].

The acetonitrile adduct $Cp^*_2Sm(hpp)(MeCN)$ (Scheme 79) was also crystallographically characterized to provide an unusual pair of eight- and nine-coordinate complexes. The coordinated MeCN can be easily removed under vacuum at room temperature to regenerate the unsolvated complex [58].

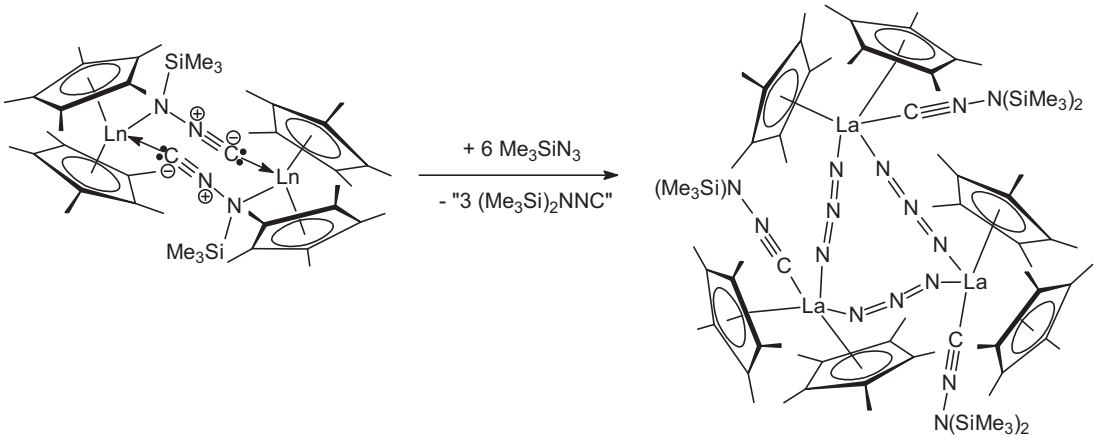

Scheme 77.

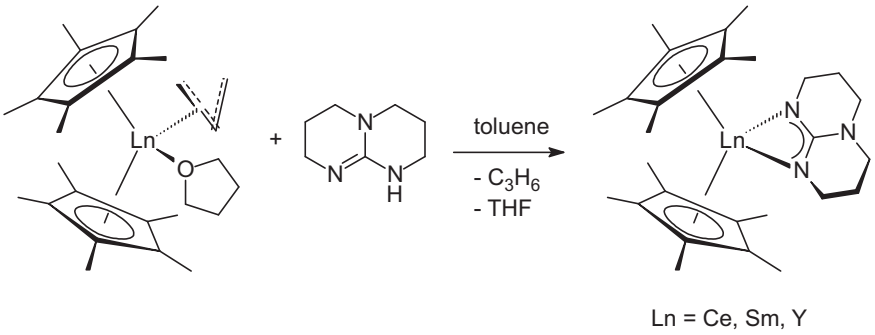

Scheme 78.

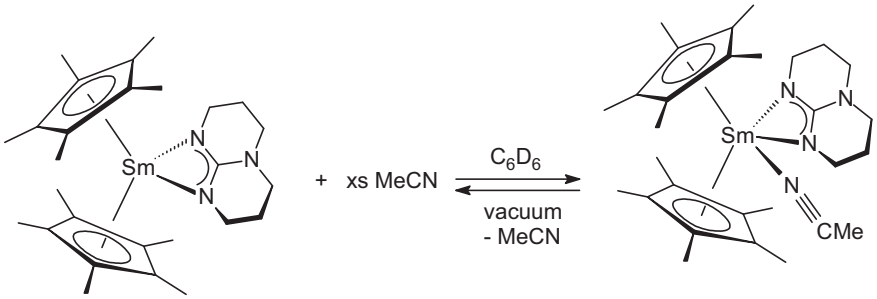

Scheme 79.

The coordination mode of the $(hpp)^-$ anion in these complexes was compared with that in other heteroallylic metallocenes like the caprolactamate $Cp^*_2Y(ONC_6H_{10})$ and the dithiocarbamate $Cp^*_2Sm(S_2CNEt_2)$, which were also structurally characterized. As shown in Scheme 80, the caprolactamate was also made *via* the allyl complex route, while the dithiocarbamate was prepared by a redox reaction between tetraethylthiuram disulfide and the divalent precursor $Cp^*_2Sm(THF)_2$ [58].

The reductive reactivity of lanthanide hydride ligands in the $[Cp^*_2LnH]_x$ complexes (Ln = Sm, La, Y) was examined to see if these hydride ligands would react like the actinide hydrides in $[Cp^*_2AnH_2]_2$ (An = U, Th) and $[Cp^*_2UH]_2$. For example, each lanthanide hydride complex reduces PhSSPh to make $[Cp^*_2Ln(\mu\text{-}SPh)]_2$ in ~90% yield. Scheme 81 illustrates the reaction with the Sm derivative [59].

$[Cp^*_2SmH]_2$ reduces phenazine and anthracene to make $[Cp^*_2Sm]_2(\mu\text{-}\eta^3\text{:}\eta^3\text{-}C_{12}H_8N_2)$ (Scheme 82) and $[Cp^*_2Sm]_2(\mu\text{-}\eta^3\text{:}\eta^3\text{-}C_{10}H_{14})$, respectively, but the analogous $[Cp^*_2LaH]_x$ and $[Cp^*_2YH]_2$ reactions were found to be more complicated [59].

All three lanthanide hydrides reduce 1,3,5,7-cyclooctatetraene (=C_8H_8) (shown in Scheme 83 for Sm) to generate $Cp^*Ln(COT)$ ($COT = C_8H_8^{2-}$) and Cp^*_3Ln, a reaction that constitutes another synthetic route to Cp^*_3Ln complexes [59].

In the analogous reaction of $[Cp^*_2YH]_2$ with C_8H_8, two unusual byproducts were obtained. In benzene, a $Cp^*Y[(\eta^5\text{-}C_5Me_4CH_2\text{-}C_5Me_4CH_2\text{-}\eta^3)]$ complex formed in which two $(C_5Me_5)^{1-}$ rings are linked to make a new type of *ansa*-allyl-cyclopentadienyl dianion that binds as a pentahapto–trihapto chelate (Scheme 84) [59].

When the same reaction was carried out in cyclohexane, a $Cp^*_2Y(\mu\text{-}\eta^8\text{:}\eta^1\text{-}C_8H_7)YCp^*$ complex was formed in which a

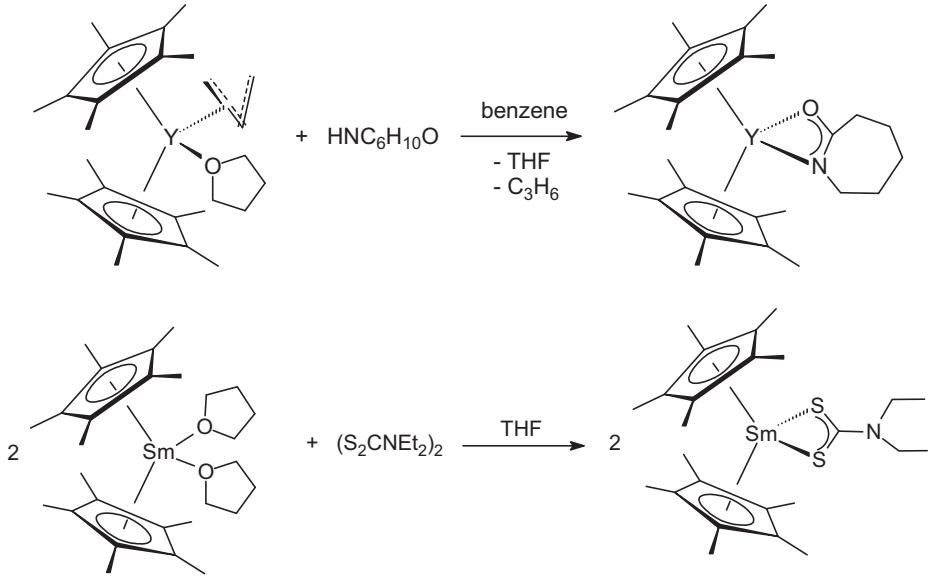

Scheme 80.

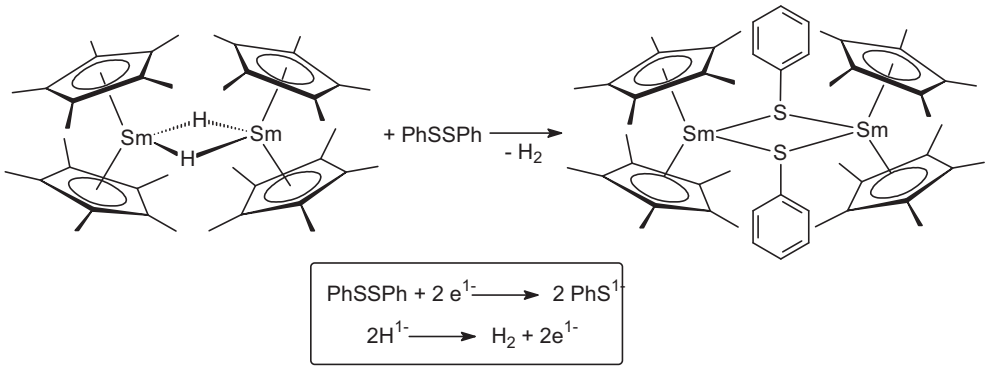

Scheme 81.

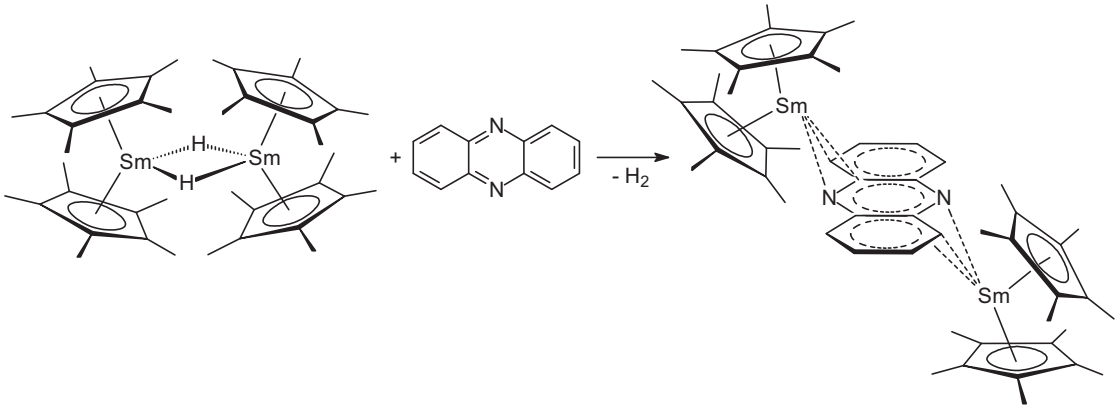

Scheme 82.

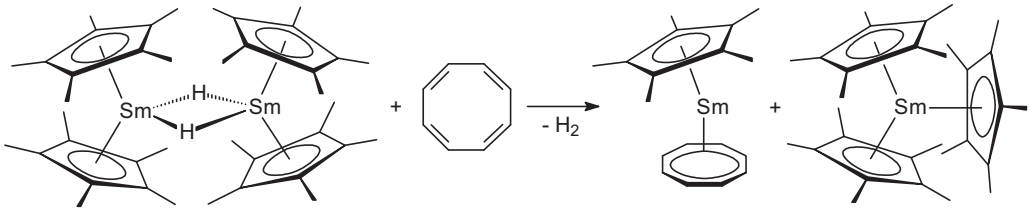

Scheme 83.

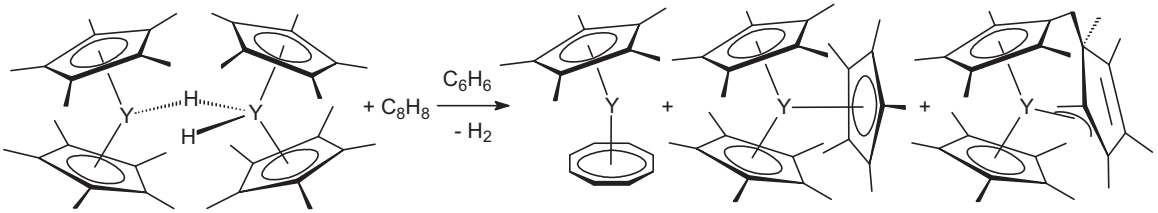

Scheme 84.

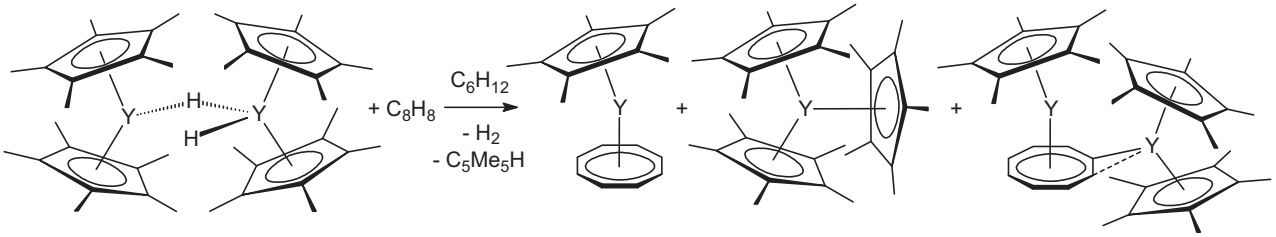

Scheme 85.

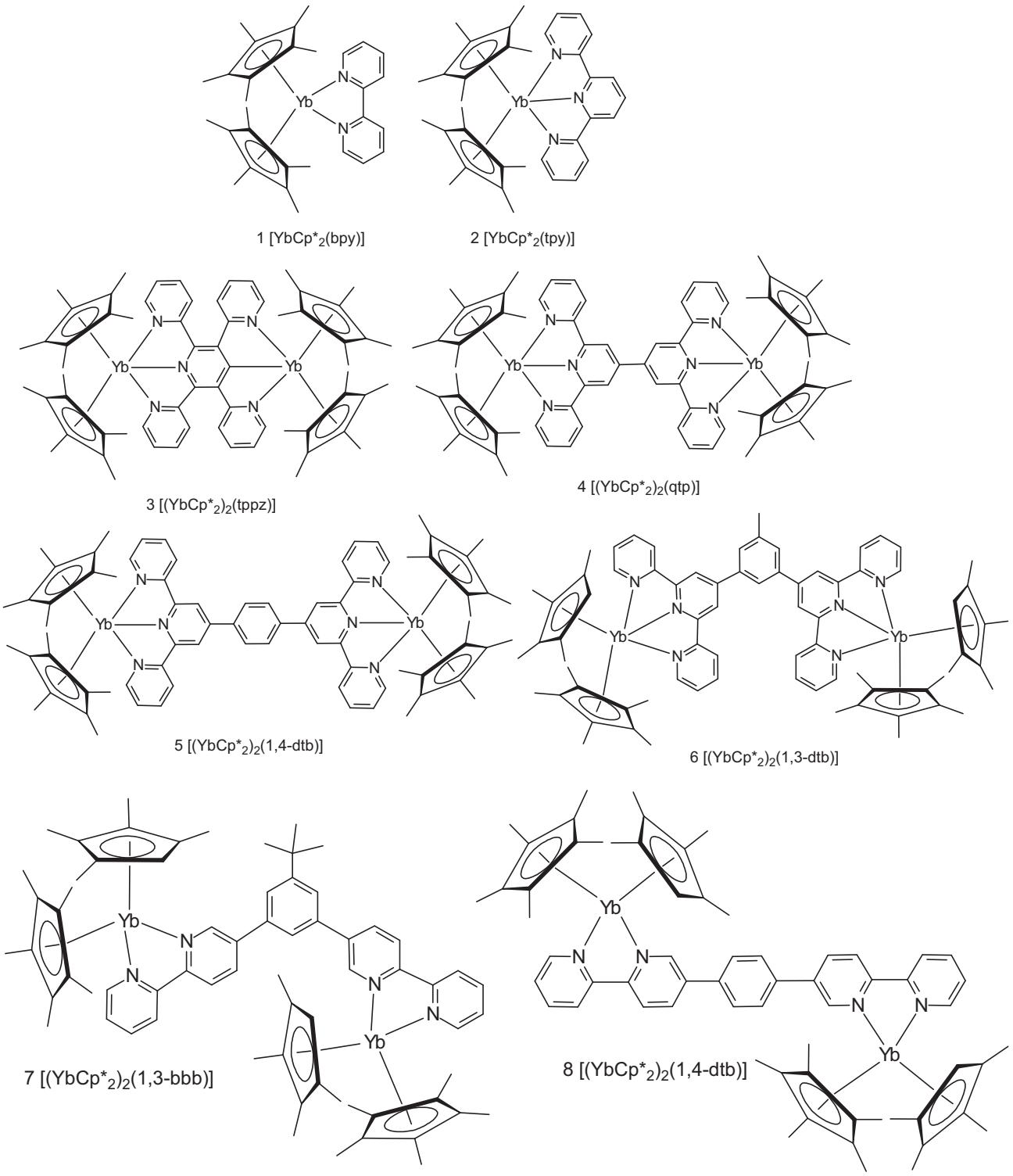

Scheme 86.

$(C_8H_8)^{2-}$ ring is metalated to form a bridging $(C_8H_7)^{3-}$ trianion (Scheme 85) [59].

Thus although the hydride ligands in lanthanide complexes $[Cp^*_2SmH]_2$, $[Cp^*_2LaH]_x$, and $[Cp^*_2YH]_2$ can act as reductants with some substrates, their reaction chemistry was found to be more complicated than that observed for the actinide hydrides, $[Cp^*_2UH]_2$, $[Cp^*_2UH_2]_2$, and $[Cp^*_2ThH_2]_2$. The latter complexes cleanly reduce C_8H_8, PhSSPh, and PhNNPh, whereas the $[Cp^*_2LnH]_x$ complexes react cleanly only with PhSSPh. The reactions of $[Cp^*_2YH]_2$ with C_8H_8 were particularly unusual and showed new opportunities in lanthanide metallocene C–H activation and insertion chemistry. The isolation of the $(\eta^8{:}\eta^1\text{-}C_8H_7)^{3-}$ and $(\eta^5\text{-}C_5Me_4CH_2\text{-}C_5Me_4CH_2\text{-}\eta^3)^{2-}$ ligands from this reaction manifold indicated that new aspects of $(C_5Me_5)^{1-}$ reaction and coordination chemistry remain to be discovered with these metals [59].

Bimetallic ytterbocene complexes with bridging *N*-heterocylic ligands have become a favorite subject of study in recent years due to their potential applications ranging from molecular wires

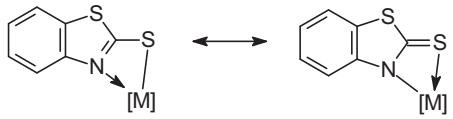

Scheme 87. Two hybrid forms of the chelating SBT ligand [62].

to single-molecule magnets. In 2008, the impact of bridging ligand geometry on the electronic and magnetic properties of bimetallic ytterbocene complexes has been studied in great detail and compiled in a "Concept" article [60]. In this article recent results have been reviewed for a series of ytterbocene polypyridyl bimetallic complexes to highlight the versatility and tunability of these systems based on simple changes in bridging ligand geometry. The neutral complexes **1**–**8** shown in Scheme 86 were prepared by adding a solution of $Cp^*_2Yb(OEt_2)$ in toluene to the nitrogen ligands at room temperature under inert atmosphere to provide complexes ranging in color from dark green to dark blue in moderate to good yield. The neutral products are soluble in toluene and THF and display limited solubility in alkane solvents. In addition, the neutral complexes react with halogenated solvents and there is some evidence that the polypyridyl ligands are displaced by solvent in acetonitrile. All products were found to be quite air and moisture sensitive, decomposing quickly to provide uncharacterized brown materials. The detailed investigations involved structural, electrochemical, optical, and magnetic measurements with the goal of better understanding the electronic and magnetic communication between the two ytterbium metal centers in this interesting class of bimetallics [60].

Terpyridine complexes have been employed for a direct comparison of the magnetic and electronic properties of samarocene and ytterbocene. For this purpose, a new complex, $Cp^*_2Sm(tpy)$ (tpy = 2,2′:6′,2″-terpyridine) and its one-electron oxidized congener $[Cp^*_2Sm(tpy)]PF_6$ have been synthesized and characterized with the aim of comparing their electronic and magnetic behavior to the known ytterbium analogues: $Cp^*_2Yb(tpy)$ and $[Cp^*_2Yb(tpy)]OTf$. These new samarium complexes have been characterized using single-crystal X-ray diffraction, ^1H NMR spectroscopy, cyclic voltammetry, optical spectroscopy, and bulk magnetic susceptibility measurements. All data for $Cp^*_2Sm(tpy)$ indicated a Sm(III)-$tpy^{\bullet-}$ $[(4f)^5\text{-}(\pi^*)^1]$ ground-state electronic configuration similar to that found previously for $Cp^*_2Yb(tpy)$ $[(4f)^{13}\text{-}(\pi^*)^1]$. Structural comparisons revealed that there are no significant changes in the overall geometries associated with the neutral and cationic samarium and ytterbium congeners aside from those anticipated based upon the lanthanide contraction. The redox potentials for the divalent $Cp^*_2Ln(THF)_n$ precursors ($E_{1/2}(Sm^{2+}) = -2.12$ V, $E_{1/2}(Yb^{2+}) = -1.48$ V) were found to be consistent with established trends, *i.e.* the redox potentials (metal-based reduction and ligand-based oxidation) for $Cp^*_2Sm(tpy)$ are nearly identical to those for $Cp^*_2Yb(tpy)$. The correlation in the optical spectra of $Cp^*_2Sm(tpy)$ and $Cp^*_2Yb(tpy)$ was excellent, as expected for this ligand-radical based electronic structural assignment, but there did appear to be a red-shift ($\sim$400 cm^{-1}) in all of the bands of $Cp^*_2Sm(tpy)$ relative to those of $Cp^*_2Yb(tpy)$ that suggested a slightly greater stabilization of the π^* level(s) in the samarium(III) complex compared to that in the ytterbium(III) complex. Similar spectroscopic overlap was observed for the monocationic complexes $[Cp^*_2Sm(tpy)]PF_6$ and $[Cp^*_2Yb(tpy)]OTf$. Bulk magnetic susceptibility measurements for $Cp^*_2Sm(tpy)$ revealed significantly different behavior than those of $Cp^*_2Yb(tpy)$ due to differences in the electronic-state structure of the two metal ions [61]. Several organolanthanide complexes containing the 2-mercapto benzothiazolate (=SBT) ligand (Scheme 87) have been synthesized and fully characterized [62].

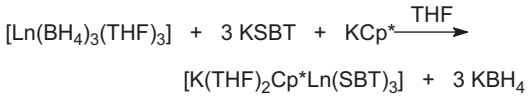

Scheme 88.

The compounds $[K(THF)_2Cp^*Ln(SBT)_3]$ (Scheme 88) were obtained by treating $Ln(BH_4)_3(THF)_3$ with KSBT and KCp*; isomorphous crystals of $[K(15\text{-crown-}5)_2][Cp^*Ln(SBT)_3]\cdot THF$ [Ln = La, Ce, Nd] were formed upon addition of 15-crown-5 [62].

2.4.6. Pentalenyl, indenyl and fluorenyl compounds

Samarium(III) pentalene sandwich compounds have been synthesized and structurally characterized. The reaction of the pentalene salt $K_2[C_8H_4\{Si^iPr_3\text{-}1,4\}_2]$ with $[Cp^*Sm(\mu\text{-}I)(THF)_2]_2$ yielded not the expected Sm(II) pentalene-bridged dimer but the Sm(III) sandwich complexes $Cp^*Sm(\eta^8\text{-}C_8H_4\{Si^iPr_3\text{-}1,4\}_2)$ and $[Sm(\eta^8\text{-}C_8H_4\{Si^iPr_3\text{-}1,4\}_2)(\eta^5\text{-}C_8H_5\{Si^iPr_3\text{-}1,4\}_2)]$ (Scheme 89) and the mixed-valence cluster $[K(THF)_6][Cp^*_6Sm_6(OMe)_8O]$ (*cf.* Section 2.4.5.1) *via* solvent activation of THF. The samarium(III) sandwich compound $[Sm(\eta^8\text{-}C_8H_4\{Si^iPr_3\text{-}1,4\}_2)(\eta^5\text{-}C_8H_5\{Si^iPr_3\text{-}1,4\}_2)]$ incorporates an η^8-pentalene ligand and an η^5-hydropentalenyl ligand [54].

Two series of new organolanthanide(II) complexes with tetrahydro-2H-pyranyl- or *N*-piperidineethyl-functionalized fluorenyl ligands were synthesized *via* one-electron reductive elimination reaction. Treatment of $[(Me_3Si)_2N]_3Ln^{III}(\mu\text{-}Cl)Li(THF)_3$ with 2 equiv. of $C_5H_9OCH_2C_{13}H_9$ or $C_5H_{10}NCH_2CH_2C_{13}H_9$, respectively, in toluene at about 80 °C produced, after workup, the corresponding organolanthanide(II) complexes with formula $[\eta^5\text{:}\eta^1\text{-}C_5H_9OCH_2C_{13}H_8]_2Ln^{II}$ (Ln = Yb, Eu) and $[\eta^5\text{:}\eta^1\text{-}C_5H_{10}NCH_2CH_2\text{-}C_{13}H_8]_2Ln^{II}$ (Ln = Yb, Eu) in good yields (Scheme 90) [63].

All new divalent lanthanide fluorenyl compounds were fully characterized by spectroscopic methods and elemental analyses. The structures of three complexes were additionally determined by single-crystal X-ray analyses. It represents the first example of solvent-free organolanthanide(II) complexes with fluorenyl ligands [63].

New bis(indenyl) silylamide complexes $(2\text{-R-Ind})_2Ln[N(SiMe_3)_2]$ (Ln = Gd, R = H, Me, Ph; Ln = Sc, R = Me) were prepared following a two step one-pot procedure, by the reaction of (2-R-Indenyl)Li (R = H, Me, Ph) with $LnCl_3$ (Ln = Gd, Sc) in THF, and treatment of the resulting chloride derivatives with $K[N(SiMe_3)_2]$ in toluene, after the removal of THF in vacuum (Scheme 91). High

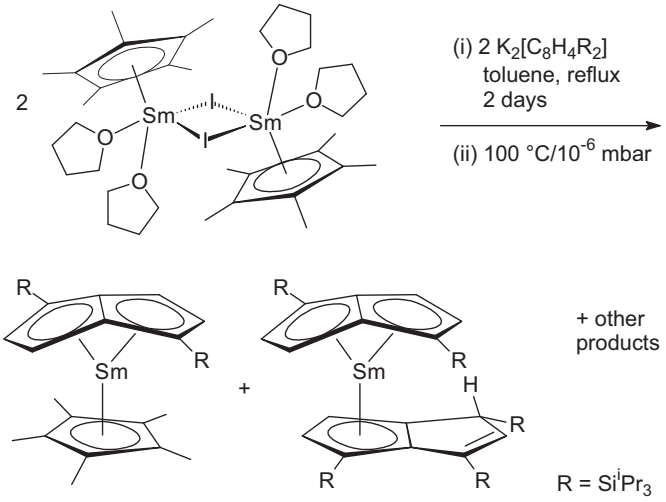

Scheme 89.

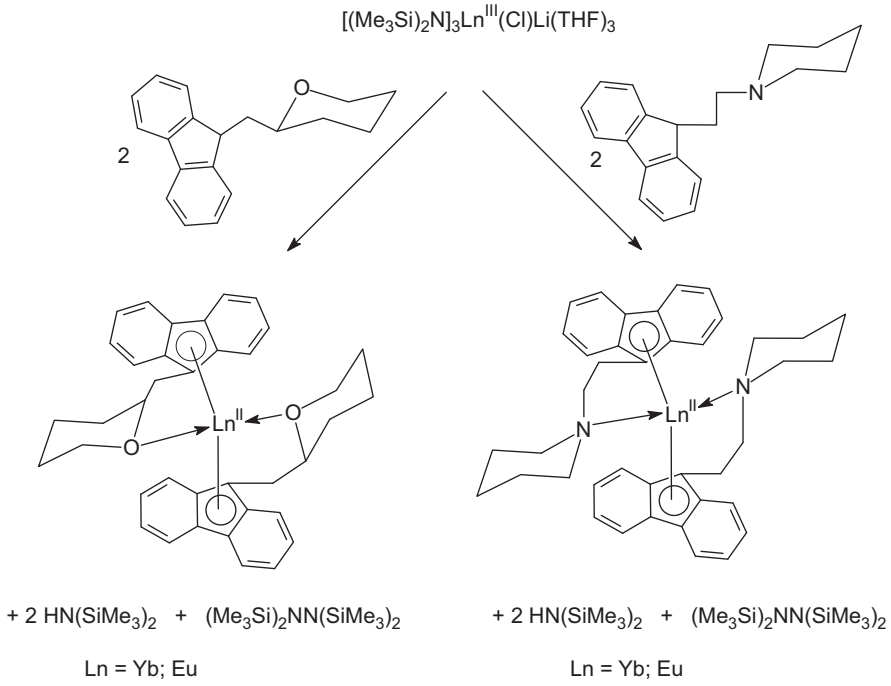

Scheme 90.

activity and extremely high yields of 1,4-*cis*- polybutadiene could be achieved by using the new bis(indenyl) silylamide rare-earth complexes in cooperation with a borate salt, and $^{i}Bu_3Al$ (*cf.* Section 2.9.1) [64].

The cationization of these complexes, using $[PhNMe_2H][B(C_6F_5)_4]$, and $[Ph_3C][B(C_6F_5)_4]$ as illustrated in Scheme 92, occurred by selective displacement of one indenyl ligand, affording new cationic mono(indenyl) amido rare-earth compounds [64].

The synthesis and structural characterization of a pending-arm mono(fluorenyl) complex, $(COT)Pr(C_{13}H_8CH_2CH_2OMe)(THF)$, containing the chelating 9-(2-methoxyethyl)fluorenyl ligand have been reported [65]. Treatment of a THF solution of $KC_{13}H_8CH_2CH_2OMe$ with $[(COT)Pr(\mu\text{-}Cl)(THF)_2]_2$ in a molar ratio of 2:1 according to Scheme 93 afforded the constrained-geometry praseodymium sandwich complex $(COT)Pr(C_{13}H_8CH_2CH_2OMe)(THF)$ in moderate yield (45%) in the form of yellow, highly air-sensitive single-crystals which were suitable for X-ray diffraction. As shown in Fig. 3, the central praseodymium atom is formally 9-coordinated by an η^8-cyclooctatetraenyl ligand, the chelating 9-(2-methoxyethyl)fluorenyl ligand bonded η^5 through the five-membered ring, and an additional THF ligand. As expected, the oxygen atom of the pendant-arm CH_2CH_2OMe functionality participates in the coordination to Pr. The corresponding Pr–O bond length is 2.5590(14) Å, while the Pr–O distance to the oxygen atom of the THF ligand is 2.6023(15) Å [65].

Fluorenyl modified *N*-heterocyclic carbene ligated rare-earth metal bis(alkyl) complexes, $(Flu\text{-}NHC)Ln(CH_2SiMe_3)_2$ (Flu-NHC=$(C_{13}H_8CH_2CH_2(NCHCCHN)\text{-}C_6H_2Me_3$-2,4,6); Ln = Sc, Y, Ho, Lu), were synthesized according to Scheme 94 and fully characterized by NMR and X-ray diffraction analyses [66].

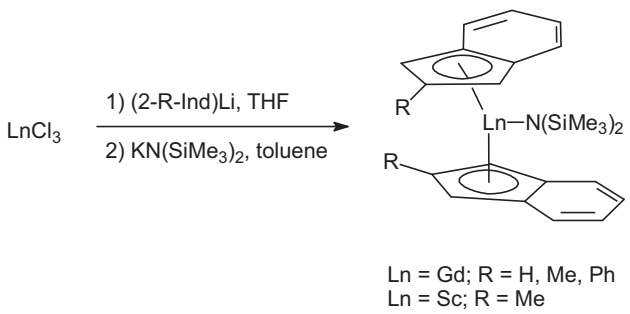

Scheme 91.

2.5. Organolanthanide complexes with cyclopentadienyl-like ligands

2.5.1. Compounds with heteroatom five-membered ring ligands

The synthesis, structural characterization, and styrene polymerization catalysis of cationic rare earth (*o*-dimethylaminobenzyl)

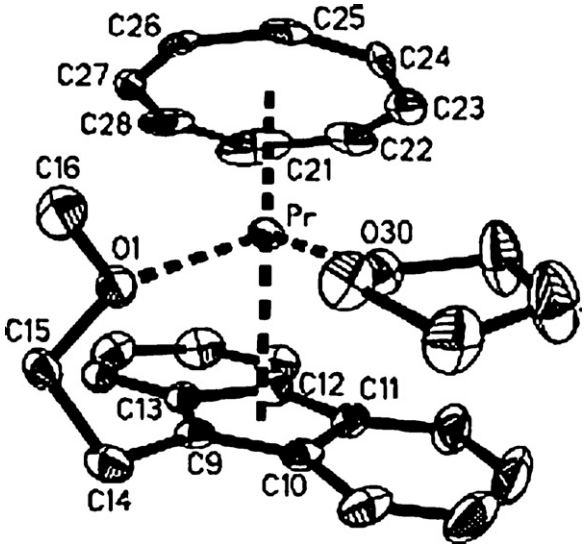

Fig. 3. Molecular structure of $(COT)Pr(C_{13}H_8CH_2CH_2OMe)(THF)$ [65].

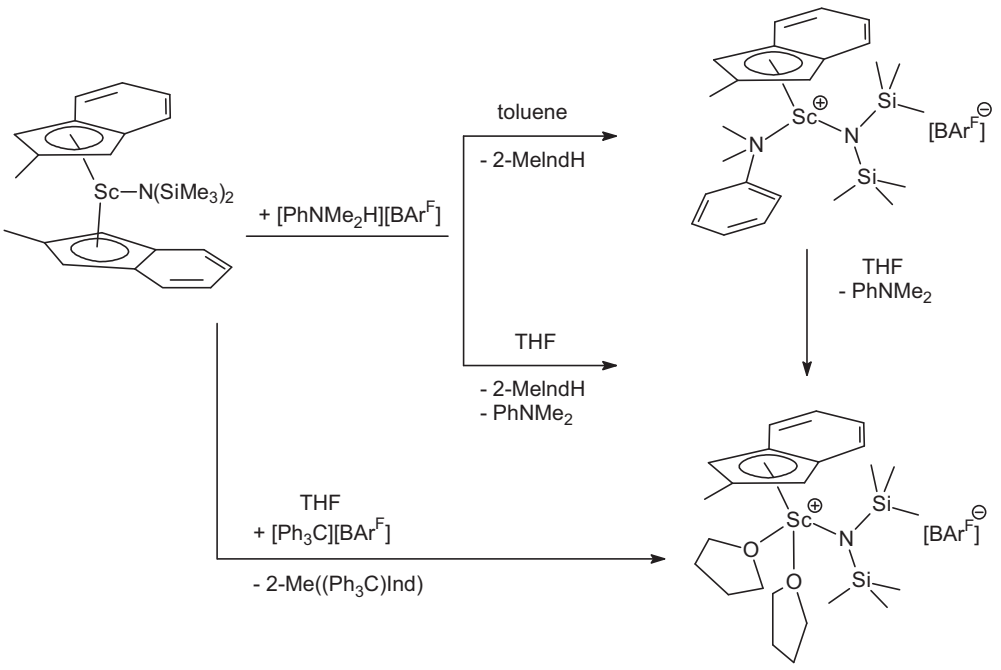

Scheme 92.

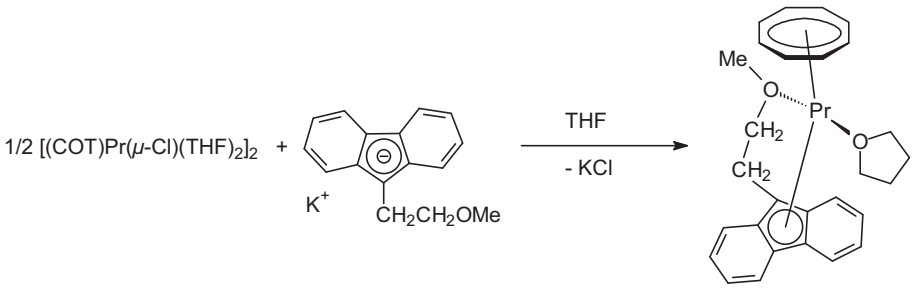

Scheme 93.

complexes bearing η^5- and η^1-pyrrolyl ligands has been reported. It was found that the coordination mode (η^1 or η^5) of the pyrrolyl ligands can show dramatic influence on the polymerization activity (*cf.* Section 2.9.1.1). The acid–base reaction of the rare earth tris(*o*-dimethylaminobenzyl) complexes $Ln(CH_2C_6H_4NMe_2\text{-}o)_3$ with 1 equiv. of 2,5-^{t}Bu$_2$C$_4$H$_2$NH gave in high yields the corresponding mono(pyrrolyl)-ligated bis(aminobenzyl) complexes (η^5-2,5-^{t}Bu$_2$C$_4$H$_2$N)Ln-$(CH_2C_6H_4NMe_2\text{-}o)_2$ (Ln = Sc, Y, La) from the smallest scandium to the largest lanthanum (Scheme 95). X-ray analyses revealed that all of these complexes adopt a similar overall structure. The pyrrolyl ligand is bonded to the metal center in an η^5-fashion as an azacyclopentadienyl ligand and the two aminobenzyl ligands are all bonded to the metal center in a chelating fashion *via* both the benzyl CH_2 carbon atom and the amino unit. The similar reaction of $Sc(CH_2C_6H_4NMe_2\text{-}o)_3$ with 1 equiv. of tetramethylpyrrole C_4Me_4NH gave (η^1-C_4Me_4N)$Sc(CH_2C_6H_4NMe_2\text{-}o)_2$ in 64% isolated yield (Scheme 95). An X-ray diffraction study revealed that the pyrrolyl ligand is now in an η^1-*N*-σ-coordination fashion

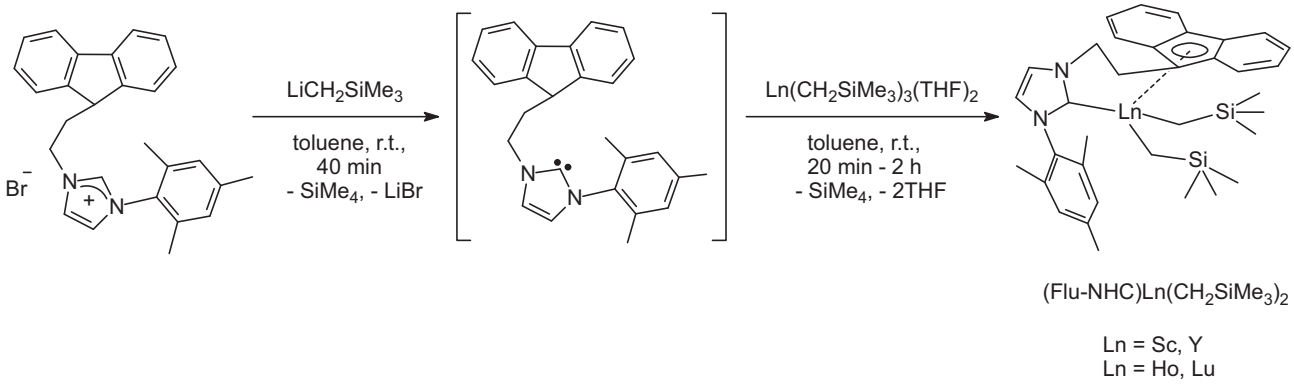

Scheme 94.

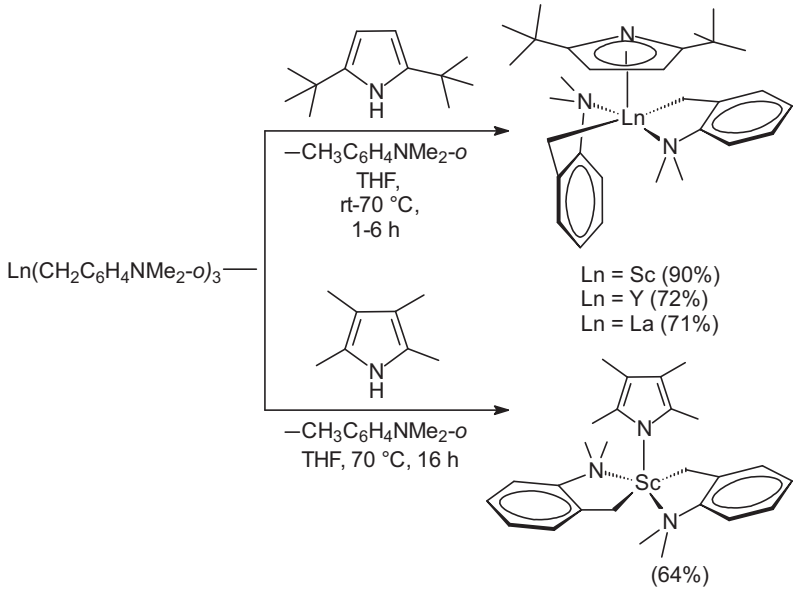

Scheme 95.

and the scandium atom lies in the pyrrolyl plane. The η^1-bonding fashion of the tetramethylpyrrolyl ligand in the Sc derivative is in sharp contrast with what was observed previously in other tetramethylpyrrolyl-coordinated metal complexes in which the pyrrolyl ligands all adopted an η^5-bonding mode. Thus this complex represents the first example of a structurally characterized η^1-bonding tetramethylpyrrolyl complex [67].

Addition of 1 equiv. of $[Ph_3C][B(C_6F_5)_4]$ to (η^5-2,5-^{t}Bu$_2$C$_4$H$_2$N)Sc($CH_2C_6H_4NMe_2$-*o*)$_2$ in toluene at 25 °C gave the corresponding cationic mono(aminobenzyl) complex [(2,5-^{t}Bu$_2$C$_4$H$_2$N)Sc($CH_2C_6H_4NMe_2$-*o*)][$B(C_6F_5)_4$] in *ca.* 90% yield (Scheme 96). Recrystallization of this product from a mixed hexane–toluene–DME solution afforded single crystals of [(2,5-^{t}Bu$_2$C$_4$H$_2$N)Sc($CH_2C_6H_4NMe_2$-*o*)(DME)][$B(C_6F_5)_4$]. An X-ray diffraction study established the presence of a separated ion pair that possesses a chelating DME ligand at the Sc center. The pyrrolyl ligand is bonded to the Sc atom in an η^5-fashion as observed in its neutral precursor. The salt represents the first example of a structurally characterized cationic pyrrolyl complex for any metal. The reaction of the η^1-tetramethylpyrrolyl-ligated complex (η^1-C_4Me_4N)Sc($CH_2C_6H_4NMe_2$-*o*)$_2$ with 1 equiv. of $[Ph_3C][B(C_6F_5)_4]$ in THF afforded [(C_4Me_4N)Sc($CH_2C_6H_4NMe_2$-*o*)(THF)$_3$][$B(C_6F_5)_4$], which possessed three THF ligands as shown by ^{1}H NMR analysis. Attempts to obtain single crystals of this compound were, however, not successful [67].

The 1,2-azaborolyl (Ab) group has been investigated as a potential isoelectronic and isolobal surrogate for the Cp ligand in many metal complexes such as Ab derivatives of group IV and VIII transition metals. In 2008, the first synthesis and characterization of a THF-coordinated bis-Ab yttrium alkyl complex, $Ab_2Y(CH_2SiMe_3)(THF)$ (Ab = 1-methyl-2-phenyl-1,2-azaborolyl), has been reported. The synthesis of this complex

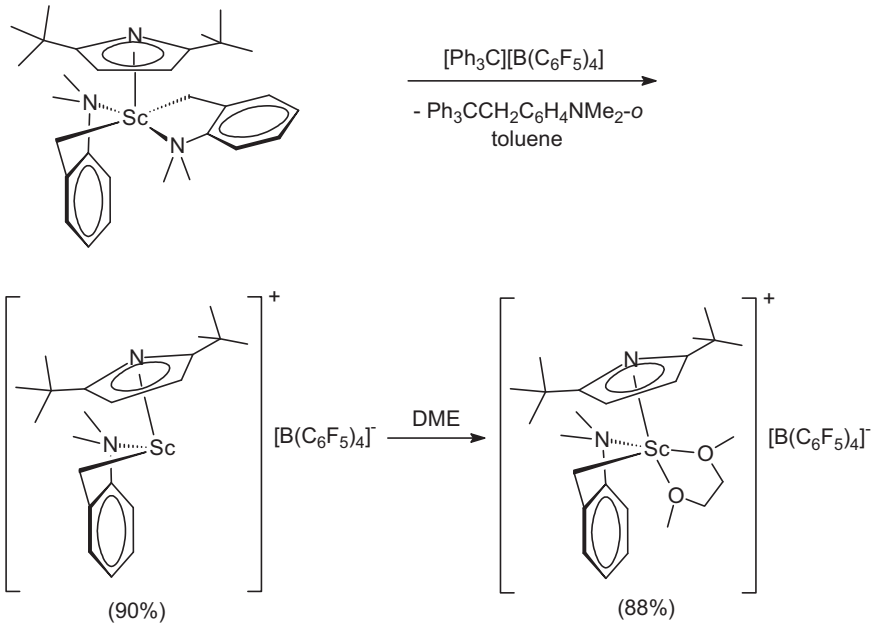

Scheme 96.

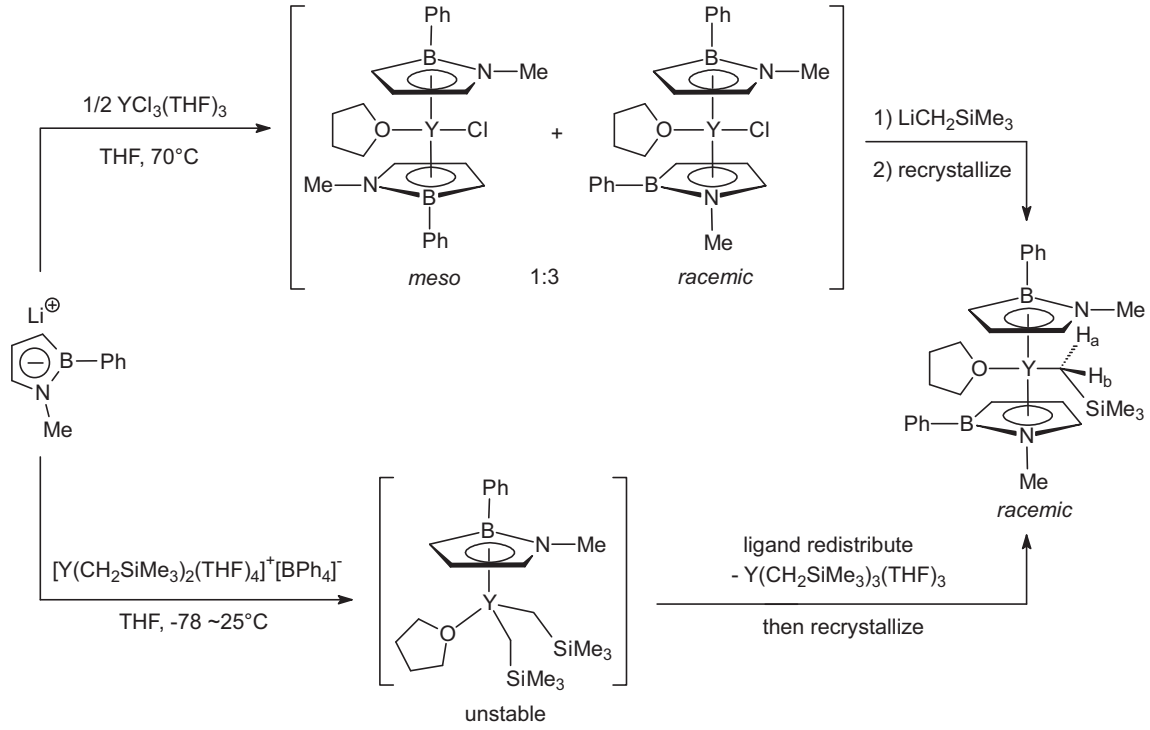

Scheme 97.

is outlined in Scheme 97. Reaction of $YCl_3(THF)_3$ with 2 equiv. of the Ab lithium species in THF afforded a THF-coordinated bis(1-methyl-2-phenyl-1,2-azaborolyl)yttrium chloride complex, which has been determined as a mixture of *meso* and *racemic* isomers in a 1:3 molar ratio by ^{1}H NMR spectroscopy. The subsequent alkylation step was carried out by treating the intermediate with 1 equiv. of $LiCH_2SiMe_3$ at −78 °C, which gave rise to the alkyl species $Ab_2Y(CH_2SiMe_3)(THF)$ (*meso*:*racemic* = 1:3) as the final product. In contrast to the chloro precursor, a *pure* racemic isomer of the alkyl complex could be obtained by repeated recrystallization in a hydrocarbon solvent such as toluene or hexane. X-ray diffraction revealed η^4-coordinated Ab rings in the racemic yttrium complex [68].

Another route for the preparation of $Ab_2Y(CH_2SiMe_3)(THF)$ was discovered unexpectedly in an attempt to synthesize a half-sandwich yttrium bis(alkyl) complex with supporting ancillary Ab ligand (Scheme 97). It was anticipated that the reaction of the monocationic yttrium species $[Y(CH_2SiMe_3)_2(THF)_4]^+[BPh_4]^-$ with the lithium salt of the Ab ligand would lead to the corresponding half-sandwich yttrium bis(alkyl) complex. However, instead of the desired bis(alkyl) derivative, only the bis-Ab yttrium complex $Ab_2Y(CH_2SiMe_3)(THF)$ and $Y(CH_2SiMe_3)_3(THF)_3$ were isolated as the final products [68].

A series of 1,2,4-diazaphospholide (dp^-) samarium complexes with a variety of coordination modes were prepared *via* the metathesis reaction of $SmCl_3(THF)_3$ and potassium 3,5-disubstituted 1,2,4-diazaphospholide or by the reaction of $Sm[N(SiMe_3)_2]_3$ with 3,5-diphenyl-1,2,4-diazaphosphole. As illustrated in Scheme 98, treatment of potassium 3,5-diphenyl-1,2,4-diazaphospholide, $[(\eta^2{:}\eta^4\text{-}3,5\text{-}Ph_2dp)K(Et_2O)]_n$, with $SmCl_3(THF)_3$ and small traces of water in THF afforded an unusual complex containing eight 3,5-Ph_2dp ligands, one oxygen, two chlorine, and four samarium atoms, as established by X-ray crystallography. The four Sm ions are arranged in a core of a tetrahedron and have a common center (O) to which the distance of each samarium is about 2.371(3) Å (average). Each samarium is seven-coordinate, being bound to three 1,2,4-diazaphospholides, to one chlorine atom (μ-bridged), and to one oxygen atom (μ_4-bridged), thus forming an oxygen-centered tetrasamarium octa(diazaphospholido) cluster. Eight phosphorus atoms are located on the sphere of the molecule [69].

A reaction of H[3,5-Ph_2dp] and $Sm[N(SiMe_3)_2]_3$ was thus carried out in toluene. After workup, the homoleptic compound Sm_2[3,5-Ph_2dp]$_4$ was isolated as yellow crystals (Scheme 99). The compound is readily soluble in aprotic polar solvents such as THF, DMSO, and hot toluene but insoluble in *n*-hexane and benzene. The X-ray structure analysis of Sm_2[3,5-Ph_2dp]$_4$ revealed a remarkable dimeric species better formulated as $[(\mu_2\text{-}\eta^2(N,N){:}\eta^5\text{-}3,5\text{-}Ph_2dp)(\eta^2(N,N)\text{-}3,5\text{-}Ph_2dp)_2Sm]_2$ containing six 3,5-Ph_2dp ligands (Fig. 4). Each Sm is 11-coordinate, being bound to four 1,2,4-diazaphospholides. In the ^{31}P{1H} NMR (DMSO-d_6, 23 °C) spectrum, only one resonance is observed at 96.08 (s) ppm, indicating that the homoleptic dimer undergoes dissociation into a solvated monomeric species in the solution (Scheme 99) [69].

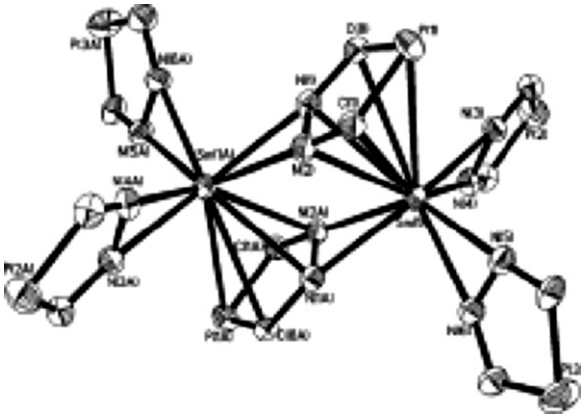

Fig. 4. Molecular structure of $[(\mu_2\text{-}\eta^2(N,N){:}\eta^5\text{-}3,5\text{-}Ph_2dp)(\eta^2(N,N)\text{-}3,5\text{-}Ph_2dp)_2Sm]_2$ [69].

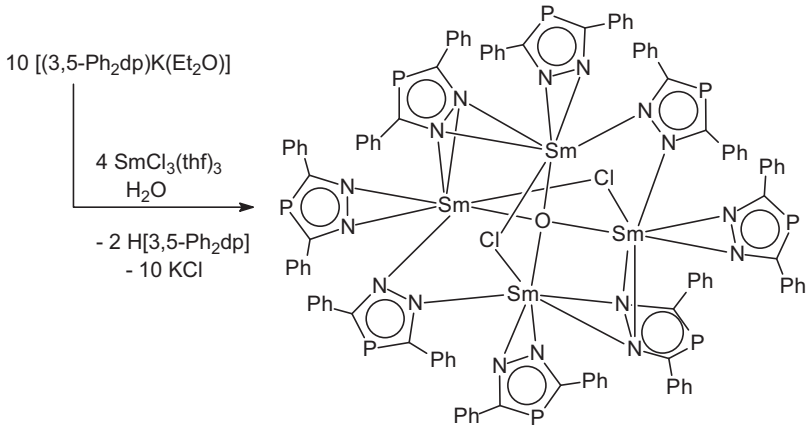

Scheme 98.

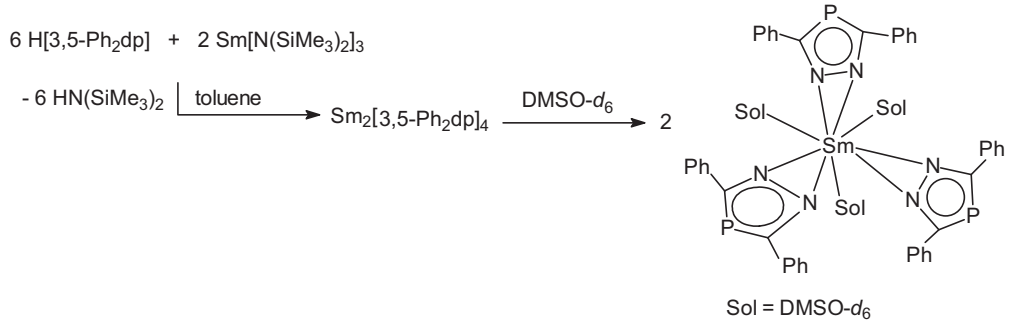

Scheme 99.

The synthesis and structural characterization of lanthanide phosphaorganometallic complexes derived from the 3,5-di-*tert*-butyl-1,2,4-triphospholyl ring anion, $P_3C_2{}^tBu^-$ have also been reported. Treatment of LnI_3 (Ln = Sc, Y, and Tm) with 3 equiv. of $KP_3C_2{}^tBu$ in refluxing toluene led to the formation and isolation of the corresponding monomeric, formally eight-coordinate complexes $Ln(\eta^5\text{-}P_3C_2{}^tBu_2)_2(\eta^2\text{-}P_3C_2{}^tBu_2)$ in moderate yields (Scheme 100). In the solid state the complexes, which are all isostructural, display an interesting assembly of ligands comprising one η^2-(bent) and two η^5-ligated triphospholyl rings. NMR studies indicated that the complexes are fluxional in solution [70].

2.5.2. Compounds with carboranyl ligands

The synthesis and structural characterization of constrained-geometry organolanthanide chlorides and alkyls incorporating the ligand $[\eta^5{:}\sigma\text{-}(C_9H_6)C_2B_{10}H_{10}]^{2-}$ have been described. Interaction of 1-indenyl-1,2-carborane with 2 equiv. of KH in refluxing THF gave the dipotassium salt $[K_2][(C_9H_6)C_2B_{10}H_{10}]$. Treatment of $[K_2][(C_9H_6)C_2B_{10}H_{10}]$ with 1 equiv. of $LnCl_3$ in THF generated the ionic complex $[K(THF)_6][\{\eta^5{:}\sigma\text{-}(C_9H_6)C_2B_{10}H_{10}\}_2La(THF)]$ for early lanthanide or organolanthanide chloride complexes $[\{\eta^5{:}\sigma\text{-}(C_9H_6)C_2B_{10}H_{10}\}Ln(THF)_2(\mu\text{-}Cl)_2K(THF)_2]_2$ (Ln = Y, Gd, Er, Yb) for late lanthanides as shown in Scheme 101 [71].

Reaction of $[\{\eta^5{:}\sigma\text{-}(C_9H_6)C_2B_{10}H_{10}\}Ln(THF)_2(\mu\text{-}Cl)_2K(THF)_2]_2$ with the nucleophiles NaCp or $KCH_2C_6H_4\text{-}o\text{-}NMe_2$ afforded the corresponding salt metathesis products $[\eta^5{:}\sigma\text{-}(C_9H_6)C_2B_{10}H_{10}]Ln(\eta^5\text{-}C_5H_5)(THF)_2$ (Ln = Y, Gd) or $[\eta^5{:}\sigma\text{-}(C_9H_6)C_2B_{10}H_{10}]Ln(CH_2C_6H_4\text{-}o\text{-}NMe_2)(DME)$ (Ln = Y, Er), respectively. The latter complexes were also synthesized *via* the alkane elimination reaction of 1-indenyl-1,2-carborane with $Ln(CH_2C_6H_4\text{-}o\text{-}NMe_2)_3$ (Scheme 102). They represent the first examples of organolanthanide alkyl complexes incorporating a carboranyl ligand. These complexes were fully characterized by various spectroscopic techniques and elemental analyses. Some were further confirmed by single-crystal X-ray analyses [70].

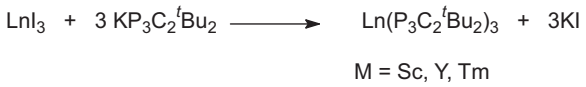

Scheme 100.

2.5.3. Compounds with heteroatom six-membered ring ligands

Synthesis, structure, and solvent-mediated redox transformations of a divalent ytterbium boratabenzene complex have been investigated. The reaction of $K[C_5H_5BNPh_2]$ with $YbI_2(THF)_2$ according to Scheme 103 provided complex $(C_5H_5BNPh_2)_2Yb(THF)_2$ as dark red, block-like crystals in 54% yield [72].

Redox reactions of $(C_5H_5BNPh_2)_2Yb(THF)_2$ with α-diimine ligands were greatly influenced by the steric environment in the α-diimines, and the reactions occurred only with less bulky α-diimines. The redox reaction of $(C_5H_5BNPh_2)_2Yb(THF)_2$ with the α-diimine PhNC(Me)C(Me)NPh in toluene afforded the trivalent ytterbium complex $[C_5H_5BNPh_2]_2Yb[PhNC(Me)C(Me)NPh]$ (Scheme 104, green crystals, 56% yield), in which the interaction between the radical-anionic α-diimine and the Yb ion is weak, and the redox process is solvent sensitive and reversible [72].

Several solvent-free boratabenzene yttrium chlorides were synthesized according to Scheme 105 and structurally characterized. In the solid-state both complexes are dimers with the Y atoms bridged by two chlorine atoms. The aminoboratabenzene ligands coordinate to Y atoms *via* the aromatic rings [73].

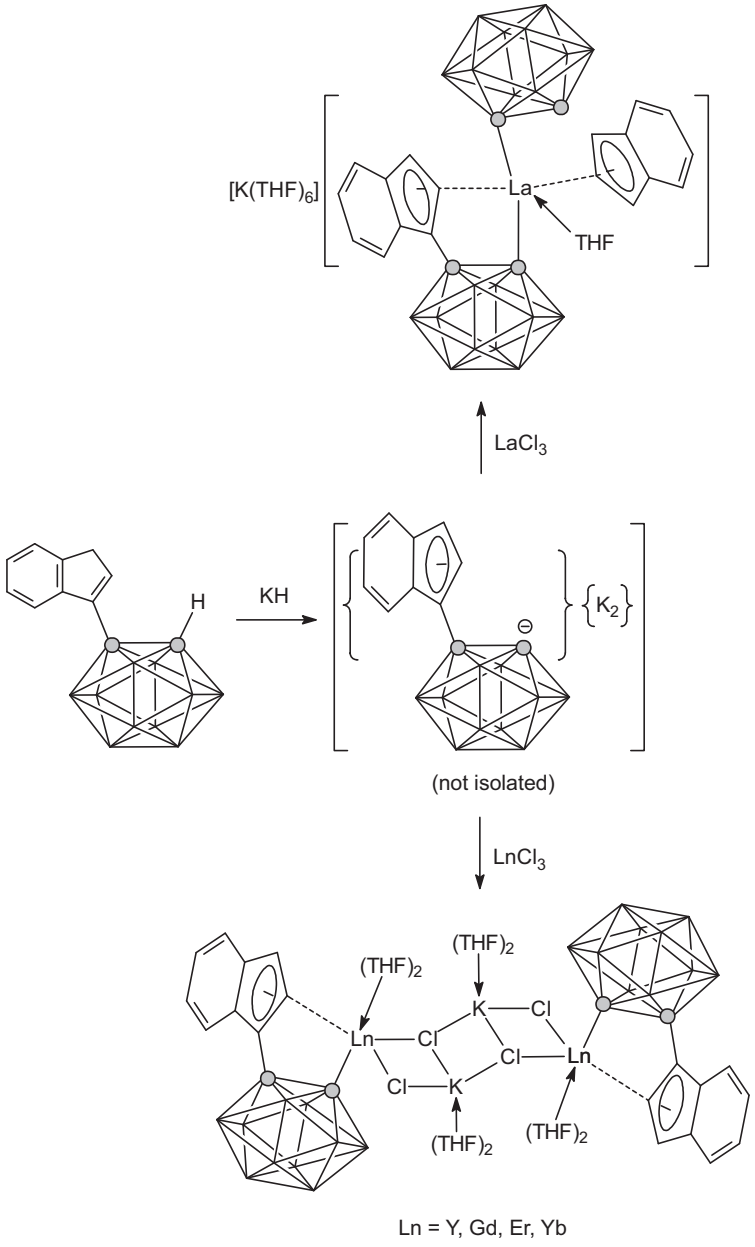

Scheme 101.

Reactions of the boratabenzene yttrium chlorides with $KN(SiMe_3)_2$ first gave boratabenzene yttrium amides *via* salt elimination. The boratabenzene yttrium amides produced reacted further with $KN(SiMe_3)_2$ to cause π-ligand displacement and generate potassium salts of boratabenzene ligands (Scheme 106). The π-ligand displacement is greatly influenced by the B substituents and decreases in the order $-Me \gg -NPh_2 > -NEt_2$ [73].

The reaction of $Yb[N(SiMe_3)_2]_2$ with the adduct borabenzene-PMe_3 according to Scheme 107 provided a novel *ansa*-heteroborabenzene divalent lanthanide amide complex through C–H bond cleavage of PMe_3. The product displays several notable structural features: (1) one metal ion is ligated by both neutral borabenzene and anionic boratabenzene groups; (2) two aromatic rings are linked through covalent and coordination bonds; (3) although a divalent lanthanide complex is formed, it has a structure similar to trivalent *ansa*-Cp lanthanide complexes [74].

The *ansa*-heteroborabenzene divalent lanthanide amide complex was found to undergo an insertion reaction of *N*,*N*′-diisopropylcarbodiimide into the metal–nitrogen bond (Scheme 108), in a similar manner to bis-Cp trivalent lanthanide amides. The resulting divalent lanthanide guanidinate was obtained in 83% yield. This work can be expected to stimulate future studies to probe the reductive properties the amide precursor as well as the nucleophilic aromatic substitution reaction on the neutral borabenzene fragment to generate new borabenzene (or boratabenzene) metal complexes [74].

2.6. Lanthanide cyclooctatetraenyl complexes

By means of *ab initio* calculations it has been predicted that it is possible to manipulate the magnetization direction in organic magnetic molecules by changing their oxidation state. This novel effect was demonstrated on the $Eu_2(C_8H_8)_3$ (C_8H_8 = 1,3,5,7-

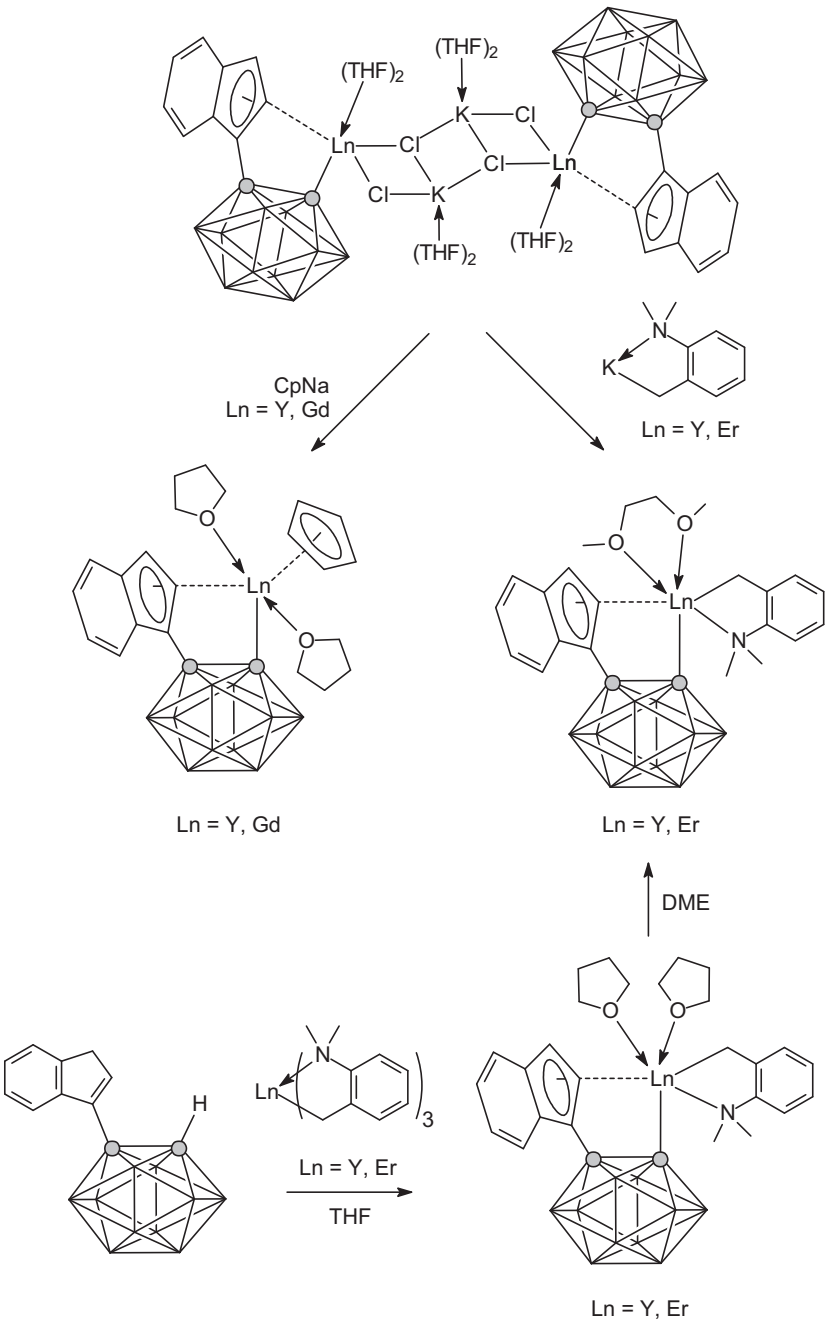

Scheme 102.

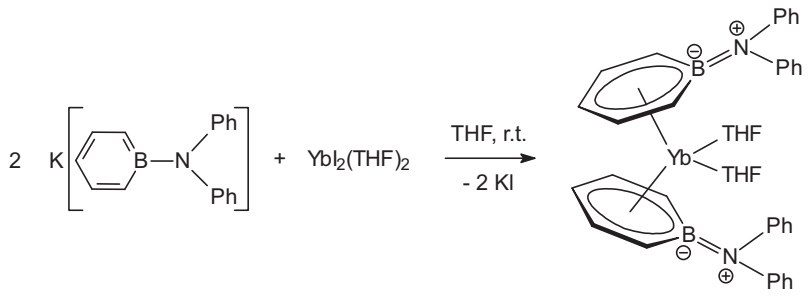

Scheme 103.

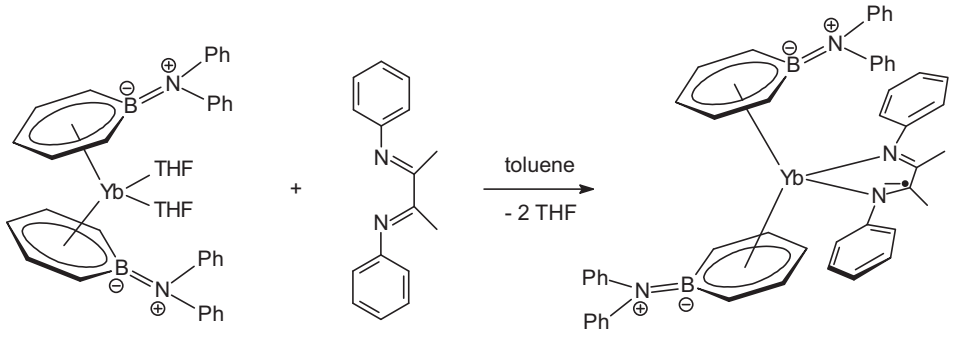

Scheme 104.

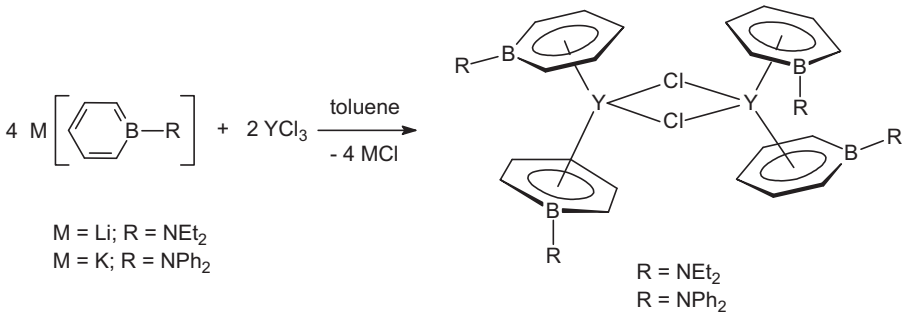

Scheme 105.

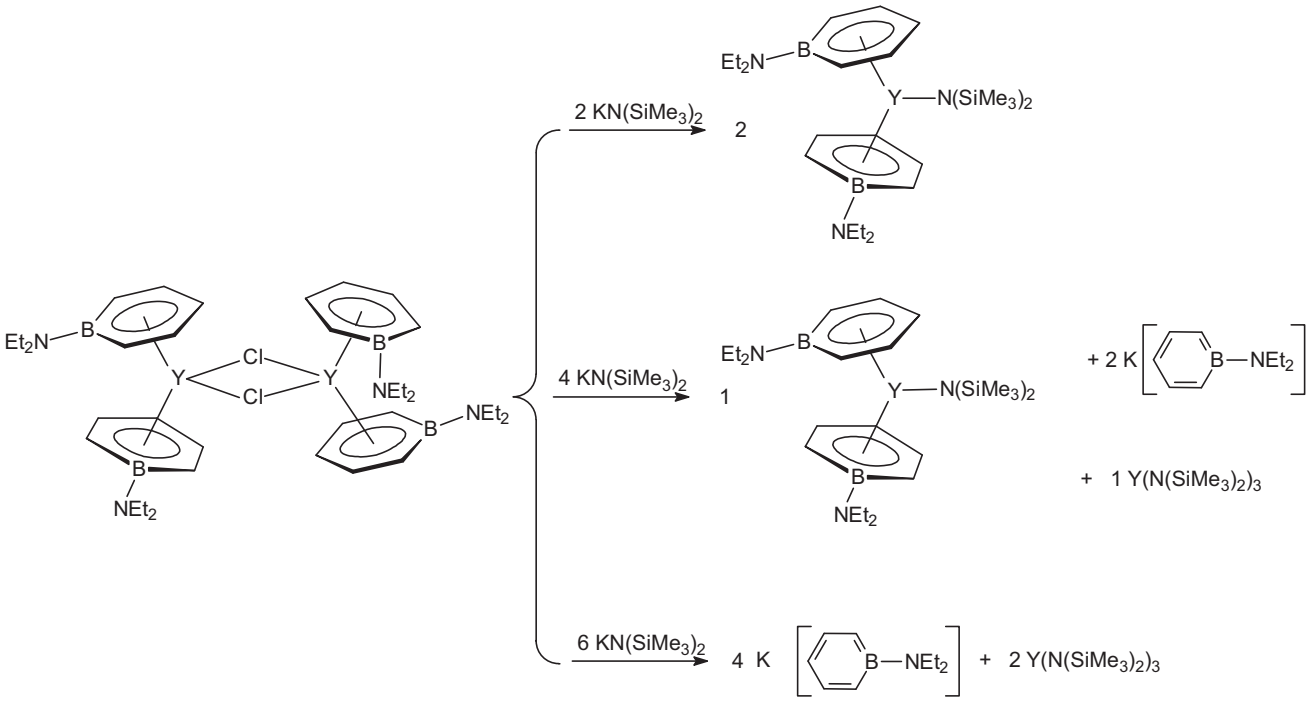

Scheme 106.

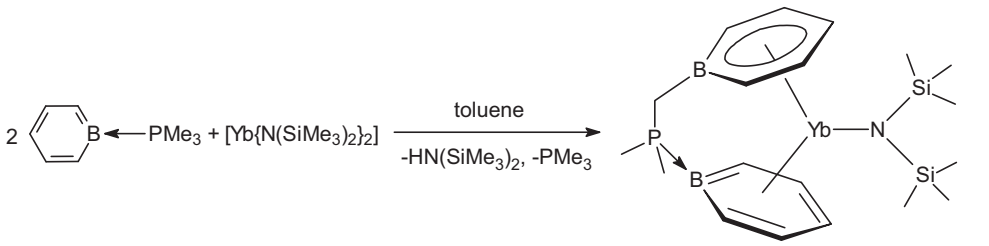

Scheme 107.

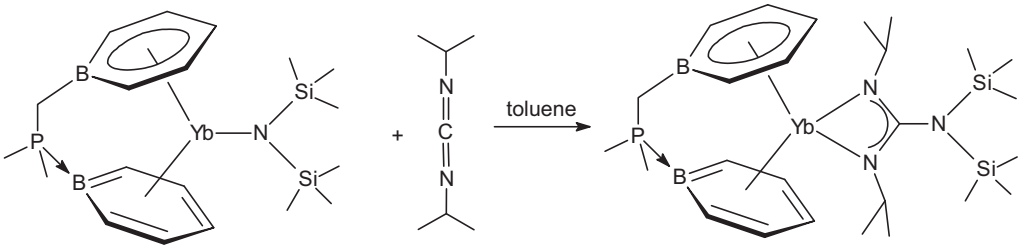

Scheme 108.

cyclooctatetraene dianion) molecule, in which the hybridization of the outer π ring states with the Eu 4*f* states causes a redistribution of the orbitals around the Fermi level leading to a strong ferromagnetism due to a hole-mediated exchange mechanism. As a key result, an oscillatory behavior of the easy axis of the magnetization as a function of the oxidation state of the molecule was predicted – a new effect, which could lead to new technological applications [75]. Multidecker sandwich clusters composed of lanthanide metal atoms and 1,3,5,7-cyclooctatetraene are concrete examples of 1-D organometallic building blocks that can be generated by the laser vaporization method and fast flow reactor in the gas phase. The bonding in Ln-C_8H_8 clusters has been theoretically elucidated to be highly ionic in nature. In 2008, multilayer lanthanide–cyclooctatetraene organometallic clusters, $Ln_n(C_8H_8)_m$ (Ln = Eu, Tb, Ho, Tm; $n = 1-7$; $m = n-1, n, n+1$) have been produced by a laser vaporization synthesis method. The magnetic deflections of these organometallic sandwich clusters were measured by a molecular beam magnetic deflection technique. Most of the sandwich species displayed one-sided deflection, while some of smaller Ln-C_8H_8 clusters showed symmetric broadening without or with only very small (or absent) net high-field deflection. In general, the total magnetic moments, calculated from the magnitude of the beams deflections, increase with the number of lanthanide atoms (*i.e.*, with increasing sandwich layers); however for Tb-, Ho-, and Tm-C_8H_8 clusters with $n > 3$, the suppression of the magnetic moments was observed, possibly through antiferromagnetic interactions. For Eu-C_8H_8 clusters, the authors observed a linear increase of the magnetic moments with the number of Eu atoms up to $n = 7$, with average magnetic moment per Eu atom around $7\mu_B$, similar to that displayed by conventionally synthesized mononuclear $Eu^{II}C_8H_8$ complexes, indicating that Eu atoms exist as Eu^{2+} ions in the full sandwich $Eu_n(C_8H_8)_{n+1}$ clusters. These results suggested that $Eu_n(C_8H_8)_{n+1}$ is a promising candidate for a high-spin, one-dimensional building block in organometallic magnetic materials [76].

2.7. Lanthanide metallofullerenes

Density functional theory (DFT) studies were performed on the endohedral scandium carbide fullerene $Sc_3C_2@C_{80}$ and its monoanion $[Sc_3C_2@C_{80}]^-$. The system consisting of a Sc_3C_2 moiety inside the I_h C_{80} fullerene was studied by using first principle molecular dynamics simulations at the DFT level. On the picosecond time scale, the triangle defined by the Sc atoms is seen to jump between orientations along the equatorial six-membered ring belt of the cage. The confined carbide unit, in turn, is engaged in a flipping motion through the Sc_3 plane. In contrast to the equilibrium geometry optimizations using large basis sets that predict a trigonal bipyramidal structure (Fig. 5), a planar Sc_3C_2-moiety is preferred during the finite-temperature simulation. In the molecular dynamics picture, $Sc_3C_2@C_{80}$ is best described as an equilibrium between the two static minimum structures. Calculations of the vibrational frequencies show that the earlier predicted C_2 and C_{2v} symmetric isomers are in fact saddle points, with one imaginary normal mode frequency that is related to the flipping motion of the confined carbon dimer. Reoptimization revealed two new minimum energy structures where the C_2 unit is tilted with respect to its orientation in the earlier suggested higher symmetry structures. The nature of the bonding in the static structures of the two isomers of $Sc_3C_2@C_{80}$ has been investigated using the electron localization function and natural population analysis. Some increased electron

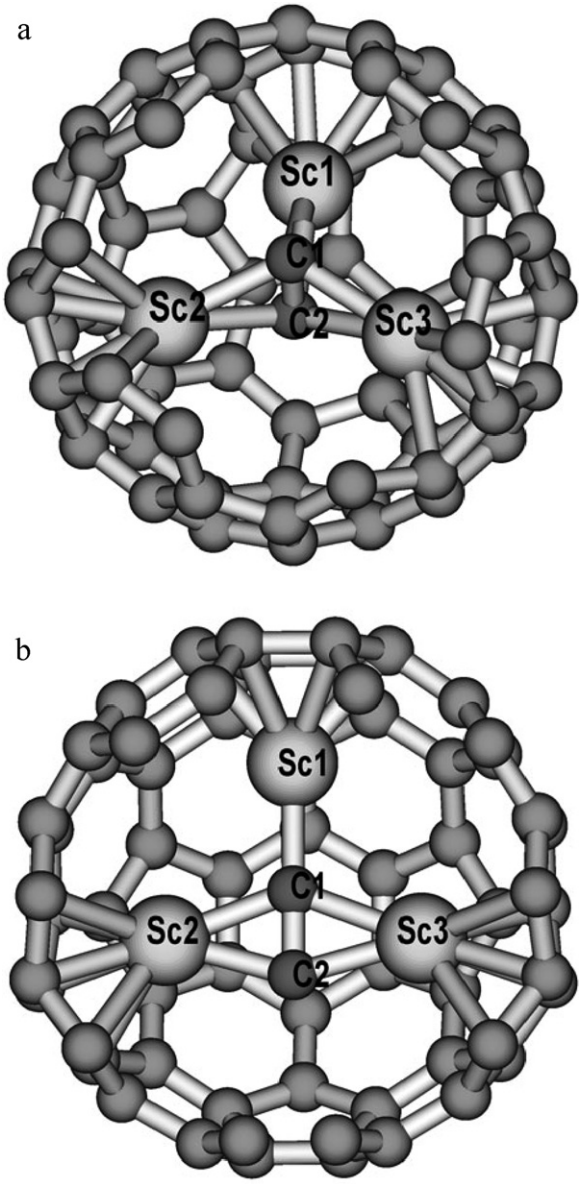

Fig. 5. Two isomers (a) and (b) of (a) of $Sc_3C_2@C_{80}$. For improved visibility of the confined moiety, part of the cage wall has been cut out [77].

pair localization was detected on the six-membered rings closest to the Sc atoms. ^{13}C NMR chemical shifts have been calculated for the closed-shell monoanion of $Sc_3C_2@C_{80}$ [77].

The ^{13}C shifts were also calculated for $Sc_2C_2@C_{84}$, for further comparison to experimentally measured spectra. The confined carbon atoms are strongly deshielded in these metallofullerenes, implying an incorrect earlier interpretation of the experimental ^{13}C NMR spectrum of $Sc_2C_2@C_{84}$. The neutral $Sc_3C_2@C_{80}$ system with one unpaired electron was further characterized by calculating the hyperfine coupling constants, the *g* tensor, as well as paramagnetic NMR (pNMR) ^{13}C shifts for both static isomers. The chemical shifts of the confined carbon atoms and the hyperfine coupling constants of all the confined atoms are strongly dependent on the conformation of the Sc_3C_2 moiety. Consequently, dynamical effects are expected to be important in the modelling of the magnetic properties of endohedral scandium carbide fullerenes. The two low-lying isomers have rather different pNMR ^{13}C shifts, implying the potential of this method in structural assignment [77]. The first experimental detection of the ^{13}C NMR chemical shifts of the C_2 unit in $Sc_2C_2@C_{82}(C_{3v})$, $Sc_2C_2@C_{84}(D_{2d})$, and $[Sc_3C_2@C_{80}(I_h)]^-$ has been achieved by using ^{13}C-enriched samples. All ^{13}C NMR chemical shifts of the cage carbon atoms for the three compounds have been successfully assigned by 2D INADEQUATE (incredible natural abundance double quantum transfer experiment) NMR measurements [78]. The electronic structure of carbide endohedral metallofullerenes of the type $Sc_2C_2@C_{82}$ has been analyzed and the possibility of rotation of the encapsulated Sc_2C_2 moiety in the interior of the cage studied. Moreover, the higher abundance of $M_2C_2@C_{82}$ (M = Sc, Y) in which the metal–carbide cluster is encapsulated in the C_{3v}–C_{82} carbon cage with respect to other carbides of the same family was rationalized on the basis of the formal transfer of four electrons from the cluster to the cage and sizeable (LUMO-3)–(LUMO-2) gap in the empty cages. This rule also applies to all those endohedral metallofullerenes in which the encapsulated cluster transfers four electrons to the carbon cage as, for example, the reduced $[M@C_{82}]^-$ systems (M = group 3 or lanthanide metal ion) [79].

The detection of a family of gadolinium-containing endohedral metallofullerenes (=EMFs) and the isolation and crystallographic characterization of one member as a metal carbide encapsulated inside a large fullerene cage has been reported. In particular, a series of di-gadolinium endohedrals extending from Gd_2C_{90} to Gd_2C_{124} has been detected by mass spectrometry of the *o*-dichlorobenzene extract of the carbon soot produced by direct current arcing of graphite rods filled with a mixture of Gd_2O_3 and graphite powder. Chromatographic separation led to the isolation of pure samples of two isomers of Gd_2C_{94} and the complete series from Gd_2C_{96} to Gd_2C_{106}. Endohedral fullerenes of the type M_2C_{2n} can exist as the conventional endohedral, $M_2@C_{2n}$, or as the carbide-containing endohedral, $M_2C_2@C_{2n-2}$. Crystallographic characterization of the more rapidly eluting isomer of Gd_2C_{94} revealed that it possesses the carbide structure, $Gd_2C_2@D_3(85)$-C_{92} (Fig. 6). Computational studies suggested that the more slowly eluting isomer of Gd_2C_{94} may be a conventional endohedral, $Gd_2@C_2(121)$-C_{94} [80].

Bis-carbene adducts of $La_2@C_{72}$ have been synthesized, isolated, and characterized as the first examples of non-IPR EMFs (IPR = isolated-pentagon rule). $La_2@C_{72}$, which has a D_2-symmetric non-IPR cage with two pairs of fused pentagons, had previously been reported to react readily with 2-adamantane-2,3-[^{3}H]-diazirine to generate six isomers of the mono-adduct $La_2@C_{72}Ad$ (Ad = adamantylidene). In this work, the reaction of $La_2@C_{72}$ with 2-adamantane-2,3-[^{3}H]-diazirine was induced by a high-pressure mercury-arc lamp in anhydrous toluene (Scheme 109) and monitored by HPLC on a Buckyprep M column. For the bis-adduct, more than fifteen isomers were distinguishable, but only seven were isolated by recycling preparative HPLC and characterized [81].

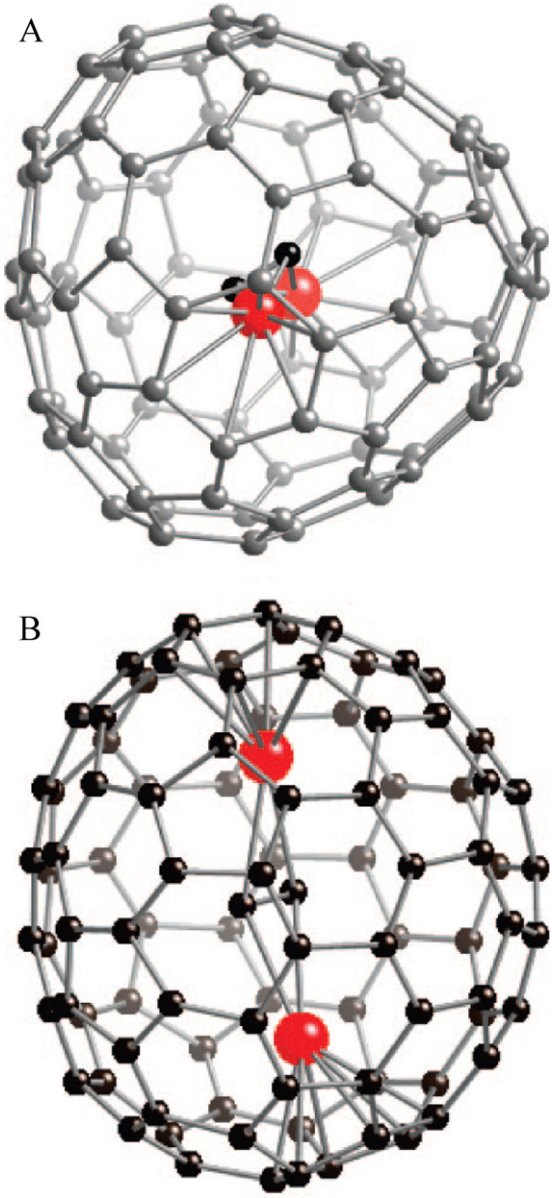

Fig. 6. Two orthogonal views of $Gd_2C_2@D_3(85)$-C_{92} with cage carbon atoms in gray, the carbide carbon atoms in black, and the gadolinium atoms in red. (a) A view down the non-crystallographic three-fold axis of the carbon cage. (b) A side view with the three-fold axis in the vertical direction. Only the major Gd sites are shown [80].

Electrochemical results revealed that the Ad groups have an electron-donating nature with respect to $La_2@C_{72}$. Structural characterization of the most abundant isomer (Fig. 7) showed that the two Ad groups are covalently bonded to the [5,6]-junctions adjacent to the two fused-pentagon bonds in a symmetric open-cage structure. Apparently the fused-pentagon sites in $La_2@C_{72}$ are clearly more reactive than other sites, as only mono- and bis-adducts were formed [81].

2.8. Heterobimetallic organolanthanide complexes

For the first time in several decades, significant progress has been achieved in the synthesis and structural characterization of compounds comprising direct lanthanide-transition metal bonds. A reaction of $[Cp^*RuH_2]_2$ with $Cp_2Y(CH_2SiMe_3)(THF)$ according to Scheme 110 afforded the unprecedented heterometallic trihydride derivative $H(Cp^*Ru)_2H_2YCp_2$ in 44% yield [82].

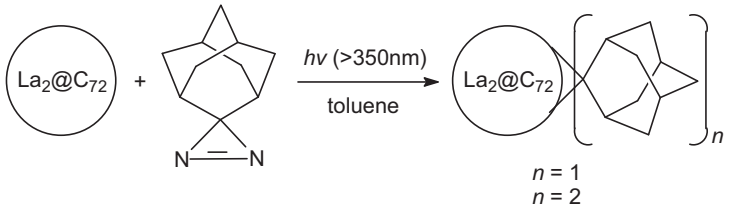

Scheme 109.

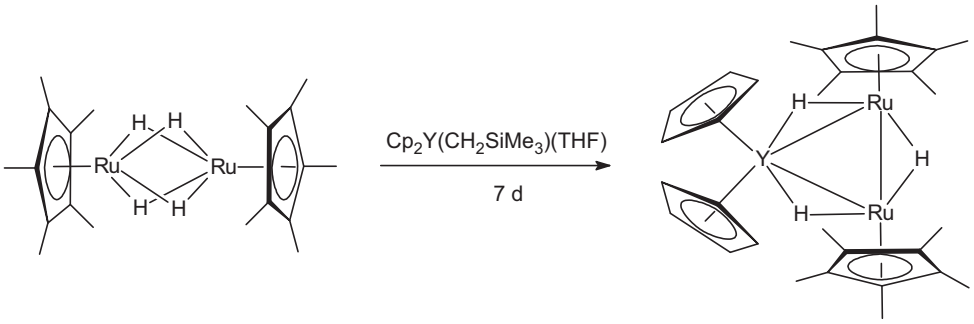

Scheme 110.

Treatment of Cp_2ReH with $Cp_2Y(CH_2SiMe_3)(THF)$ in toluene at −80 °C followed by stirring at room temperature for 3 h afforded the orange bis(metallocene) Cp_2ReYCp_2 in 91% yield (Scheme 111). Dark green $Cp_2ReYbCp_2$ was obtained in an analogous manner from Cp_2ReH and *in situ*-prepared $Cp_2Yb(CH_2SiMe_3)(THF)$. The ^1H NMR spectrum of the Y derivative showed only two signals typical for Cp ligands. A single-crystal X-ray analysis confirmed the presence of the first heterometallic bis(metallocene) comprising an unsupported Y–Re bond [82].

Characterization and reactivity of peralkylated $Ln^{II}Al^{III}$ heterobimetallic complexes have been studied in detail. The heterobimetallic peralkylated complexes $[Ln(AlR_4)_2]_n$ (Ln = Sm, Yb; R = Me, Et) were synthesized by a silylamide elimination route from $Ln[N(SiMe_3)_2]_2(THF)_2$ and an excess of AlR_3. The solid-state structure of $[Sm(AlEt_4)_2]_n$ is isomorphous to that of the ytterbium derivative. Polymeric $[Yb(AlMe_4)_2]_n$ was examined by ^1H and ^{13}C MAS NMR spectroscopy revealing the presence of distinct bridging methyl groups. The reaction of $[Yb(AlMe_4)_2]_n$ and 1,10-phenanthroline (Phen) afforded the monomeric donor adduct $Yb(AlMe_4)_2(Phen)$ as green plate-like crystals in 83% yield, while the protonolysis reaction with 2 equiv. C_5Me_5H (HCp^*) yielded a separated ion pair of composition $[Cp^*Yb(THF)_4][AlMe_4]$. Single-crystal X-ray diffraction data have been provided for both ytterbium(II) complexes. Solid-state magnetic measurements (SQUID) were performed on $[Sm(AlMe_4)_2]_n$, $[Sm(AlEt_4)_2]_n$, $SmI_2(THF)_2$ and $Sm[N(SiMe_3)_2]_2(THF)_2$ showing high effective magnetic moments $3.67\mu_B < \mu_{eff} < 4.43\mu_B$ [83]. Protonolysis reactions of heterobimetallic peralkylated complexes $[Ln(AlR_4)_2]_n$ (Ln = Sm, Yb; R = Me, Et) with 2 equiv. of $HOC_6H_2{}^tBu_2$-2,6-Me-4 afforded the bis(trialkylaluminum) adducts $Ln[(\mu\text{-}OAr^{tBu,Me})(\mu\text{-}R)AlR_2]_2$ in good yields. Analogous reactions with the less sterically demanding ^{i}Pr-substituted phenol result in ligand redistributions and formation of X-ray structurally evidenced $Ln[(\mu\text{-}OAr^{iPr,H})_2AlR_2]_2$ (Ln = Yb, R = Me; Ln = Sm, R = Et), $Yb[(\mu\text{-}OAr^{iPr,H})(\mu\text{-}Et)AlEt_2]_2(THF)$, and $[Et_2Al(\mu\text{-}OAr^{iPr,H})_2Yb(\mu\text{-}Et)_2AlEt_2]_2$. The solid-state structures of the serendipitous alumoxane complex $Sm[(\mu\text{-}OAr^{tBu,Me})AlEt_2OAlEt_2(\mu\text{-}OAr^{tBu,Me})](toluene)$ and the dimeric $AlMe_3$-adduct complex $[(AlMe_3)(\mu\text{-}OAr^{tBu,Me})Sm(\mu\text{-}OAr^{tBu,Me})_2Sm(\mu\text{-}OAr^{tBu,Me})(AlMe_3)]$ were also determined by X-ray crystallography. While the former can be discussed as a typical hydrolysis product of $Sm[(\mu\text{-}OAr^{tBu,Me})(\mu\text{-}Et)AlEt_2]_2$, the latter was isolated from the 1:1 reaction of $[Sm(AlEt_4)_2]_n$ with $HOAr^{tBu,Me}$. Scheme 112 summarizes these reactions [84].

The mono(amidinato) yttrium bis-alkyl complex shown in Scheme 20 reacts rapidly with 5 equiv. of $AlMe_3$ in toluene at room temperature to give a heterotrinuclear Y/Al complex in 80% yield (Scheme 113). As shown by an X-ray diffraction study, the product can formally be viewed as a combination of one molecule of $(NCNdipp)YMe_2$ with two molecules of $AlMe_3$. The Y atom and each of the two Al atoms in this complex are bridged by two Me groups, and a crystallographic two-fold axis passes through the Y atom and the central carbon atom of the NCNdipp amidinate unit. The eight methyl groups exhibit only one singlet at around $\delta = 0.02$ ppm in the ^1H NMR spectrum in $[D_8]$toluene at both room temperature and −60 °C, thereby suggesting a rapid exchange between the bridging and terminal methyl groups in solution [19].

Salt-metathesis reactions between the homoleptic lanthanide tetramethylaluminates $Ln(AlMe_4)_3$ and a bulky scorpionate ligand (Scheme 114) revealed a marked dependence on the ionic radius of the lanthanide metal [85].

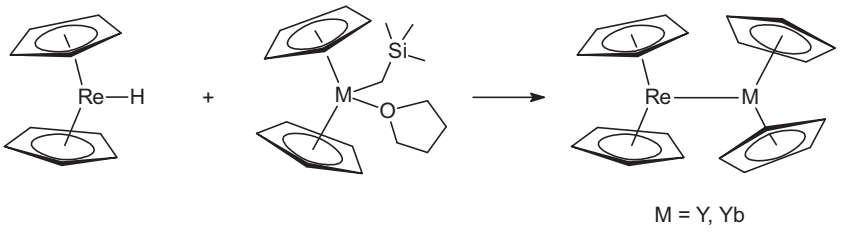

Scheme 111.

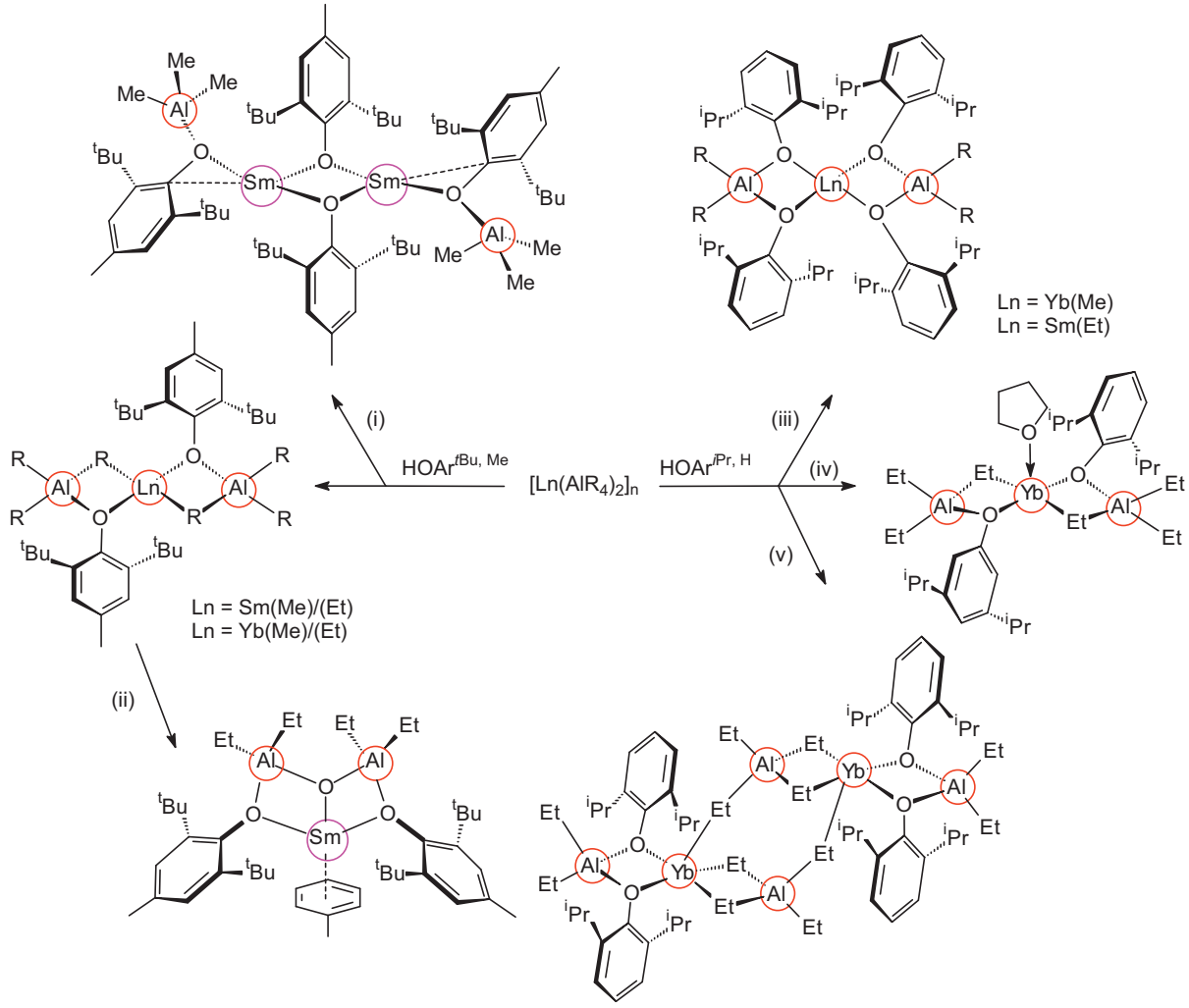

Scheme 112. Reactivity of $[Ln(AlR_4)_2]_n$ (R = Me, Et; Ln = Sm, Yb) toward bulky phenols $HOAr^{iPr,H}$ and $HOAr^{tBu,Me}$. All reactions were performed in toluene or hexane with 2 equiv. of HOArR. Isolated complexes are shown only. (i) Reaction performed in toluene with 1 equiv. $HOAr^{tBu,Me}$. (ii) Degradation product, most likely the result of the presence of traces of H_2O. (iii) This compound was also obtained with 4 equiv. of $HOAr^{iPr,H}$. (iv) Coordinated THF possibly originates from $Yb(AlEt_4)_2(THF)_2$ present as a minor impurity. (v) Main product, but slower crystallization.

In the case of Ln = Y, the X-ray structural analysis revealed the formation of a distorted trigonal–bipyramidal complex comprising a σ-methyl group as well as a monodentate tetramethylaluminate ligand (Fig. 8) [85].

In contrast, with Ln = La an unprecedented heterobimetallic complex was formed which can be regarded as a rare-earth metal variant of the well-known Tebbe reagent, $Cp_2Ti[(\mu\text{-}CH_2)(\mu\text{-}Cl)Al(CH_3)_2]$. It contains a Tebbe-like, butterfly-shaped $(\mu\text{-}CH_2)[(\mu\text{-}CH_3)Al(CH_3)_2]_2$ unit comprising a relatively short La–C(methylene) bond (2.519(2) Å) (Fig. 9). Initial experiments showed that the La compound even show Tebbe-type reactivity. A reaction with 9-fluorenone afforded the carbonyl-methylenation product 9-methylidenefluorene in 50% yield [85].

The analogous reaction of $Ln(AlMe_4)_3$ (Ln = Y, Lu) with the bulky hydro-tris(pyrazolyl)borate $(Tp^{tBu,Me})H$ proceeds *via* a sequence of methane elimination and C–H bond activation,

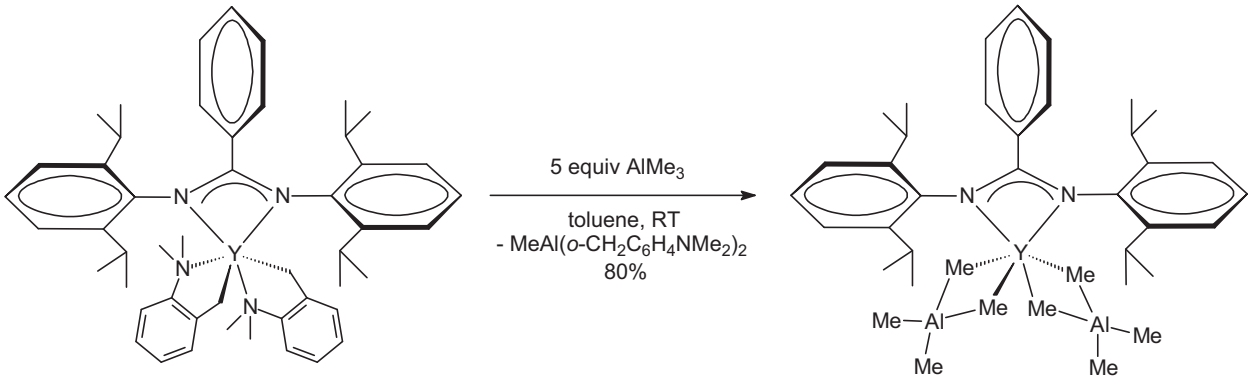

Scheme 113.

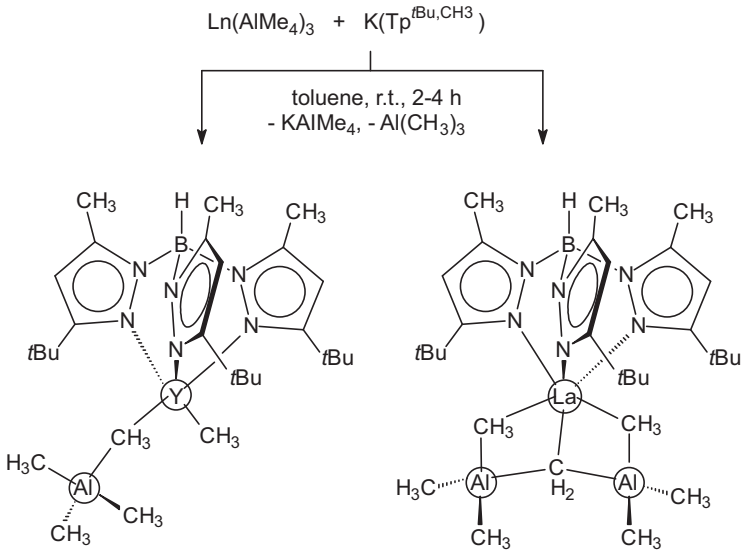

Scheme 114.

affording unprecedented rare-earth metal ligand moieties including Ln(Me)[(μ-Me)$AlMe_3$] and X-ray structurally characterized "Tebbe-like" Ln[(μ-CH_2)$_2$$AlMe_2$] (Scheme 115) [86].

Reactions of La($AlMe_4$)$_3$ and Y($AlMe_4$)$_3$ with PMe_3 showed that the phosphine can cleave Ln–CH_3–Al linkages, separating $Me_3Al(PMe_3)$. PMe_3 (3 mol equiv.) was found to react with Y($AlMe_4$)$_3$ to give $(YMe_3)_n$ contaminated with by-products containing phosphorus and aluminum. The La-based analogue, $(LaMe_3)_n$, was not formed selectively from the reaction of La($AlMe_4$)$_3$ with PMe_3 or Et_2O, which rather yielded insoluble La/Al heterobimetallic products. Three multinuclear La-based clusters were obtained from a reaction of La($AlMe_4$)$_3$ with PMe_3 (1 equiv.) and identified by X-ray structure analyses (Scheme 116) [87].

Each cluster exhibits extensive methyl group degradation and contains methylene, methine, or carbide moieties. $La_4Al_8(CH)_4(CH_2)_2(CH_3)_{20}(PMe_3)$ (**A**) has a {$La_4(CH)_4$} cuboid core supported by $AlMe_3$, $Me_2AlCH_2AlMe_2$, and PMe_3 ligands. $La_4Al_8(C)(CH)_2(CH_2)_2(CH_3)_{22}$(toluene) (**B**) also contains a cuboid core, {$La_3Al(C)(CH)_2(CH_2)$}, which includes one exo cubic lanthanum atom, and is supported by $AlMe_3$, $Me_3AlCH_2AlMe_2$, $(AlMe_4)^-$, and toluene ligands. The lanthanum atoms in $La_5Al_9(CH)_6(CH_3)_{30}$ (**C**) are arranged in a trigonal bipyramidal fashion with (CH) functionalities capping each face. The

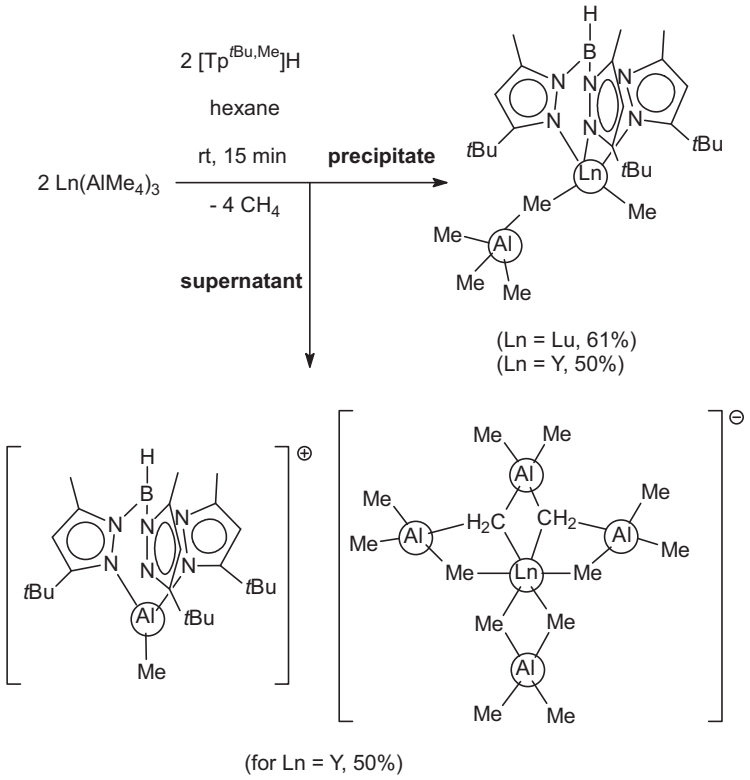

Scheme 115.

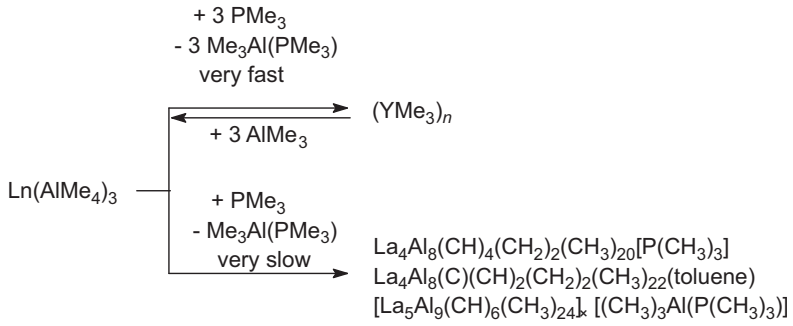

Scheme 116.

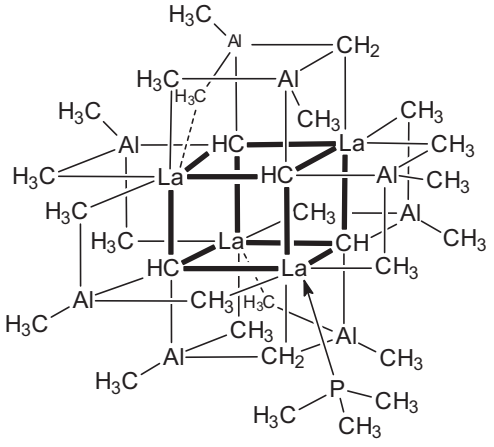

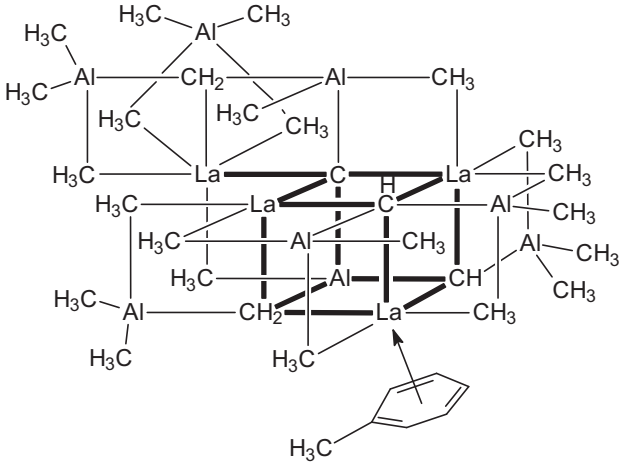

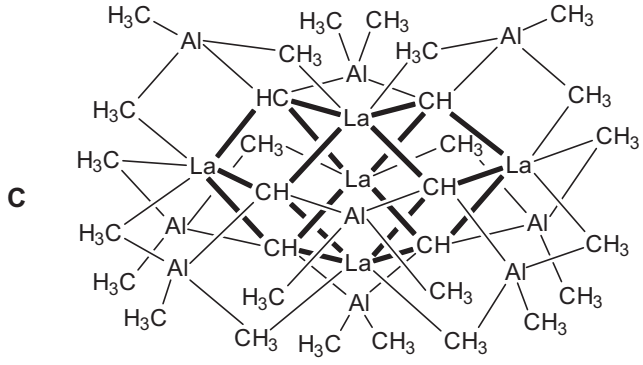

Scheme 117.

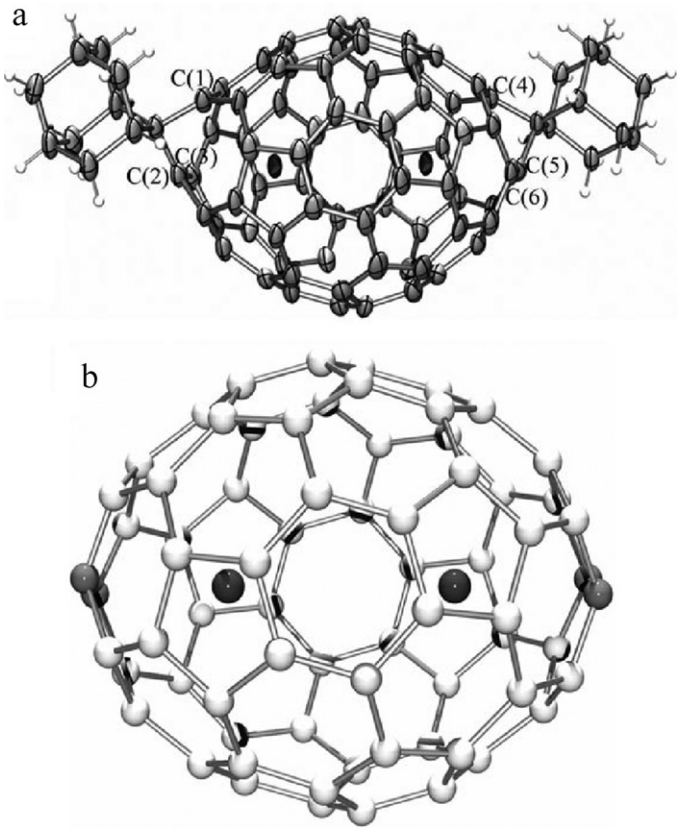

Fig. 7. (a) ORTEP drawing of one enantiomer of the most abundant bis-adduct isomer showing thermal ellipsoids at the 50% probability level. (b) Molecular structure of $La_2@C_{72}$ with the four [5,5]-junction carbon atoms highlighted as darker spheres [81].

$[La_5(CH)_6]^{3-}$ core is formally balanced by three $AlMe^{2+}$ moieties and is additionally supported by six $AlMe_3$ ligands. The unit cell contains two independent La_5 clusters, one with *pseudo*-C_{3h} and the other with *pseudo*-D_3 symmetry, as well as two molecules of the separation co-product $Me_3Al(PMe_3)$ (Scheme 117) [87].

As a synthetic equivalent for the elusive trimethyl complex $LnMe_3$, lithium methylates of the approximate composition $Li_3LnMe_6(THF)_n$ were prepared by treating rare-earth metal

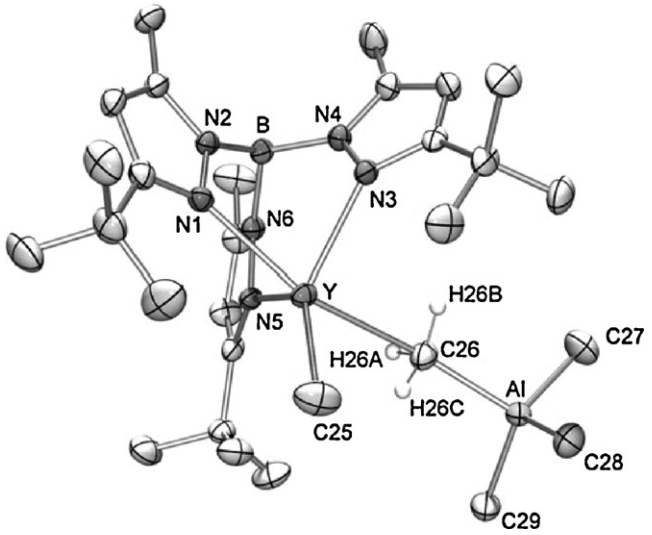

Fig. 8. Molecular structure of $(Tp^{tBu,CH3})Y(CH_3)[(\mu\text{-}CH_3)Al(CH_3)_3]$ [85].

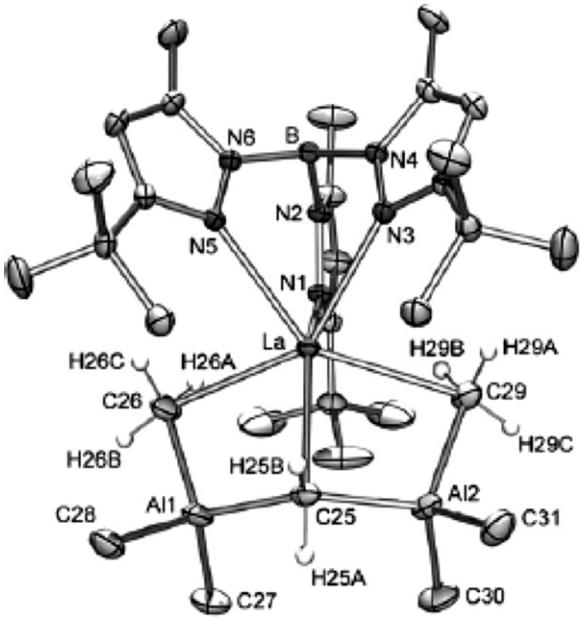

Fig. 9. Molecular structure of $[(Tp^{tBu,CH3})La[(\mu\text{-}CH_2)\{(\mu\text{-}CH_3)Al(CH_3)_2\}_2]$ [85].

trichlorides $LnCl_3(THF)_n$ with 6 equiv. of methyllithium in diethyl ether. Heteronuclear complexes of the formula $Li_3Ln_2Me_9L_n$ (Ln = Sc, Y, Tb; L = Et_2O, THF) were isolated by crystallization from diethyl ether (Scheme 118). Single crystal X-ray diffraction studies revealed a heterometallic aggregate of composition $Li_3Ln_2Me_9(THF)_n(Et_2O)_m$ with a $[LiLn_2Me_9]^{2-}$ core (Ln = Sc, Y, Tb) [8].

The protonolysis reaction of $Ln(AlMe_4)_3$ with various substituted cyclopentadienyl derivatives HCpR provided access to a series of half-sandwich complexes $(CpR)Ln(AlMe_4)_2$ (Scheme 119). Whereas bis(tetramethylaluminate) complexes

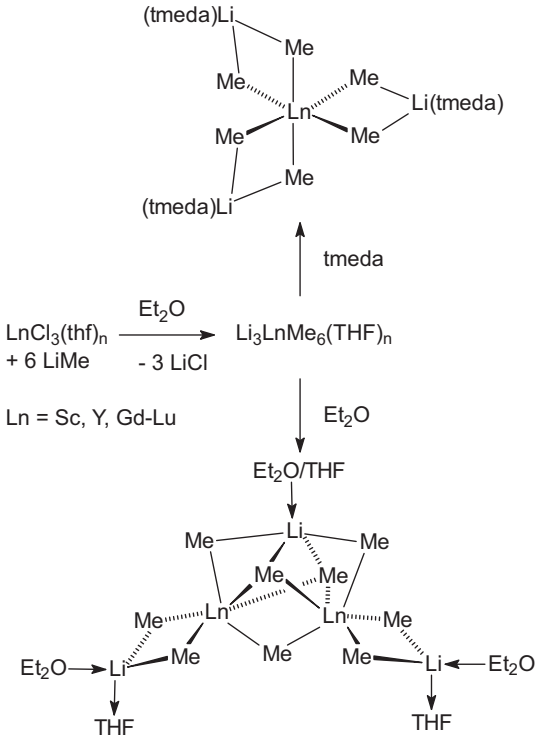

Scheme 118.

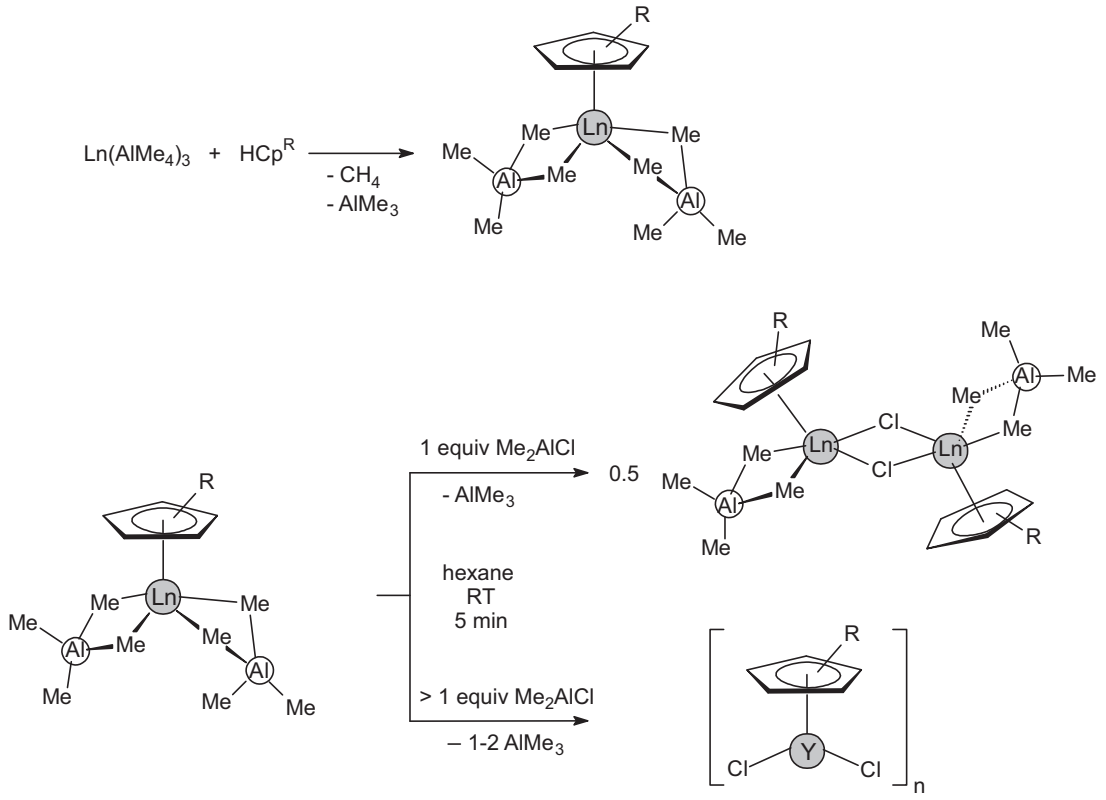

Scheme 119.

with 1,3-$(Me_3Si)_2C_5H_3$ and $C_5Me_4SiMe_3$ ancillary ligands formed easily at ambient temperature for the entire Ln^{III} cation size range (Ln = Y, La, Nd, Sm, Lu), exchange with the less reactive 1,2,4-$(Me_3C)_3C_5H_3$ was only obtained at elevated temperatures and for the larger metal centers Sm, Nd, and La. X-ray structure analyses of seven representative complexes of the type $(CpR)Ln(AlMe_4)_2$ revealed a similar distinct $AlMe_4$-coordination (one η^2, one bent η^2). Subsequent treatment with Me_2AlCl leads to $AlMe_4 \rightarrow Cl$ exchange and, depending on the Al/Ln ratio and the CpR ligand, varying amounts of partially and fully exchanged products $[(CpR)Ln(AlMe_4)(\mu\text{-}Cl)]_2$ and $[(CpR)Ln(\mu\text{-}Cl)_2]_n$, respectively, have been identified. The complexes $[(C_5Me_4SiMe_3)Y(AlMe_4)(\mu\text{-}Cl)]_2$ and $[\{1,2,4\text{-}(Me_3C)_3C_5H_2\}Nd(AlMe_4)(\mu\text{-}Cl)]_2$ were characterized by X-ray structure analysis [88].

In a similar manner, $Cp^*Ln(AlMe_4)_2$ half-sandwich complexes (Ln = Y, La, Nd) were prepared *via* alkane elimination from $Ln(AlMe_4)_3$ and HCp^*. Treatment with either $[Ph_3C][B(C_6F_5)_4]$ or $[PhNMe_2H][B(C_6F_5)_4]$ according to Scheme 120 afforded the corresponding cationic mono(tetramethylaluminate) complexes [89].

Similar treatment of the lanthanum bis(tetramethylaluminate) precursor with 1 equiv. of the strong Lewis acid $B(C_6F_5)_3$ in C_6H_5Cl at room temperature led to immediate and quantitative formation of $[Cp^*La\{(\mu\text{-}Me)_2AlMe(C_6F_5)\}\{Me_2Al(C_6F_5)_2\}]_2$ as a result of very rapid sequential CH_3/C_6F_5 exchange processes (Scheme 121). An X-ray diffraction study revealed the presence of two close La···F contacts (La···F 2.62(1) Å) in the crystal structure [89].

The ethyl substituted aluminum hydroxide LAlEt(OH) (L = HC[C(Me)N(Ar)]$_2$; Ar = 2,6-^{i}Pr$_2$C$_6$H$_3$) was prepared by the hydrolysis of LAlEt(Cl) in the presence of an *N*-heterocyclic carbene. Subsequent reactions of LAlEt(OH) with Cp_3Ln in THF led to the intermolecular elimination of HCp and formation of LAlEt(μ-O)M(THF)Cp$_2$ (Ln = Y, Dy, Er, Yb) (Scheme 122) [90].

A series of unusual yttrium and erbium halides with $(\mu_3\text{-}N)[\{Ti(\eta^5\text{-}C_5Me_5)(\mu\text{-}NH)\}_3]$ as a neutral tridentate ligand has been synthesized as outlined in Scheme 123 and structurally characterized. These experiments showed that the titanium imido-nitrido complex acts as a rigid facially coordinating ligand to yttrium and erbium halide complexes [91].

The synthesis of a scandium dimethylbenzyl complex supported by a ferrocene diamide ligand was accomplished as shown in Scheme 124 by alkane elimination from $Sc(CH_2Xy\text{-}3,5)_3(THF)_2$ (*cf.* Scheme 15). The scandium dimethylbenzyl complex $Sc(fc[NSi(^tBu)Me_2]_2)(CH_2Xy\text{-}3,5)(THF)$ was used as a starting material for the synthesis of the corresponding chloride-

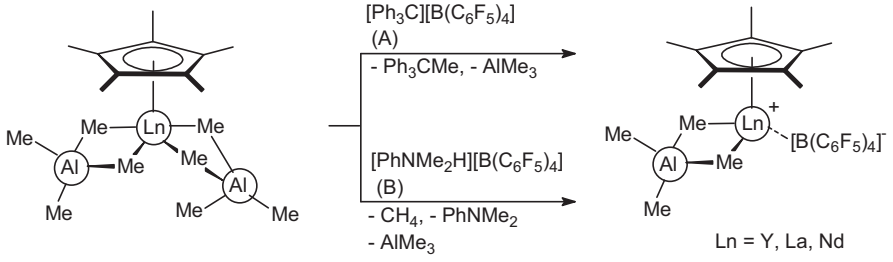

Scheme 120.

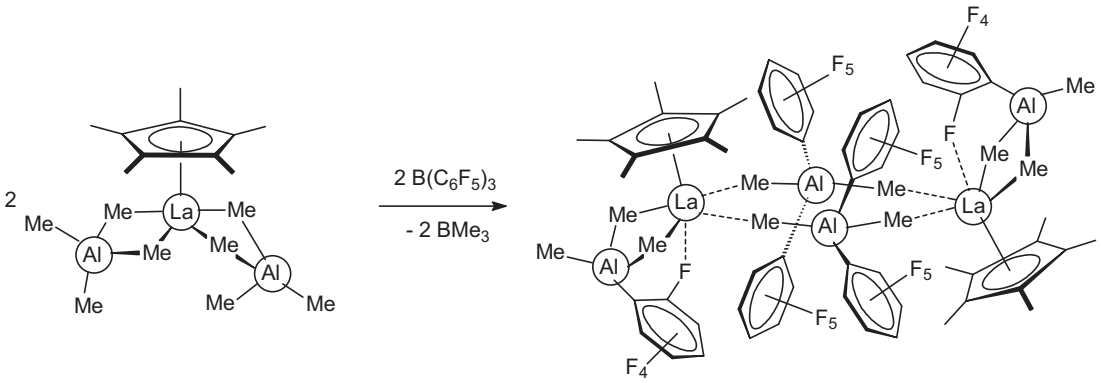

Scheme 121.

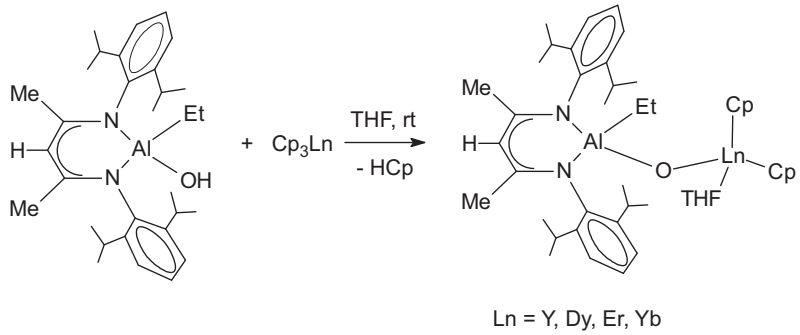

Scheme 122.

bridged dimer, which, in turn, led to a scandium bis(*neo*-pentyl) "ate" salt [17].

Attempts to remove the coordinated THF molecule from Sc(fc[NSi(^{t}Bu)Me$_2$]$_2$)(CH$_2$Xy-3,5)(THF) with AlMe$_3$ led to the isolation of a scandium methyl complex with two coordinated AlMe$_3$ molecules. This compound afforded a scandium methyl complex by stirring in THF (Scheme 125). All ferrocene diamido compounds were characterized by X-ray crystallography. DFT calculations on model compounds were used to explain the stability of the compounds synthesized and to probe the existence of an iron–scandium interaction [17].

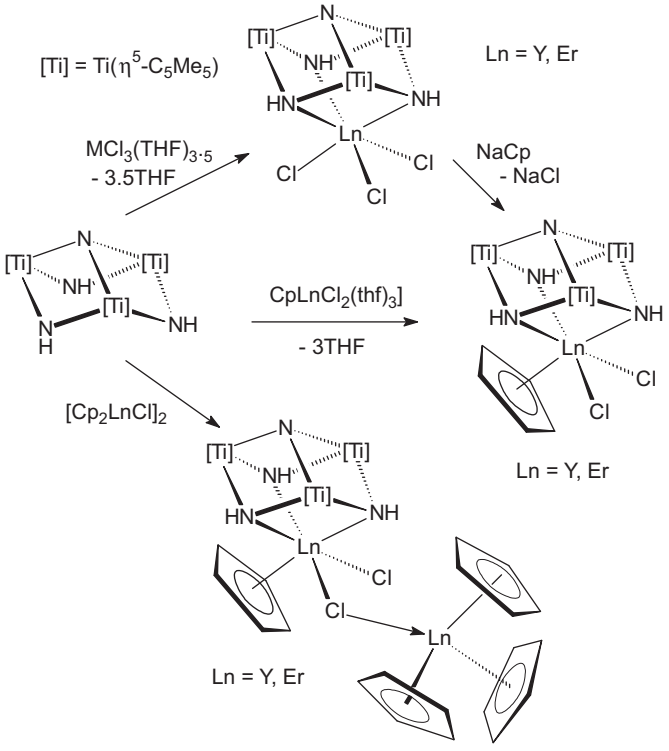

Scheme 123.

Reactions of the ferrocene 1,1′-diamide scandium benzyl complex Sc(fc[NSi(^{t}Bu)Me$_2$]$_2$)(CH$_2$Xy-3,5)(THF) with aromatic *N*-aromatic heterocycles have been studied in detail, including metalation and C–C coupling of pyridine rings and unusual ring-opening of 1-methylimidazole. Scheme 126 summarizes the products obtained by the treatment of Sc(fc[NSi(^{t}Bu)Me$_2$]$_2$)(CH$_2$Xy-3,5)(THF) with 2-phenylpyridine under different reaction conditions. Besides regular *N*-coordination, *ortho*-metalation of the pyridine ring was observed as well as a product resulting from C–C coupling of two pyridine rings, in which one ring is dearomatized [92].

The reaction of a yellow toluene solution of Sc(fc[NSi(^{t}Bu)Me$_2$]$_2$)(CH$_2$Xy-3,5)(THF) (=**1^{Sc}-THF**) with 3 equiv. of 1-methylimidazole resulted in the formation of a dark purple mixture after heating for 5 h at 70 °C. After workup, a crystalline material was isolated and its X-ray crystal was structure determined. That study revealed that the product (**4Sc**) contained an imidazole–imine–amide fragment, in which one imidazole molecule was ring-opened. The solid-state structure is preserved in solution, as confirmed by ^{1}H NMR spectroscopy. An analogous product was isolated from the reaction of the yttrium benzyl complex Y(fc[NSi^{t}BuMe$_2$]$_2$)(CH$_2$Ph)(THF) (**1^{Y}-THF**) and 1-methylimidazole, although the formation of the ring-opened product was slower than that in the scandium case. Scheme 127 illustrates the proposed mechanism for the ring-opening of 1-methylimidazole by the scandium benzyl complex **1Sc-THF** [92].

Conversion of 1,1′-dianilinoferrocenes of the composition [3,4-R$_2$C$_5$H$_2$(NHPh)]$_2$Fe (R = H, Ph) with 1 equiv. of the rare-earth

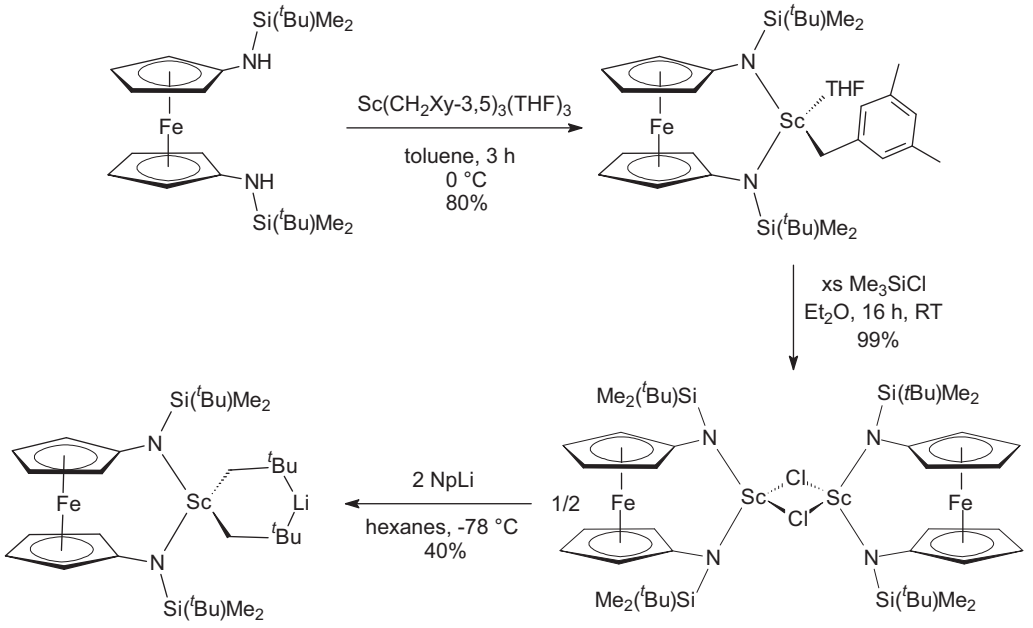

Scheme 124.

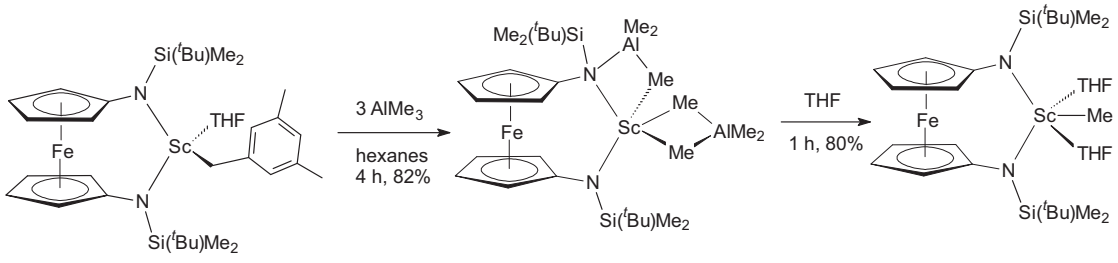

Scheme 125.

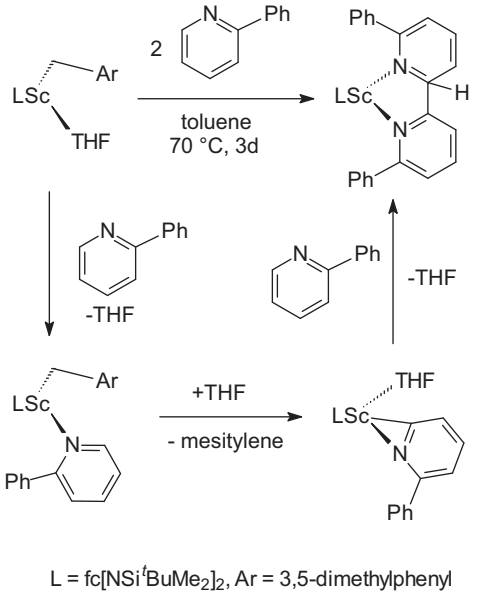

Scheme 126.

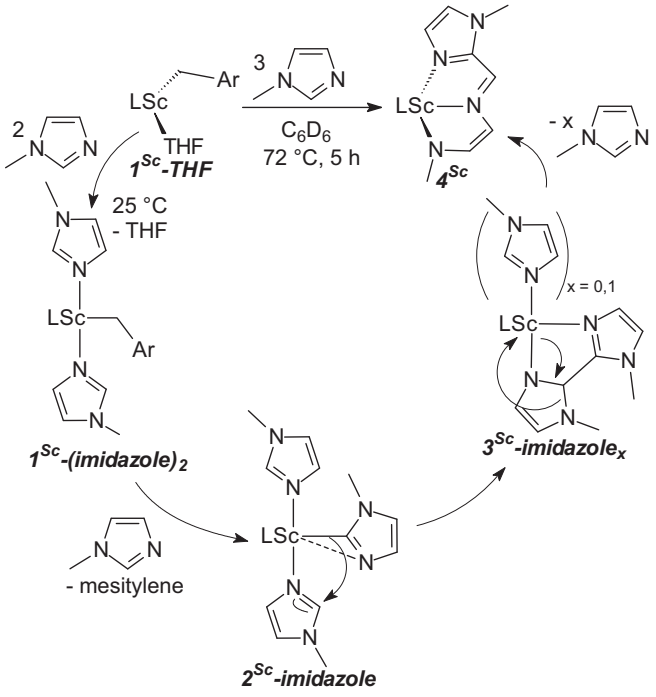

Scheme 127.

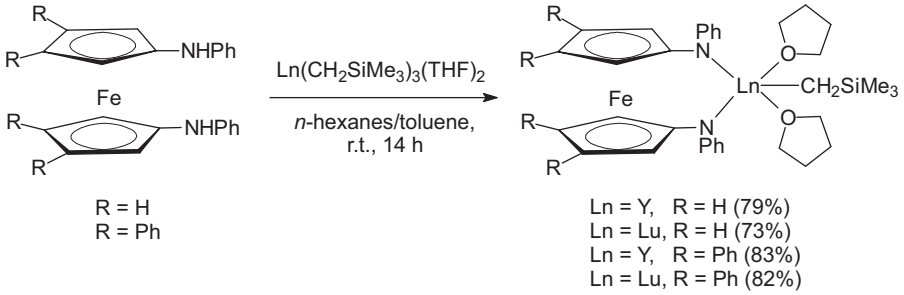

Scheme 128.

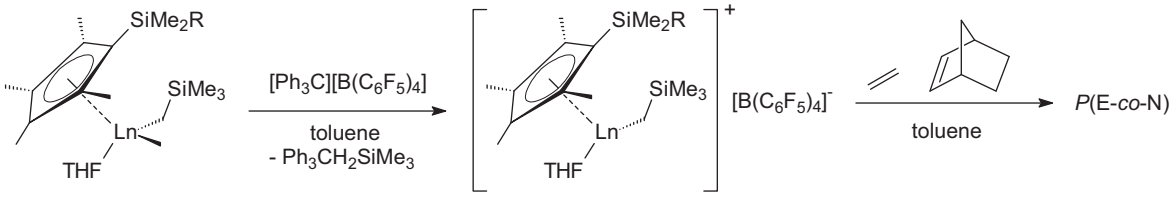

Scheme 129.

metal alkyl precursors $Ln(THF)_2(CH_2SiMe_3)_3$ (Ln = Lu, Y) affords $[R_4Fc(NPh)_2]Ln(THF)_2CH_2SiMe_3$ in yields of 73–83% (Scheme 128). The steric bulk of the ferrocene moiety induces a pronounced stabilization of the complexes in comparison to alkyl-bridged analogues. Correspondingly, the products are stable in solution at room temperature and were characterized by multinuclear NMR spectroscopy and elemental analysis. A single-crystal X-ray diffraction study was performed for the complex with Ln = Lu and R = Ph [11].

2.9. Organolanthanide catalysis

2.9.1. Organolanthanide-catalyzed polymerization reactions

2.9.1.1. Monoolefins (ethylene, propene, styrene, etc.). A toluene solution of the phenanthrene-fused cyclopentadienyl yttrium complex $(PCp^*)Y(CH_2SiMe_3)_2(THF)$ (*cf.* Scheme 59) and 1 equiv. of $[Ph_3C]^+[B(C_6F_5)_4]^-$ showed modest catalytic activity for the polymerization of ethylene at room temperature ($20\ kg\ mol^{-1}\ h^{-1}\ bar^{-1}$) [45]. The olefin polymerization capabilities of a series of complexes $M(L)R_3$ containing neutral *fac*-N_3 and *fac*-S_3 donor ligands have been determined. The scandium complexes were found to be very productive for ethylene polymerization for $L = HC(Me_2pz)_3$, Me_3[9]aneN$_3$, or [9]aneS$_3$ (*cf.* Schemes 9 and 10) and $R = CH_2SiMe_3$ when activated with 1 equiv. of $[CPh_3][BAr^F{}_4]$. When activated with 2 equiv. of $[CPh_3][BAr^F{}_4]$, the compounds were also very active for the polymerization of 1-hexene [13]. Activation of amido-pyridine-supported rare-earth metal alkyl by borate cocatalysts $[Ph_3C][B(C_6F_5)_4]$ and $[PhNMe_2H][B(C_6F_5)_4]$ was reported to give ion pairs that polymerize ethylene in moderate yields (activity: Sc > Lu) [32]. Copolymerizations of ethylene with norbornene were successfully achieved with half-sandwich rare-earth metal catalysts generated by activation of dialkyl complexes $[Ln(\eta^5\text{-}C_5Me_4SiMe_2R)(\eta^1\text{-}CH_2SiMe_3)_2(THF)]$ (Ln = Sc, R = Me, C_6F_5; Ln = Y, Lu, R = C_6F_5) with $[Ph_3C][B(C_6F_5)_4]$ (Scheme 129). Both scandium complexes showed excellent activities, whereas the Y complex gave poor activity and the Lu derivative was practically inactive. Weak stabilization of metal center by a bulkier silyl group of the tetramethylcyclopentadienyl ring in the complexes with $R = C_6F_5$ allowed controlled copolymerization ($M_w/M_n < 1.3$). Mainly atactic alternating P(E-*co*-N) copolymers were obtained with the active catalytic systems. These copolymerizations were well described by first-order Markov statistics [93].

Scope and mechanism of the organolanthanide-mediated synthesis of amine-capped polyethylenes have been studied in detail. Amines of varying Brønsted acidity and steric encumberance were investigated as chain-transfer agents to functionalize polyolefins *via* organolanthanide-mediated olefin polymerization processes. Ethylene homopolymerizations were carried out with activated $Cp^*{}_2LnCH(SiMe_3)_2$ (Ln = La, Sm, Y, Lu) precatalysts in the presence of aniline, *n*-propylamine, *N*,*N*-bis(trimethylsilyl)amine, di-*sec*-butylamine, *N*-*tert*-butyl(trimethylsilyl)amine, di-*iso*-propylamine, and dicyclohexylamine. In the presence of these amines, polymerization activities up to 10^4 g polymer/(mol of Ln atm ethylene h) and narrow product polymer polydispersities were observed, consistent with single-site polymerization processes. Amine chain-transfer efficiency was found to follow the trend $PhNH_2 \approx {}^nPrNH_2 \ll HN(SiMe_3)_2 \approx {}^sBu_2NH < N\text{-}{}^tBu(SiMe_3)NH \approx {}^iPr_2NH < Cy_2NH$ to yield polyethylenes of the structure $H(CH_2CH_2)_nNRR'$, where an efficient chain-transfer agent is defined as a reagent that both terminates polymer chain growth and facilitates the reinitiation of polymer chain growth. Under the conditions investigated, primary amines were found to be the most inert toward Cp'_2La-mediated polymerizations, affording no detectable insertion products, while di-*sec*-butylamine and *N*,*N*-bis(trimethylsilyl)amine were marginally efficient and produced monoethylene insertion products. In contrast, *N*-*tert*-butyl(trimethylsilyl)amine and di-*iso*propylamine afforded amine-capped oligoethylenes, while dicyclohexylamine was the most efficient chain-transfer agent investigated, producing high molecular weight amine-terminated polyethylenes. For these Ln catalysts, dicyclohexylamine chain transfer exhibits a linear relationship between product M_n and $[dicyclohexylamine]^{-1}$, consistent with a well-behaved aminolysis chain termination pathway. In all of the above systems, protonolysis appears to be the dominant chain-transfer pathway. Scheme 130 illustrates a simplified catalytic cycle for the single-site-mediated olefin polymerization in the presence of monofunctional electron-rich chain-transfer agents [94].

The hybrid scorpionate/cyclopentadienyl complexes $(bpzcp)MCl_2(THF)$ (*cf.* Scheme 62, M = Sc, Y) were reported to be active olefin polymerization catalysts after activation with methylaluminoxane. These compounds gave atactic polystyrenes with narrow molecular weight distribution (M_n/M_w 1.26–1.91) and with low molecular weights [46]. In the presence of 1 equiv. of $[Ph_3C][B(C_6F_5)_4]$, the scandium bis(aminobenzyl) complex $(\eta^5\text{-}2,5\text{-}{}^tBu_2C_4H_2N)Sc(CH_2C_6H_4NMe_2\text{-}o)_2$ (*cf.* Scheme 95) showed high activity for the polymerization

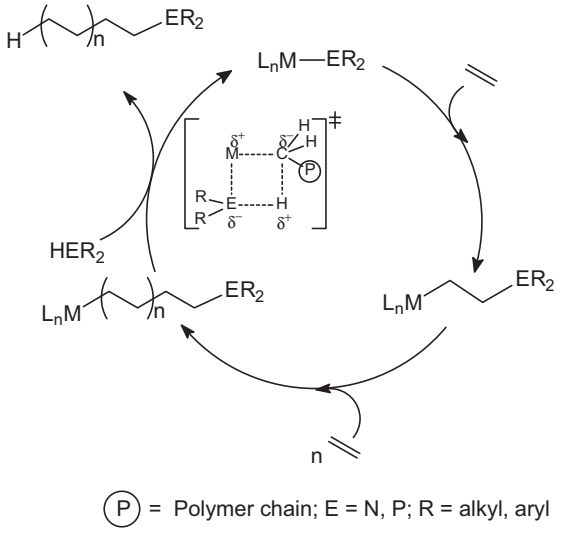

Scheme 130.

of styrene, yielding syndiotactic polystyrene with high molecular weight and moderate molecular distribution. The yttrium complex (η^5-2,5-^{t}Bu$_2$C$_4$H$_2$N)Y(CH$_2$C$_6$H$_4$NMe$_2$-*o*)$_2$ could also produce syndiotactic polystyrene but with much lower activity, whereas the lanthanum analogue (η^5-2,5-^{t}Bu$_2$C$_4$H$_2$N)La(CH$_2$C$_6$H$_4$NMe$_2$-*o*)$_2$ showed no activity under the same conditions. The isolated cationic benzyl species [(2,5-^{t}Bu$_2$C$_4$H$_2$N)Sc(CH$_2$C$_6$H$_4$NMe$_2$-*o*)][B(C$_6$F$_5$)$_4$] alone also showed high activity for the syndiospecific polymerization of styrene, while the neutral complex (η^5-2,5-^{t}Bu$_2$C$_4$H$_2$N)Sc(CH$_2$C$_6$H$_4$NMe$_2$-*o*)$_2$ was inactive under the same conditions. The cationic complex [(2,5-^{t}Bu$_2$C$_4$H$_2$N)Sc(CH$_2$C$_6$H$_4$NMe$_2$-*o*)(DME)][B(C$_6$F$_5$)$_4$] showed no activity, apparently due to the strong coordination of the DME ligand to the metal center. The η^1-C$_4$Me$_4$N-ligated Sc complex (η^1-C$_4$Me$_4$N)Sc(CH$_2$C$_6$H$_4$NMe$_2$-*o*)$_2$ did not show any activity for the polymerization of styrene either in the presence or absence of [Ph$_3$C][B(C$_6$F$_5$)$_4$]. In comparison, the analogous η^5-tetramethylcyclopentadienyl scandium complex (C$_5$Me$_4$H)Sc(CH$_2$C$_6$H$_4$NMe$_2$-*o*)$_2$ afforded syndiotactic polystyrene in the presence of 1 equiv. of [Ph$_3$C][B(C$_6$F$_5$)$_4$]. These results demonstrate that an η^5-π-bonding ligand system is superior to an η^1-bonding analogue for such types of polymerization catalysts [67]. The mixed hydride/aryloxide derivatives [Cp′Ln(μ-H)(OAr)]$_2$ (Ln = Y, Dy, Lu) complexes shown in Scheme 53 were reported to initiate the copolymerization of CO$_2$ and cyclohexene oxide (CHO) (Scheme 131) under mild conditions to afford polymers with modest molecular weights and high carbonate linkages (92–99%). No co-catalyst is required for this copolymerization reaction [42].

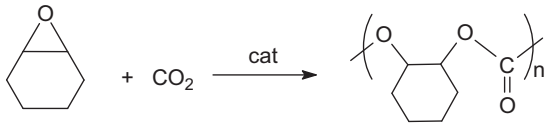

Scheme 131.

2.9.1.2. Dienes (butadiene, isoprene, etc.). The iminophosphonamido bis(alkyl) scandium complex (NPNPh)Sc-(CH$_2$SiMe$_3$)$_2$(THF) depicted in Scheme 30 in combination with [PhNHMe$_2$][B(C$_6$F$_5$)$_4$] and Al^{i}Bu$_3$ forms the first non-Cp-ligated rare earth metal based catalyst system to provide extremely high activity and 3,4-selectivity for the polymerization of isoprene. The resultant high molecular weight polymer (M_n = 99 × 104) with nar-

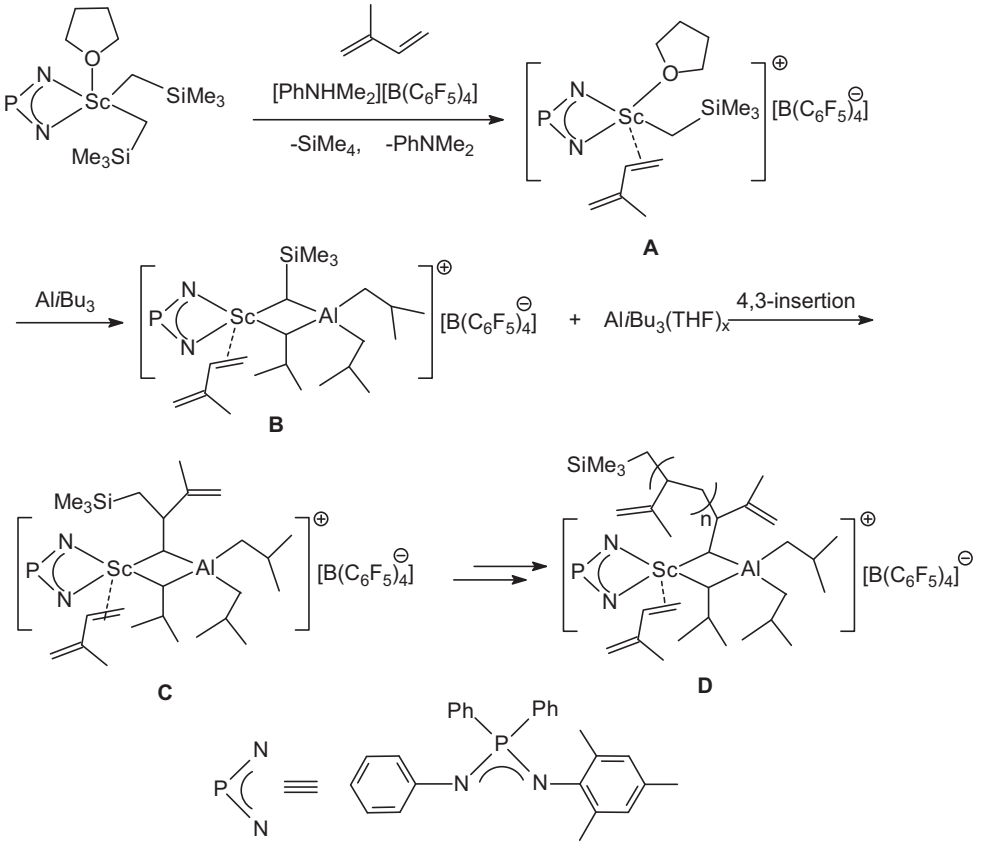

Scheme 132.

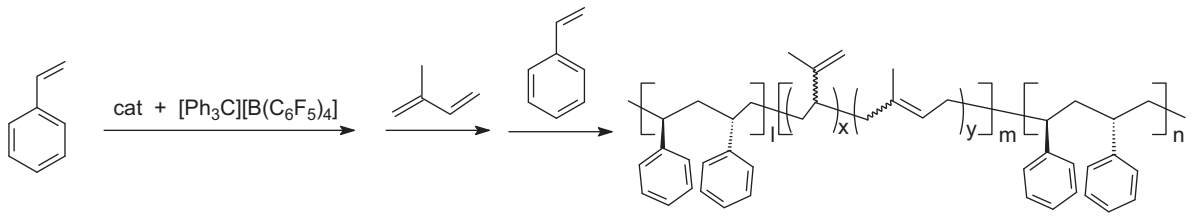

Scheme 133.

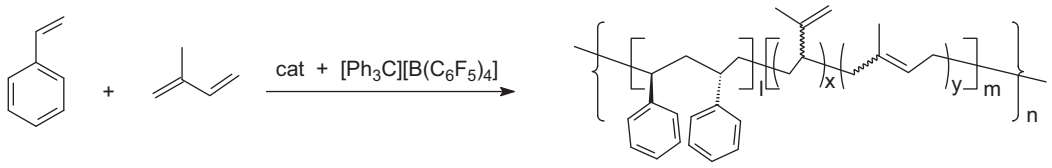

Scheme 134.

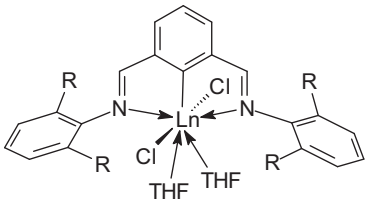

Ln = Y: R = Me, Et, ^{i}Pr
R = Et: Ln = La, Nd, Gd
Sm, Eu, Tb
Dy, Ho
Yb, Lu

Scheme 135.

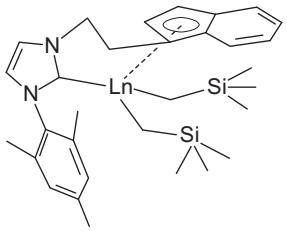

(Ind-NHC)Ln(CH_2SiMe_3)$_2$

Ln = Sc, Y
Ln = Ho, Lu

Scheme 137.

row molecular weight distribution (PDI = 1.55) had a 3,4-regularity up to 94.7% (Tp = −40 °C, toluene, 2 h, 100% yield). The analogous yttrium and lutetium complexes, with a larger ionic radius, were less regioselective, and the derivative with an electron-donating pyridyl moiety was found to be inert. The probable initiation species and mechanistic scenario are summarized in Scheme 132 [25].

In combination with AlR_3 and borate, the thiophene-NPN ligand supported rare-earth metal bis(alkyl) complexes shown in Schemes 26 and 27 were also found to exhibit medium activity and good *trans*-1,4 selectivity for the polymerization of butadiene. The resultant polymer had moderate molecular weight (M_n = 10 000–18 000) with narrow molecular weight distribution (M_w/M_n < 1.6) and *trans*-1,4 regularity varying from 49.2% up to 91.3%. The catalyst performances were found to be strongly dependent on the *ortho* substituent of the *N*-aryl ring, the presence of the thiophene moiety of the ligands, the type of aluminum alkyls and the lanthanide metal used. The scandium complex derived from HL^2 displayed the highest *trans*-1,4 selectivity [23]. By the use of a cationic half-sandwich scandium alkyl catalyst, the syndiospecific living copolymerization of styrene with isoprene has been achieved for the first time, which afforded a new family of styrene–isoprene copolymers that possess stereoregular syndiotactic styrene–styrene blocks and were difficult to be prepared previously, such as AB type styrene–isoprene diblock copolymers, ABA type styrene–isoprene–styrene triblock copolymers (Scheme 133), and multiblock styrene–isoprene copolymers (Scheme 134). The catalyst was prepared from $(C_5Me_4SiMe_3)Sc(CH_2SiMe_3)_2(THF)$ and 1 equiv. of $[Ph_3C][B(C_6F_5)_4]$ in toluene at room temperature [95].

The heterobimetallic (Ln/Al) chlorinated half-sandwich complexes shown in Scheme 119 were found to be inactive in isoprene polymerization. However, activation of the complexes

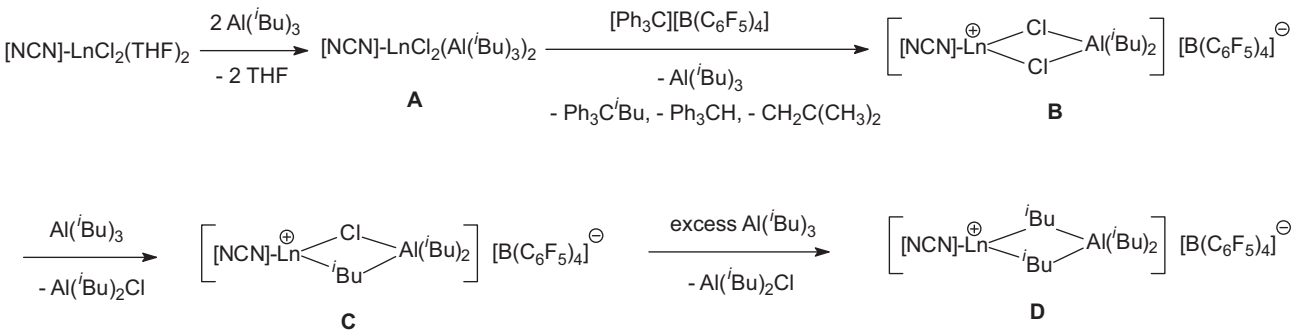

Scheme 136.

(CpR)Ln($AlMe_4$)$_2$ with boron-containing cocatalysts, such as [Ph_3C][$B(C_6F_5)_4$], [$PhNMe_2H$][$B(C_6F_5)_4$], or $B(C_6F_5)_3$, produced initiators for the fabrication of *trans*-1,4-polyisoprene. The choice of rare-earth metal cation size, CpR ancillary ligand, and type of boron cocatalyst crucially affects the polymerization performance, including activity, catalyst efficiency, living character, and polymer stereoregularity. Systematic investigations of the effects of metal cation size, the substituents on the cyclopentadiene ligand, and cocatalyst interactions (borate *vs.* borane) revealed: (a) good (for systems activated with $B(C_6F_5)_3$) to excellent catalytic activities for (CpR)Ln($AlMe_4$)$_2$ activated by borate cocatalysts [Ph_3C][$B(C_6F_5)_4$] or [$PhNMe_2H$][$B(C_6F_5)_4$], (b) increased *trans*-1,4-selectivity with increasing size of the rare-earth metal cation (Y < Nd « La), (c) increased *trans*-1,4-selectivity with enhanced chemical "innocence" and stability of the CpR ligand (1,3-$(Me_3Si)_2C_5H_3$ ≪ 1,2,4-$(Me_3C)_3C_5H_2$ < $C_5Me_4SiMe_3$ ≪ Cp*). The highest stereoselectivities were observed for the precatalyst/cocatalyst systems ($C_5Me_4SiMe_3$)La($AlMe_4$)$_2$/$B(C_6F_5)_3$ (*trans*-1,4-content: 95.6%, M_w/M_n = 1.26) and Cp*La($AlMe_4$)$_2$/$B(C_6F_5)_3$ (*trans*-1,4-content: 99.5%, M_w/M_n = 1.18) [88]. Similarly, fluorinated borates [Ph_3C][$B(C_6F_5)_4$] and [$PhNMe_2H$][$B(C_6F_5)_4$] as well as the borane reagent $B(C_6F_5)_3$ activate rare-earth-metal bis(tetramethylaluminate) complexes in a distinct and efficient manner (an activated catalyst is shown in Scheme 120) for the fabrication of synthetic gutta-percha *via* living isoprene polymerization (99.5% *trans*-1,4-polyisoprene, M_n = 0.8–4.4 × 10^5 g mol^{-1}, M_n/M_w = 1.18) [89]. Highly *cis*-1,4 selective polymerization of dienes has been achieved with homogeneous Ziegler-Natta catalysts based on the NCN-pincer rare-earth metal dichloride

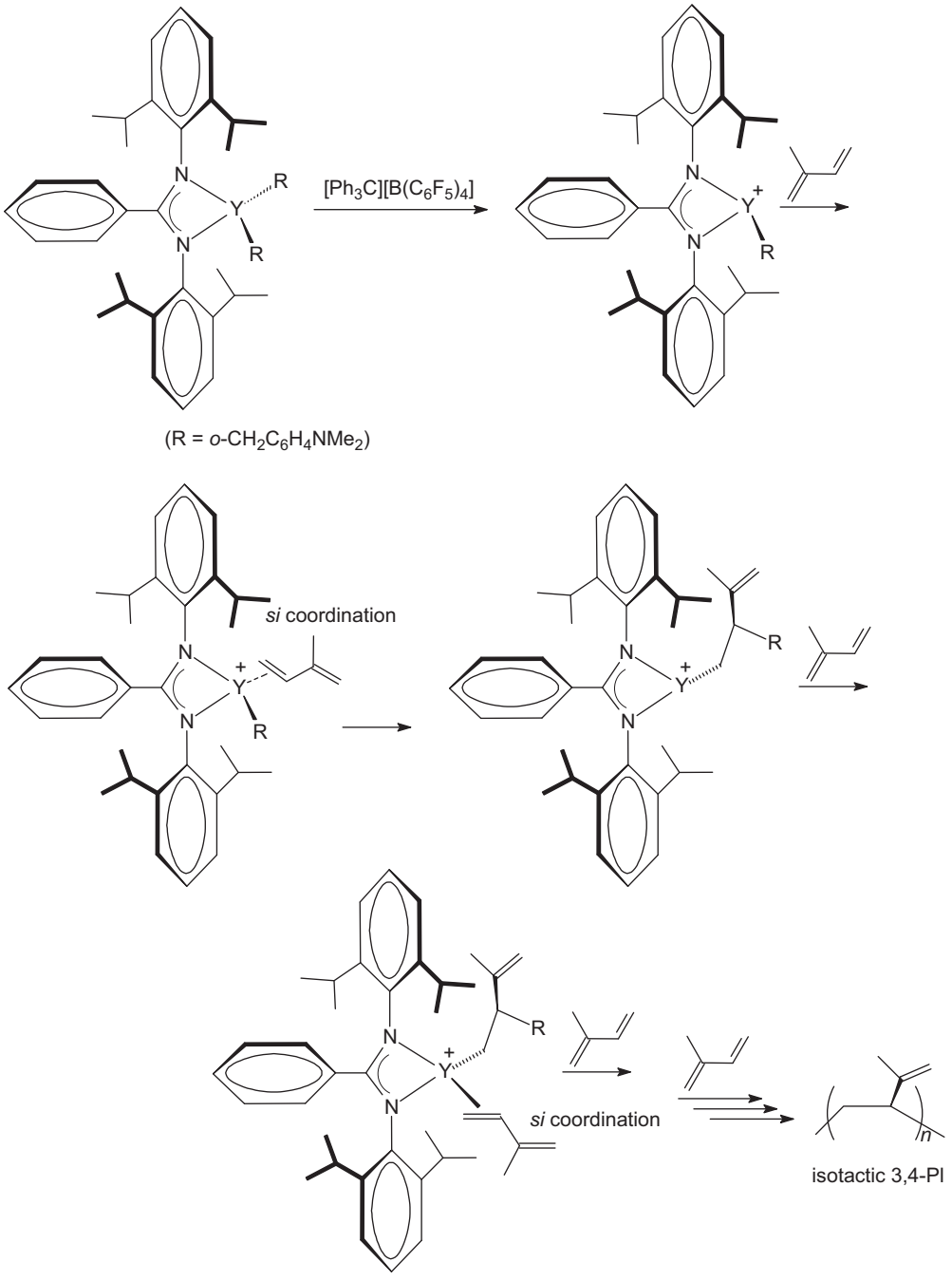

Scheme 138.

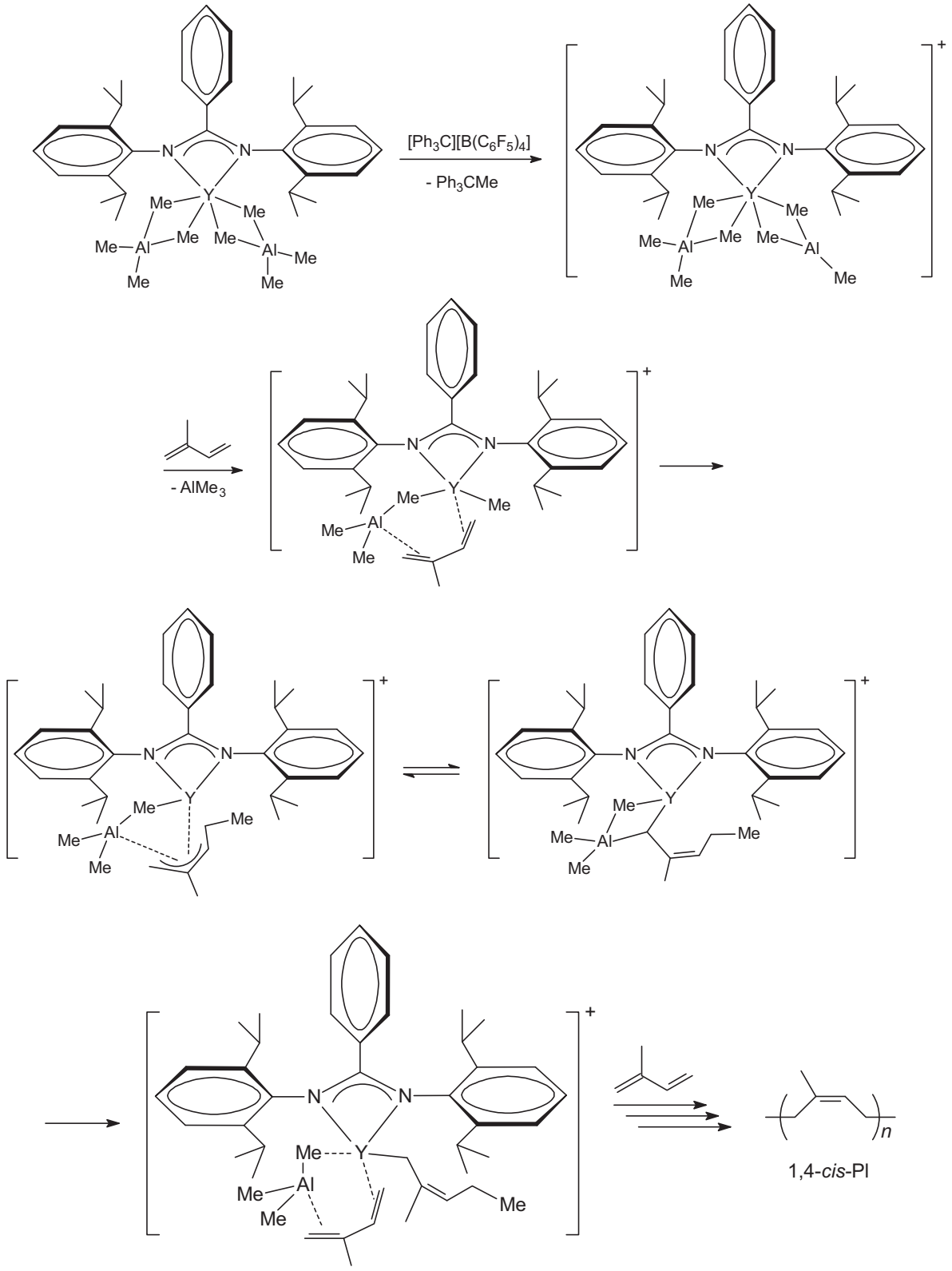

Scheme 139.

precursors shown in Scheme 135. The dichlorides combined with aluminum tris(alkyl)s and $[Ph_3C][B(C_6F_5)_4]$ established a homogeneous Ziegler-Natta catalyst system, which exhibited high activities and excellent *cis*-1,4 selectivities for the polymerizations of butadiene (T_p = 25 °C, 99.9%; 0 °C, 100%) and isoprene (T_p = 25 °C, 98.8%). Remarkably, such high *cis*-1,4-selectivity almost remained at elevated polymerization temperatures up to 80 °C and did not vary with the type of the central lanthanide element, however, it was influenced obviously by the *ortho*-substituent of the *N*-aryl ring of the ligands and the bulkiness of the aluminum alkyls [96].

As illustrated in Scheme 136, alkyl-bridged Ln–Al bimetallic cations were proven to be the actual active species [96].

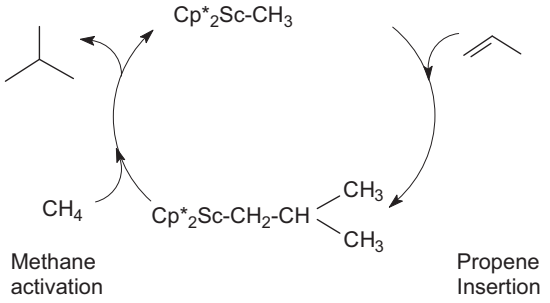

Scheme 140.

Highly 3,4-selective living polymerization of isoprene with has been achieved with rare-earth metal fluorenyl *N*-heterocyclic carbene precursors (*cf.* Scheme 94). With the activation of Al^iBu_3 and $[Ph_3C][B(C_6F_5)_4]$ they exhibited high activity, medium syndio- but remarkably high 3,4-regioselectivity, and the unprecedented livingness for the polymerization of isoprene. Such distinguished catalytic performances could be maintained under various monomer-to-initiator ratios (500–5000) and broad polymerization temperatures (25–80 °C). The resultant polymers are crystalline, having syndiotactically enriched (racemic enchainment triad *rr* = 50%, pentad *rrrr* = 30%) 3,4-regulated (99%) microstructure and high glass-transition temperatures (40–49 °C). In contrast, the scandium complex was almost inert, while complexes bearing indenyl modified *N*-heterocyclic carbene moiety, (Ind-NHC)Ln$(CH_2SiMe_3)_2$ (Ind-NHC = $C_9H_6CH_2CH_2$(NCHCCHN)-$C_6H_2Me_3$-2,4,6; Ln = Sc, Y, Ho, Lu) (Scheme 137) also showed low activity or selectivity. These differences in catalytic performance could be attributed mainly to the electronics and spacial sterics of the metal center of these precursors [66].

It was reported that the neutral mono(amidinato) yttrium dialkyl complex depicted in Scheme 20 does not catalyze the polymerization of isoprene but it becomes extremely active in the presence of 1 equiv. of $[Ph_3C][B(C_6F_5)_4]$, whereby it converts 750 equiv. of isoprene quantitatively into polyisoprene in 2 min at room temperature. This reaction proceeds with high 3,4-regioselectivity (91%) and some degree of isotacticity (*mm* ≈ 50%). When the polymerization is carried out at low temperature (≤−10 °C), an even higher regio- and stereoselectivity was achieved and almost perfectly isotactic 3,4-polyisoprene was obtained (3,4-selectivity up to 99.5%, *mmmm* up to 99%). A possible mechanism for the isospecific 3,4-polymerization of isoprene by this catalyst system was proposed (Scheme 138). Thus, the reaction of the neutral mono(amidinato) yttrium dialkyl complex with $[Ph_3C][B(C_6F_5)_4]$ gives a cationic aminobenzyl species. The steric hindrance and C_2 symmetry of the (NCNdipp)Y unit means that the coordination of isoprene to the Y center in the latter species takes place preferably in a 3,4-η^2 fashion through the *si* face to an isoprene adduct. Subsequent migratory addition of the aminobenzyl group to the coordinated isoprene affords a tricoordinate intermediate, followed by multiple subsequent 3,4-coordination and isoprene insertion steps, eventually leading to the formation of isotactic 3,4-polyisoprene [19].

More remarkably, the regio- and stereoselectivities of this polymerization system can be dramatically switched from 3,4-isospecific to 1,4-*cis*-selective by the addition of $AlMe_3$. Isolation of a heterotrinuclear Y/Al complex (*cf.* Scheme 113) from the reaction of $(NCN^{dipp})Y(o\text{-}CH_2C_6H_4NMe_2)_2$ with $AlMe_3$, and the 1,4-*cis*-specificity of the (NCNdipp)Y$[(\mu\text{-}Me)_2AlMe_2]_2$/$[Ph_3C][B(C_6F_5)_4]$ system for the polymerization of isoprene, suggested that this selectivity switching from 3,4-isospecific to 1,4-*cis*-selective could be due to the involvement of a cationic, heterobimetallic Y/Al catalyst species. A possible mechanism for the 1,4-*cis*-polymerization of isoprene by the heterobimetallic catalyst system is illustrated in Scheme 139. Although alkylaluminum compounds have often been used as additives or cocatalysts in various isoprene polymerization catalyst systems, this was the first report to unambiguously show that the incorporation of an alkylaluminum species can dramatically change the regio- and stereoselectivities of a catalyst system [19].

2.9.1.3. Cyclic esters and amides (ε-caprolactone, δ-valerolactone, lactide, etc.). The mechanisms of polymerization of ε-caprolactone (CL) initiated by either the rare-earth hydride $Cp_2Eu(H)$ or the borohydrides $Cp_2Eu(BH_4)$ or $(N_2NN')Eu(BH_4)$ (N_2NN' = (2-$C_5H_4N)CH_2(CH_2CH_2NMe)_2$) have been studied at the DFT level. For all compounds the reaction proceeds in two steps: hydride transfer from the rare-earth initiator to the carbonyl carbon of the lactone, followed by ring-opening of the monomer. In the last step a difference was observed between the hydride and borohydride complexes, because for the latter the ring-opening is induced by an additional B–H bond cleavage leading to a terminal $–CH_2OBH_2$ group. This corresponds to the reduction by BH_3 of the carbonyl group of CL. Upon reaction of $Cp_2Eu(H)$ with CL, the alkoxy–aldehyde complex produced, $Cp_2Eu[O(CH_2)_5C(O)H]$, is the first-formed initiating species. In contrast, for the reaction of CL with the borohydride complexes $(L_x)Eu(BH_4)$ (L_x = Cp_2 or N_2NN'), an aliphatic alkoxide with a terminal $–CH_2OBH_2$ group, $(L_x)Eu[O(CH_2)_6OBH_2]$ is formed and subsequently propagates the polymerization. These DFT investigations were fully compatible with previously reported mechanistic studies of experimental systems [97]. The dialkyllanthanide complexes shown in Scheme 25 were found to display high activities for the ring-opening polymerization of ε-caprolactone, in which narrow-polydispersity polymers were produced. The size of the pendant arm has a significant effect on the molecular weight of the polymer obtained. In comparison to the Y complex with an $–NMe_2$ group, the Y complexes with $–NEt_2$ and $–N((CH_2CH_2)_2CH_2)$ groups yield much higher molecular weight polymers (60 000 *vs* 20 000) [22]. Rare-earth metal bis(alkyls) supported by a quinolinyl anilido-imine ligand (Scheme 32) were reported to catalyze the ring-opening polymerization of ε-caprolactone with high activities in living fash-

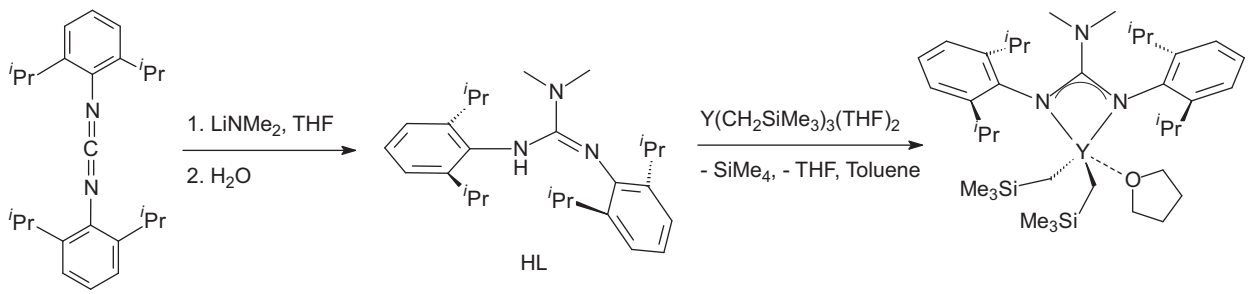

Scheme 141.

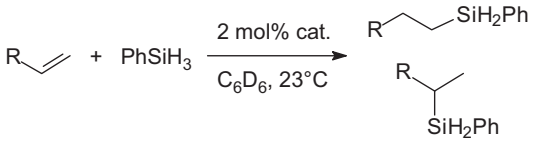

Scheme 142.

ion, among which the Lu complex was proved to be more active than its Sc and Y analogues [27]. The scandium dimethylbenzyl complex Sc(fc[NSi(^{t}Bu)Me$_2$]$_2$)(CH$_2$Xy-3,5)(THF) and its adduct with AlMe$_3$ (*cf.* Scheme 125) were reported to polymerize L-lactide [17].

2.9.1.4. Acrylic monomers (methyl methacrylate (MMA), acrylonitrile, etc.). A combined experimental and computational approach has been employed to gain new insights into the polymerization of methyl methacrylate (MMA) initiated by rare-earth borohydride complexes. Polymerization of MMA initiated by Ln(BH$_4$)$_3$(THF)$_3$ (Ln = Nd, Sm) or Cp*$_2$Sm(BH$_4$)(THF) proceeds at ambient temperature to give rather syndiotactic poly(methyl methacrylate) (PMMA) with molar masses M_n higher than expected and quite broad molar mass distributions, which is consistent with a poor initiation efficiency. The polymerization of MMA was investigated by performing density functional theory (DFT) calculations on an η-C$_5$H$_5$ model metallocene and showed that in the reaction of Cp$_2$Eu(BH$_4$) with MMA the borate Cp$_2$Eu[(OBH$_3$)(OMe)C = C(Me)$_2$] complex, which forms *via* the enolate Cp$_2$Eu[O(OMe)C=C(Me)$_2$], was calculated to be exergonic and is the most likely of all of the possible products. This product is favored because the reaction that leads to the formation of the carboxylate Cp$_2$Eu[OOC–C(Me)(=CH$_2$)] is thermodynamically favorable, but kinetically disfavored, and both of the potential products from a Markovnikov Cp$_2$Eu[O(OMe)C–CH(Me)(CH$_2$BH$_3$)] or *anti*-Markovnikov Cp$_2$Eu[O(OMe)C–C(Me$_2$)(BH$_3$)] hydroboration reaction are also kinetically inaccessible. Similar computational results were obtained for the reaction of Eu(BH$_4$)$_3$ and MMA with all of the products showing extra stabilization. The DFT calculations performed by using Cp$_2$EuH to model the mechanism previously reported for the polymerization of MMA initiated by [Cp*$_2$SmH]$_2$ confirmed the favorable exergonic formation of the intermediate Cp$_2$Eu[O(OMe)C=C(Me)$_2$] as the kinetic product, this enolate species ultimately leads to the formation of PMMA as experimentally observed. Replacing H by BH$_4$ thus prevents the 1,4-addition of the Cp$_2$Eu(BH$_4$) borohydride ligand to the first incoming MMA molecule and instead favors the formation of the borate complex Cp$_2$Eu[(OBH$_3$)(OMe)C=C(Me)$_2$]. This intermediate is the somewhat active species in the polymerization of MMA initiated by the borohydride precursors Ln(BH$_4$)$_3$(THF)$_3$ or Cp*$_2$Sm(BH$_4$)(THF) [98].

The catalytic properties of the organolanthanide(II) fluorenyl complexes shown in Scheme 90 on the polymerization of ε-caprolactone and methyl methacrylate have been studied. The temperatures, solvents and coordination effects on the catalytic activities of the complexes were examined. It was found that both series of complexes containing heterocyclic-functionalized fluorenyl ligands can act as single-component catalysts for ring-opening of ε-caprolactone and MMA polymerization with very good catalytic activities. The experimental results of the catalytic activities of the complexes indicated that organolanthanide(II) complexes incorporating fluorenyl ligands have an advantage as catalysts for MMA and ε-caprolactone polymerization over the complexes with indenyl ligands with similar substituents. It was also found that temperatures, solvents and the central metals have influences on the catalytic activities of catalysts, the molecular weights, and the molecular weight distributions of polymers [63]. The monoalkyl diamido-pyridine compound [**L1**]Ln(CH$_2$SiMe$_3$)(THF)$_x$ (H**L1** = [2,6-{(2,6-^{i}Pr$_2$C$_6$H$_3$)NHCH$_2$}C$_5$H$_3$N] (Scheme 39) has been reported to polymerize methyl methacrylate [32]. Good MMA polymerization activity has also been found for the THF-coordinated bis-Ab yttrium alkyl complex, Ab$_2$Y(CH$_2$SiMe$_3$)(THF) (Ab = 1-methyl-2-phenyl-1,2-azaborolyl) shown in Scheme 97. This compound serves as an efficient single-component initiator to initiate MMA polymerization with living character, and the polymerization is more consistent with a site-control mechanism [68]. Rare-earth metal alkyls embedded into a 1,1′-diamidoferrocene framework (*cf.* Scheme 128) effectively initiate the polymerization of MMA at room temperature, producing isotactic enriched poly(methyl methacrylate) (PMMA). The properties of the produced PMMAs are mainly governed by the substitution patterns of the ferrocenyl backbone [11].

2.9.2. Organolanthanide-catalyzed hydrosilylation, hydroamination and hydrophosphination reactions

Density functional theory (B3PW91) calculations have been carried out for the hydromethylation of propene (Scheme 140) and isobutene catalyzed by the scandium complex *ansa*-Me$_2$Si(C$_5$Me$_4$)$_2$ScCH, as modeled by H$_2$Si(C$_5$H$_4$)$_2$ScCH$_3$. The calculations showed that the hydromethylation of isobutene, but not propene, could be catalytic, and the difference may be attributed to a combination of electronic and steric factors. Several side reactions have also been considered. The catalytic cycle is completed only for cases in which both the olefin and methane can interact with the Lewis acidic metal center in separate steps. Olefins have greater coordination strengths than methane unless steric factors dominate. In the case of the *ansa* complex, which is more Lewis acidic and slightly more open than a non-*ansa* complex, calculations show that the strong binding of propene blocks the cat-

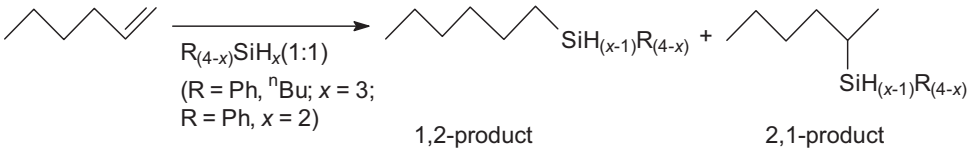

Scheme 143.

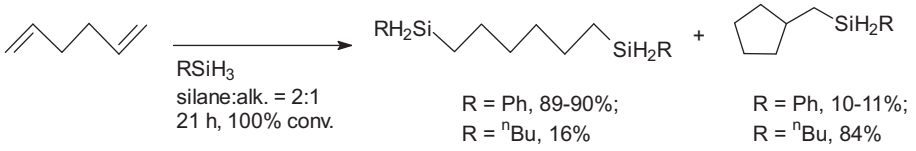

Scheme 144.

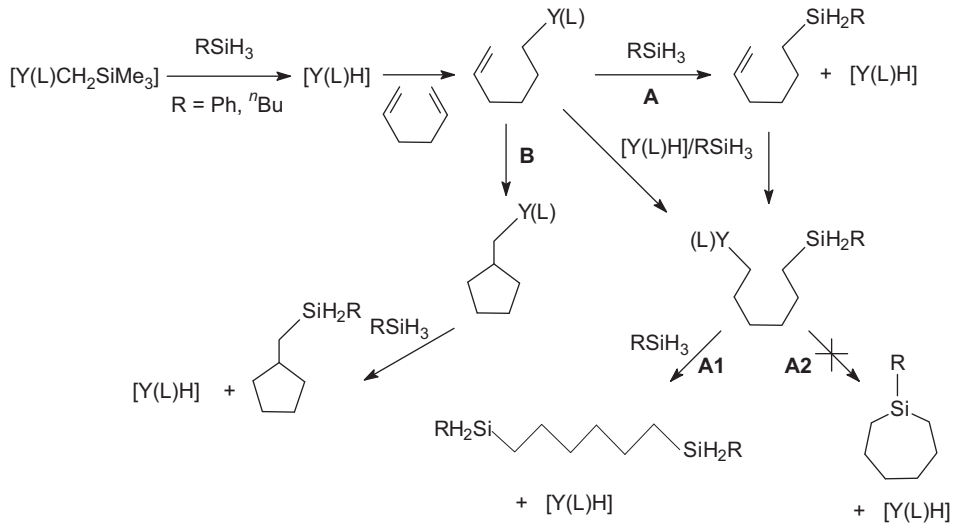

Scheme 145.

alytic cycle. This is not the case for the more bulky isobutene, which is a poorer ligand and thus allows competitive access of methane to the metal center [99].

The highly efficient hydrosilylation of alkenes by organoyttrium catalysts with sterically demanding amidinate and guanidinate ligands has been reported. The sterically demanding guanidine ArNHC(NMe_2)NAr (Ar = 2,6-diisopropylphenyl, HL) reacts with $Y(CH_2SiMe_3)_3(THF)_2$ to give the yttrium dialkyl complex (L)$Y(CH_2SiMe_3)_2(THF)$, which was structurally characterized (Scheme 141). Electronic interaction of the –NMe_2 group with the conjugated ligand backbone could be inferred from structural and spectroscopic data [100].

The new yttrium guanidinate complex and its related amidinate analogue [PhC($NAr)_2$]$Y(CH_2SiMe_3)_2(THF)$ were found to be highly active and selective catalysts for alkene hydrosilylation with $PhSiH_3$ (Scheme 142, tof > 600 h^{-1} at 23 °C). For unfunctionalized olefins, full selectivity toward *anti*-Markovnikov products was obtained. The more electron donating guanidinate ligand afforded the highest activities with heteroatom-functionalized substrates [100].

Several rare-earth metal alkyl complexes with tridentate [OSO]-type and tetradentate [OSSO]-type bis(phenolato) ligands shown in Scheme 36 have been found to be effective catalysts for olefin hydrosilylation (Scheme 143). These complexes were tested in the hydrosilylation of a wide variety of aliphatic and aromatic 1-alkenes and 1,5-hexadiene with various silanes ($PhSiH_3$, $^nBuSiH_3$, and Ph_2SiH_2). In the case of terminal aliphatic alkenes an *anti*-Markovnikov (1,2) addition takes place with 80–99% regioselectivity. The hydrosilylation of styrene afforded the Markovnikov (2,1) addition product PhHC(SiH_2Ph)Me with 97% regioselectivity [29].

The hydrosilylation of 1,5-hexadiene by $PhSiH_3$ catalyzed by a bis(phenolato)-stabilized yttrium alkyl resulted in the formation of a linear product, 1,6-bis(phenylsilyl)hexane (*ca.* 90%), and a cyclic product, (phenylsilylmethyl)cyclopentane (*ca.* 10%), whereas with $^nBuSiH_3$ 84% of the cyclic product was obtained (Scheme 144) [29].

The proposed mechanism for the hydrosilylation of 1,5-hexadiene catalyzed by the bis(phenolato)-stabilized yttrium alkyl is presented in Scheme 145. Analogous to the hydrosilylation of monoolefins, it is likely that the reaction of the yttrium alkyl complex with $RSiH_3$ initiates the catalytic cycle with concomitant generation of the yttrium hydride. The *anti*-Markovnikov addition of the hydride to 1,5-hexadiene leads to the intermediate yttrium 5-hexenyl complex, which further reacts *via* two competing reaction pathways, **A** and **B**. In the case of $PhSiH_3$ pathway **A** is favored, yielding the linear product **A1**. The ring closure pathway (**A2**) to give silacycloheptane was not observed. In contrast to the reaction with $PhSiH_3$, intramolecular insertion of the yttrium 5-hexenyl complex leads to the yttrium methylcyclopentyl complex in the presence of $^nBuSiH_3$, which undergoes intermolecular σ-bond metathesis with $^nBuSiH_3$ to yield (silylmethyl)cyclopentane. This distinctly different reactivity of $PhSiH_3$ and $^nBuSiH_3$ can be rationalized by the slower attack on the 1-hexenyl yttrium species by the bulkier $^nBuSiH_3$. In addition, intramolecular (labile) coordination of the dangling double bond at the Lewis acidic yttrium center may play a role [29].

The neutral dialkyl complexes shown in Scheme 12 and their cationic derivatives (Scheme 19) have been studied as catalysts for the hydroamination/cyclization of 2,2-diphenylpent-4-en-1-amine and *N*-methylpent-4-en-1-amine reference substrates (Scheme 146) and compared with ligand-free Sc, Y, and La neutral and cationic catalysts. The most effective catalysts in the series were the cationic L-yttrium catalyst (for 2,2-diphenylpent-4-en-1-amine) and the cationic lanthanum systems (for *N*-methylpent-4-en-1-amine). For the La catalysts, evidence was obtained for the release of L from the metal during catalysis [15].

Good catalytic activities for intramolecular hydroamination have also been found for the boratabenzene yttrium amides shown

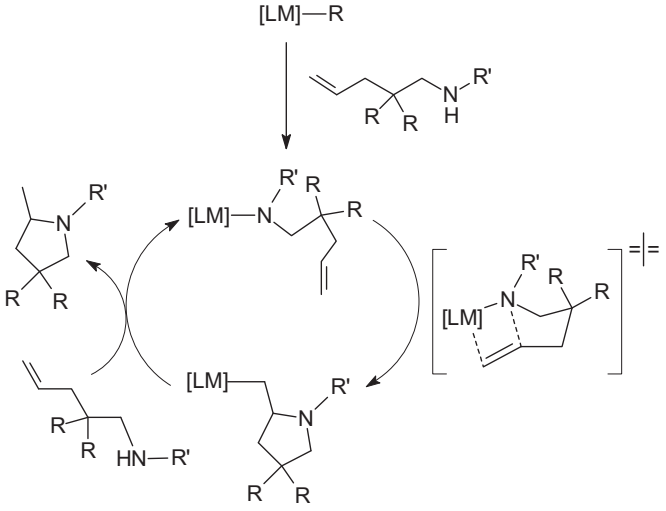

Scheme 146.

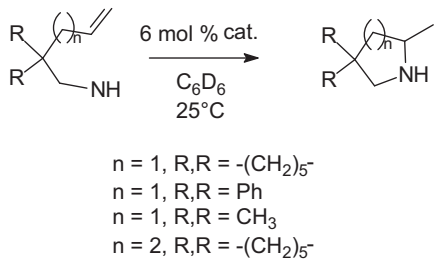

Scheme 147.

in Scheme 106 [73] as well as for the phenylene-bridged binuclear organolanthanide complexes of Scheme 56. Reactivity studies revealed that these binuclear organolanthanide complexes efficiently catalyze the intramolecular hydroamination/cyclization of aminoalkenes, aminoalkynes, and aminodienes, with turnover frequencies as high as $10\,h^{-1}$ at 60 °C [43]. The new chiral binaphthylamido alkyl "ate" and neutral yttrium and ytterbium complexes illustrated in Scheme 44 have proven to be very efficient catalysts for enantioselective intramolecular hydroamination of aminopentenes or aminohexene at room temperature with enantiomeric excesses up to 83%. The reactions were tested with the substrates shown in Scheme 147 [34].

2.9.3. Other organolanthanide-catalyzed reactions

It has been demonstrated that half-sandwich rare-earth metal alkyl complexes can act as excellent catalyst precursors for the cross-coupling of various terminal alkynes with isocyanides, selectively affording the (*Z*)-1-aza-1,3-enyne products (Scheme 148) [101].

The half-sandwich lanthanide alkyl complexes used in this study are summarized in Scheme 149 [101].

On the basis of detailed experimental results, a possible catalytic cycle for this cross-coupling reaction was proposed as illustrated in Scheme 150. The acid–base reaction between a half-sandwich rare-earth alkyl and a terminal alkyne should yield a dimeric alkynide species such as **A**. Coordination of an isocyanide to one of the metal centers of the dimeric alkynide species could afford **B** by breaking one of the two alkynide bridges. Attack of the terminal alkynide to the coordinated isocyanide on another metal center in binuclear species **B** in an intermolecular fashion should give **C**, which upon abstraction of a proton from another molecule of the alkyne would yield the corresponding (*Z*)-1-aza-1,3-enyne and regenerate the alkynide **A**. Apparently, having the coupling reaction take place at the two metal centers in a binuclear species such as **B** is the key to the selective formation of the *Z*-isomer product in the catalyst system [101].

Various divalent lanthanide complexes with the formula $LnL_2(sol)_x$ (L = N(TMS)$_2$, sol = THF, x = 3, Ln = Sm (**I**), Eu (**II**), Yb (**III**); L = MeC_5H_4, sol = THF, x = 2, Ln = Sm (**IV**); L = ArO (Ar = [2,6-^{t}Bu$_2$-4-MeC_6H_2]), sol = THF, x = 2, Ln = Sm (**V**)), especially complexes **I**–**III**, have been found to serve as excellent catalyst precursors for catalytic addition of various primary and secondary amines to carbodiimides, efficiently providing the corresponding guanidine derivatives with a wide range of substrates under solvent-free condition (Scheme 151). The reaction showed good functional groups tolerence [102].

Complexes **I**–**III** are also excellent precatalysts for the addition of terminal alkynes to carbodiimides yielding a series of propiolamidines. The active sequence of Yb < Eu < Sm for metal and MeC_5H_4 < ArO < N(SiMe$_3$)$_2$ for the ligands around the lanthanide ion was observed for both reactions. A plausible mechanism for the addition of amines and terminal alkynes to carbodiimides is illustrated in Scheme 152. The first step in both reactions was supposed to include the formation of a bimetallic bis(amidinate) samarium species originating from the reduction-coupling reaction of carbodiimide promoted by the lanthanide(II) complex. The active species is proposed to be a lanthanide guanidinate and a lanthanide amidinate [102].

The half-sandwich rare-earth metal aminobenzyl complexes depicted in Scheme 57 can serve as efficient catalyst precursors for the catalytic addition of various phosphine P–H bonds to carbodiimides to form a series of phosphaguanidine derivatives with excellent tolerability to aromatic carbon–halogen bonds (Scheme 153). A significant increase in the catalytic activity was observed as a result of an increase in the metal size with a general trend of La > Pr, Nd > Sm > Gd > Lu > Sc [44].

Based upon the preparative results illustrated in Scheme 58, a possible mechanism has been formulated (Scheme 154). These results suggest that the catalytic formation of a phosphaguanidine compound proceeds through the nucleophilic addition of a phosphide species, which is formed by the acid–base reaction between a rare-earth metal *o*-dimethylaminobenzyl bond and a phosphine P–H bond, to a carbodiimide, followed by the protonolysis of the

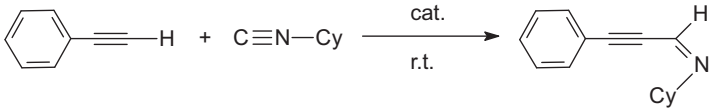

Scheme 148.

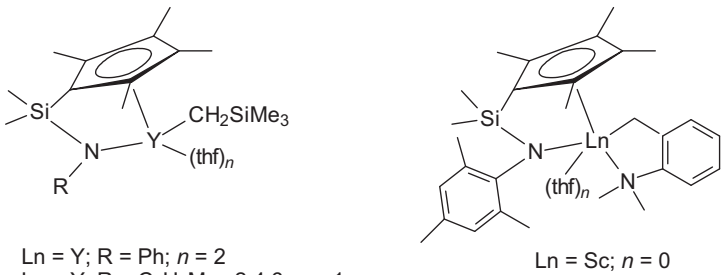

Ln = Y; R = Ph; n = 2
Ln = Y; R = $C_6H_2Me_3$-2,4,6; n = 1
Ln = Y; R = ^{t}Bu; n = 1
Ln = Yb; R = Ph; n = 2
Ln = Lu; R = Ph; n = 2

Ln = Sc; n = 0
Ln = Y; n = 1
Ln = Sm; n = 1
Ln = Nd; n = 1
Ln = La; n = 1

Scheme 149.

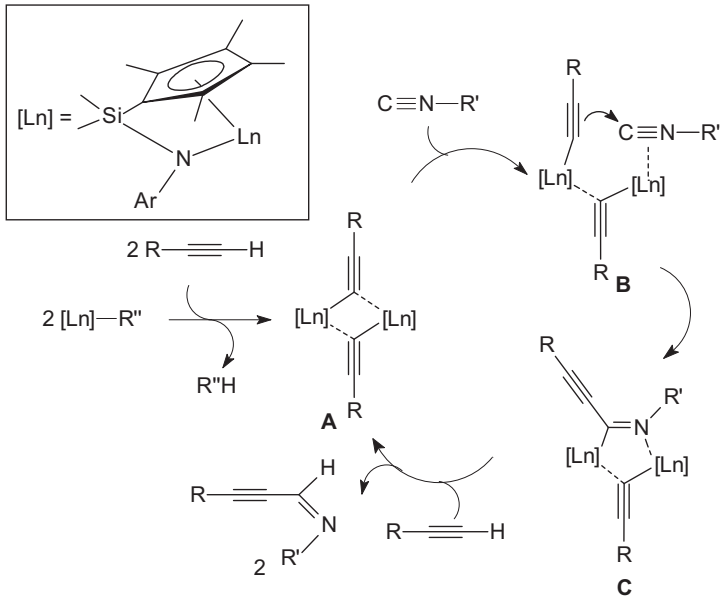

Scheme 150.

resultant phosphaguanidinate species by a phosphine P–H bond [44].

2.10. Organolanthanides in materials science

The year 2008 witnessed continued interest in the production of lanthanide oxide (Ln_2O_3) thin films through MOCVD or ALD techniques using liquid organolanthanide precursors. The most useful lanthanide precursors are ring-alkylated (ethyl, *iso*-propyl) tris(cyclopentadienyl)lanthanide complexes, many of which are now commercially available. For example, lanthanum hafnium oxide (LHO) thin films were grown using an electron cyclotron resonance atomic layer deposition technique. Tetrakis(ethylmethyl-amido)hafnium (TEMAHf) and tris(ethylcyclopentadienyl)lanthanum(III), $La(EtCp)_3$, were employed as the hafnium and lanthanum precursors, respectively, and an O_2 plasma was used as a reactant gas. Transmission electron microscopy analyses revealed that the as-deposited LHO film had a crystalline structure at a deposition temperature of 400 °C. Rapid thermal annealing of the LHO films induced dramatic changes in the electrical properties. The V_{FB} (=flatband voltage) for the films shifted toward the ideal V_{FB} and the amount of positive fixed charge disappeared in the LHO films. The leakage current density of the film deposited at 400 °C was estimated to be 4.6×10^{-7} A/cm^2 at −1 V. The leakage characteristic of the LHO films was improved with annealing at temperatures above 900 °C [103]. In a closely related study, La aluminate $(La_2O_3)_x(Al_2O_3)_{1-x}$ thin films were grown on *p*-Si (1 0 0) wafers by atomic layer deposition. In this case, $Al(CH_3)_3$ and $La(^iPrCp)_3$ were used as precursors, and O_3 gas served as the oxygen source. The films were grown in Ar ambient atmosphere, which was supplied as the purge and carrier gas. The growth temperature was 450 °C, and the thickness of the resulting La aluminate films was about 20 nm. The conduction band offset, valence band offset, and band gap were obtained by using X-ray photoelectron spectroscopy and reflection electron energy loss spectroscopy. The valence band offsets were nearly unchanged within the range from 2.23 to 2.37 eV with increasing Al content. The conduction band offsets were changed from 2.40 to 2.86 eV for the above dielectrics. Remarkably, the band gap could be engineered from 5.75 to 6.35 eV by increasing Al content [32]. Correlation between structure and properties of Er_2O_3 nanocrystalline thin films produced from a tris(cyclopentadienyl) erbium precursor have been studied. Er_2O_3 thin films were deposited by low-pressure metalorganic chemical vapor deposition (MOCVD) and also plasma-assisted (RP-MOCVD), using tris(isopropylcyclopentadienyl)erbium and O_2 on Si(1 0 0), Si(1 1 1) and corning glass substrates. The RP-MOCVD approach produced highly (1 0 0)-oriented, dense and mechanically stable Er_2O_3 films with columnar structure, while films with (1 1 1) texture are deposited by MOCVD. A high refractive index of 2.1

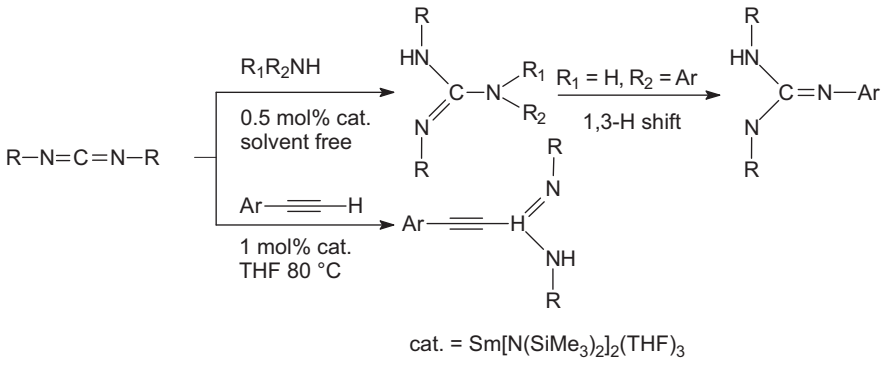

Scheme 151.

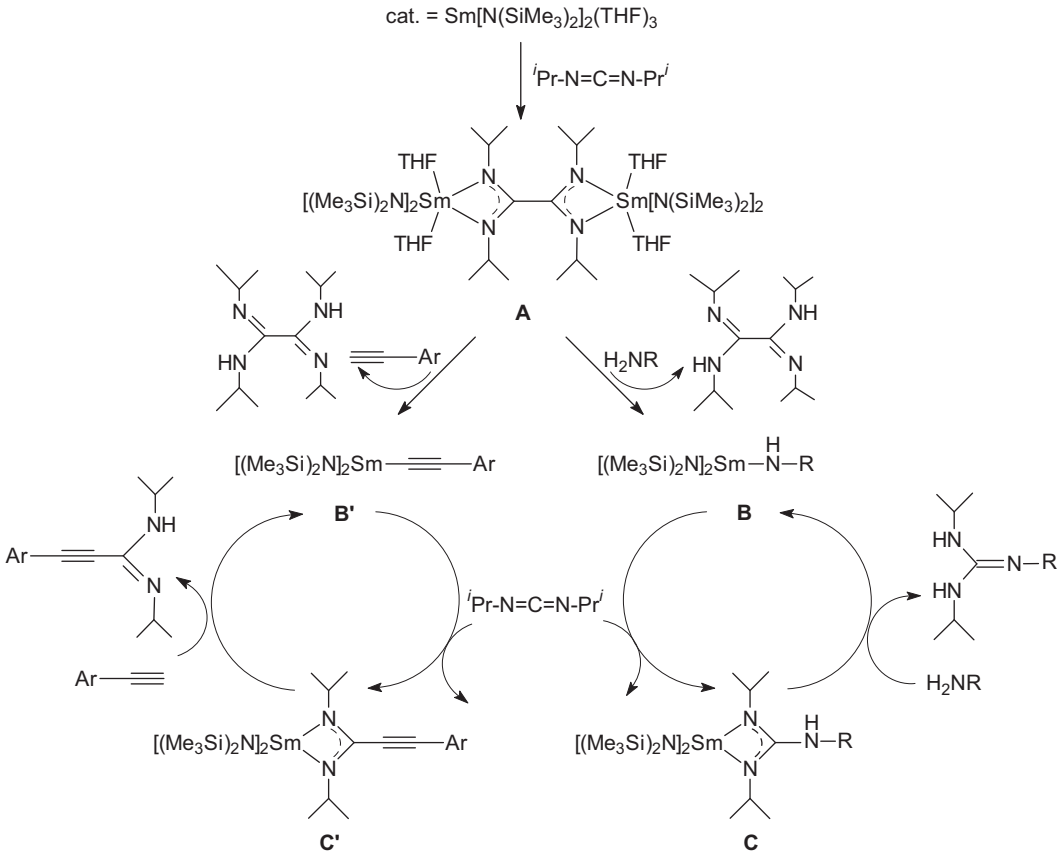

Scheme 152.

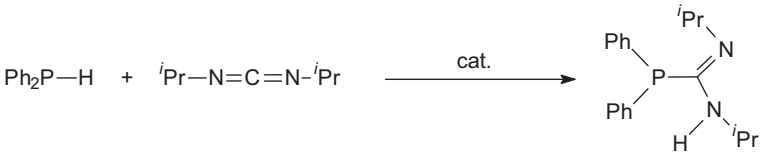

Scheme 153.

at 589.3 nm comparable to that of bulk single-crystalline Er_2O_3, a high transparency in the vis–near UV range and an optical band-gap of 6.5 eV have been found, which make Er_2O_3 interesting as antireflective and protective coating. A static dielectric constant $k \sim 12$, a density of interface traps as low as $4.2 \times 1010\,cm^2\,eV^{-1}$, for 5–10 nm thick Er_2O_3 layers grown on Si(1 0 0), render the Er_2O_3 films interesting also as high-κ dielectric in CMOS devices [104].

Two interesting organometallic precursor approaches leading to the hitherto-unknown dioxo monocarbodiimides ($Ln_2O_2CN_2$) of the late lanthanides Ho, Er, and Yb as well as yttrium have been

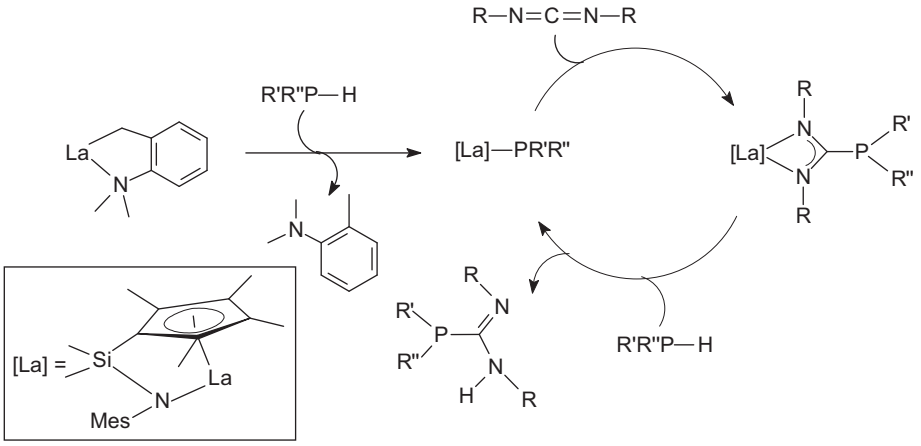

Scheme 154.

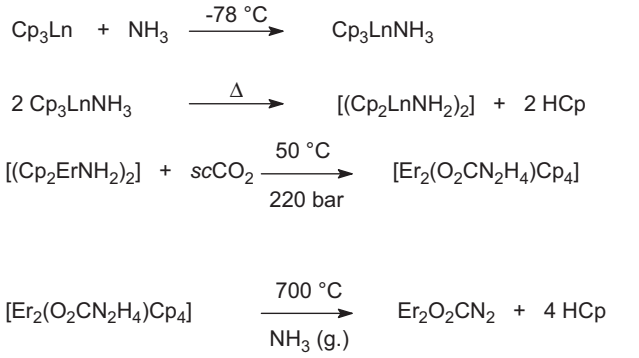

Scheme 155.

Scheme 156.

reported. One involves the insertion of CO_2, and the other one is a straightforward route using a molecular single-source precursor. To this end the reactivity of the activated amido lanthanide compound $(Cp_2ErNH_2)_2$ (Scheme 155) toward carbon dioxide absorption under supercritical conditions was studied. Selective insertion of CO_2 into the amido complex yielded the single-source precursor $Cp_4Er_2(O_2CN_2H_4)$, which was characterized by vibrational spectroscopy and thermal and elemental analyses. Ammonolysis of this amorphous compound at 700 °C afforded $Er_2O_2CN_2$ (Scheme 155) [105].

The overall yield of $Er_2O_2CN_2$ obtained in four reaction steps based on Cp_3Er as starting material (Scheme 155) was 26 mol%. Thus it was possible to synthesize pure lanthanide dioxo monocarbodiimides starting from ammonia and CO_2 by employing the well-known Cp_3Ln complexes as molecular precursors as summarized in Scheme 156. The oxophilic character of the lanthanides is the driving force for the reaction [105].

To gain deeper insight into the structural characteristics of the amorphous precursor, a similar molecular carbamato complex was synthesized as shown in Scheme 157 and fully characterized. X-ray structure analysis of the dimeric complex $Cp_4Ho_2[\mu\text{-}\eta^1\text{:}\eta^2\text{-}OC(O^tBu)NH]$ showed an unusual bonding mode of the *tert*-butylcarbamate ligand, which acts as both a bridging and side-

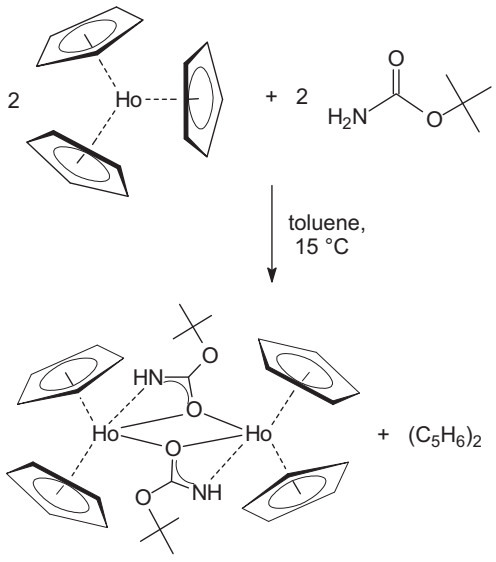

Scheme 157.

on chelating group. Ammonolysis of this compound also yielded dioxo monocarbodiimides, and therefore the crystalline carbamato complex turned out to be an alternative precursor for the straightforward synthesis of $Ln_2O_2CN_2$. Analogously, the dioxo monocarbodiimides of Y, Ho, Er, and Yb were synthesized by this route. The crystal structures were determined from X-ray powder diffraction data and refined by the Rietveld method (Ln = Ho, Er). Further spectroscopic characterization and elemental analysis evidenced the existence of phase-pure products. The dioxo monocarbodiimides of holmium and erbium crystallize in a trigonal space group. According to X-ray powder diffraction, they adopt the $Ln_2O_2CN_2$ (Ln = Ce–Gd) structure type [105].

3. Actinides

There has been a recent resurgence of interest in understanding the electronic structure of 5*f*-block element compounds. This is driven principally by the desire to predict the behavior of actinide species in a variety of applications, from waste repositories to the design of selective chemical separation methodologies. Noteworthy is for example the unique bonding pattern in the U_2 diatomic molecule that corresponds to a quintuple bond involving three electron-pair bonds and four one-electron bonds. In a 2008 theoretical study, the molecular and electronic structures, stabilities, bonding features and magnetic properties of prototypical planar isocyclic *cyclo*-U_nX_n (n = 3, 4; X = O, NH) and heterocyclic *cyclo*-$U_n(\mu_2\text{-}X)_n$ (n = 3, 4; X = C, CH, NH) clusters as well as the E@[*c*-$U_4(\mu_2\text{-}C)_4$], (E = H^+, C, Si, Ge) and U@[*c*-$U_5(\mu_2\text{-}C)_5$] molecules including a planar tetracoordinate element E (ptE) and pentacoordinate U (ppU) at the ring centers, respectively, have been thoroughly investigated by means of electronic structure calculation methods at the DFT level. It was shown that 5*f* orbitals play a key role in the bonding of these *f*-block metal systems significantly contributing to the cyclic electron delocalization and the associated magnetic diatropic (magnetic aromaticity) response. The aromaticity of the perfectly planar *cyclo*-U_nX_n (n = 3, 4; X = O, NH), *cyclo*-$U_n(\mu_2\text{-}X)_n$ (n = 3, 4; X = C, CH, NH), E@[*c*-$U_4(\mu_2\text{-}C)_4$], (E = H^+, C, Si, Ge) and U@[*c*-$U_5(\mu_2\text{-}C)_5$] clusters was verified by an efficient and simple criterion in probing the aromaticity/antiaromaticity of a molecule, that of the nucleus-independent chemical shift, NICS(0), NICS(1), $NICS_{zz}(0)$ and the most refined $NICS_{zz}(1)$ index in conjunction with the NICS scan profiles. Natural bond orbital analyses provided a clear picture of the bonding pattern in the planar isocyclic and heterocyclic uranium clusters and revealed the features that stabilize the ptE's inside the six- and eight-member uranacycle rings. The ptE's benefit from a considerable electron transfer from the surrounding uranium atoms in the E@[*c*-$U_4(\mu_2\text{-}C)_4$], (E = H^+, C, Si, Ge) and U@[*c*-$U_5(\mu_2\text{-}C)_5$] clusters justifying the high occupancy of the *np* orbitals of the central atom E [106].

3.1. Actinide hydrocarbyls

Reactions of thorium atoms with polyhalomethanes have been reported and the infrared spectra of the resulting $CH_2{=}ThX_2$, HC–ThX_3, and XC–ThX_3 molecules have been investigated. Laser-ablated thorium atoms were found to react with methylene fluoride to form singlet $CH_2{=}ThF_2$, with fluoroform to give triplet HC–ThF_3, and with CF_4 to produce triplet FC–ThF_3 molecules as the major products trapped in solid argon. Infrared spectroscopy, isotopic substitution, and density functional theoretical calculations confirmed the identity of these methylidene and methylidyne complexes. Parallels with the analogous chloromethane and Group 4 metal reaction products were also discussed. Structure calculations showed that the C=Th bond lengths decrease and the agostic distortion increases from $CH_2{=}ThF_2$ to $CH_2{=}ThFCl$ to $CH_2{=}ThCl_2$

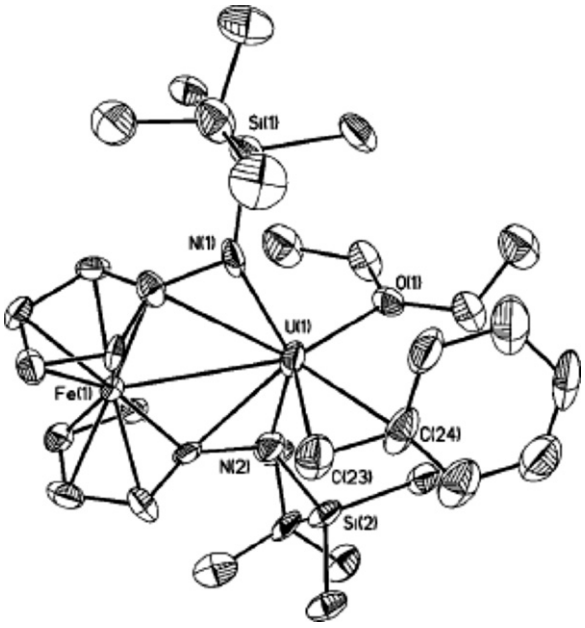

Fig. 10. ORTEP view of the cation in [{fc(NSi^{t}BuMe$_2$)$_2$}U(Bz)(Et$_2$O)][BPh$_4$] [111].

for the methylidene complexes. The triplet-state HC–ThF$_3$ and FC–ThF$_3$ electron-deficient methylidyne complexes exhibit delocalized π-bonding as evidenced by spin densities comparable to those calculated for the analogous zirconium complexes. Chlorine substitution for fluorine supports stronger C–Th bonds. Thus, thorium appears to react as an early transition-metal atom with fluoro- and chloromethanes. However, there is a substantial contribution from Th 5*f* orbitals in addition to 6*d* in the SOMO forming the weak π-bonds in these electron-deficient methylidyne complexes [107]. In a similar manner, reactions of actinide metal atoms with ethane have been studied and the computation and observation of new Th and U ethylidene dihydride, metallacyclopropane dihydride, and vinyl metal trihydride complexes reported. A combined computational and experimental investigation provided evidence that excited thorium and uranium atoms activate ethane to form the vinyl metal trihydride, metallacyclopropane dihydride, and ethylidene metal dihydride for thorium, and the latter complex and the inserted ethyl metal hydride for uranium. These products were trapped in solid argon and identified through deuterium isotopic substitution and vibrational frequencies calculated by density functional theory. Comparisons were made with group 4 and methane reaction products. Numerous calculations using several methods showed that these simple ethylidene complexes are more distorted by the agostic interaction than the

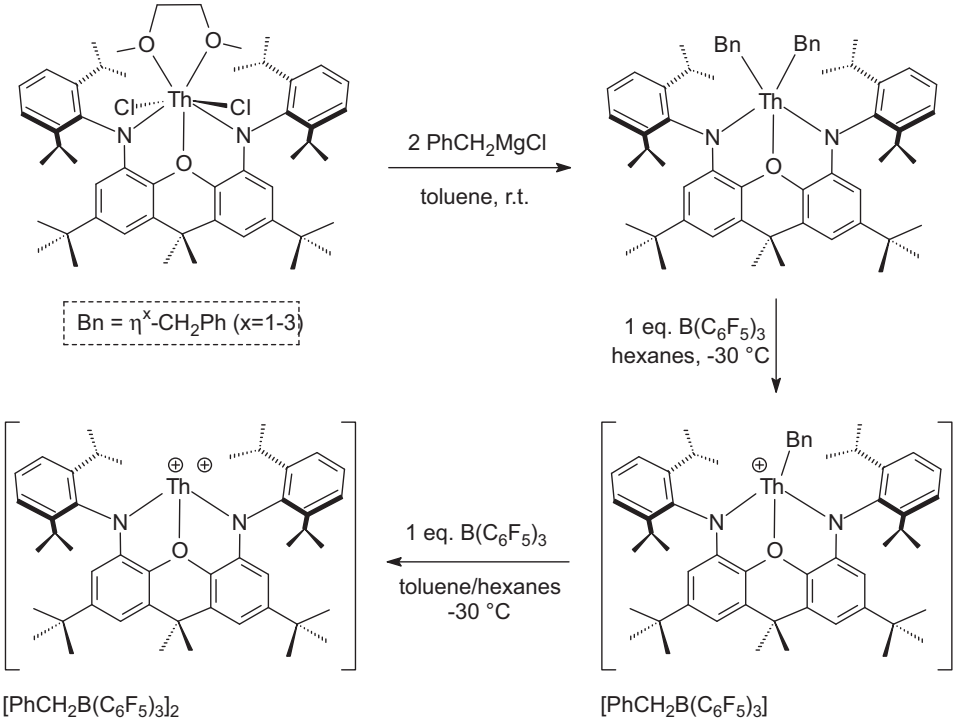

Scheme 158.

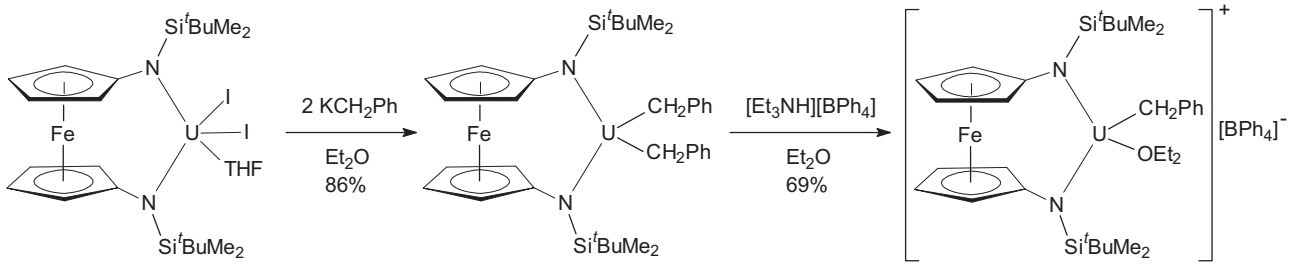

Scheme 159.

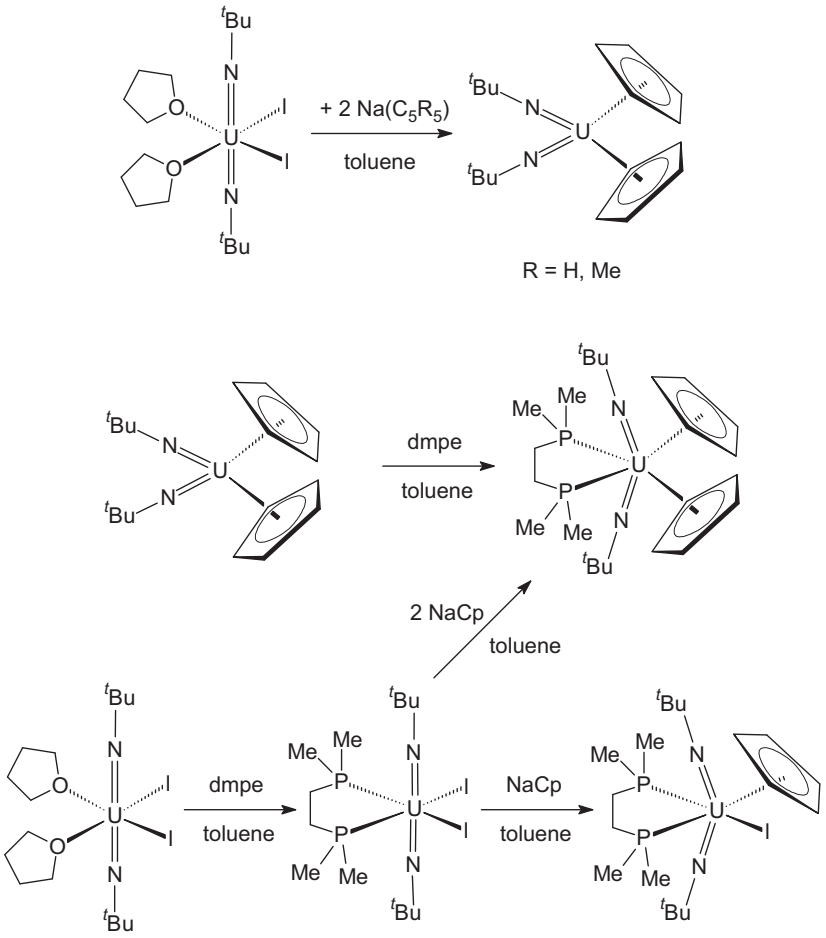

Scheme 160.

corresponding methylidene species. This enhanced agostic interaction probably arises from methyl hydrogen to α-H repulsions, which leads to a substantial decrease in the α-H to Th agostic interaction distance, and contributes to our understanding of agostic distortion in organometallic complexes [108]. Infrared spectra and electronic structures of agostic uranium methylidene molecules have been investigated in the same way. Through reactions of laser-ablated uranium atoms with methylene halides CH_2XY (XY = F_2, FCl, and Cl_2), a series of new actinide methylidene molecules CH_2=UF_2, CH_2=UFCl, and CH_2=UCl_2 were formed as the major products. The identification of these complexes was accomplished *via* matrix infrared spectra, isotopic substitution, and relativistic density functional calculations of the vibrational frequencies and infrared intensities. Density functional calculations using the generalized gradient approach (PW91) showed that these CH_2=UXY methylidene complexes prefer highly distorted agostic structures rather than the ethylene-like symmetric structures. The calculated agostic angles (∠H–C–U) are around 89° for all the three uranium complexes, and the predicted vibrational modes and isotopic shifts agree well with experimental values. Electronic structure calculations revealed that these U(IV) molecules all have strong C=U double bonds in the triplet ground states with $5f^2$ configurations. The calculated bond lengths and bond energies indicate that the C=U double bonds are slightly weaker in the fluoride species than in the chloride species because of the radial contraction of the U (6*d*) orbitals by the inductive effect of the fluorine substituent. The agostic uranium methylidene complexes were compared with analogous transition metal and thorium complexes, which revealed interesting differences in their chemistries [109].

Actinide hydrocarbyls stabilized by other ligands than substituted cyclopentadienyl remain quite rare. The isolation of an organothorium cation and a thorium dication *via* single and double alkyl abstraction from a bis(anilido)xanthene thorium(IV) dibenzyl complex have been reported. Reaction of $(XA_2)ThCl_2(dme)$ [XA_2 = 4,5-bis(2,6-diisopropylanilido)-2,7-di-*tert*-butyl-9,9-dimethylxanthene, dme = 1,2-dimethoxyethane)] with 2 equiv. of $PhCH_2MgCl$ resulted in the formation of solvent-free $(XA_2)Th(CH_2Ph)_2$ (light yellow solid, 56% yield). Subsequent reaction of the dibenzyl complex with either 1 or 2 equiv. of $B(C_6F_5)_3$ allowed the isolation of the first non-cyclopentadienyl actinide alkyl cation, $[(XA_2)Th(CH_2Ph)][PhCH_2B(C_6F_5)_3]$, and a rare example of an actinide dication, $[(XA_2)Th][PhCH_2B(C_6F_5)_3]_2$. The reaction sequence is summarized in Scheme 158 [110].

X-ray quality crystals of $(XA_2)Th(CH_2Ph)_2$ were grown from hexanes at −30 °C. The unit cell contains two distinct molecules of [Th–CH_2 = 2.503(3)–2.545(3) Å], and in both cases, one benzyl group is located in the ligand plane while the other occupies an apical site. For both molecules, the in-plane benzyl group adopts a bonding mode intermediate between η^2- and η^3-coordination (Fig. 10) [110].

Alkyl complexes of uranium supported by ferrocene diamide ligands have been described along with the corresponding cationic species. Synthesis of uranium dialkyl compounds $[fc(NSi^tBuMe_2)_2]UR_2$ [R = Np (*neo*-pentyl), Bz (benzyl)] was accomplished by salt metathesis between $[fc(NSi^tBuMe_2)_2]UI_2(THF)$ and *neo*-pentyllithium or benzylpotassium. Protonation of one alkyl ligand led to the isolation of a cationic uranium alkyl complex (Scheme 159). DFT calculations and X-ray crystallography data

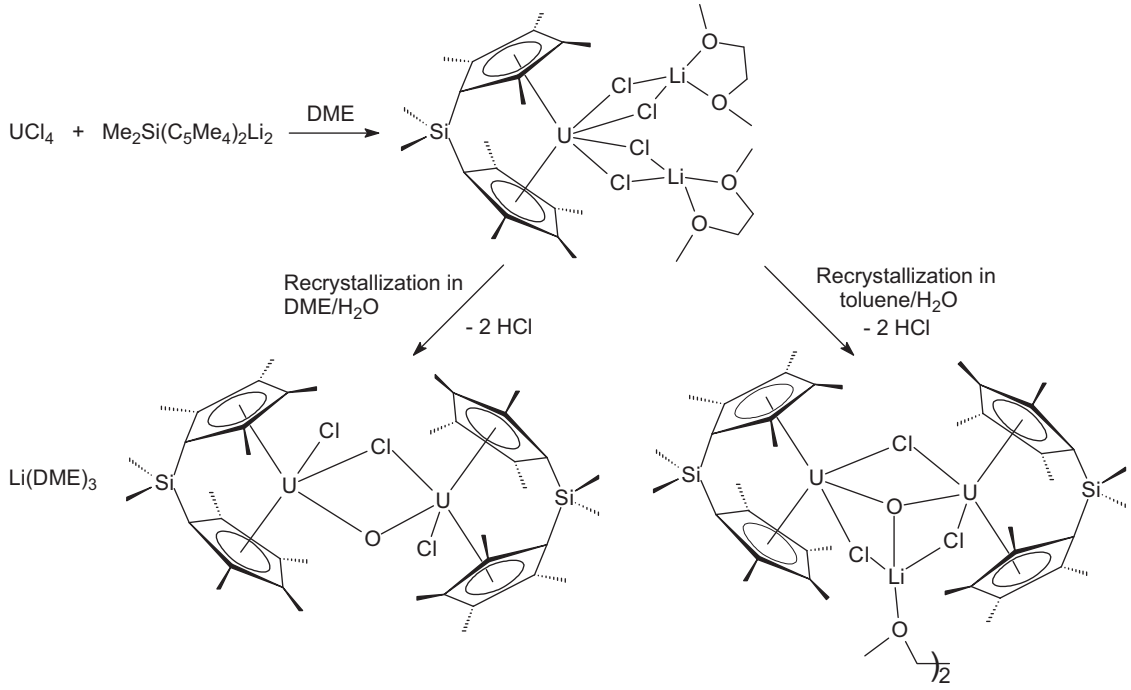

Scheme 161.

supported the existence of a donor–acceptor, weak interaction between iron and uranium [111].

The X-ray crystal structure of the cationic complex (Fig. 10) showed an η^2-coordination of the benzyl group and a pseudotetrahedral coordination around uranium [111].

Notable in this context is an important paper reporting straightforward solution syntheses of UI_3 and UI_4 etherates because such halides are to be expected to become widely used starting materials for the synthesis of organouranium complexes. Historically, UI_3 has been synthesized by the reduction of UI_4 with zinc metal in sealed silica vessels at about 600 °C. The solid-state metal iodide synthesis was optimized by synthesizing UI_3 from uranium and HgI_2 at 320 °C in a sealed glass ampule. A mercury-free synthesis involves the controlled reaction of the elements at elevated temperature. Although these reactions produce UI_3 in excellent yields, they involve the heating of uranium turnings to red heat or utilize mercury and are thus potentially dangerous or have undesirable environmental implications, respectively. It was now found that uranium turnings react with elemental iodine in diethyl ether at room temperature, with sonication and/or stirring, over a period of days to afford UI_3, $UI_4(OEt_2)_2$, or $UI_4(O^nBu_2)$ depending on the stoichiometry or ether solvent. This was the first room temperature, and thus safe and convenient, synthesis of UI_3. In order to demonstrate the utility of these solution-based syntheses, UI_3 and $UI_4(OEt_2)_2$ have been used to prepare other uranium(III) and uranium(IV) starting materials. For example, the uranium tris(silylamide), $U[N(SiMe_3)_2]_3$, can be

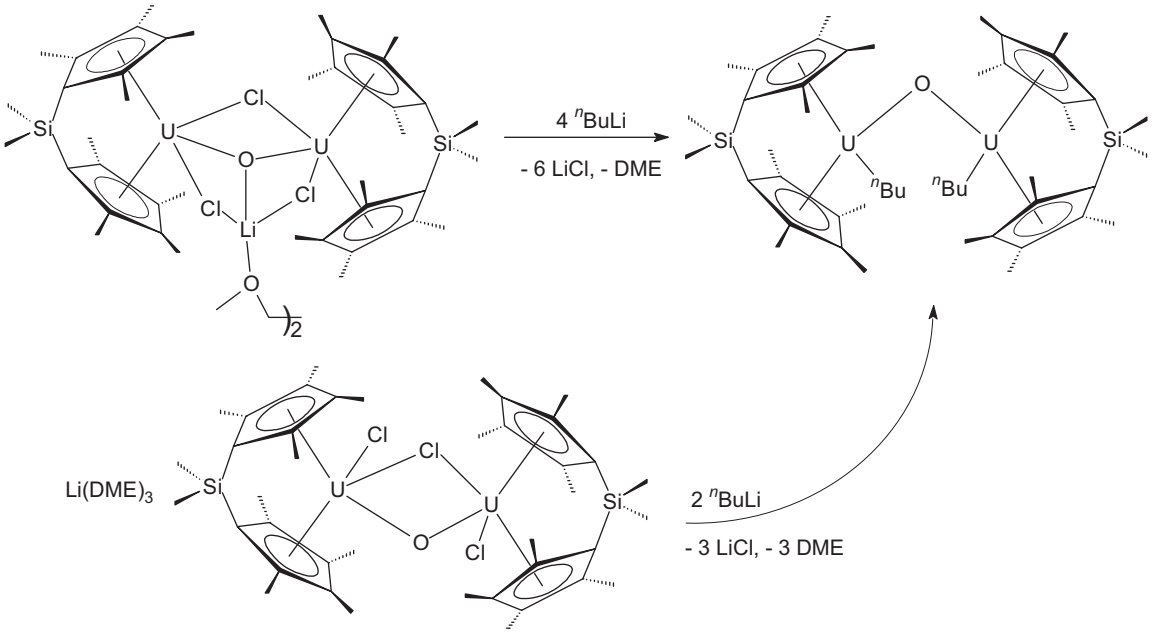

Scheme 162.

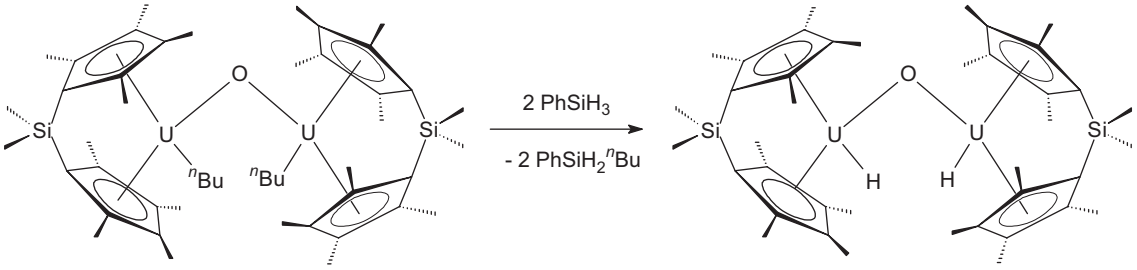

Scheme 163.

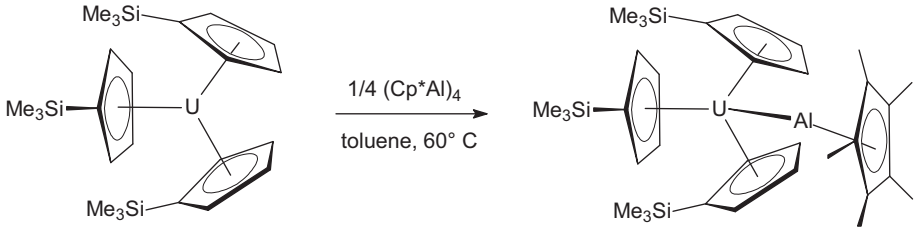

Scheme 164.

efficiently synthesized from $UI_3(THF)_4$ and $NaN(SiMe)_3$ in THF in 82% yield (on a 19 g scale). The addition of toluene to a mixture of UI_3 and $KN(SiMe_3)_2$ on a small scale afforded a dark-red-purple solution from which $U[N(SiMe_3)_2]_3$ was isolated in 63% yield, lower mainly because of the small scale of the reaction. Likewise, Cp_3UI can be made in 71% yield from $UI_4(OEt_2)_2$ and NaCp [112].

3.2. Actinide cyclopentadienyl compounds

3.2.1. $CpAnX_3$, Cp_2AnX_2 and Cp_3AnX compounds

A DFT study of the isostructural compounds $[UO_2L_5]^{n-}$ with $n = 3–5$ and linear $[Cp_2UL_5]^{m-}$ with $m = 1–3$ has been carried out for two different anionic ligands. Structurally stable structures were obtained for all systems. The coordination competition between cyanide (CN^-) and isocyanide (NC^-) as well as between cyanate (OCN^-) and isocyanate (NCO^-) has been studied in the uranyl case. A clear preference for cyanide and isocyanate complexes was reported. The coordination of five ligands in the equatorial plane was rationalised by the analysis of the MO diagram of both systems. The existence of linear $[Cp_2UL_5]^-$ organometallic U(VI) complexes was thus proposed, as well as the possibility of obtaining complexes of both types for U(VI) and U(V) with OCN^- ligands. In addition, the U(IV) linear metallocene was calculated to be stable for the latter ligand. Two structurally stable structures have been predicted with cyanide ligands: $[UO_2(CN)_5]^{4-}$ and $[Cp_2U(CN)_5]^-$. Their existence has been rationalised by the analysis of the MO diagrams and follows the isolobality concept [113].

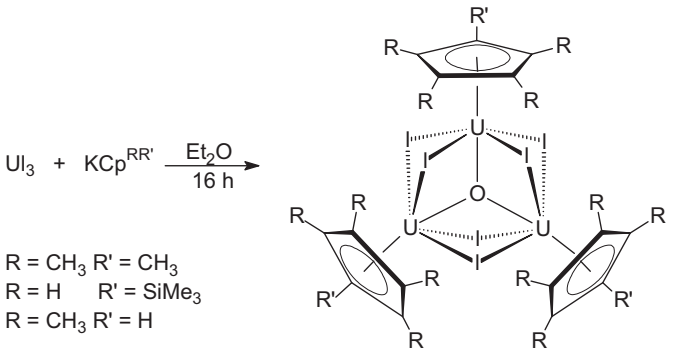

Scheme 165.

The hexavalent bis(imido) uranium(VI)-C_5H_5 and -C_5Me_5 complexes $Cp_2U(N^tBu)_2$, $Cp^*_2U(N^tBu)_2$, $CpU(N^tBu)_2(I)(dmpe)$, and $Cp_2U(N^tBu)_2(dmpe)$ can be synthesized from reactions between $U(N^tBu)_2(I)_2(L)_x$ (L = THF, $x = 2$; L = dmpe, $x = 1$) and $Na(C_5R_5)$ (R = H, Me). The synthetic routes are outlined in Scheme 160. These complexes represent the first structurally characterized C_5H_5-compounds of uranium(VI) and they further highlight the differences between UO_2^{2+} and the bis(imido) fragment [114].

The synthesis, structures, and reactivity of a series of *ansa*-dimethylsilyl oxo-bridged uranium metallocenes have been investigated in great detail. Uranium tetrachloride reacts with 1 equiv. of the lithium ligand $Li_2[(C_5Me_4)_2SiMe_2]$ in DME to form the complex $[\eta^5\text{-}(C_5Me_4)_2SiMe_2]UCl_2{\cdot}2LiCl{\cdot}2DME$, which undergoes a rapid hydrolysis either in DME with equimolar amounts of water to give the coordinatively unsaturated bridged mono-oxide and monochloride uranium lithium salt complex $\{[\eta^5\text{-}(C_5Me_4)_2SiMe_2]UCl\}_2(\mu\text{-O})(\mu\text{-Cl}){\cdot}Li(DME)_3{\cdot}DME$ or in toluene to yield the dimeric bridged monochloride mono-oxide lithium

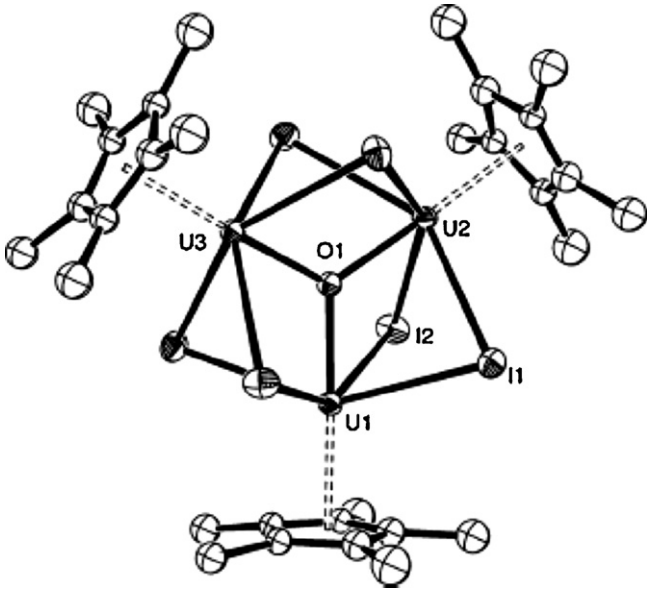

Fig. 11. Molecular structure of $[Cp^*U(\mu\text{-I})_2]_3(\mu^3\text{-O})$ [117].

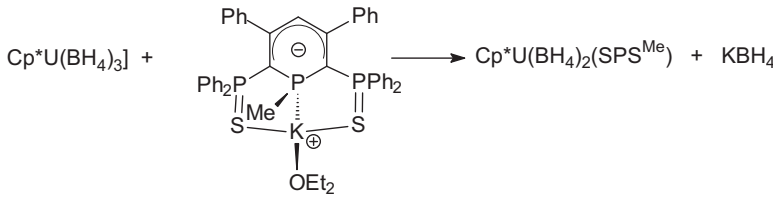

Scheme 166.

salt complex [{[η^5-(C_5Me_4)$_2$$SiMe_2$]UCl}$_2$($\mu$-O)($\mu$-Cl)·Li·1/2DME]$_2$ (Scheme 161). The complex [η^5-(C_5Me_4)$_2$$SiMe_2$]$UCl_2$·2LiCl·2DME was structurally characterized by X-ray diffraction [115].

Alkylation of either mono-oxide complex with ^{n}BuLi in DME afforded the mono-bridged dibutyl complex {[η^5-(C_5Me_4)$_2$$SiMe_2$]U^{n}Bu}$_2$($\mu$-O) (Scheme 162) [115].

Although the elemental analysis of the complex was excellent, it was extremely important to prove the presence of the two butyl groups, as X-ray quality single crystals were not available. To corroborate the existence of these alkyl moieties, the complex {[η^5-(C_5Me_4)$_2$$SiMe_2$]U^{n}Bu}$_2$($\mu$-O) was treated with excess amounts of $PhSiH_3$ (Scheme 163), producing only 2 equiv. of the corresponding $PhSiH_2{}^nBu$. This result corroborated the presence of the two butyl groups as described in {[η^5-(C_5Me_4)$_2$$SiMe_2$]U^{n}Bu}$_2$($\mu$-O). Any attempts to crystallize the hydride complex or to get an informative NMR have been unsuccessful. Only cryoscopic measurements of the *in situ* solution of the hydride complex in frozen benzene solutions showed an $M_w = 1150 \pm 10\%$ ($M_{w\,calc}$ for a monomer = 1091) [115].

The synthesis and characterization of the first example of a complex with an unsupported bond between an actinide and group 13 element have been achieved in 2008. Stirring a mixture of ($CpSiMe_3$)$_3$U and (Cp*Al)$_4$ in toluene at 60 °C for several hours resulted in a dark brown solution. Evaporation and crystallization from pentane at −80 °C produced dark brown X-ray quality blocks of ($CpSiMe_3$)$_3$UAlCp* in 38% yield (Scheme 164). The new complex was structurally autheticated by X-ray diffraction. It is stable in solution and DFT calculations suggested that the U–Al bond exhibits some covalent character owing to charge transfer from the Cp*Al ligand onto uranium [116].

3.2.2. Pentamethylcyclopentadienyl compounds

*3.2.2.1. Cp*AnX$_2$ and Cp*$_2$AnX compounds.* The activation and reduction of diethyl ether by low valent uranium resulting in the surprising formation of the trimetallic, mixed-valence uranium oxo species [U(Cp$^{RR'}$)(μ-I)$_2$]$_3$(μ^3-O) (Cp$^{RR'}$ = C_5Me_5, C_5Me_4H, $C_5H_4SiMe_3$) has been reported. When UI_3 was stirred with an equimolar amount of KCp$^{RR'}$ in diethyl ether for 16 h a green solution with white precipitate (KI) was observed in each case. Filtration followed by cooling to −50 °C resulted in the formation of green needles of the trinuclear compounds (Scheme 165) [117].

The molecular structures of the new trimetallic uranium oxo complexes were confirmed by X-ray diffraction studies (Fig. 11). Notably their formation was quite reproducible, and carried out with strict exclusion of oxygen and water, the obvious potential sources of the oxo unit. The source of the latter was confirmed as the ether solvent by GC–MS analysis of the reaction mixture, which showed the presence of butane. On the basis of the latter,

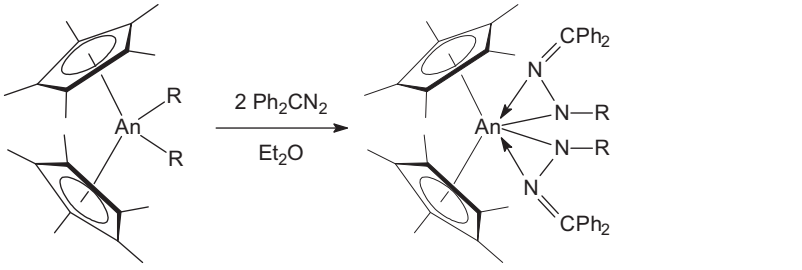

An = U, R = CH_2Ph
An = Th, R = CH_2Ph
An = Th, R = Ph

An = U, R = CH_2Ph, 82%, orange crystals
An = Th, R = CH_2Ph, 52%, colorless crystals
An = Th, R = Ph, 56%, pale yellow crystals

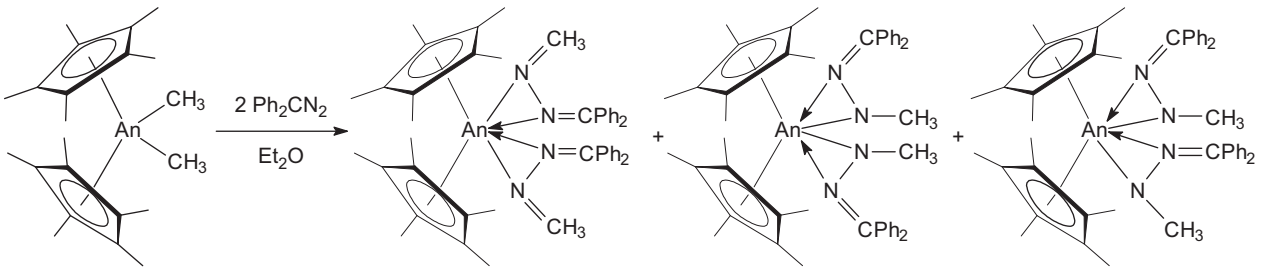

An = U
An = Th

a **b** **c**

a-c, An = U, 71%, red crystals
a-c, An = Th, 63%, colorless crystals

Scheme 167.

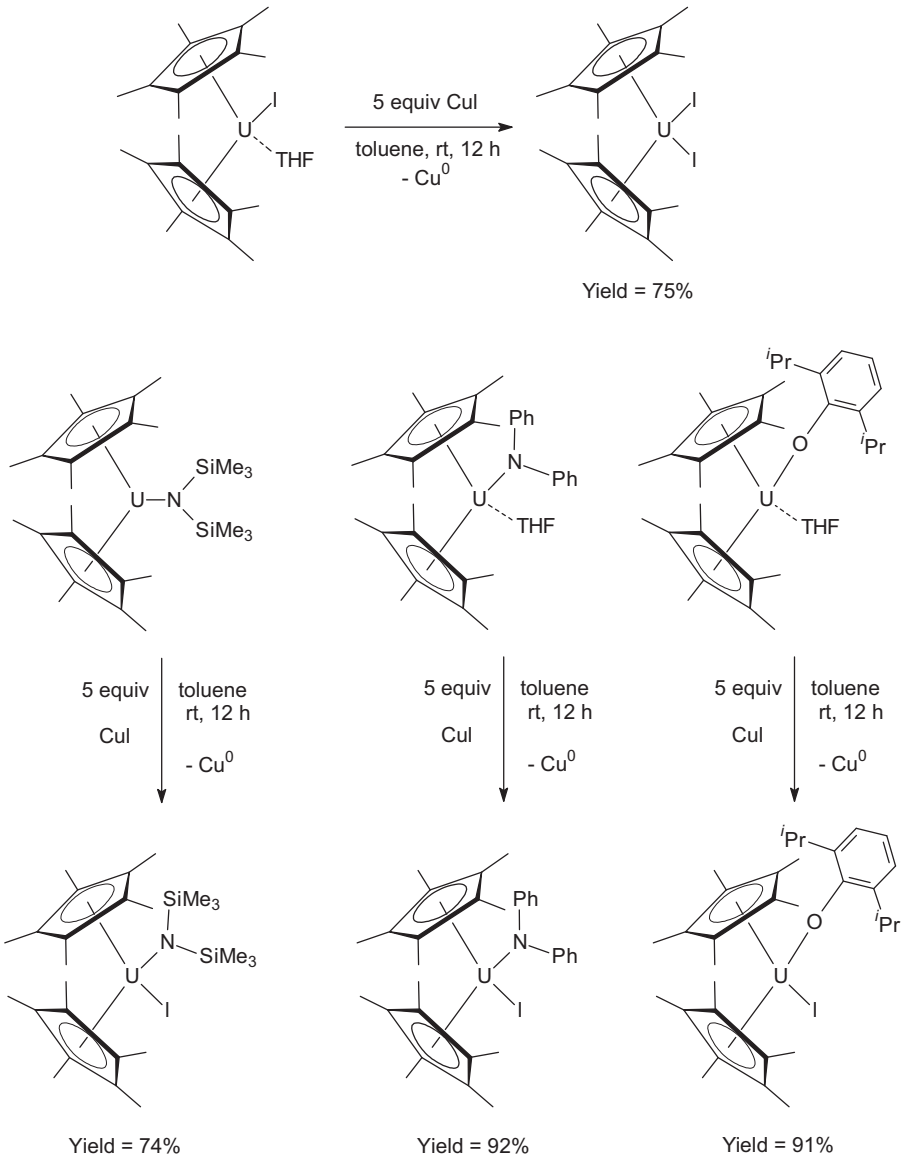

Scheme 168.

the formation of the oxo complexes presumably involves a radical mechanism [117].

3.2.2.2. Pentamethylcyclopentadienyl actinide(IV)-, (V)-, and (VI)-compounds. A mono(pentamethylcyclopentadienyl) uranium complex with a phosphinine-based SPS pincer ligand has been reported. Reaction of $[K(Et_2O)][SPSMe]$ with $Cp^*U(BH_4)_3$ in THF according to Scheme 166 gave the expected substitution product $Cp^*U(BH_4)_2(SPSMe)$. The X-ray crystal structures of this compound indicated that the central moiety of the SPS ligand can be considered as a classical phosphine, the anionic charge being stabilized by delocalization over the five carbon atoms of the phosphahexadienyl anion and negative hyperconjugation into the two Ph_2PS pendant arms [118].

The bis(pentamethylcyclopentadienyl) actinide metallocene platform continues to be a favorite subject of study among organoactinide chemists. For example, migratory insertion of diphenyldiazomethane into both metal-carbon bonds of the bis(alkyl) and bis(aryl) complexes $Cp^*_2AnR_2$ as illustrated in Scheme 167 yielded the first *f*-element bis(hydrazonato) complexes $Cp^*_2An[\eta^2\text{-}(N,N')\text{-}R\text{-}N\text{-}N{=}CPh_2]_2$ (An = Th, R = CH_3, $PhCH_2$, Ph; An = U, R = CH_3, $PhCH_2$), which have been characterized by a combination of spectroscopy, electrochemistry, and X-ray crystallography [119].

The two hydrazonato ligands adopt an η^2-coordination mode leading to 20-electron (for Th) and 22-electron (for U) complexes that have no transition-metal analogues. In fact, reaction of $Cp_2Zr(CH_3)_2$ or $Cp^*_2Hf(CH_3)_2$ with diphenyldiazomethane is limited to the formation of the corresponding mono(hydrazonato) complex $(C_5R_5)_2M[\eta^2\text{-}(N,N')\text{-}CH_3\text{-}N\text{-}N{=}CPh_2](CH_3)$ (M = Zr, R = H or M = Hf, R = CH_3). The difference in the reactivities of the group 4 metal complexes and the actinides was used as a unique platform for investigating in depth the role of 5*f* orbitals on the reactivity and bonding in actinide organometallic complexes. The electronic structure of the $Cp_2M[\eta^2\text{-}(N,N')\text{-}CH_3\text{-}N\text{-}N{=}CH_2]_2$ (M = Zr, Th, U) model complexes was studied using density functional theory (DFT) calculations and compared to experimental structural, electrochemical, and spectroscopic results [119]. Ultrafast pump-probe spectroscopic studies have been performed on the closely related uranium(IV) and thorium(IV) bis(ketimide) complexes $Cp^*_2U[\text{-}N{=}C(Ph)(CH_2Ph)]_2$ and $Cp^*_2Th[\text{-}N{=}C(Ph)(CH_2Ph)]_2$ including, for the uranium complex, the first direct measurement of dynamics of electronic deactivation within a 5*f*-electron manifold. Evidence has been found for strong coupling between the electronic ground

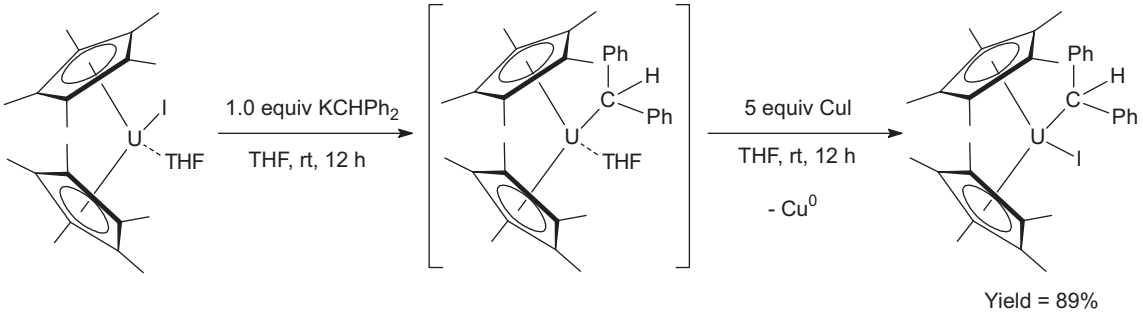

Scheme 169.

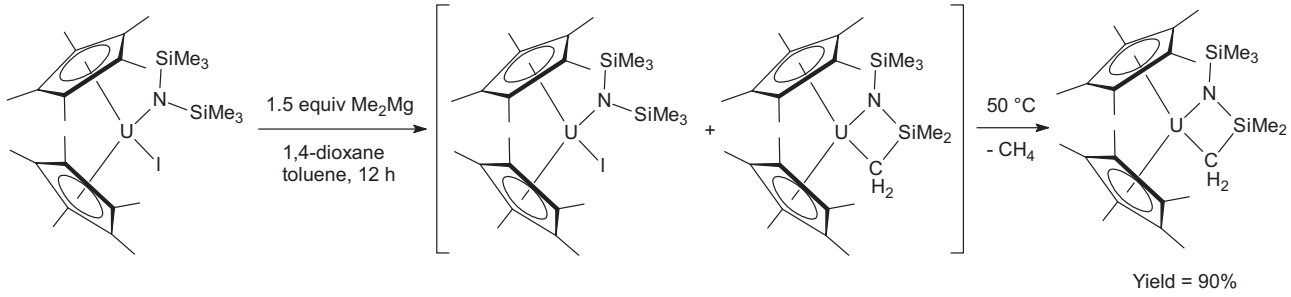

Scheme 170.

state and the *f*-electron manifold which dominates the dynamics of the excited states of the bis(ketimide) uranium complex. These also demonstrated strong singlet-*f* manifold coupling, which assists in the deactivation of the photoexcited state of the uranium complex, and provided information on intersystem crossing and internal conversion processes in both complexes [120].

A mild protocol to generate uranium(IV) mixed-ligand metallocene complexes using copper(I) iodide has been developed. Reaction of the trivalent uranium complexes $Cp^*_2UI(THF)$, $Cp^*_2U[N(SiMe_3)_2]$, $Cp^*_2U(NPh_2)(THF)$, and $Cp^*_2U(O\text{-}2,6\text{-}{}^iPr_2C_6H_3)(THF)$ with copper(I) iodide afforded the corresponding tetravalent uranium diiodide, amide iodide, and aryloxide iodide complexes $Cp^*_2UI_2$, $Cp^*_2U[N(SiMe_3)_2](I)$, $Cp^*_2U(NPh_2)(I)$ and $Cp^*_2U(O\text{-}2,6\text{-}{}^iPr_2C_6H_3)(I)$, respectively. These reactions are summarized in Scheme 168 [121].

This protocol was also extended to the synthesis of the alkyl iodide complex $Cp^*_2U(CHPh_2)(I)$ (Scheme 169). The isolation of this complex from the *in situ* generated trivalent uranium alkyl complex $Cp^*_2U(CHPh_2)(THF)$ nicely illustrated the synthetic value of this oxidation procedure in those situations where the uranium(III) metallocene complex cannot be isolated or is unstable. Overoxidation and ligand redistribution were not observed with this Cu-based $U^{III} \rightarrow U^{IV}$ oxidation procedure [121].

Attempted functionalization of the UIV amide iodide complex $Cp^*_2U[N(SiMe_3)_2](I)$ with Me_2Mg afforded the novel azametallacycle $Cp^*_2U[\eta^2\text{-}(N,C)\text{-}CH_2SiMe_2N(SiMe_3)]$ by intramolecular C–H

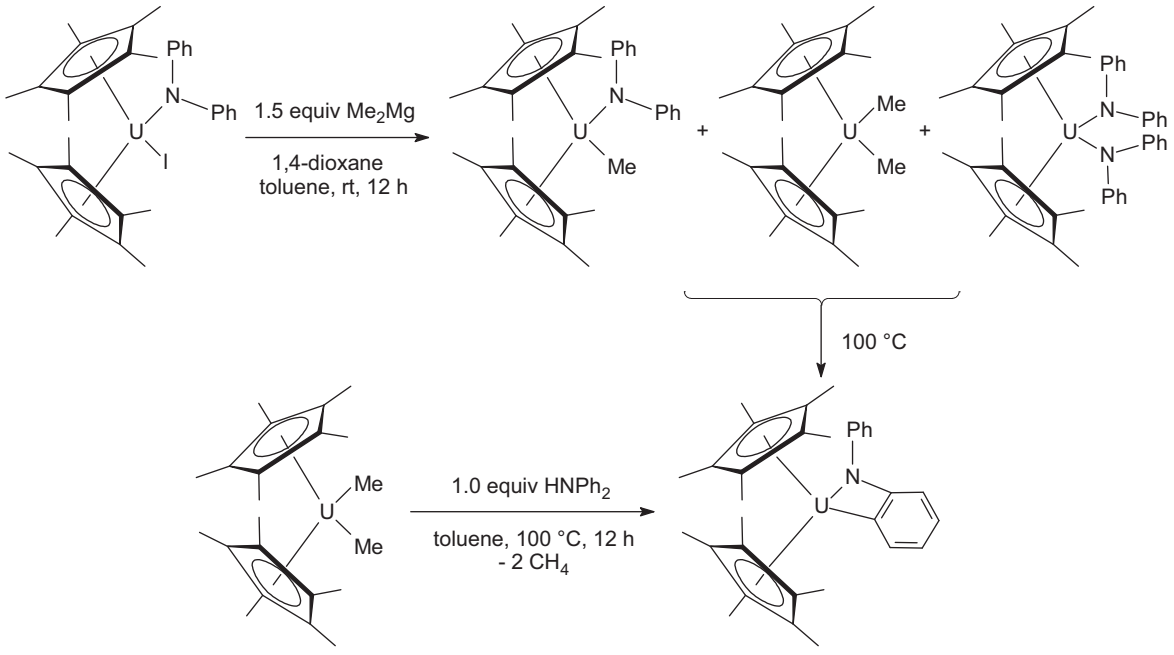

Scheme 171.

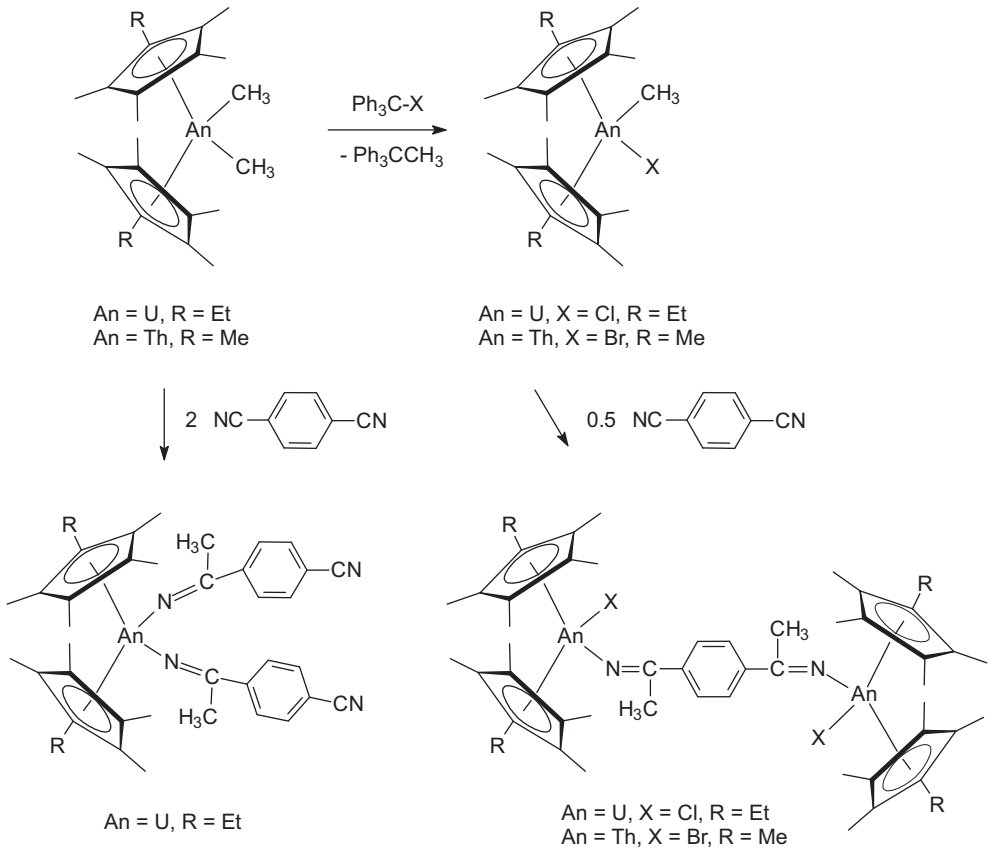

Scheme 172.

activation and liberation of methane as illustrated in Scheme 170 [121].

Reaction between $Cp^*_2U(NPh_2)(I)$ and Me_2Mg afforded a mixture of the products $Cp^*_2U(NPh_2)(Me)$, $Cp^*_2UMe_2$, and $Cp^*_2U(NPh_2)_2$ at room temperature. Heating this mixture smoothly furnished the azametallacycle $Cp^*_2U[\eta^2\text{-}(N,C)\text{-}(o\text{-}C_6H_4)NPh]$. Similarly, reaction between $Cp^*_2UMe_2$ and $HNPh_2$ at 100 °C produced the azametallacycle by aminolysis and subsequent intramolecular C–H activation. Scheme 171 highlights these reaction sequences [121].

Reactions of two equivalents of $(C_5Me_4Et)_2U(CH_3)(Cl)$ or $Cp^*_2Th(CH_3)(Br)$ with 1,4-dicyanobenzene according to Scheme 172 led to the formation of the novel 1,4-phenylenediketimide-bridged bimetallic organoactinide complexes $(\mu\text{-}[N{=}C(CH_3)C_6H_4(CH_3)C{=}N])[(C_5Me_4Et)_2U(Cl)]_2$ and $(\mu\text{-}[N{=}C(CH_3)C_6H_4(CH_3)C{=}N])\text{-}[Cp^*_2Th(Br)]_2$, respectively. These complexes were structurally characterized by single-crystal X-ray diffraction and NMR spectroscopy. Metal–metal interactions in these isovalent bimetallic systems were assessed by means of cyclic voltammetry, UV–visible/NIR absorption spectroscopy, and variable-temperature magnetic susceptibility. Although evidence for magnetic coupling between metal centers in the bimetallic U^{IV}/U^{IV} ($5f^2$–$5f^2$) complex is ambiguous, the complex was found to display appreciable electronic communication between the metal centers through the π-system of the dianionic diketimide bridging ligand, as judged by voltammetry. The transition intensities of the *f*–*f* bands for the bimetallic U^{IV}/U^{IV} system decrease substantially compared to the related monometallic ketimide chloride complex $Cp^*_2U(Cl)[\text{-}N{=}C(CH_3)(3,4,5\text{-}F_3C_6H_2)]$ [122].

Also reported in this contribution were new synthetic routes to the actinide starting materials $(C_5Me_4Et)_2U(CH_3)(Cl)$ and $Cp^*_2Th(CH_3)(Br)$ in addition to the syntheses and structures of the monometallic uranium complexes $(C_5Me_4Et)_2UCl_2$, $(C_5Me_4Et)_2U(CH_3)_2$, $(C_5Me_4Et)_2U[\text{-}N{=}C(CH_3)C_6H_4C{=}N]_2$ and $Cp^*_2U(Cl)[\text{-}N{=}C(CH_3)(3,4,5\text{-}F_3C_6H_2)]$. The synthetic route leading to the latter is outlined in Scheme 173 [122].

To probe the correlation of unusual $(C_5Me_5)^{1-}$ reactivity with steric crowding in complexes such as Cp^*_3UMe and Cp^*_3UCl,

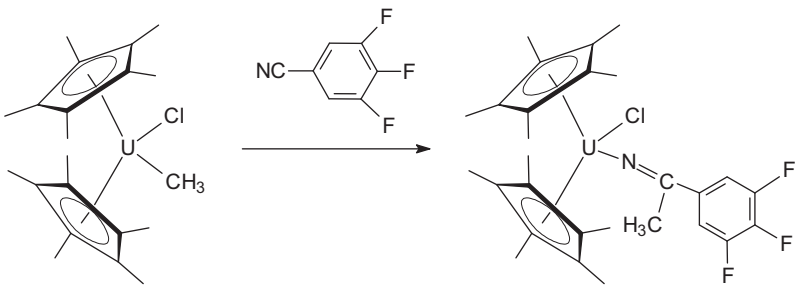

Scheme 173.

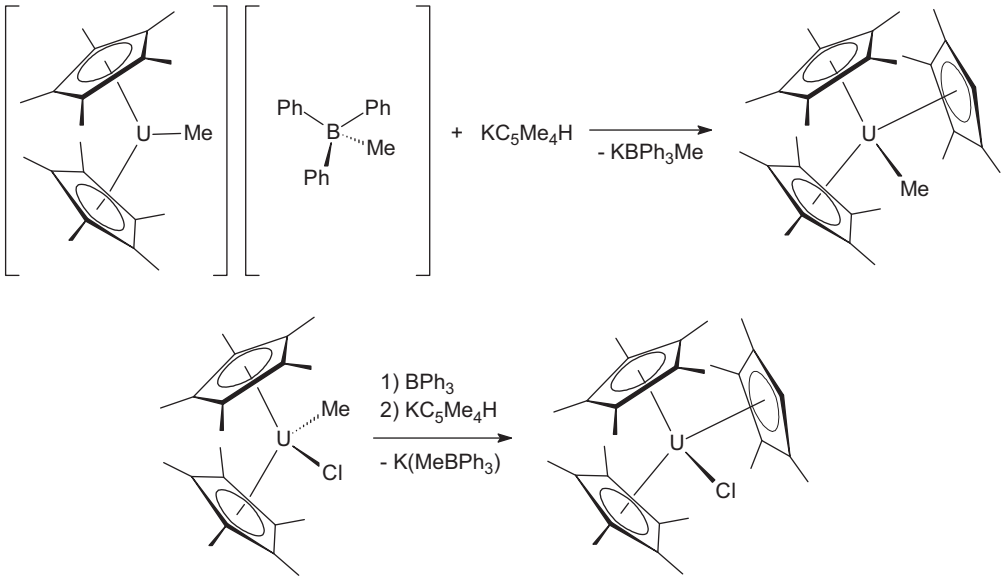

Scheme 174.

slightly less crowded $Cp^*_2(C_5Me_4H)UX$ analogues (X = Me, Cl) were synthesized and their reactivity was evaluated. The utility of the cationic precursors $[Cp^*_2UMe]^{1+}$ and $[Cp^*_2UCl]^{1+}$ in the synthesis of $Cp^*_2(C_5Me_4H)UMe$, and $Cp^*_2(C_5Me_4H)UCl$ was also explored. Since the use of precursor $[Cp^*_2UMe][MeBPh_3]$, is complicated by the equilibrium between $[Cp^*_2UMe][MeBPh_3]$ and $Cp^*_2UMe_2/BPh_3$, the reactivity of $[Cp^*_2UMe(OTf)]_2$ (OTf = O_3SCF_3), prepared from $Cp^*_2UMe_2$ and AgOTf, was also studied. Both $[Cp^*_2UMe][MeBPh_3]$ and $[Cp^*_2UMe(OTf)]_2$ react with KC_5Me_4H to form $Cp^*_2(C_5Me_4H)UMe$. Complex $Cp^*_2(C_5Me_4H)UCl$ readily forms by the addition of KC_5Me_4H to $[Cp^*_2UCl][MeBPh_3]$, generated *in situ* from Cp^*_2UMeCl and BPh_3 (Scheme 174). A closely related cyclopentadienyl complex, $Cp^*_2(C_5H_5)UMe$, was prepared in the same manner (Scheme 175) [123].

Complex $[Cp^*_2UMe(OTf)]_2$ was preferred to $[Cp^*_2UMe][MeBPh_3]$ for the synthesis of $Cp^*_2(C_5H_5)UMe$ and $Cp^*_2UMe[CH(SiMe_3)_2]$, from KC_5H_5 and $LiCH(SiMe_3)_2$, respectively (Scheme 176) [123].

The bis(alkyl) complex $Cp^*_2UMe[CH(SiMe_3)_2]$ is the first example of a mixed alkyl uranium metallocene complex. Since the complex $Cp^*_2(C_5Me_4H)UMe$ had a maximum methyl displacement in the range of SIR-active compounds, its reactivity with reducible substrates was examined. Complex $Cp^*_2(C_5Me_4H)UMe$ reacts with AgOTf to form silver metal and $(C_5Me_5)_2$, the two products expected from sterically induced reduction. However, those products would also be formed from the abstraction of a $(C_5Me_5)^{1-}$ ligand and decomposition of AgC_5Me_5. Attempts to characterize the uranium-containing product of the reaction of $Cp^*_2(C_5Me_4H)UMe$ with AgOTf led to the isolation of a product derived from an adventitious source of oxygen, $[(C_5Me_5)(C_5Me_4H)(OTf)U]_2(\mu\text{-}O)$ (Scheme 177). In summary, sterically induced reduction (SIR) reactivity was not observed with the new complexes although the methyl displacements from the $(C_5Me_5)^{1-}$ ring plane for $Cp^*_2(C_5Me_4H)UMe$ are the closest observed to date to those of SIR-active complexes. The ^1H NMR spectra of $Cp^*_2(C_5Me_4H)UMe$ and $Cp^*_2(C_5Me_4H)UCl$ are unusual in that all of the $(C_5Me_4H)^{1-}$ methyl groups are inequivalent. This structural rigidity is consistent with density-functional theory calculations [123].

Multielectron reduction chemistry has been recently expanded in the organoactinide area by the realization that traditional metal-based redox couples can be combined with a growing list of ligand-based redox processes. In 2008, it was reported that the combination of one alkyl and one hydride ligand in U^{4+} complexes can effectively function as a two-electron reductant to make U^{4+} products. The alkyl hydride reductive reactivity was observed in the course of characterizing the product of heating $[Cp^*_2UH]_2$ shown in Scheme 178 [124]. This complex, $Cp^*U[\mu\text{-}\eta^5\text{:}\eta^1\text{:}\eta^1\text{-}C_5Me_3(CH_2)_2](\mu\text{-}H)_2UCp^*_2$, comprises a $[C_5Me_3(CH_2)_2]^{3-}$ ligand that has one methylene group "tucked-in" to bind to the uranium of its ring and one "tucked-over" to the uranium of another metallocene unit. Since $Cp^*U[\mu\text{-}\eta^5\text{:}\eta^1\text{:}\eta^1\text{-}C_5Me_3(CH_2)_2](\mu\text{-}H)_2UCp^*_2$ is a U^{4+} hydride, like $[Cp^*_2UH_2]_2$, it was expected to have hydride reduction chemistry that would generate new tuck-in and tuck-over derivatives. Accordingly, the reductive chemistry of this compound was examined [125].

As shown in Scheme 179, complex $Cp^*U[\mu\text{-}\eta^5\text{:}\eta^1\text{:}\eta^1\text{-}C_5Me_3(CH_2)_2](\mu\text{-}H)_2UCp^*_2$ was found to quantitatively reduce 2 equiv. of PhSSPh in benzene in a four electron reduction pro-

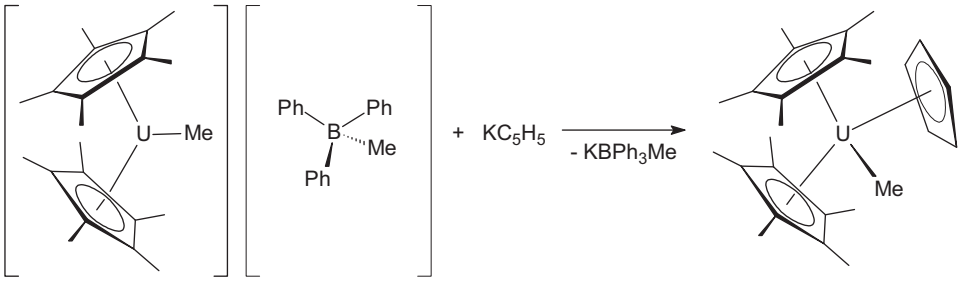

Scheme 175.

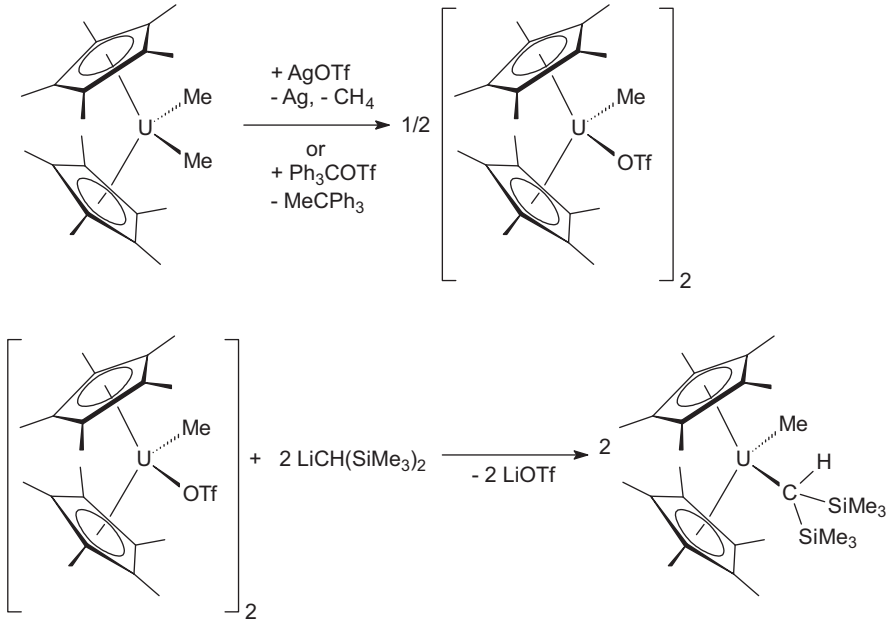

Scheme 176.

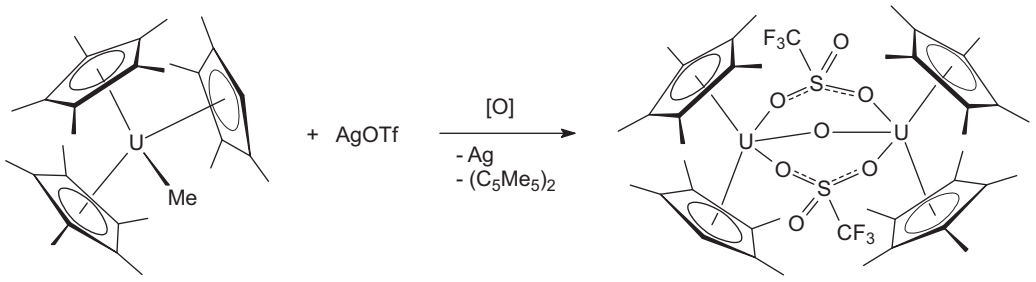

Scheme 177.

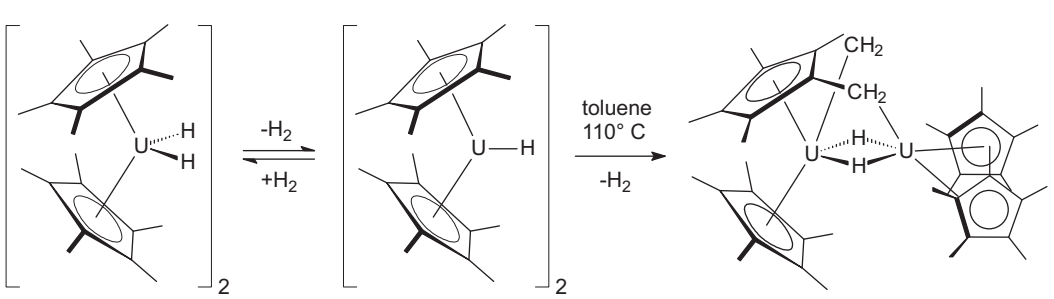

Scheme 178.

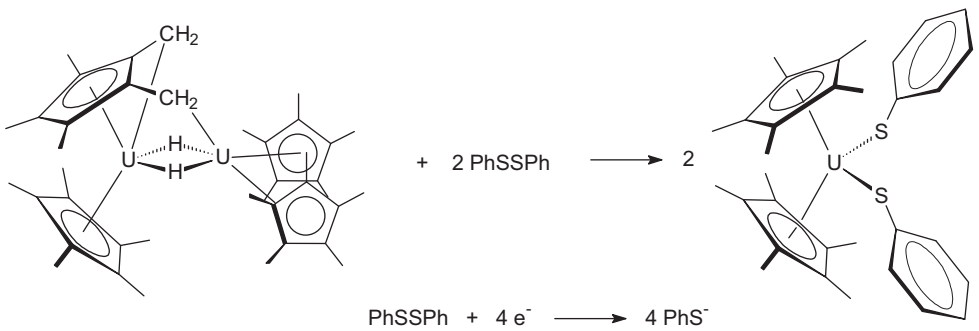

Scheme 179.

$$[C_5Me_3(CH_2)_2]^{3-} + 2\,H^- \longrightarrow (C_5Me_5)^- + 4\,e^-$$

Scheme 180.

cess, but the product $Cp^*_2U(SPh)_2$ contained neither tuck-in nor tuck-over ligands [125].

In fact, the cyclopentadienide ligands in the product contain no metalated methylene groups. It was concluded that since the starting material and product both contain U^{4+} and there are only two hydride ligands, two additional electrons in the four electron reduction must come from some other source. Since the methylene groups in the starting material have regained hydrogen to become methyl groups and there is no other obvious source of hydrogen in the reaction other than the hydride ligands, the four electron reduction can be explained by the formal half-reaction shown in Scheme 180 [125].

It was further found that $Cp^*U[\mu\text{-}\eta^5\text{:}\eta^1\text{:}\eta^1\text{-}C_5Me_3(CH_2)_2](\mu\text{-}H)_2UCp^*_2$ can also function as a six-electron reductant in the reduction of C_8H_8 to $[(C_5Me_5)(C_8H_8)U]_2(C_8H_8)$, in benzene (Scheme 181). Again, in this case, there is no obvious source of hydrogen for the intact $(C_5Me_5)^{1-}$ ligands in the product except the hydride ligands. The quantitative six electron reduction formally can be accounted for by two two-electron alkyl hydride reductions and two one-electron $(C_5Me_5)^{1-}$-based reductions which give the $(C_5Me_5)_2$ byproduct observed [125].

Complex $Cp^*U[\mu\text{-}\eta^5\text{:}\eta^1\text{:}\eta^1\text{-}C_5Me_3(CH_2)_2](\mu\text{-}H)_2UCp^*_2$ can also quantitatively reduce 2 equiv. of PhN=NPh in benzene to form the previously characterized U^{6+} imido complex $Cp^*_2U(=NPh)_2$ (Scheme 182). In this case, an eight-electron reduction occurs involving two two-electron alkyl hydride reductions and two two-electron U^{4+} to U^{6+} processes [125].

To determine if the alkyl hydride reductive chemistry was specific to the unusual tuck-in tuck-over complex $Cp^*U[\mu\text{-}\eta^5\text{:}\eta^1\text{:}\eta^1\text{-}C_5Me_3(CH_2)_2](\mu\text{-}H)_2UCp^*_2$, reactions of combinations of U^{4+} hydride and methyl complexes were examined. Combination of $Cp^*_2UMe_2$ and $[Cp^*_2UH_2]_2$ achieved an even more surprising reduction. As shown in Scheme 183, the combination of U^{4+} hydrides and methyls reduces benzene to make the formally trivalent complex of $(C_6H_6)^{2-}$, that is, the previously characterized $(\mu\text{-}C_6H_6)[Cp^*_2U]_2$. Methane was observed as a byproduct and again the formal half-reaction is as shown in Scheme 183 [125].

More conventional reactions of the tuck-in tuck-over complex $Cp^*U[\mu\text{-}\eta^5\text{:}\eta^1\text{:}\eta^1\text{-}C_5Me_3(CH_2)_2](\mu\text{-}H)_2UCp^*_2$ include its reaction with $[Et_3NH][BPh_4]$ to form the cationic species $[Cp^*_2U][BPh_4]$ as depicted in Scheme 184 [124].

Reaction of $Cp^*U[\mu\text{-}\eta^5\text{:}\eta^1\text{:}\eta^1\text{-}C_5Me_3(CH_2)_2](\mu\text{-}H)_2UCp^*_2$ with phenol yielded H_2 and the bis(phenoxide) complex $Cp^*_2U(OPh)_2$ in 92% yield (Scheme 185). The identity of $Cp^*_2U(OPh)_2$ was confirmed by X-ray crystallography [124].

The investigation of uranium imido complexes continues to be a hot topic in organoactinide chemistry. For example, an interesting series of organometallic uranium(V) imido halide complexes have been synthesized and their electronic structure and bonding elucidated. Reactions of $Cp^*_2U(=N\text{-}2,4,6\text{-}{}^tBu_3C_6H_2)$ or $Cp^*_2U(=N\text{-}2,6\text{-}{}^iPr_2C_6H_3)(THF)$ with 5 equiv. of CuX_n ($n = 1$, X = Cl, Br, I; $n = 2$, X = F) affords the corresponding uranium(V)-imido halide complexes, $Cp^*_2U(=N\text{-}Ar)(X)$ (where Ar = 2,4,6-${}^tBu_3C_6H_2$ and X = F, Cl, Br, I; Ar = 2,6-${}^iPr_2C_6H_3$ and X = F, Cl, Br, I), in good isolated yields of 75–89% (Scheme 186) [126].

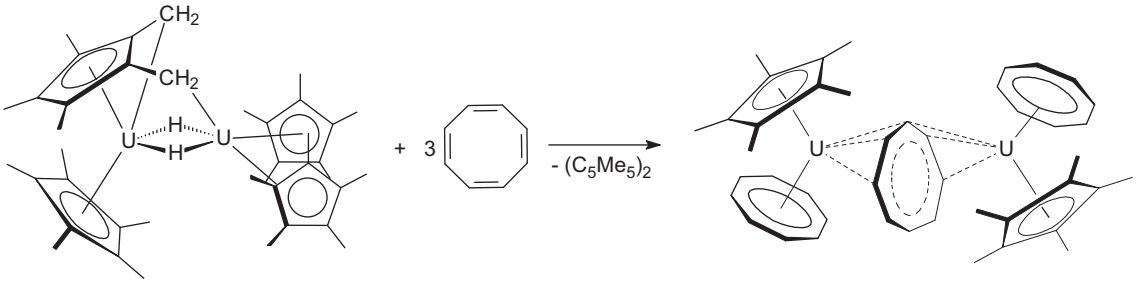

$$3\,C_8H_8 + 6\,e^- \longrightarrow 3\,(C_8H_8)^{2-}$$
$$[C_5Me_3(CH_2)_2]^{3-} + 2\,H^- \longrightarrow (C_5Me_5)^- + 4\,e^-$$
$$2\,(C_5Me_5)^- \longrightarrow (C_5Me_5)_2 + 2\,e^-$$

Scheme 181.

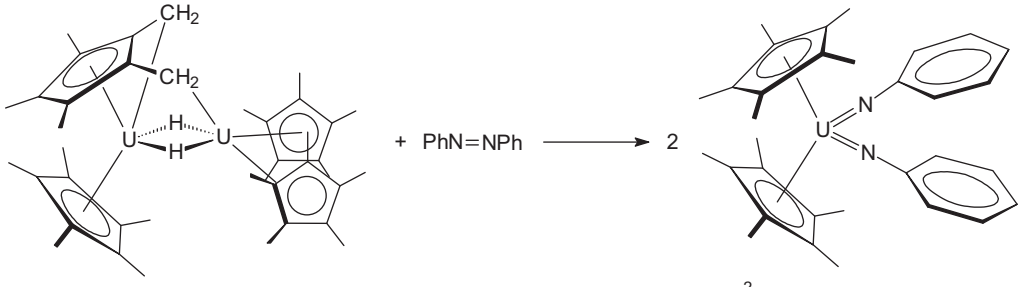

$$2\,PhN{=}NPh + 8\,e^- \longrightarrow 4\,(PhN)^{2-}$$
$$[C_5Me_3(CH_2)_2]^{3-} + 2\,H^- \longrightarrow (C_5Me_5)^- + 4\,e^-$$
$$2\,[(C_5Me_5)_2U]^{2-} \longrightarrow 2\,[(C_5Me_5)_2U]^{4+} + 4\,e^-$$

Scheme 182.

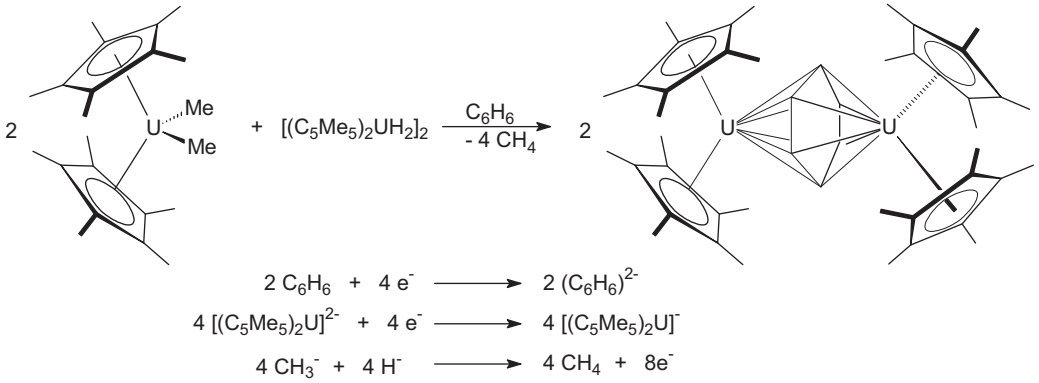

Scheme 183.

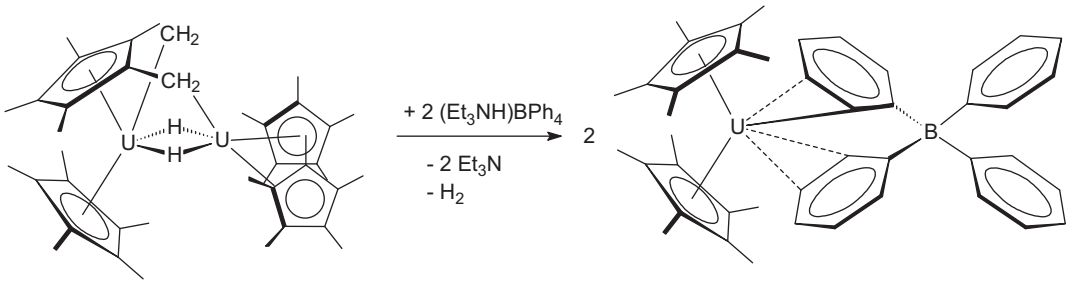

Scheme 184.

All new imido complexes have been thoroughly characterized by a combination of single-crystal X-ray diffraction, ^{1}H NMR spectroscopy, elemental analysis, mass spectrometry, cyclic voltammetry, UV–visible–NIR absorption spectroscopy, and variable-temperature magnetic susceptibility. The uranium L_{III}-edge X-ray absorption spectrum of $Cp^*_2U(=N\text{-}2,4,6\text{-}{}^tBu_3C_6H_2)(Cl)$ was analyzed to obtain structural information, and the $U{=}N_{imido}$ (1.97(1) Å), U–Cl (2.60(2) Å), and U–C_5Me_5 (2.84(1) Å) distances were consistent with those observed for the compounds which were characterized by single-crystal X-ray diffraction studies. All $Cp^*_2U(=N\text{-}Ar)(X)$ complexes exhibit U^V/U^{IV} and U^{VI}/U^V redox couples by voltammetry, with the potential separation between these metal-based couples remaining essentially constant at ~1.50 V. The electronic spectra comprise $\pi \rightarrow \pi^*$ and $\pi \rightarrow nb_{5f}$ transitions involving electrons in the metal-imido bond, and metal-centered *f–f* bands illustrative of spin–orbit and crystal-field influences on the $5f^1$ valence electron configuration. Two distinct sets of bands were attributed to transitions derived from this $5f^1$ configuration, and the intensities in these bands increase dramatically over those found in spectra of classical $5f^1$ actinide coordination complexes. Temperature-dependent magnetic susceptibilities are reported for all complexes with μ_{eff} values ranging from 2.22 to 2.53 μ_B. The onset of quenching of orbital angular momentum by ligand fields was observed to occur at ~40 K in all cases. Density functional theory results for the model complexes $Cp^*_2U(=NC_6H_5)(F)$ and $Cp^*_2U(=N\text{-}C_6H_5)(I)$ showed good agreement with the experimental structural and electrochemical data and provided a basis for the assignment of spectroscopic bands. The bonding analysis describes multiple bonding between the uranium metal center and imido nitrogen which comprises one σ and two π interactions with variable participation of 5*f* and 6*d* orbitals from the uranium center [126]. In a similar manner, tetravalent and pentavalent uranium acetylide complexes have been prepared by oxidative functionalization with CuC≡CPh (Scheme 187). Oxidation of $Cp^*_2U(NPh_2)(THF)$ and $Cp^*_2U(=N\text{-}2,6\text{-}{}^iPr_2C_6H_3)(THF)$ with CuC≡CPh yields the corresponding U^{IV} and U^V acetylide complexes $Cp^*_2U(NPh_2)(C{\equiv}CPh)$ and $Cp^*_2U(=N\text{-}2,6\text{-}{}^iPr_2C_6H_3)(C{\equiv}CPh)$, respectively. The complexes were characterized using a combination of ^{1}H NMR, X-ray crystallography, UV–Visible–near-IR spectroscopy, and cyclic voltammetry. $Cp^*_2U(=N\text{-}2,6\text{-}{}^iPr_2C_6H_3)(C{\equiv}CPh)$ represents the first example of a pentavalent uranium complex with an anionic carbon ligand other than a carbocyclic (C_5R_5, C_7H_7, C_8H_8) ligand. This work clearly showed that the Cu-based oxidative functionalization using CuC≡CPh is applicable to both U^{III} and U^{IV} oxidation states through the synthesis of the respective U^{IV} amide and U^V imide acetylide

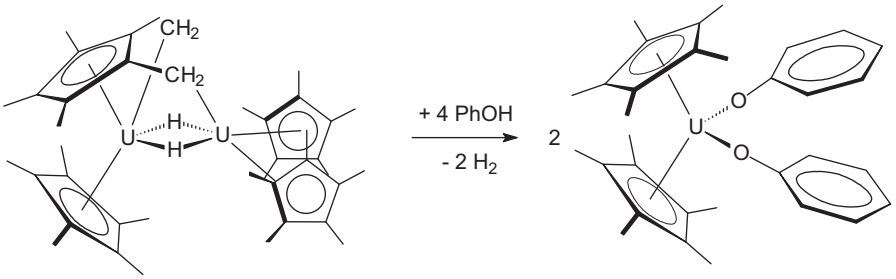

Scheme 185.

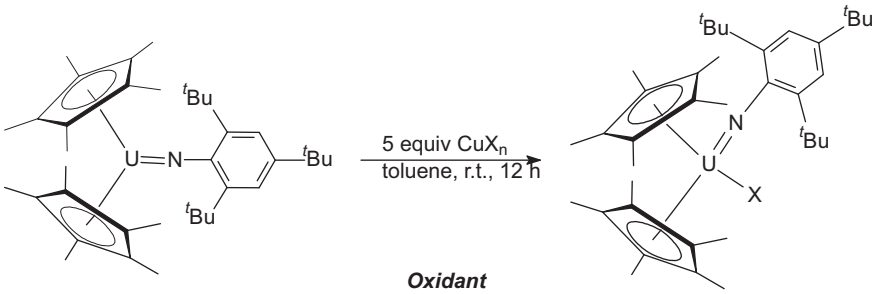

Oxidant		
CuF_2	X = F	81% Yield
CuCl	X = Cl	75% Yield
CuBr	X = Br	77% Yield
CuI	X = I	78% Yield

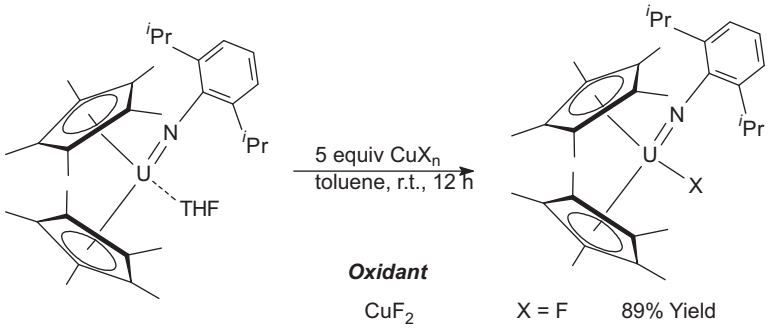

Oxidant		
CuF_2	X = F	89% Yield
CuCl	X = Cl	80% Yield
CuBr	X = Br	88% Yield
CuI	X = I	81% Yield

Scheme 186.

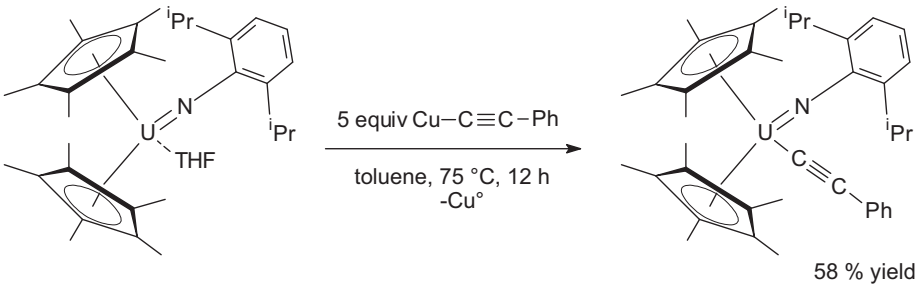

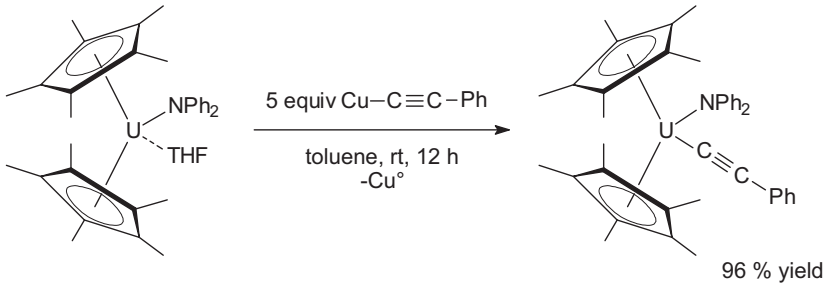

Scheme 187.

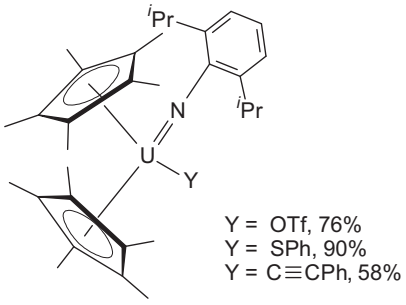

Scheme 188.

complexes. The isolation of the U^V acetylide complex reported in this work clearly demonstrated that pentavalent uranium can support anionic carbon ligands other than carbocycles and, therefore, may serve as a useful platform for the generation of carbon-based functional groups on uranium [127].

In an extension of this work, the chemistry, electronic structure and redox energetics in these organometallic pentavalent uranium complexes has been investigated in detail. Utilizing the direct oxidation of $Cp^*_2U(=N\text{-}2,6\text{-}{}^iPr_2C_6H_3)(THF)$ with the appropriate copper(I) salt yielded the triflate (Y = OTf (=OSO_2CF_3)), thiolate (Y = SPh), and the previously reported acetylide (Y=C≡CPh) complexes (Scheme 188) [128].

In addition, a salt metathesis route between the U^V-imido $Cp^*_2U(=N\text{-}2,6\text{-}{}^iPr_2C_6H_3)$(I) and various alkali salts gave the diphenylamide (Y = NPh_2), aryloxide (Y = OPh), alkyl (Y = Me), and aryl (Y = Ph) complexes (Scheme 189). The successful isolation of the acetylide as well as the methyl and phenyl derivatives clearly shows that UV can support the full range of carbon anions (sp, sp^2, and sp^3), and these represent the first examples of pentavalent uranium complexes with anionic carbon moieties other than carbocyclic (C_5R_5, C_7H_7, C_8H_8) ligands [128].

Finally, both protonolysis and insertion pathways according to Scheme 190 afforded the U^V-imido ketimide complex $Cp^*_2U(=N\text{-}2,6\text{-}{}^iPr_2C_6H_3)(N=CPh_2)$ [128].

All pentavalent uranium imido complexes shown in Schemes 188–190 have been isolated in good yield and characterized using various combinations of ^1H NMR spectroscopy, elemental analysis, mass spectrometry, single crystal X-ray diffraction, cyclic voltammetry, UV/Vis/NIR absorption spectroscopy, and magnetic susceptibility measurements. All $Cp^*_2U(=N\text{–}Ar)(X)$ (X = F, Cl, Br, I) and $Cp^*_2U(=N\text{–}Ar)(Y)$ complexes exhibited U^{VI}/U^V and U^V/U^{IV} redox couples by voltammetry. The potential separation between these couples remains essentially constant at ~1.50 V, but both processes shift in tandem in potential by ~700 mV across the series of X/Y ligands. No significant differences between μ_{eff} values or temperature dependencies in the magnetic susceptibility were observed for these complexes regardless of the identity of the ancillary X/Y ligand. However, an excellent linear correlation was observed between the chemical shift values of C_5Me_5 ligand protons in the ^1H NMR spectra and the oxidation potentials of $Cp^*_2U(=N\text{-}2,4,6\text{-}{}^tBu_3C_6H_2)(X/Y)$, suggesting that there is a common origin, overall σ-/π-donation from the ancillary X/Y ligand to the metal, contributing to both observables. Combined, these data confer the following trend in increasing σ/π-donating ability of the X/Y ligand to the UV metal center: OTf < I < Br < Cl < SPh < C≡CPh < F < [OPhMePh] ≪ NPh_2 < N = CPh_2.
These $Cp^*_2U(=N\text{-}2,4,6\text{-}{}^tBu_3C_6H_2)(X/Y)$ complexes also showed distinct hallmarks of a covalent bonding interaction between the metal and the imide ligand that is modulated to varying degrees by the interaction between the X/Y ancillary ligand and the UV metal center. These signatures of covalency include stabilization of multiple metal oxidations states [U^{VI}, U^V, and U^{IV}] and enhanced intensities in the intraconfiguration (*f–f*) transitions. Of particular note in this regard is the more than 20-fold enhancement in the *f–f* intensities observed for Y=C≡CPh and N = CPh_2, which is a clear

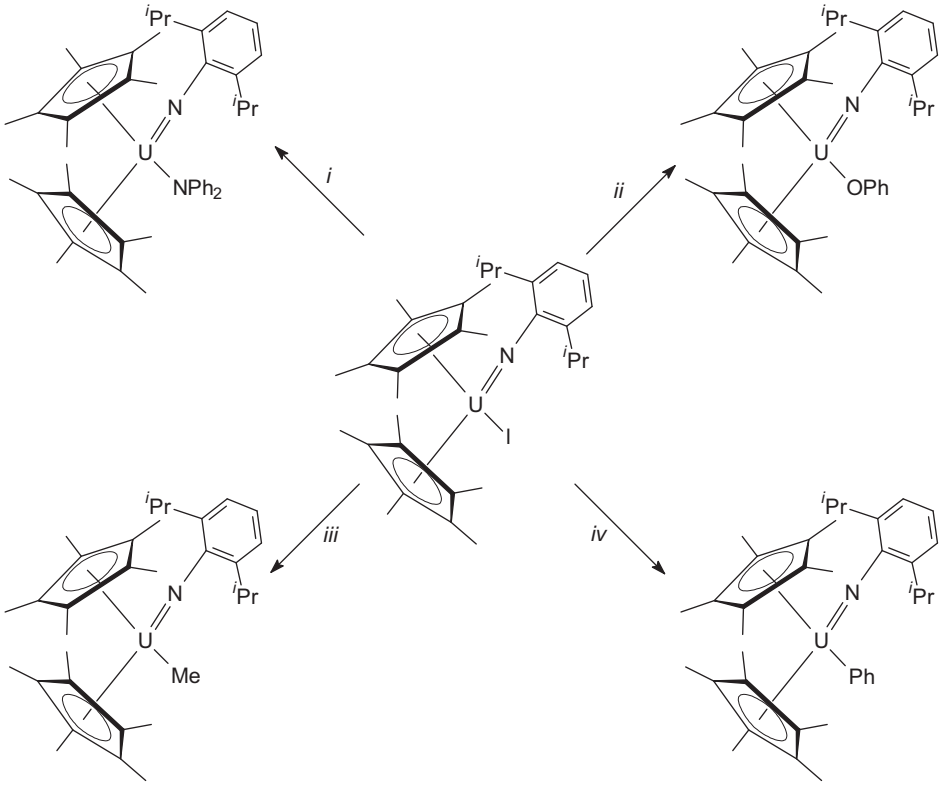

Scheme 189. (i) 1.2 equiv. $KNPh_2$, toluene, 25 °C, 12 h, 80%; (ii) 1.2 equiv. KOPh, toluene, 75 °C, 12 h, 75%; (iii) 1.5 equiv. Me_2Mg, 1,4-dioxane, toluene, 25 °C, 12 h, 70%; (iv) 2.0 equiv. $Ph_2Mg(THF)_2$, 1,4-dioxane, toluene, 25 °C, 12 h, 80%.

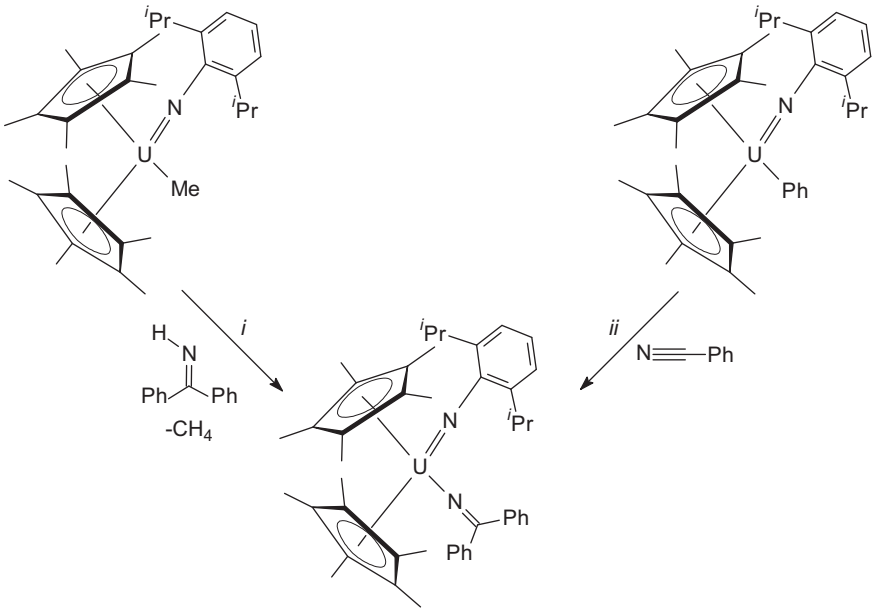

Scheme 190.

reflection of the covalent metal–ligand bonding interactions sustained by the acetylide and ketimide ligands in these pentavalent systems [128].

Unusual mixed-valent An^{IV}/U^{III}_2 complexes (An = Th, U) have been synthesized as outlined in Scheme 191 and fully characterized by X-ray crystallography as well as their magnetic properties and UV/Vis/NIR absorption data [129].

The reductive coupling of acetonitrile by uranium and thorium hydride complexes to give the cyanopentadienyl dianion, $(C_6N_3H_7)^{2-}$, has been reported. Addition of CH_3CN to a brown-green solution of the trivalent uranium hydride $[Cp^*_2UH]_2$ in toluene formed a dark red solution, from which $[Cp^*_2U\{(CH_3C(NH)=CHC(NH)=CHCN)]_2$ could be isolated in 69% yield upon heating (Scheme 192). The complex was identified by X-ray crystallography and characterized by spectroscopic and analytical methods. During the course of the reaction, three molecules of acetonitrile had been coupled to give a dianionic tridentate ligand containing a six carbon atom chain with concomitant loss of six hydrogen atoms. Although nitriles have been previously condensed in many ways to monoanionic ligands by insertion and metalation reactions initiated by alkyl and amide metal complexes, the combination of reduction, insertion, deprotonation, and rearrangement that contributed to the formation of this diaminocyanopentadienyl dianion unit appears to be unique [130].

The analogous reaction of $[Cp^*_2UH]_2$ and CD_3CN suggested that none of the hydrogen atoms in $(C_6N_3H_7)^{2-}$ arose from the hydride ligands in $[Cp^*_2UH]_2$, as the ^1H NMR resonances attributable to the $(C_6N_3H_7)^{2-}$ ligand in the spectrum of $[Cp^*_2U\{(CH_3C(NH)=CHC(NH)=CHCN)]_2$ were absent in the ^1H NMR spectrum of the CD_3CN product. It was pointed out that, normally, it would not be possible to obtain reductive thorium chemistry analogous to that accessible from U^{III} complexes, as only very few Th^{III} compounds are known. For example, there is no thorium analogue of $[Cp^*_2UH]_2$. However, the tetravalent thorium

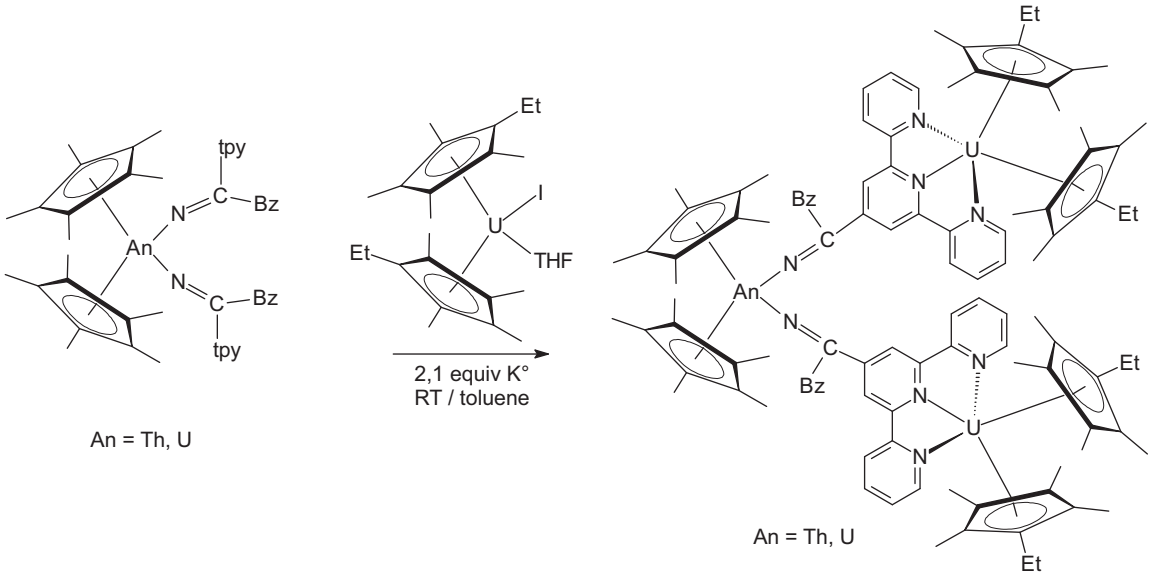

Scheme 191.

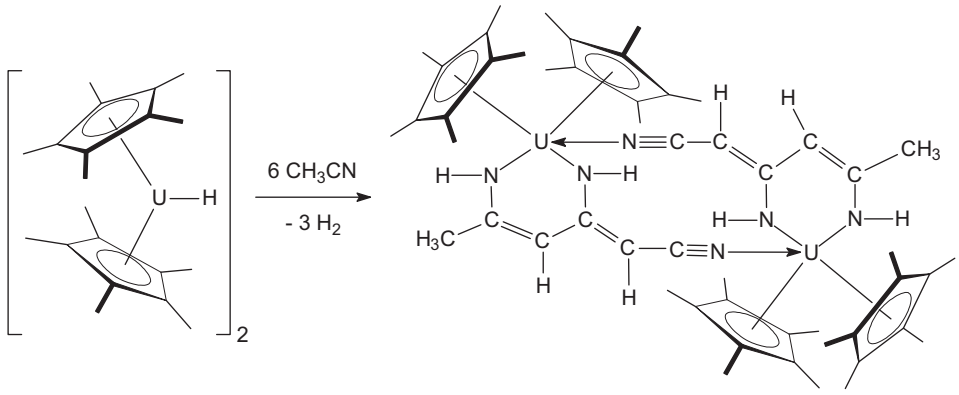

Scheme 192.

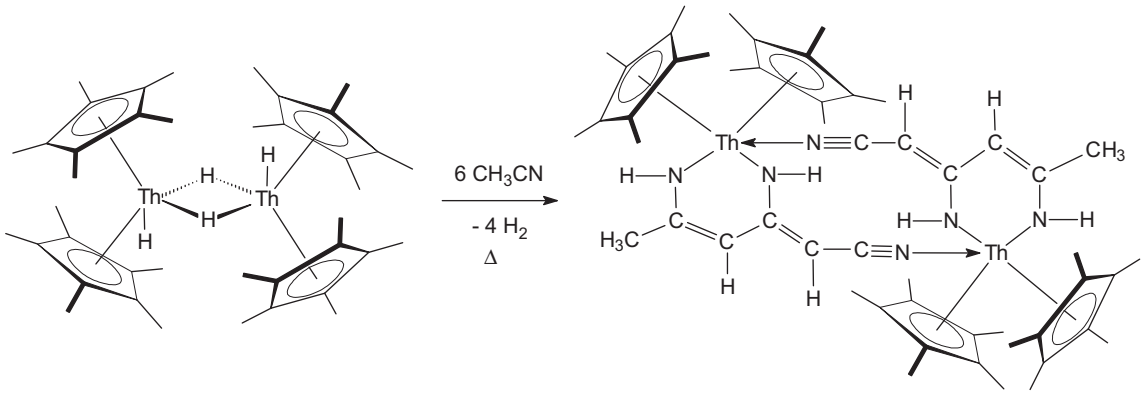

Scheme 193.

hydride $[Cp^*_2ThH_2]_2$ has been found to have chemistry similar to that of $[Cp^*_2UH]_2$ in some cases. The four hydride ligands in $[Cp^*_2ThH_2]_2$ can provide the same reductive capacity generated from the two U^{III} and two hydride ions in $[Cp^*_2UH]_2$. Hence, the reaction of $[Cp^*_2ThH_2]_2$ with CH_3CN was also studied. Despite the complexity of the reaction in Scheme 192 and the presence of U^{III} in that case, Th^{IV} complex $[Cp^*_2ThH_2]_2$ afforded an analogous product (Scheme 193) [130].

Organouranium complexes containing the 2-mercapto benzothiazolate (=SBT) ligand (Scheme 194) have been synthesized and fully characterized [62].

Treatment of $Cp^*_2UCl_2$ with KSBT in THF gave $Cp^*_2U(SBT)_2$, which exhibits the usual bent sandwich configuration in the solid state with the two SBT ligands adopting the bidentate ligation mode. The monocyclopentadienyl compound $Cp^*U(SBT)_3$ was synthesized by reaction of $Cp^*U(BH_4)_3$ with KSBT in THF, and its reduction with potassium amalgam in the presence of 18-crown-6 afforded the corresponding anionic complex [K(18-crown-6)$(THF)_2$][$Cp^*U(SBT)_3$]. These reactions are summarized in Scheme 195 [62].

Reports on organoactinide complexes comprising five-membered heterocyclic ring ligands remain scarce. Treatment of UI_3 with three equivalents of $KP_3C_2{}^tBu_2$ in refluxing toluene (Scheme 196) led to the corresponding monomeric, formally eight

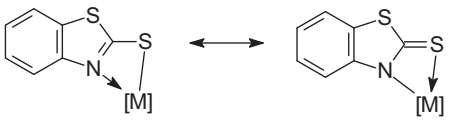

Scheme 194. Two hybrid forms of the chelating SBT ligand [62].

$$Cp^*_2UCl_2 + KSBT \xrightarrow{THF} Cp^*_2U(SBT)Cl] + KCl$$

$$Cp^*U_2Cl_2 + 2\,KSBT \xrightarrow{THF} Cp^*_2U(SBT)_2 + 2KCl$$

$$Cp^*U(BH_4)_3 + 3\,KSBT \xrightarrow{THF} Cp^*U(SBT)_3 + 3KBH_4$$

$$Cp^*U(SBT)_3] + K(Hg) + 18\text{-crown-6} \xrightarrow{THF} [K(18\text{-crown-6})(THF)_2][Cp^*U(SBT)_3]$$

Scheme 195.

coordinate complex $U(\eta^5\text{-}P_3C_2{}^tBu_2)_2(\eta^2\text{-}P_3C_2{}^tBu_2)$ which was isolated as a dark brown crystalline solid in 36% yield. In the solid state, the complex displays an interesting assembly of ligands comprising one η^2-(bent) and two η^5-ligated triphospholyl rings. An NMR study indicated fluxional behavior in solution [70].

3.3. Actinide cyclooctatetraenyl complexes

In 2006, the reductive cyclooligomerization of CO by the U(III) mixed-sandwich complexes $[\eta\text{-}C_8H_6(Si^iPr_3\text{-}1,4)_2]U(\eta\text{-CpR})(THF)$

$$UI_3 + 3\,KP_3C_2{}^tBu_2 \longrightarrow U(P_3C_2{}^tBu_2)_3 + 3\,KI$$

Scheme 196.

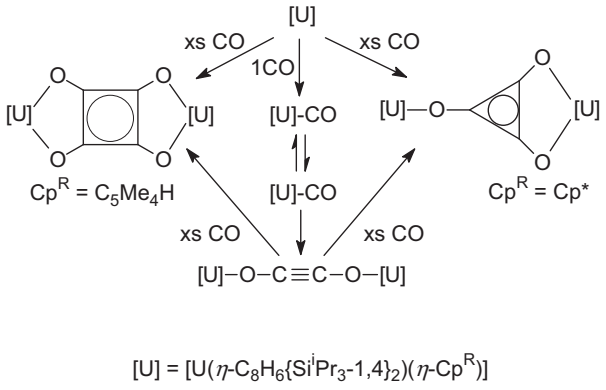

Scheme 197.

(CpR = Cp* or C_5Me_4H) had been reported. The resultant deltate and squarate complexes, $(\mu\text{-}\eta^1\text{:}\eta^2\text{-}C_3O_3)[\eta\text{-}C_8H_6(Si^iPr_3\text{-}1,4)_2]U(\eta\text{-}Cp^*)]_2$ and $(\mu\text{-}\eta^2\text{:}\eta^2\text{-}C_4O_4)[\eta\text{-}C_8H_6(Si^iPr_3\text{-}1,4)_2]U(\eta\text{-}C_5Me_4H)]_2$, were derivatives of the first two cyclic members of the oxocarbon dianions. A potential mechanism for the U(III)-induced formation of the latter is shown in Scheme 197. More recently, in 2008, detailed mechanistic studies on this reductive cyclooligomerization of CO by U(III) mixed sandwich complexes have been carried out, leading to the isolation of a third unusual compound resulting from this system, *i.e.* the binuclear ynediolate complex $(\mu\text{-}\eta^1\text{:}\eta^1\text{-}C_2O_2)[\eta\text{-}C_8H_6(Si^iPr_3\text{-}1,4)_2]U(\eta\text{-}Cp^*)]_2$, the molecular structure of which was determined by X-ray diffraction. In conclusion of this investigation it was shown that the role of the actinide in the initial C–C bond formation is not only to reduce the bound CO but also to act as a Lewis acid binding an additional CO oxygen, and thus aligning the two CO groups in a favorable orientation for the C–C bond forming process [131].

Mono(cyclooctatetraenyl) complexes of uranium with a phosphinine-based SPS pincer ligand have been reported. Reaction of $[K(Et_2O)][SPS^{Me}]$ with $(COT)U(BH_4)_2(THF)$ in THF according to Scheme 198 gave the expected substitution product $(COT)U(BH_4)(SPS^{Me})$. The X-ray crystal structure indicated that the central moiety of the SPS ligand can be considered as a classical phosphine, the anionic charge being stabilized by delocalization over the five carbon atoms of the phosphahexadienyl anion and negative hyperconjugation into the two Ph_2PS pendant arms [118].

Protonolysis of $(COT)U(BH_4)(SPS^{Me})$ with $[NEt_3H][BPh_4]$ afforded the cationic complex $[U(COT)(SPS^{Me})(NEt_3)][BPh_4]$, which was transformed into $[U(COT)(SPSMe)(L)][BPh_4]$ (L = $OPPh_3$ or HMPA] (Scheme 199). Changing $[K(Et_2O)][SPS^{Me}]$ with $[Na][SPS^{OMe}]$ in its reaction with $(COT)U(BH_4)_2(THF)$ afforded a mixture of complexes, among which $(COT)U(BH_4)(SPS^{H})$ was deposited as red crystals of a THF solvate. Complex $(COT)U(BH_4)(SPS^{H})$ was isolated in 79% yield from the reaction of $(COT)U(BH_4)_2(THF)]$ and SPS in the presence of a catalytic amount of $NaBH_4$; the key intermediate of the reaction is $[Na(THF)_x][SPS^{H}\cdot BH_3]$, formed by the addition of $NaBH_4$ to SPS, which reacts with $(COT)U(BH_4)_2(THF)$ to give $(COT)U(BH_4)(SPS^{H})$ and $NaBH_4$. The X-ray crystal structures of $[(COT)U(S_2PPh_2)(\mu\text{-}OMe)]_2$ and $[U(COT)]_4\{U(THF)_3\}_2(\mu^3\text{-}S)_8$, which resulted from decomposition of the SPS ligand, were also presented. The structure of the latter exhibits an octahedron-like skeleton of uranium atoms that are held together with triply bridging sulfur atoms located above each face of the octahedron (Fig. 12). The U_6S_8 core of the complex is a tetrakis-hexahedron, that is, a cube of S atoms each face of which is covered by a square pyramid with a uranium atom at the apex. While octahedral thiolato clusters of the type M_6S_8 are quite common for *d* transition metals, especially for M = Re, Mo, and W, such compounds of the *f* elements had not been previously reported [118].

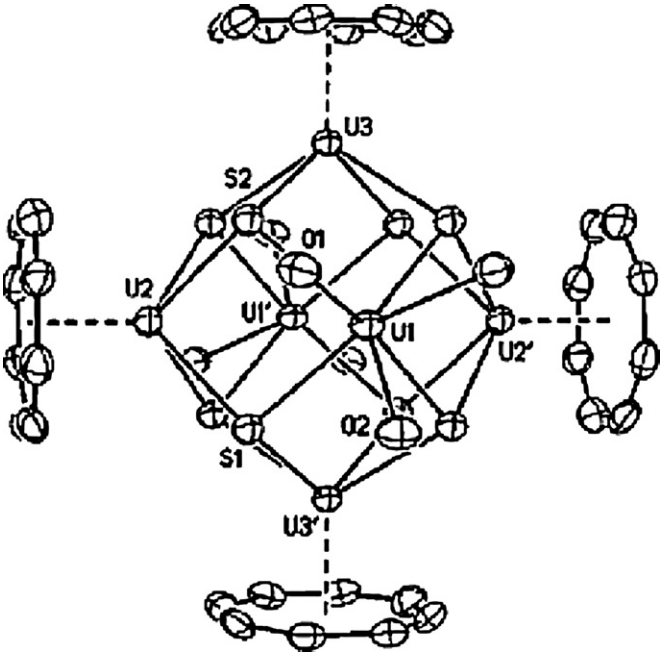

Fig. 12. Molecular structure of $[U(COT)]_4\{U(THF)_3\}_2(\mu^3\text{-}S)_8$ (for clarity the hydrogen atoms and carbon atoms of the THF molecules are omitted) [118].

The synthesis and crystal structure of the uranocene-derived cyano complex $[NEt_4][(\eta^8\text{-}COT)_2U(CN)]$ have been reported. Addition of slightly less than 1 mol equiv. of NEt_4CN to a suspension of $(\eta^8\text{-}COT)_2U$ in pyridine at 50 °C gave rapidly a clear solution of color varying from green to red depending on lighting conditions, from which thin brown needles of $[NEt_4][(\eta^8\text{-}COT)_2U(CN)]$ crystallized on cooling to room temperature in a combined yield of 86% (Scheme 200) The structure of the anion in the product showed the coordination of a single carbon-bound cyanide ligand in the equatorial girdle of a bent "uranocene". In contrast to known $(\eta^8\text{-}COT)_2An^{q-}$ (*q* = 0, 1) complexes, where the Cnt–An–Cnt angles (Cnt = ring centroid) deviate from linearity by a maximum of 4°, the $(\eta^8\text{-}COT)_2U$ moiety in $[NEt_4][(\eta^8\text{-}COT)_2U(CN)]$ adopts an unprecedented bent configuration with a Cnt–U–Cnt angle of 153.3°. In an analogous manner, the derivative $[N^nBu_4][(\eta^8\text{-}C_8H_8)_2U(CN)]$ was prepared in quantitative yield by addition of 1 mol equiv. of N^nBu_4CN to a suspension of uranocene in THF [132].

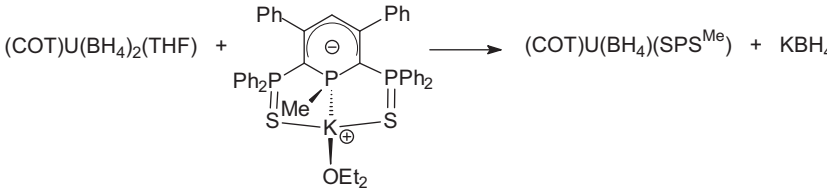

Scheme 198.

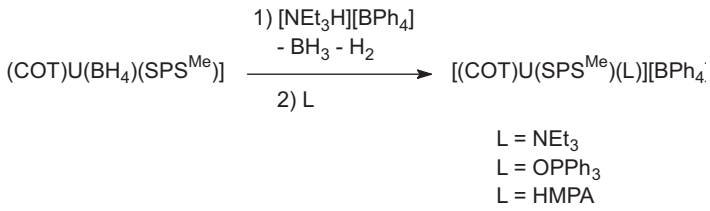

Scheme 199.

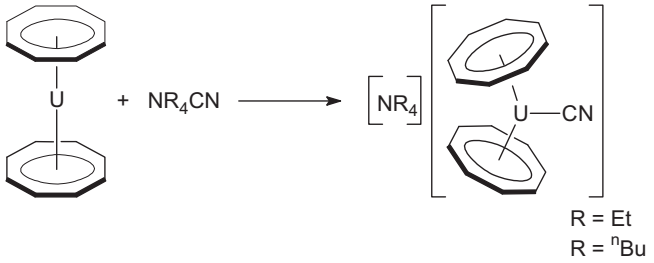

Scheme 200.

3.4. Organoactinides in catalysis

In earlier work, the thorium(IV) and uranium(IV) alkyl complexes $Cp^*_2AnR_2$ (where An = Th, U; R = CH_3, CH_2Ph, Ph) had proven to be versatile starting materials for the synthesis of a diverse array of actinide organometallic systems containing An–N bonds such as imido, hydrazonato, and ketimido complexes, which feature novel electronic properties. It has also been shown that these actinide alkyl complexes undergo interesting C–H and C–N bond cleavage chemistry with *N*-heterocycles. For example, the Th(IV) complexes $Cp^*_2Th(CH_3)_2$ and $Cp^*_2Th(CH_2Ph)_2$ readily react with the sp^2 C–H bonds in pyridine *N*-oxide and the sp^3 C–H bonds in 2,6-lutidine *N*-oxide, whereas the corresponding U(IV) complexes activate only the sp^2 C–H bonds in pyridine *N*-oxide (Scheme 201). Thus the C–H bond activation chemistry of $Cp^*_2Th(CH_3)_2$ and $Cp^*_2U(CH_3)_2$ with 2-picoline (2-methylpyridine) has been examined with the use of density functional techniques. In particular, the differences between insertion into the *ortho* ring sp^2 C–H bond and the methyl sp^3 C–H bond were explored. The energies to form the η^2-(*N*,*C*)-pyridyl products resulting from the activation of the aromatic ring sp^2 C–H bond were calculated as thermodynamic products for both thorium and uranium systems with similar reaction energies of −15.8 kcal/mol. The products corresponding to insertion into the methyl sp^3 C–H bond were found to be higher in energy by 3.5 and 5.4 kcal/mol for Th and U, respectively. In the transition state, the actinide atom mediates the hydrogen migration from 2-picoline

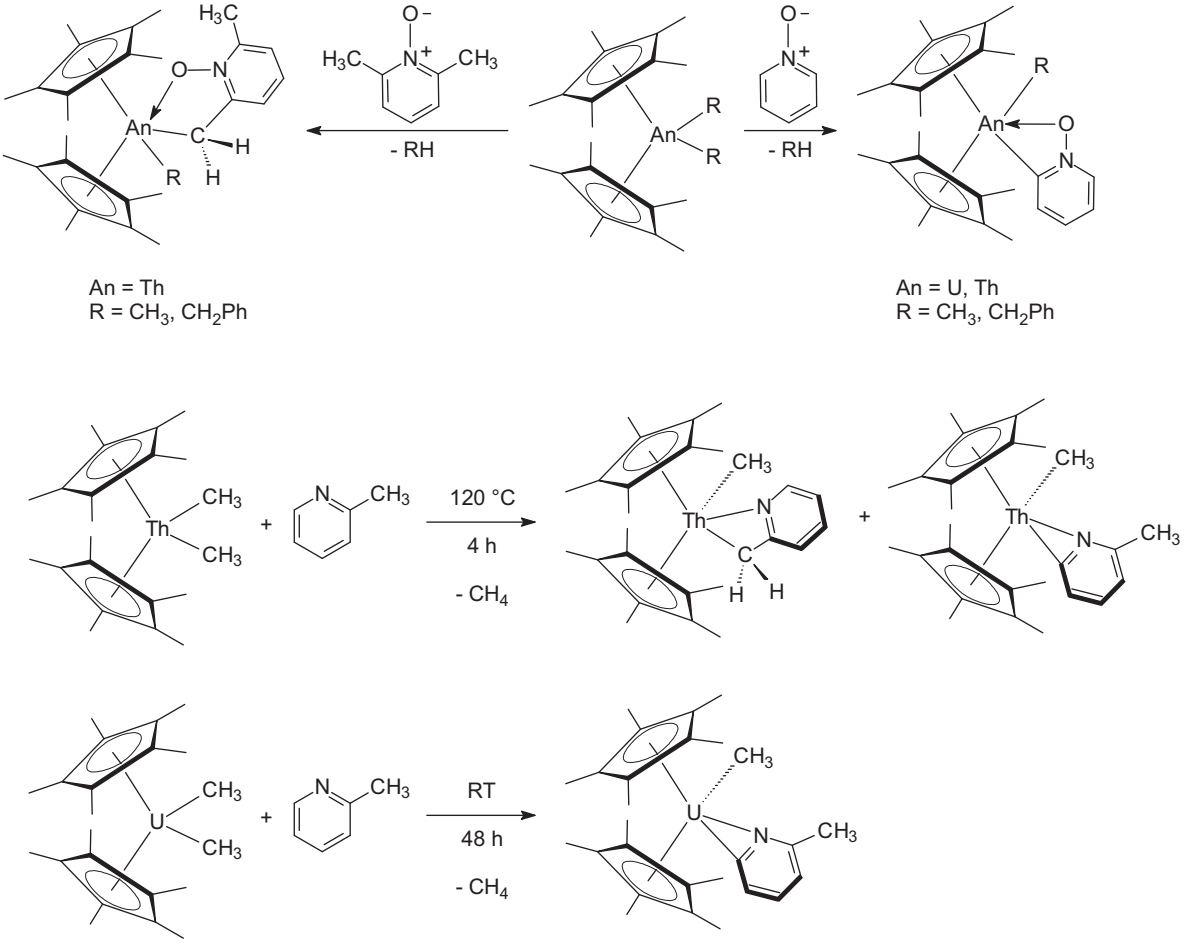

Scheme 201.

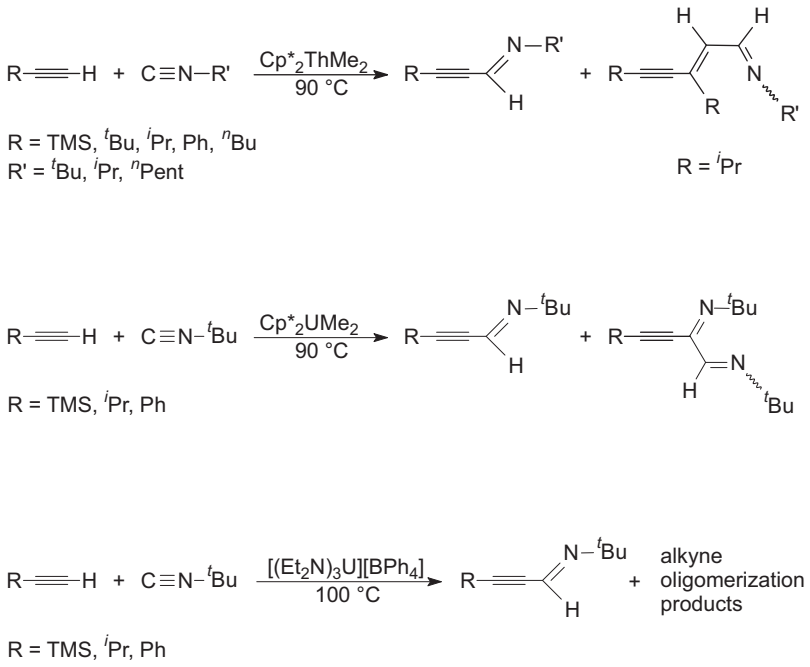

Scheme 202.

to the leaving methyl group by forming an agostic five-centered C–H complex. The relative activation energies between sp^2 and sp^3 C–H bond activation differ slightly between Th, $\Delta E^{\ddagger}(sp^2) > \Delta E^{\ddagger}(sp^3)$ and U, $\Delta E^{\ddagger}(sp^2) < \Delta E^{\ddagger}(sp^3)$. These results are in agreement with the experimental observations that the sp^2 insertion product is the thermodynamic product in both cases, but that the sp^3 insertion product is the kinetic product in the case of Th [133].

The coupling reaction of terminal alkynes with several isonitriles, catalyzed by the neutral organoactinide complexes $Cp^*_2AnMe_2$ (An = Th, U) or the cationic complex $[(Et_2N)_3U][BPh_4]$, yielded substituted α,β-acetylenic aldimines, in good to excellent yields. The reaction proceeded *via* a 1,1-insertion of the isonitrile carbon into a metal–acetylide bond, followed by a protonolysis by the acidic proton of the terminal alkyne. Additional insertion products were obtained by altering the catalyst and the reactant ratios (Scheme 202) [134].

A plausible mechanism for the catalytic reaction is also presented, based on kinetics measurements and thermodynamic studies of the coupling reaction with $Cp^*_2ThMe_2$ or $[(Et_2N)_3U][BPh_4]$ as catalysts (Schemes 203 and 204). The reaction is first-order in catalyst and isonitrile and zero-order in alkyne. This coupling of terminal alkynes and isonitriles by catalyzed organoac-

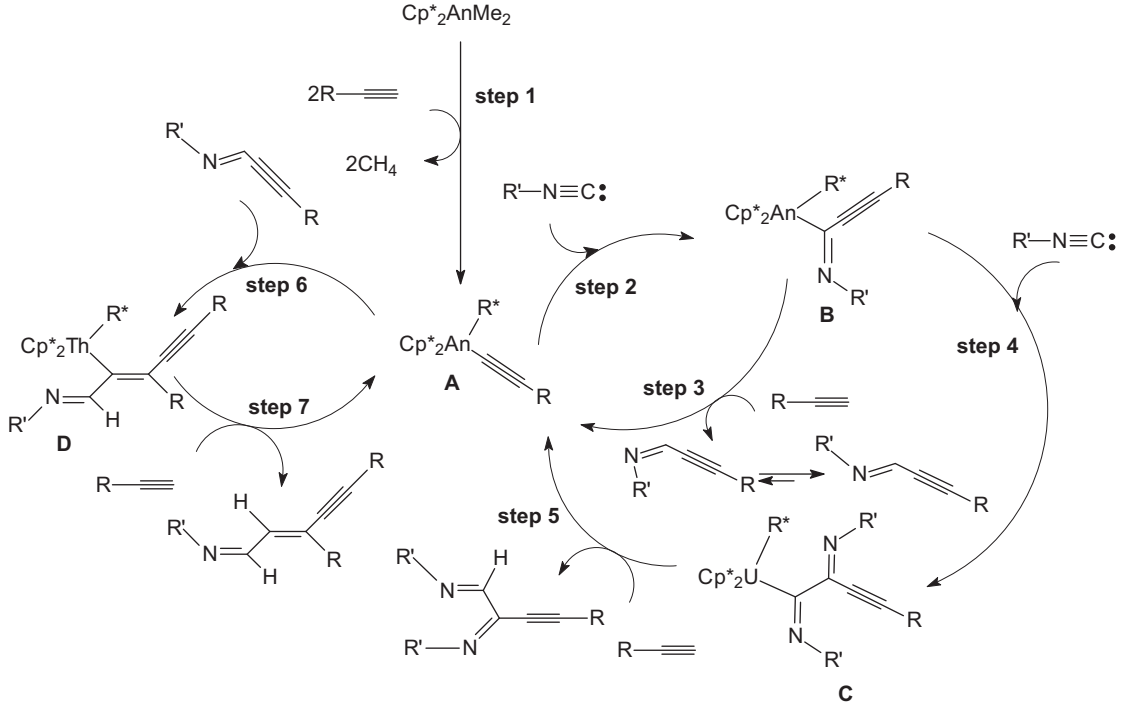

Scheme 203. Plausible mechanism for the catalytic coupling of isonitriles and terminal alkynes mediated by $Cp^*_2AnMe_2$ (An = Th, U) (for clarity R^* is used instead of RC≡C).

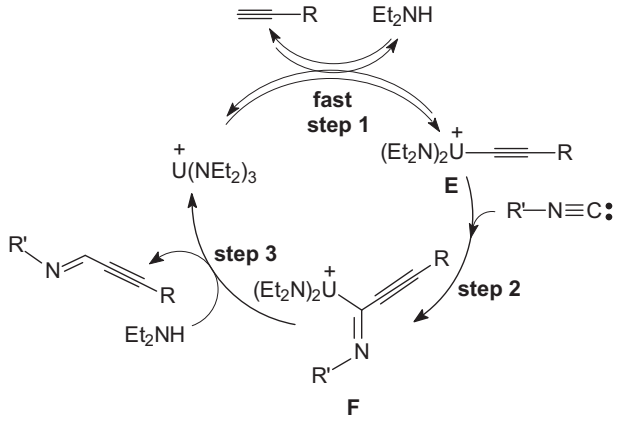

Scheme 204. Plausible mechanism for the catalytic coupling of isonitriles and terminal alkynes mediated by $[(Et_2N)_3U][BPh_4]$.

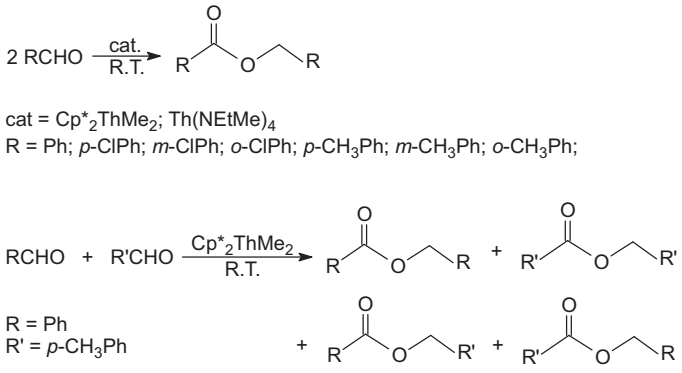

Scheme 205.

tinide complexes certainly introduced a new chapter in the field of catalytic activity of organoactinide complexes [134].

The mono-bridged dibutyl complex $\{[\eta^5\text{-}(C_5Me_4)_2SiMe_2]U^nBu\}_2(\mu\text{-}O)$ (Scheme 162) was found to be an active catalyst for the disproportionation metathesis of $Me_3SiC{\equiv}CH$ and the cross-metathesis of $Me_3SiC{\equiv}CH$ or $Me_3SiC{\equiv}CSiMe_3$ with various terminal alkynes. To shed some light on the possible mechanistic scenario, different alkynes, $Me_3SiC{\equiv}CH$, $Me_3SiC{\equiv}CSiMe_3$, or $Me_3SiC{\equiv}C^iPr$, were treated in the presence of $\{[\eta^5\text{-}(C_5Me_4)_2SiMe_2]U^nBu\}_2(\mu\text{-}O)$ with $PhSiH_3$, producing a myriad of products in addition to the unexpected Me_3SiH and SiH_4, indicating the cleavage of the trimethylsilyl group from the alkyne and the formation of a uranium-silyl intermediate. Complex $\{[\eta^5\text{-}(C_5Me_4)_2SiMe_2]U^nBu\}_2(\mu\text{-}O)$ was also found to be an active catalyst for the phenyl cleavage metathesis of $PhSiH_3$ to form Ph_2SiH_2 and Ph_3SiH. In C_6D_6 solutions, the C–D activation of the aromatic ring takes place, forming $C_6D_5SiH_3$. Plausible mechanisms for all the catalytic processes have been presented [115].

Certain organoactinide complexes and actinide amides have been shown to promote the catalytic Tishchenko reaction between two similar or different aldehydes to give the symmetric or asymmetric esters, correspondingly. To show the generality of the process, and to be able to propose a suitable mechanistic pathway, the thorium complexes $Cp^*_2ThMe_2$ and $Th(NEtMe)_4$ have been employed in addition to kinetic and thermodynamic studies using complex $Cp^*_2ThMe_2$. The two actinide complexes were found to be highly to moderately active (yields 85–65%) in the catalytic dimerization of benzaldehyde and gave the corresponding ester with no side products. Scheme 205 illustrates the dimerization reactions of benzaldehyde and other substituted benzaldehydes [135].

Based on the kinetic and thermodynamic data a plausible mechanism for the Tishchenko reaction was presented which is depicted in Scheme 206. In the first step of the reaction, the precatalyst $Cp^*_2ThMe_2$ reacts with 2 equiv. of the aldehyde to give the alkoxo

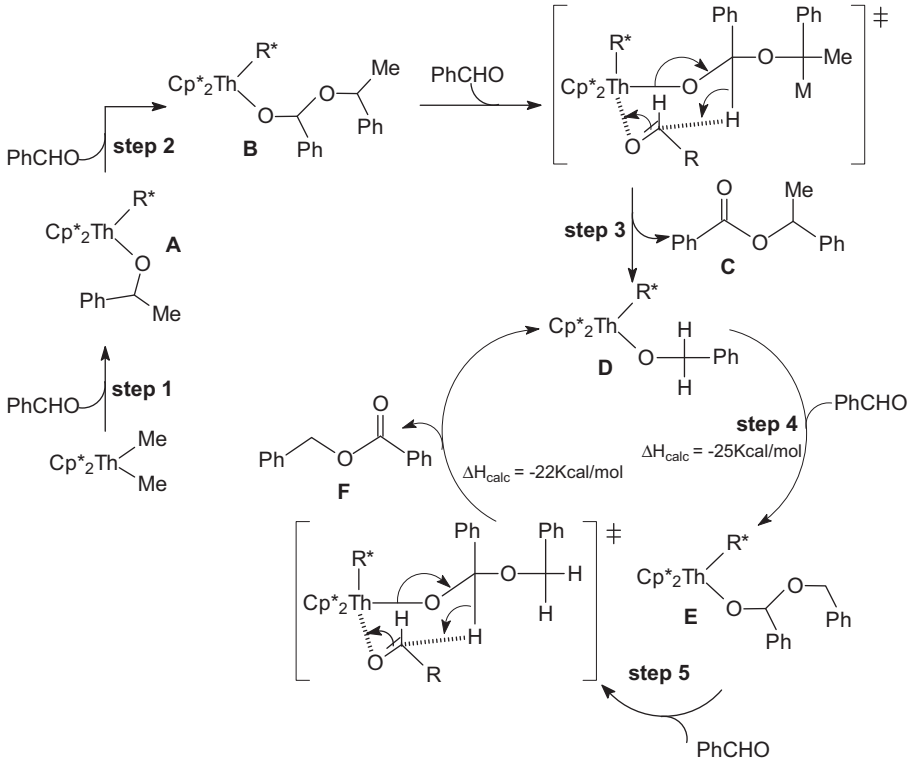

Scheme 206.

complex **A**, *via* a four-center transition state. The first step is thermodynamically favorable because of the oxophilic nature of thorium ($\Delta H_{calcd} = -68$ kcal/mol). A second insertion of an aldehyde into the thorium–alkoxide bond produces complex **B**. The following metathesis of complex **B** with an additional aldehyde releases the ester **C**, thereby producing the active catalytic species **D**. The catalytic insertion of an aldehyde into a thorium-alkoxo bond takes place in step 4 to give complex **E**, and its hydride transfer reaction (step 5, rate determining step) with an additional aldehyde *via* a plausible six-centered chairlike transition state produces the ester **F** and regenerates the active complex. Apparently, this was the first example of a catalytic coupling process of aldehydes mediated by actinide complexes. Unexpectedly, the reaction was found to proceed *via* an actinide-alkoxo bond activation, which was previously believed to be a dead end for actinide complexes in terms of catalysis [135].

References

[1] G. Wu, J. Wang, Y. Lu, M. Yang, J. Chem. Phys. 128 (2008) 224315/1.
[2] L. Jiang, Q. Xu, J. Chem. Phys. 128 (2008) 124317/1.
[3] L. Jiang, X.-B. Zhang, S. Han, Q. Xu, Inorg. Chem. 47 (2008) 4826.
[4] J. Marcalo, M. Santos, A. Pires de Matos, J.K. Gibson, R.G. Haire, J. Phys. Chem. 112 (2008) 12647.
[5] J. Cheng, J. Takats, M.J. Ferguson, R. McDonald, J. Am. Chem. Soc. 130 (2008) 1544.
[6] J. Scott, H. Fan, B.F. Wicker, A.R. Fout, M.-H. Baik, D.J. Mindiola, J. Am. Chem. Soc. 130 (2008) 14438.
[7] S.T. Liddle, J. McMaster, J.C. Green, P.L. Arnold, Chem. Commun. (2008) 1747.
[8] M.U. Kramer, D. Robert, S. Arndt, P.M. Zeimentz, T.P. Spaniol, A. Yahia, L. Maron, O. Eisenstein, J. Okuda, Inorg. Chem. 47 (2008) 9265.
[9] H. Fan, D. Adhikari, A.A. Saleh, R.L. Clark, J.F. Zuno-Cruz, C.G. Sanchez, J.C. Huffman, M. Pink, D.J. Mindiola, M.-H. Baik, J. Am. Chem. Soc. 130 (2008) 17351.
[10] X. Wei, Y. Cheng, P.B. Hitchcock, M.F. Lappert, Dalton Trans. (2008) 5235.
[11] J. Eppinger, K.R. Nikolaides, M. Zhang-Presse, F.A. Riederer, G.W. Rabe, A.L. Rheingold, Organometallics 27 (2008) 736.
[12] B. Shen, L. Ying, J. Chen, Y. Luo, Inorg. Chim. Acta 361 (2008) 1255.
[13] C.S. Tredget, E. Clot, P. Mountford, Organometallics 27 (2008) 3458.
[14] M. Ohashi, M. Konkol, I. Del Rosal, R. Poteau, L. Maron, J. Okuda, J. Am. Chem. Soc. 130 (2008) 6920.
[15] S. Ge, A. Meetsma, B. Hessen, Organometallics 27 (2008) 5339.
[16] N. Meyer, P.W. Roesky, S. Bambirra, A. Meetsma, B. Hessen, K. Saliu, J. Takats, Organometallics 27 (2008) 1501.
[17] C.T. Carver, M.J. Monreal, P.L. Diaconescu, Organometallics 27 (2008) 363.
[18] S. Bambirra, F. Perazzolo, S.J. Boot, T.J.J. Sciarone, A. Meetsma, B. Hessen, Organometallics 27 (2008) 704.
[19] L. Zhang, M. Nishiura, M. Yuki, Y. Luo, Z. Hou, Angew. Chem. Int. Ed. 47 (2008) 2642.
[20] J.D. Masuda, K.C. Jantunen, B.L. Scott, J.L. Kiplinger, Organometallics 27 (2008) 1299.
[21] J.D. Masuda, K.C. Jantunen, B.L. Scott, J.L. Kiplinger, Organometallics 27 (2008) 803.
[22] X. Xu, X. Xu, Y. Chen, J. Sun, Organometallics 27 (2008) 758.
[23] D. Wang, S. Li, X. Liu, W. Gao, D. Cui, Organometallics 27 (2008) 6531.
[24] K.D. Conroy, W.E. Piers, M. Parvez, J. Organomet. Chem. 693 (2008) 834.
[25] S. Li, W. Miao, T. Tang, W. Dong, X. Zhang, D. Cui, Organometallics 27 (2008) 718.
[26] J.D. Masuda, K.C. Jantunen, O.V. Ozerov, K.J.T. Noonan, D.P. Gates, B.L. Scott, J.L. Kiplinger, J. Am. Chem. Soc. 130 (2008) 2408.
[27] W. Gao, D. Cui, Organometallics 27 (2008) 5889.
[28] X. Liu, D. Cui, Dalton Trans. (2008) 3747.
[29] M. Konkol, M. Kondracka, P. Voth, T.P. Spaniol, J. Okuda, Organometallics 27 (2008) 3774.
[30] K. Lv, D. Cui, Organometallics 27 (2008) 5438.
[31] J. Zhang, H. Yao, Y. Zhang, H. Sun, Q. Shen, Organometallics 27 (2008) 2672.
[32] H. Jin, Y.J. Cho, S.K. Oh, H.J. Kang, J.C. Park, S. Heo, J.C. Lee, Appl. Phys. Lett. 93 (2008) 052904/1.
[33] D.M. Lyubov, C. Doring, G.K. Fukin, A.V. Cherkasov, A.S. Shavyrin, R. Kempe, A.A. Trifonov, Organometallics 27 (2008) 2905.
[34] I. Aillaud, D. Lyubov, J. Collin, R. Guillot, J. Hannedouche, E. Schulz, A. Trifonov, Organometallics 27 (2008) 5929.
[35] J. Cheng, K. Saliu, G.Y. Kiel, M.J. Ferguson, R. McDonald, J. Takats, Angew. Chem. Int. Ed. 47 (2008) 4910.
[36] Y.-L. Teng, Q. Xu, J. Phys. Chem. 112 (2008) 10274.
[37] G.B. Deacon, C.M. Forsyth, F. Jaroschik, P.C. Junk, D.L. Kay, T. Maschmeyer, A.F. Masters, J. Wang, L.D. Field, Organometallics 27 (2008) 4772.
[38] C. Ruspic, J.R. Moss, M. Schürmann, S. Harder, Angew. Chem. Int. Ed. 47 (2008) 2121.
[39] M. Yousufuddin, M.J. Gutmann, J. Baldamus, O. Tardif, Z. Hou, S.A. Mason, G.J. McIntyre, R. Bau, J. Am. Chem. Soc. 130 (2008) 3888.
[40] B.-Y. Li, Y.-M. Yao, Y.-R. Wang, Y. Zhang, Q. Shen, Polyhedron 27 (2008) 709.
[41] R. Qi, B. Liu, X. Xu, Z. Yang, Y. Yao, Y. Zhang, Q. Shen, Dalton Trans. (2008) 5016.
[42] D. Cui, M. Nishiura, O. Tardif, Z. Hou, Organometallics 27 (2008) 2428.
[43] H.F. Yuen, T.J. Marks, Organometallics 27 (2008) 155.
[44] W.-X. Zhang, M. Nishiura, T. Mashiko, Z. Hou, Chem. Eur. J. 14 (2008) 2167.
[45] J. Sun, D.J. Berg, B. Twamley, Organometallics 27 (2008) 683.
[46] A. Otero, J. Fernandez-Baeza, A. Lara-Sanchez, A. Antinolo, J. Tejeda, E. Martinez-Caballero, I. Marquez-Segovia, I. Lopez-Solera, L.F. Sanchez-Barba, C. Alonso-Moreno, Inorg. Chem. 47 (2008) 4996.
[47] A. Venugopal, A. Hepp, T. Pape, A. Mix, N.W. Mitzel, Dalton Trans. 46 (2008) 6628.
[48] J. Zhang, Y. Han, F. Han, Z. Chen, L. Weng, X. Zhou, Inorg. Chem. 47 (2008) 5552.
[49] R. Liu, P. Zheng, L. Weng, X. Zhou, C. Liu, J. Organomet. Chem. 693 (2008) 1614.
[50] E.L. Werkema, R.A. Andersen, J. Am. Chem. Soc. 130 (2008) 7153.
[51] P.B. Hitchcock, M.F. Lappert, L. Maron, A.V. Protchenko, Angew. Chem. Int. Ed. 47 (2008) 1488.
[52] H.-D. Amberger, H. Reddmann, Z. Anorg. Allg. Chem. 634 (2008) 1542.
[53] H.-D. Amberger, H. Reddmann, Z. Anorg. Allg. Chem. 634 (2008) 173.
[54] O.T. Summerscales, D.R. Johnston, F.G.N. Cloke, P.B. Hitchcock, Organometallics 27 (2008) 5612.
[55] V.F. Quiroga Norambuena, A. Heeres, H.J. Heeres, A. Meetsma, J.H. Teuben, B. Hessen, Organometallics 27 (2008) 5672.
[56] W.J. Evans, E. Montalvo, T.M. Champagne, J.W. Ziller, A.G. DiPasquale, A.L. Rheingold, Organometallics 27 (2008) 3582.
[57] W.J. Evans, E. Montalvo, T.M. Champagne, J.W. Ziller, A.G. DiPasquale, A.L. Rheingold, J. Am. Chem. Soc. 130 (2008) 16.
[58] W.J. Evans, E. Montalvo, D.J. Dixon, J.W. Ziller, A.G. DiPasquale, A.L. Rheingold, Inorg. Chem. 47 (2008) 11376.
[59] W.J. Evans, B.M. Schmiege, S.E. Lorenz, K.A. Miller, T.M. Champagne, J.W. Ziller, A.G. DiPasquale, A.L. Rheingold, J. Am. Chem. Soc. 130 (2008) 8555.
[60] C.N. Carlson, J.M. Veauthier, K.D. John, D.E. Morris, Chem. Eur. J. 14 (2008) 422.
[61] J.M. Veauthier, E.J. Schelter, C.N. Carlson, B.L. Scott, R.E. Da Re, J.D. Thompson, J.L. Kiplinger, D.E. Morris, K.D. John, Inorg. Chem. 47 (2008) 5841.
[62] M. Roger, L. Belkhiri, T. Arliguie, P. Thuery, A. Boucekkine, M. Ephritikhine, Organometallics 27 (2008) 33.
[63] Y. Wei, Z. Yu, S. Wang, S. Zhou, G. Yang, L. Zhang, G. Chen, H. Qian, J. Fan, J. Organomet. Chem. 693 (2008) 2263.
[64] O. Tardif, S. Kaita, Dalton Trans. (2008) 2531.
[65] A. Zaeni, F. Olbrich, A. Fischer, F.T. Edelmann, J. Organomet. Chem. 693 (2008) 3791.
[66] B. Wang, D. Cui, K. Lv, Macromolecules 41 (2008) 1983.
[67] M. Nishiura, T. Mashiko, Z. Hou, Chem. Commun. 17 (2008) 2019.
[68] X. Fang, Y. Deng, Q. Xie, F. Moingeon, Organometallics 27 (2008) 2892.
[69] C. Pi, L. Wan, Y. Gu, W. Zheng, L. Weng, Z. Chen, L. Wu, Inorg. Chem. 47 (2008) 9739.
[70] G.K.B. Clentsmith, F.G.N. Cloke, M.D. Francis, J.R. Hanks, P.B. Hitchcock, J.F. Nixon, J. Organomet. Chem. 693 (2008) 2287.
[71] H. Shen, H.-S. Chan, Z. Xie, Organometallics 27 (2008) 5309.
[72] P. Cui, Y. Chen, G. Wang, G. Li, W. Xia, Organometallics 27 (2008) 4013.
[73] Y. Yuan, Y. Chen, G. Li, W. Xia, Organometallics 27 (2008) 6307.
[74] P. Cui, Y. Chen, G. Li, W. Xia, Angew. Chem. Int. Ed. 47 (2008) 9944.
[75] N. Atodiresei, P.H. Dederichs, Y. Mokrousov, L. Bergqvist, G. Bihlmayer, S. Blugel, Phys. Rev. Lett. 100 (2008) 117207/1.
[76] K. Miyajima, M.B. Knickelbein, A. Nakajima, J. Phys. Chem. 112 (2008) 366.
[77] S. Taubert, M. Straka, T.O. Pennanen, D. Sundholm, J. Vaara, Phys. Chem. Chem. Phys. 10 (2008) 7158.
[78] Y. Yamazaki, K. Nakajima, T. Wakahara, T. Tsuchiya, M.O. Ishitsuka, Y. Maeda, T. Akasaka, M. Waelchli, N. Mizorogi, S. Nagase, Angew. Chem. Int. Ed. 47 (2008) 7905.
[79] R. Valencia, A. Rodriguez-Fortea, J.M. Poblet, J. Phys. Chem. 112 (2008) 4550.
[80] H. Yang, C. Lu, Z. Liu, H. Jin, Y. Che, M.M. Olmstead, A.L. Balch, J. Am. Chem. Soc. 130 (2008) 17296.
[81] X. Lu, H. Nikawa, T. Tsuchiya, Y. Maeda, M.O. Ishitsuka, T. Akasaka, M. Toki, H. Sawa, Z. Slanina, N. Mizorogi, S. Nagase, Angew. Chem. 120 (2008) 8770.
[82] M.V. Butovskii, O.L. Tok, F.R. Wagner, R. Kempe, Angew. Chem. Int. Ed. 47 (2008) 6469.
[83] H.-M. Sommerfeldt, C. Meermann, M.G. Schrems, K.W. Törnroos, N.A. Froystein, R.J. Miller, E.-W. Scheidt, W. Scherer, R. Anwander, Dalton Trans. (2008) 1899.
[84] H.-M. Sommerfeldt, C. Meermann, K.W. Törnroos, R. Anwander, Inorg. Chem. 47 (2008) 4696.
[85] R. Litlaboe, M. Zimmermann, K. Saliu, J. Takats, K.W. Törnroos, R. Anwander, Angew. Chem. Int. Ed. 47 (2008) 9560.
[86] M. Zimmermann, J. Takats, G. Kiel, K.W. Törnroos, R. Anwander, Chem. Commun. (2008) 612.
[87] L.C.H. Gerber, E. Le Roux, K.W. Törnroos, R. Anwander, Chem. Eur. J. 14 (2008) 9555.
[88] M. Zimmermann, K.W. Törnroos, H. Sitzmann, R. Anwander, Chem. Eur. J. 14 (2008) 7266.
[89] M. Zimmermann, K.W. Törnroos, R. Anwander, Angew. Chem. Int. Ed. 47 (2008) 775.

[90] Y. Yang, P.M. Gurubasavaraj, H. Ye, Z. Zhang, H.W. Roesky, P.G. Jones, J. Organomet. Chem. 693 (2008) 1455.
[91] J. Caballo, M. Garcia-Castro, A. Martin, M. Mena, A. Perez-Redondo, C. Yelamos, Inorg. Chem. 47 (2008) 7077.
[92] C.T. Carver, P.L. Diaconescu, J. Am. Chem. Soc. 130 (2008) 7558.
[93] A. Ravasio, C. Zampa, L. Boggioni, I. Tritto, J. Hitzbleck, J. Okuda, Macromolecules 41 (2008) 9565.
[94] S.B. Amin, S.Y. Seo, T.J. Marks, Organometallics 27 (2008) 2411.
[95] H. Zhang, Y. Luo, Z. Hou, Macromulecules 41 (2008) 1064.
[96] W. Gao, D. Cui, J. Am. Chem. Soc. 130 (2008) 4984.
[97] N. Barros, P. Mountford, S.M. Guillaume, L. Maron, Chem. Eur. J. 14 (2008) 5507.
[98] N. Barros, M. Schappacher, P. Dessuge, L. Maron, S.M. Guillaume, Chem. Eur. J. 14 (2008) 1881.
[99] N. Barros, O. Eisenstein, L. Maron, T.D. Tilley, Organometallics 27 (2008) 2252.
[100] S. Ge, A. Meetsma, B. Hessen, Organometallics 27 (2008) 3131.
[101] W.-X. Zhang, M. Nishiura, Z. Hou, Angew. Chem. Int. Ed. 47 (2008) 9700.
[102] Z. Du, W. Li, X. Zhu, F. Xu, Q. Shen, J. Org. Chem. 73 (2008) 8966.
[103] W.-S. Kim, T.-S. Kim, B.-W. Kang, M.-G. Ko, S.-K. Park, J.-W. Park, J. Vac. Sci. Technol. B 26 (2008) 1588.
[104] M.M. Giangregorio, A. Sacchetti, M. Losurdo, P. Capezzuto, G. Bruno, J. Non-Cryst. Solids 354 (2008) 2853.
[105] M. Zeuner, S. Pagano, W. Schnick, Chem. Eur. J. 14 (2008) 1524.
[106] A.C. Tsipis, C.E. Kefalidis, C.A. Tsipis, J. Am. Chem. Soc. 130 (2008) 9144.
[107] J.T. Lyon, L. Andrews, Eur. J. Inorg. Chem. (2008) 1047.
[108] H.-G. Cho, J.T. Lyon, L. Andrews, J. Phys. Chem. 112 (2008) 6902.
[109] J.T. Lyon, L. Andrews, H.-S. Hu, J. Li, Inorg. Chem. 47 (2008) 1435.
[110] C.A. Cruz, D.J.H. Emslie, L.E. Harrington, J.F. Britten, Organometallics 27 (2008) 15.
[111] M.J. Monreal, P.L. Diaconescu, Organometallics 27 (2008) 1702.
[112] C.D. Carmichael, N.A. Jones, P.L. Arnold, Inorg. Chem. 47 (2008) 8577.
[113] N. Iche-Tarrat, N. Barros, C.J. Marsden, L. Maron, Chem. Eur. J. 14 (2008) 2093.
[114] L.P. Spencer, R.L. Gdula, T.W. Hayton, B.L. Scott, J.M. Boncella, Chem. Commun. (2008) 4986.
[115] J. Wang, Y. Gurevich, M. Botoshansky, M.S. Eisen, Organometallics 27 (2008) 4494.
[116] S.G. Minasian, J.L. Krinsky, V.A. Williams, J. Arnold, J. Am. Chem. Soc. 130 (2008) 10086.
[117] C.P. Larch, F.G.N. Cloke, P.B. Hitchcock, Chem. Commun. (2008) 82.
[118] T. Arliguie, M. Blug, P. Le Floch, N. Mezailles, P. Thuery, M. Ephritikhine, Organometallics 27 (2008) 4158.
[119] T. Cantat, C.R. Graves, K.C. Jantunen, C.J. Burns, B.L. Scott, E.J. Schelter, D.E. Morris, P.J. Hay, P.J.L. Kiplinger, J. Am. Chem. Soc. 130 (2008) 17537.
[120] D.J. Hilton, R.P. Prasankumar, E.J. Schelter, V.K. Thorsmolle, S.A. Trugman, A.P. Shreve, J.L. Kiplinger, D.E. Morris, A.J. Taylor, J. Phys. Chem. 112 (2008) 7840.
[121] C.R. Graves, E.J. Schelter, T. Cantat, B.L. Scott, J.L. Kiplinger, Organometallics 27 (2008) 5371.
[122] E.J. Schelter, J.M. Veauthier, C.R. Graves, K.D. John, B.L. Scott, J.D. Thompson, J.A. Pool-Davis-Tournear, D.E. Morris, J.L. Kiplinger, Chem. Eur. J. 14 (2008) 7782.
[123] W.J. Evans, J.R. Walensky, F. Furche, J.W. Ziller, A.G. DiPasquale, A.L. Rheingold, Inorg. Chem. 47 (2008) 10169.
[124] W.J. Evans, K.A. Miller, A.G. DiPasquale, A.L. Rheingold, T.J. Stewart, R. Bau, Angew. Chem. Int. Ed. 47 (2008) 5075.
[125] W.J. Evans, E. Montalvo, S.A. Kozimor, K.A. Miller, J. Am. Chem. Soc. 130 (2008) 12258.
[126] C.R. Graves, P. Yang, S.A. Kozimor, A.E. Vaughn, D.L. Clark, S.D. Conradson, E.J. Schelter, B.L. Scott, J.D. Thompson, P.J. Hay, D.E. Morris, J.L. Kiplinger, J. Am. Chem. Soc. 130 (2008) 5272.
[127] C.R. Graves, B.L. Scott, D.E. Morris, J.L. Kiplinger, Organometallics 27 (2008) 3335.
[128] C.R. Graves, A.E. Vaughn, E.J. Schelter, B.L. Scott, J.D. Thompson, D.E. Morris, J.L. Kiplinger, Inorg. Chem. 47 (2008) 11879.
[129] E.J. Schelter, R. Wu, B.L. Scott, J.D. Thompson, D.E. Morris, J.L. Kiplinger, Angew. Chem. Int. Ed. 47 (2008) 2993.
[130] W.J. Evans, K.A. Miller, J.W. Ziller, Angew. Chem. Int. Ed. 47 (2008) 589.
[131] A.S. Frey, F.G.N. Cloke, P.B. Hitchcock, I.J. Day, J.C. Green, G. Aitken, J. Am. Chem. Soc. 130 (2008) 13816.
[132] J.-C. Berthet, P. Thuery, M. Ephritikhine, Organometallics 27 (2008) 1664.
[133] P. Yang, I. Warnke, R.L. Martin, P.J. Hay, Organometallics 27 (2008) 1384.
[134] E. Barnea, T. Andrea, J.-C. Berthet, M. Ephritikhine, M.S. Eisen, Organometallics 27 (2008) 3103.
[135] T. Andrea, E. Barnea, M.S. Eisen, J. Am. Chem. Soc. 130 (2008) 2454.